Investigating SAMHD1 restriction of HIV-1 in stem cell-derived macrophages



Damien Warner
Sir William Dunn School of Pathology
Brasenose College
University of Oxford

A thesis submitted for the degree of
Doctor of Philosophy
Trinity Term 2019



Abstract

Investigating SAMHD1 restriction of HIV-1 in stem cell-derived macrophages

A thesis submitted for the degree of Doctor of Philosophy at the University of Oxford by Damien Warner, Brasenose College, Trinity Term 2019

SAMHD1 is potent in restriction of lentiviruses in primary bone marrow-derived monocytes, macrophages, and dendritic cells and is variably neutralised in these cells by the SIV accessory protein Vpx [1-3]. However, the dynamics of SAMHD1 restriction of lentiviruses in yolk sac derived tissue-resident macrophages has not been formally demonstrated. Here I use a human stem cell differentiation protocol, competent in the production of macrophages that are developmentally related to, and thus a good model for, tissue-resident macrophages such as microglia, Langerhans cells, and alveolar macrophages [4, 5]. This system produced stem cell origin Yolk-sac-Derived-like Macrophage Precursor cells (scYDMPs) and Macrophages (scYDMs) over extended periods, which were subsequently used as a tool to investigate SAMHD1 restriction of HIV-1 and antagonisation by Vpx. Using a loss-of-function approach, I showed that the phenotype of SAMHD1 expression, hydrolysis of dNTPs, restriction of HIV-1, and antagonisation by Vpx in scYDMs is very similar to that reported in blood MDMs. I also showed that Vpx-mediated rescue of HIV-1 infection was more potent than the shRNA knockdown of SAMHD1. I, therefore, hypothesised that either Vpx facilitates HIV-1 infection via a SAMHD1 independent mechanism or the SAMHD1 protein remaining after knockdown was of sufficient potency to facilitate HIV-1 restriction and dNTP hydrolysis. I used a CRISPR-Cas9 knockout strategy to show that Vpx did not rescue HIV-1 infection by a SAMHD1 independent mechanism in scYDMs. However, the application of Vpx to SAMHD1 knockout cells was concomitant with an increase in dNTPs. This showed that in scYDMs, Vpx functions to increase dNTPs by a mechanism independent of SAMHD1. Using a dNTPase defective SAMHD1 mutant scYDM cell line, I was able to show for the first time that the dNTPase function of SAMHD1 is dispensable for HIV-1 infection in scYDMs. I also showed for the first time that Vpr of SIVmac degrades SAMHD1 and rescues HIV-1 infection in scYDMs. Moreover, and in contrast to Vpx-mediated rescue of HIV-1 infection at the steady-state in scYDMs, Vpx (and Vpr) rescued HIV-1 infection from the antiviral state established by type I interferons and LPS in scYDMs. This result implies that in scYDMs, Vpx and Vpr may interact with additional components of the innate immune system that are independent of SAMHD1. Taken together, these results highlight the experimental flexibility and integrity of data generated using a stem cell to macrophage differentiation strategy combined with genetic modification, and show that these cells represent a good model for investigating SAMHD1 restriction of HIV-1.

Acknowledgements

This thesis is dedicated to Leonie, Michelle, Brian, and Racheal, whose constant presence and encouragement provided both nourishment and inspiration; and without whom, this work would not have been possible.

I would like to show my appreciation for primary supervision provided by Dr Michael (Kenny) Moore and Prof. William James; and additional supervision provided by Dr Frank Vreede, Prof. Ervin Fodor and Prof. Anton van der Merwe.

I am also grateful to the Biotechnology and Biological Sciences Research Fund (BBSRC), the Sir William Dunn School of Pathology, and Brasenose College for the funding that made my endeavour to pursue a D.Phil., possible.

Table of Contents

ABSTRACT **5**

ACKNOWLEDGEMENTS **7**

TABLE OF CONTENTS **9**

LIST OF FIGURES **13**

LIST OF TABLES **15**

LIST OF ABBREVIATIONS **16**

CHAPTER 1: INTRODUCTION **30**

1.1 PRIMATE IMMUNODEFICIENCY VIRUSES 30
1.1.1 HIV and SIV origin *30*
1.1.2 HIV and SIV genome *37*
1.1.3 HIV and SIV core proteins *39*
1.1.3.1 Regulatory proteins 39
1.1.3.2 Structural proteins 40
1.1.4 HIV and SIV Accessory proteins *40*
1.1.4.1 Nef, Vif and Vpu 41
1.1.4.2 Vpr 41
1.1.4.3 Vpx 48
1.1.5 Restriction factors *53*
1.1.5.1 APOBEC3G 54
1.1.5.2 TRIM5α 54
1.1.5.3 Tetherin 55
1.1.5.4 SAMHD1 55
1.1.6 HIV and SIV lifecycle *64*
1.2 LENTIVIRAL VECTORS 70
1.3 MACROPHAGES 72
1.3.1 Development *72*
1.3.2 Homeostasis *74*
1.3.3 Macrophages and Immunity *75*
1.3.4 Ontogenesis *77*
1.3.5 Differentiation *79*
1.3.6 Activation and polarisation *83*
1.3.7 Macrophages and HIV *84*
1.3.7.1 Tropism 85
1.3.7.2 HIV-1 Infection of macrophages 86
1.3.7.3 HIV-1 Infection from macrophages 88
1.3.7.4 Macrophages as reservoirs 88
1.4 GENE EDITING 90
1.4.1. Meganucleases *90*
1.4.2 Zinc finger nucleases and Transcription activator-like effectors nucleases *91*
1.4.3 CRISPR- Cas9 ..... *92*
1.5 THESIS PROPOSITUM 95

CHAPTER 2: GENERAL MATERIALS AND METHODS **97**

2.1 CELL CULTURE 98
2.1.1 Cell Lines *98*
2.1.2 Human es cell and iPS cell culture *98*
2.1.3 Es and iPS macrophage differentiation *99*
2.1.3.1 Embryoid Body (EB) formation – Aggrewell™ 800 99

2.1.3.2 Directed differentiation of Embryoid Bodies into Stem Cell origin Yolk sac Derived-like Macrophage Precursors (scYDMPs) 100
2.1.3.3 Differentiation of Stem Cell origin Yolk sac Derived-like Macrophages (scYDMs) 101
2.1.4 Freezing and thawing of cell lines *103*
2.1.5 Freezing and thawing of stem cells *103*
2.1.6 Cell counts and viability *103*
2.1.7 Microscopy *104*
2.1.8 Electroporation *104*
2.1.9 Staining for cell surface receptor expression levels *104*
2.1.10 Flow cytometry *105*
2.1.11 Co-transfection of HEK293T cells *105*
2.2 QUANTIFICATION ASSAYS 106
2.2.1 SIV p27 antigen ELISA *106*
2.2.2 Western Blot *106*
2.2.3 ATP (Adenosine 5'-triphosphate) determination *107*
2.3 CLONING TECHNIQUES 107
2.3.1 Bacterial transformation *107*
2.3.2 Restriction enzyme digest of DNA *108*
2.3.3 DNA amplification using the polymerase chain reaction (PCR) *108*
2.3.4 Agarose gel purification and separation of DNA in solution *108*
2.3.5 DNA ligation *109*
2.3.6 Preparation of oligonucleotides for cloning *109*
2.3.7 Vector design and sequence analysis *110*
2.4 HIV-1 ASSAYS 114
2.4.1 Viruses used in this thesis *114*
2.4.1.1 HIV-1.GIP (EF1-GFP-Ires-Puro-SIN) 114
2.4.1.2 HIV-1.NLU (NL4-3.Luc.R-E) 114
2.4.2 Viral lentivector like particles (VLP) *114*
2.4.2.1 Vpx-VLP (CMV-SIV4+Vpx) 114
2.4.2.2 Vpr-VLP (CMV-SIV4+Vpr) 115
2.4.2.3 Empty-VLPs (CMV-SIV4+CTRL) 115
2.4.2.4 Vpr_{HIV-1}-VLP (CMV-HIV-1+Vpr) 115
2.4.3 HIV-1 Infection assays *115*
2.4.3.1 HIV-1 Infection assay (GFP) 115
2.4.3.2 HIV-1 Infection assay (GFP) with VLPs 116
2.4.3.3 HIV-1 Infection assay (Luciferase) 116
2.4.3.4 HIV-1 Infection assay (Luciferase) with VLPs 117
2.5 LENTIVIRAL PARTICLE PRODUCTION 117
2.5.1 HIV-1 virus *117*
2.5.2 Viral Lentivector Like Particles (VLPs) *118*
2.6 LENTIVECTOR TRANSDUCTION OF THP-1 CELLS 119
2.7 STATISTICAL ANALYSIS 119

CHAPTER 3: SAMHD1 ACTIVITY IN STEM CELL-DERIVED MACROPHAGES 121

3.1 INTRODUCTION 122
3.2 METHODS AND MATERIALS 124
3.2.1 Generation of scYDMs expressing Vpx and shRNA targeting SAMHD1 ..... *124*
3.2.1.1 Lentivector particles for transduction of stem cells 124
3.2.1.2 Transduction of stem cells 125
3.2.1.3 Differentiation of transduced scYDMs 125
3.2.2 Tritium based enzymatic assay for the determination of intracellular dNTP concentrations *127*
3.3 RESULTS 130
3.3.1 Successful differentiation of es cells and iPS cells into macrophages *130*
3.3.2 SAMHD1 is phosphorylated and highly expressed in esYDMs *135*

3.3.3 Vpx degrades SAMHD1 in esYDMs and ipsYDMs *138*
3.3.4 Quantification of dNTPs using the Tritiated (^{3}H) dNTP enzymatic assay (dNTP assay) *139*
3.3.5 SAMHD1 hydrolyses dNTPs in esYDMs and ipsYDMs *142*
3.3.6 SAMHD1 restricts HIV-1 in esYDMs and ipsYDMs *146*
3.3.7 SAMHD1 independent functions of Vpx in esYDMs and ipsYDM *148*
3.4 Discussion 154

CHAPTER 4: CRISPR- CAS9 GENE EDITING OF SAMHD1 165

4.1 Introduction 166
4.2 Methods and Materials 167
4.2.1 CRISPR Design Considerations *167*
4.2.2 High-Resolution Melt Analysis (HRM) primer design *168*
4.2.3 Vector cloning *170*
4.2.4 CRISPR- Cas9: Validations of gRNAs activity in HEK293T cells using T7 Endonuclease 1 ..... *170*
4.2.5 Electroporation of stem cells, selection, and expansion of potential SAMHD1 KO clones *172*
4.2.6 DNA Extraction for HRM *174*
4.2.7 Identification of SAMHD1 mutants using HRM *174*
4.2.8 DNA Extraction and Illumina SNP array *177*
4.3 Results 177
4.3.1 Genomic structure of SAMHD1 ..... *177*
4.3.2 Genotypic characterisation of SAMHD1 knockout EScs *178*
4.3.3 Macrophage differentiation of SAMHD1 knockout EScs *184*
4.3.4 Phenotypic characterisation of SAMHD1 knockout esYDMs *188*
4.4 Discussion 190

CHAPTER 5: VPX AND VPR ANTAGONISATION OF SAMHD1 195

5.1 Introduction 196
5.2 Methods and Materials 198
5.2.1 Immunoprecipitation & Mass Spectrometry Analysis *198*
5.2.2 Cloning for the production of SIVmac-Vpx, SIVmac-Vpr, and HIV-1 Vpr expressing plasmids *201*
5.3 Results 203
5.3.1 Modulation of dNTP concentrations and HIV-1 restriction by SAMHD1 RKP *203*
5.3.2 Probing the identity of SAMHD1 independent Vpx interacting partners *207*
5.3.3 SIVmac251 Vpr rescues HIV-1 infection in esYDMs in a SAMHD1 dependent manner *213*
5.3.4 HIV-1 Vpr rescues HIV-1 infection in esYDMs *217*
5.3.5 The dNTPase function of SAMHD1 is dispensable for restriction of HIV-1 in esYDMs *218*
5.3.6 Env effects on HIV-1 infection in esYDMs *219*
5.3.7 Vpx and Vpr mediated rescue from the innate immune response in esYDMs *221*
5.3.8 LPS assists HIV-1 infection in esYDMs *225*
5.4 Discussion 227

CHAPTER 6: DISCUSSION 239

6.1 Summary of Results 240
6.2 Implications and perspectives 247
6.2.1 Implications *247*
6.2.2 Perspectives *255*

CHAPTER 7: REFERENCES 257

7.1 Licences 258
7.1.1 Licence for Figure 1.2 "Phylogeny of lentiviruses". *258*
7.1.2 Licence for Figure 1.6 "Some Vpr Proteins Degrade SAMHD1" and Table 1.2 "Species-Specific SAMHD1 Degradation by Vpr and Vpx". *258*
7.2 Bibliography 258

List of Figures

Figure 1.1 Global prevalence of HIV among adults aged 15 to 49 in 2017 [20]. 32

Figure 1.2 Phylogeny of lentiviruses. 33

Figure 1.3 Primate lentiviral genomes. 39

Figure 1.4 Structure of Vpx and Vpr proteins. 44

Figure 1.5 Comparative models for Vpx and Vpr interaction with DCAF1. 45

Figure 1.6 Some Vpr Proteins Degrade SAMHD1. 48

Figure 1.7 Structure of SAMHD1. 58

Figure 1.8 Regulation of SAMHD1 catalytic activity by nucleotide concentrations. 59

Figure 1.9 The HIV and SIV lifecycle. 68

Figure 1.10 HIV and SIV Reverse transcription. 69

Figure 1.11 Macrophage heterogeneity in development, homeostasis, and disease. 73

Figure 1.12 Myeloid lineages in the mouse. 78

Figure 1.13 Macrophage polarisation continuum 82

Figure 2.1 Directed differentiation of embryonic stem cells. 102

Figure 3.1 Lentiviral vectors for constitutive expression of Vpx, VpxQ76A, and shRNA. 126

Figure 3.2 Tritium based enzymatic assay for the quantification of dNTPs (dNTP assay). 129

Figure 3.3 Embryoid body (EB), esYDMP and esYDM morphology. 132

Figure 3.4 Production timing of stem cell-derived factories. 134

Figure 3.5 SAMHD1 protein expression profile. 137

Figure 3.6 dNTP quantification by enzymatic incorporation of tritiated dNTPs. 140

Figure 3.7 dNTP concentrations in relation to Vpx and SAMHD1 in PMA treated THP-1 cells. 144

Figure 3.8 dNTP concentrations in relation to Vpx and SAMHD1 in esYDMs. 145

Figure 3.9 HIV-1 infection dynamics in relation to Vpx and SAMHD1. 152

Figure 3.10 Potential SAMHD1 independent Vpx functions. 153

Figure 3.11 Rescue of HIV-1 infection by VpxQ76A in esYDMPs. 154

Figure 4.1 CRISPR- Cas9 Primer and target RNA design. 169

Figure 4.2 Gel separation for the T7 Endonuclease I Assay. 171

Figure 4.3 Flow diagram of CRISPR- Cas9 gene editing protocol. 173

Figure 4.4 High resolution melt analysis (HRM). 176

Figure 4.5 HRM Melt curves. 179

Figure 4.6 Immunoblot of SAMHD1 in es cells. 181

Figure 4.7 SAMHD1 knockout (E2) via targeting of exon 4. 182

Figure 4.8 SAMHD1 dNTPase null mutant (G9) via targeting of exon 4. 183

Figure 4.9 SAMHD1 mutant via targeting of exon 5. 184

Figure 4.10 SAMHD1-KO esYDMPs are produced later than wild type esYDMPs. 185

Figure 4.11 SAMHD1 knockout esYDM maintains karyotype. 186

Figure 4.12 esYDM SAMHD1 mutant and esYDM WT markers are comparable. 188

Figure 4.13 Immunoblot of SAMHD1 in esYDMs. 189

Figure 4.14 dNTP levels in SAMHD1 KO cells. 189

Figure 5.1 Plasmid pEF1-IRES-Puro-SIN. 202

Figure 5.2 SIVmac251 Vpr incorporation into pEF1-IRES-Puro. 202

Figure 5.3 HIV-1 Vpr incorporation into pVpr (HIV-1) 203

Figure 5.4 HIV-1 infection and dNTP concentrations in SAMHD1-KO cells. 206

Figure 5.5 Potential novel Vpx interacting partners. 209

Figure 5.6 Vpr regulation of HIV-1 infection in esYDMs. 215

Figure 5.7 HIV-1 Vpr regulation of HIV-1 infection in esYDMs. 216

Figure 5.8 dNTPase independent mechanism for HIV-1 restriction encoded by SAMHD1 may be sensitive to env. 223

Figure 5.9 Vpx, Vpr, and $Vpr_{(HIV-1)}$ rescue HIV-1 infection from the antiviral state. 224

Figure 5.10 LPS regulation of HIV-1 infection in esYDMs. 226

List of Tables

Table 1.1 Primate Lentiviruses. 34

Table 1.2 Species-Specific SAMHD1 Degradation by Vpr and Vpx. 51

Table 1.3 The major genetic elements of HIV-1 and their role in lentiviral vectors. 71

Table 1.4 Comparison of monocyte and multi-lineage macrophage cell surface receptors. 81

Table 2.1 Antibodies for detection of surface CD4, CCR5, CD14, CXCR4, CD45, CD16 and CD11b. 110

Table 2.2 Antibodies used for western blotting. 111

Table 2.3 Sequences of primers. 111

Table 2.4 Sequences for the generation of shRNA. 111

Table 2.5 Plasmid DNA constructs used in this thesis. 112

Table 3.1 Reported dNTP concentrations for several cell types. 141

Table 3.2 Reported change in dNTPs for the addition of Vpx. 146

Table 3.3 Reported rescue of HIV-1 infection by Vpx. 148

Table 5.1 Mass Spectrometry. 212

List of Abbreviations

°C	Degrees Celsius
~	Approximately
<	Is less than
>	Is greater than
=	Is equal to
3’	3 prime
5’	5 prime
ΔU3	Truncated U3 region in the LTR
Ψ	“Psi” HIV-1 packaging RNA sequence
ADP	Adenosine diphosphate
AGS	Aicardi Goutières Syndrome
AIDS	Acquired Immune Deficiency Syndrome
APOBEC3A	Apolipoprotein B mRNA-editing, enzyme-catalytic, polypeptide-like 3A
APOBEC3G	Apolipoprotein B mRNA-editing, enzyme-catalytic, polypeptide-like 3G
AMP	Adenosine monophosphate
ATP	Adenosine Triphosphate
bp	Base pairs
CA	Capsid
cAMP	Cyclic adenosine monophosphate
Cas-	CRISPR-associated protein
cGAS	Cyclic GMP-AMP synthase

CCR-	Chemokine (C-C motif) Receptor-
CD	Cluster of Differentiation
CDK-	Cyclin dependent kinase
cDNA	Complementary Deoxyribonucleic Acid
CLR4	Cullin 4-RING E3 ligase
CMV	Cytomegalovirus
CNS	Central nervous system
CO_2	Carbon dioxide
COS-1	Cell Line from African green monkey kidney expressing SV40 T antigen
cPPT	Central polypurine tract
CRISPR	Clustered regularly interspaced short palindromic repeats
CSF	Colony stimulating factor
CSFR	Colony stimulating factor receptor
CtIP	CtBP-interacting protein
CtBP	C-terminal-binding protein
CTS	Central termination sequence
CXCR	C-X-C chemokine receptor
BMP4	Bone morphogenetic protein 4
Da	Daltons
dATP	Deoxyadenosine triphosphate
DAMP	Damage associated molecular patterns
DAPI	4',6-Diamidino-2-Phenylindole
DCAF1	DDB1-Cullin 4-Associated Factor 1
DDB1	Damage Specific DNA Binding Protein 1

dCTP	Deoxycytidine triphosphate
DC	Dendritic Cells
DC-SIGN	Dendritic Cell-Specific Intercellular adhesion molecule-3-Grabbing Non-integrin
dGTP	Deoxyguanosine triphosphate
DMEM	Dulbecco's modified Eagle's medium
DMSO	Dimethyl sulfoxide
DNA	Deoxyribonucleic Acid
DNase	Deoxyribonuclease
dNTP	Deoxynucleotide triphosphate
dNTPase	Deoxynucleotide triphosphate hydrolase
dTTP	Deoxythymidine triphosphate
EB	Embryoid Body
EDTA	Ethylenediaminetetraacetic Acid
EF1α	Elongation Factor-1 alpha
EGF	Epidermal growth factor
Env	Envelope
Esc	Embryonic stem cell (human)
esYDM	Embryonic stem cell origin yolk-sac-derived-like macrophage (human)
esYDMP	Embryonic stem cell origin yolk-sac-derived-like macrophage precursor (human)
FACS	Fluorescence-Activated Cell Sorting
FCS	Foetal Calf Serum
FITC	Fluorescein isothiocyanate
FL	Foetal liver

fmol	Fentomolar
FSC	Forward scatter
G2 phase	Gap 2 phase of mitotic interphase
g	Gravitational force
Gag	Group-specific antigen
GAPDH	Glyceraldehyde 3-Phosphate Dehydrogenase
GDP	Guanosine diphosphate
GFP	Green fluorescent protein
GM-CSF	Granulocyte Macrophage-colony Stimulating Factor
GMP	Guanosine monophosphate
GOI	Gene of Interest
GP	Glycoprotein
GPI	Glycophosphatidylinositol
GTP	Guanosine triphosphate
GTPase	GTP hydrolysing enzymes
H+	Hydrogen ion
HA	Haemagglutinin
HEK293	Human embryonic kidney 293 cell
HEK293T	HEK293 cells expressing SV40 T antigen
HeLa	Henrietta lacks cervical cancer cell line
hESC	Human Embryonic Stem Cell
HDR	Homology directed repair
HDAC	Histone deacetylase
HIV-1	Human Immunodeficiency Virus-1

HNH	Homing endonuclease
Hrs	Hours
HPV	Human papilloma virus
HR	Homologous recombination
HRP	Horseradish peroxidase
HSC	Haematopoietic stem cell
HSV	Herpes Simplex Virus
HTLV	Human T-lymphotropic virus
HUES	Human Embryonic Stem Cell line
IBD	Irritable bowel disorder
ICAM	Intracellular adhesion molecule
IFN-	Interferon-
IgG	Immunoglobulin G
IκBα	Nuclear factor of kappa light polypeptide gene enhancer in B-cells inhibitor, alpha
IN	Integrase
IL	Interleukin
IPMC	Intracellular plasma membrane-connected compartments
iPS	Induced pluripotent stem cell
IRES	Internal ribosome entry site
IRF	Interferon regulatory factor
ipsYDM	Induced pluripotent stem cell origin yolk-sac-derived-like Macrophage (human)
ipsYDMP	Induced pluripotent stem cell origin yolk-sac-derived-like Macrophage Precursor (human)

ISG	Interferon stimulated gene
JAK	Janus kinase
kbp	Kilobase pairs
K_d	Dissociation constant
kDa	Kilo Dalton
LINE	Long interspersed nuclear elements
LB	Lysogeny broth
LC	Langerhans Cells
LDS	Lithium Dodecyl Sulfate
Log	Logarithm to base 10
Log_2	Logarithm to base 2
LPS	Lipopolysaccharide
LTR	Long Terminal Repeat
LUC	A firefly luciferase reporter gene
LY-27632	L Rho-kinase inhibitor Y-27632
M13	M13 filamentous bacteriophage
MA	Matrix
mAb	Monoclonal antibody
M-CSF	Macrophage-Colony Stimulating Factor
MACS	Magnetic Activated Cell Sorting
MAL	Myelin and lymphocyte protein
MDM	Monocyte-Derived Macrophages
MDDC	Monocyte-Derived dendritic cell

mDC	Myeloid dendritic cell
MEF	Mitomycin C-inactivated mouse embryo fibroblasts
MFI	Mean Fluorescence Intensity
MHC	Major Histocompatibility Complex
Mins	Minutes
MRN	MRE11-RAD50-NBS1 (endonuclease)
mir	MicroRNA
µg	Microgram
mg	Milligram
µL	Microlitre
mL	Millilitre
MLV	Murine leukaemia virus
µM	Micromolar
mM	Millimolar
MOI	Multiplicity of Infection
mRNA	Messenger RNA
M-Sec	Tumor necrosis factor alpha-induced protein 2 (also called B94)
n	Number
Na+	Sodium ion
NADPH	Nicotinamide adenine dinucleotide phosphate-oxidase
NADH	Nicotinamide adenine dinucleotide
NBT	Nitro Blue Tetrazolium
NC	Nucleocapsid

NCBI	National Centre for Biotechnology Information
Nef	Negative factor
Neo	Neomycin
NFAT	Nuclear factor of activated T-cells
NFκB	Nuclear factor kappa-light-chain-enhancer of activated B cells
NHEJ	Non-homologous end joining
NIAID	National Institute of Allergy and Infectious Diseases
NIH	National Institute of Health
ng	Nanogram
nM	Nanomolar
NMD	Nonsense-mediated mRNA decay
NOS	Nitric oxide synthase
NK	Natural Killer
NLS	Nuclear Localization Signal
ns	Non Significant
p	plasmid
p-value	Probability value
pAb	Polyclonal Antibodies
PAM	Protospacer adjacent motif
PAMP	Pathogen associated molecular pattern
PBMC	Peripheral Blood Mononuclear Cell
PBS	Phosphate buffer saline
PBS-T	Phosphate buffer saline with Tween
PCR	Polymerase chain reaction

pDC	Plasmacytoid dendritic cell
PEI	Polyethylenimine
PES	Phenazine ethosulfate
PGK	Phosphoglycerate kinase
pH	Equal to $-\log_{10} c$, where c is the hydrogen ion concentration in moles per litre
PIC	Pre-integration complex
PIPES	Piperazine-N,N′-bis(2-ethanesulfonic acid)
PKC	Protein kinase C
pM	Picomolar
PMA	Phorbol 12-myristate 13-acetate
Pol	Polymerase
PolyA	Poly-adenylation
PPT	Polypurine tract
PR	Protease
PRR	Pattern recognition receptor
Puro	Puromycin
PuroR	Puromycin resistance
PVDF	Polyvinylidene fluoride
qPCR	Quantitative polymerase chain reaction
R	Repeat region in HIV-1 LTR
R5-tropic	CCR5-tropic
RCL	Replication competent lentivirus
Rev	Regulator of expression of virion proteins
RIPA	Radioimmunoprecipitation assay (Buffer)

RLR	RIG-I like receptors
RLU	Relative light units
RNA	Ribonucleic acid
RNase H	Ribonuclease H
ROS	Reactive Oxygen Species
RPMI	Roswell Park Memorial Institute
RRE	Rev Responsive Element
RT	Reverse Transcription or Reverse Transcriptase
RTC	Reverse Transcription Complex
RUCV	A common endonuclease domain
SAMHD1	Sterile alpha domain and HD domain-containing protein 1
SCC	Side scatter
SCF	Stem cell factor
Sec	Seconds
scYDM	Stem cell origin yolk-sac-derived-like Macrophage (human)
scYDMP	Stem cell origin yolk-sac-derived-like Macrophage Precursor (human)
SD	Standard Deviation
SDF	Stromal cell-derived factor
SDS	S*odium dodecyl sulfate*
SOC	Super Optimal broth with Catabolite repression
shRNA	Short hairpin RNA
SIN	Self-inactivating
siRNA	Short interfering RNA
SIV	Simian Immunodeficiency Virus

SOX	Sry-related HMG box
SP-1	Specificity protein 1
Src	Sarcoma
STAT	Signal transducers and activators of transcription
STING	Stimulator of interferon genes
SU	Surface glycoprotein
SupT1	T-cell lymphoblastic lymphoma cell line
SV40	Simian Virus 40
T4	T4 Bacteriophage
T7	T7 Bacteriophage
TALEN	Transcription activator-like effector nucleases
TAE	Tris base, acetic acid and EDTA
TAM	Tumor associated macrophage
TAR	Transactivation response region
TAT	Trans-activator of transcription
Taq	Polymerase from *Thermus aquaticus*
TCR	T-cell antigen receptor
TEAB	Triethylammonium bicarbonate buffer
TGF-	Transforming growth factor
TH-1	Type 1 helper T-cell
TH-2	Type 2 helper T- cell
THP-1	Human monocytic cell line derived from an acute monocytic leukemia patient
TLR	Toll-like receptors
TM	Transmembrane glycoprotein

TNF	Tumour necrosis factor
tRFP	Turbo RFP
Trio	Triple functional domain protein
Tris	Tris(hydroxymethyl)aminomethane
TZM-bl	HeLa cell line expressing high levels CD4 and CCR5
U/mL	Units per millilitre
U3	Untranslated 3’ region in the LTR
U5	Untranslated 5’ region in the LTR
U937	Human cell line isolated from a histiocytic lymphoma
UBC	Ubiquitin C
UNG-	Uracil DNA glycosylase
UV	Ultraviolet
v	Virus
V	Volts
VEGF	Vascular endothelial growth factor
VCC	Virus containing compartment
Vif	Viral infectivity factor
VS	Virological synapse
VLP	Virus Lentivector-like particles
VP16	Viral protein 16
Vpr	Viral protein R
VprBP	Vpr Binding Protein (also known as DCAF1)
Vpu	Viral protein U
Vpx	Viral protein x

VS	Virological synapse
VSV	Vesicular Stomatitis Virus
VSV-G	Vesicular Stomatitis Virus glycoprotein
WPRE	Woodchuck Posttranscriptional Regulatory Element
X4-tropic	CXCR4-tropic
ZFN	Zinc finger nuclease
ZFP	Zinc finger protein

Chapter 1

Chapter 1: Introduction

1.1 Primate Immunodeficiency Viruses

1.1.1 HIV and SIV origin

In North America, in 1981, an increasing number of individuals all of the same sexual demographic were admitted to hospital exhibiting symptoms consisting of the overgrowth of opportunistic infections concurrent with a functional decline of the adaptive immune system. The spectrum of conditions identified was collectively termed acquired immune deficiency syndrome (AIDS) and proved ultimately fatal. In 1983 the causative agent of AIDS was isolated and identified as a lentivirus of genus retrovirus, termed human immunodeficiency virus (HIV) [8-12].

HIV infects and replicates in cells of the immune system; primarily T-lymphocytes, monocytes, macrophages, and dendritic cells (DC). HIV is transmitted via bodily fluids such as blood, semen, vaginal secretions, breast milk, and cerebral spinal fluid. Thus, transmission mainly occurs as a result of sexual intercourse, reuse of infected intravenous equipment, or from mother to child during birth [13].

As of 2018, approximately 37.9 million people worldwide were infected with HIV-1, of which 1 million represent new infections; there were also 770,000 HIV associated deaths. Figure 1.1 shows global prevalence of HIV-1 in 2017 [14]. Recent advances in antiretroviral therapies mean that, for relatively rich countries at least, HIV infection is now a manageable disease with life expectancies comparable to those observed with non-infected individuals [15, 16]. These advances in therapeutics, combined with preventative measures such as antiretroviral prophylaxis [17], has seen global HIV-1 related deaths reduce by 51% since the peak in 2004 of 1.9 million. However, in regions where HIV infections are most prevalent, antiretroviral therapies can prove inaccessible due to, for example, financial constraints or cultural stigmatisation of those accessing treatments [18]. As such a curative strategy is still required to enable eradication of HIV worldwide.

HIV-1 has been categorised into four lineages or groups, M, N, O, and P [19]. HIV-1 group M is the most prevalent and is the causative agent of the current pandemic [20]. HIV-2, a closely related yet genetically distinct virus to HIV-1, was isolated in 1986 from a Cape Verdean patient [21] and similarly has been categorised, into nine groups: A-I [22, 23]. HIV-2 groups A and B are most prevalent [24], located primarily in West Africa, where HIV-2 is endemic [25]. HIV-2 is substantially less virulent than HIV-1, both in terms of infectivity and pathogenicity. Recent reports on HIV-2 prevalence are lacking. However, historical estimates suggest that approximately 1-2 million people were infected with HIV-2 circa 2010 [26].

Early investigations into the origins of HIV identified a closely related lentivirus infecting old world monkeys [27-30] and apes [31-34] inhabiting sub-Saharan Africa, collectively termed simian immunodeficiency virus (SIV). Approximately 37 species of sub-Saharan primates have been identified as natural hosts for SIV [35, 36]. SIV transmission predominantly appears to be intraspecific evidenced by monophyletic clade formation of distinct strains isolated from a single species [34, 35]. However, primate lentiviruses HIV and SIV form a distinct phylogenetic clade within genus Lentivirus, indicating interspecific transmission does occur and that the source of zoonosis is other primates [37]. Primate lentiviruses are listed in Table 1.1; relationships are depicted in (Figure 1.2).

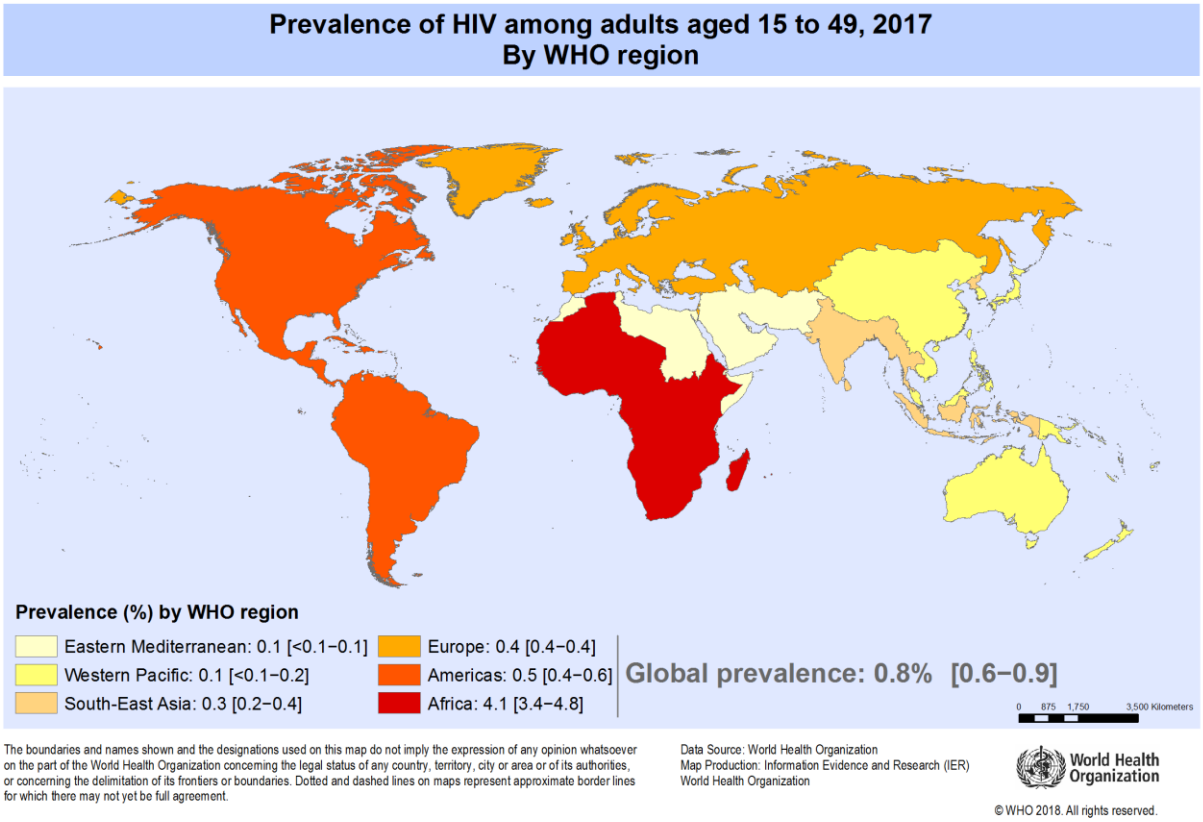


Figure 1.1 Global prevalence of HIV among adults aged 15 to 49 in 2017 [20].

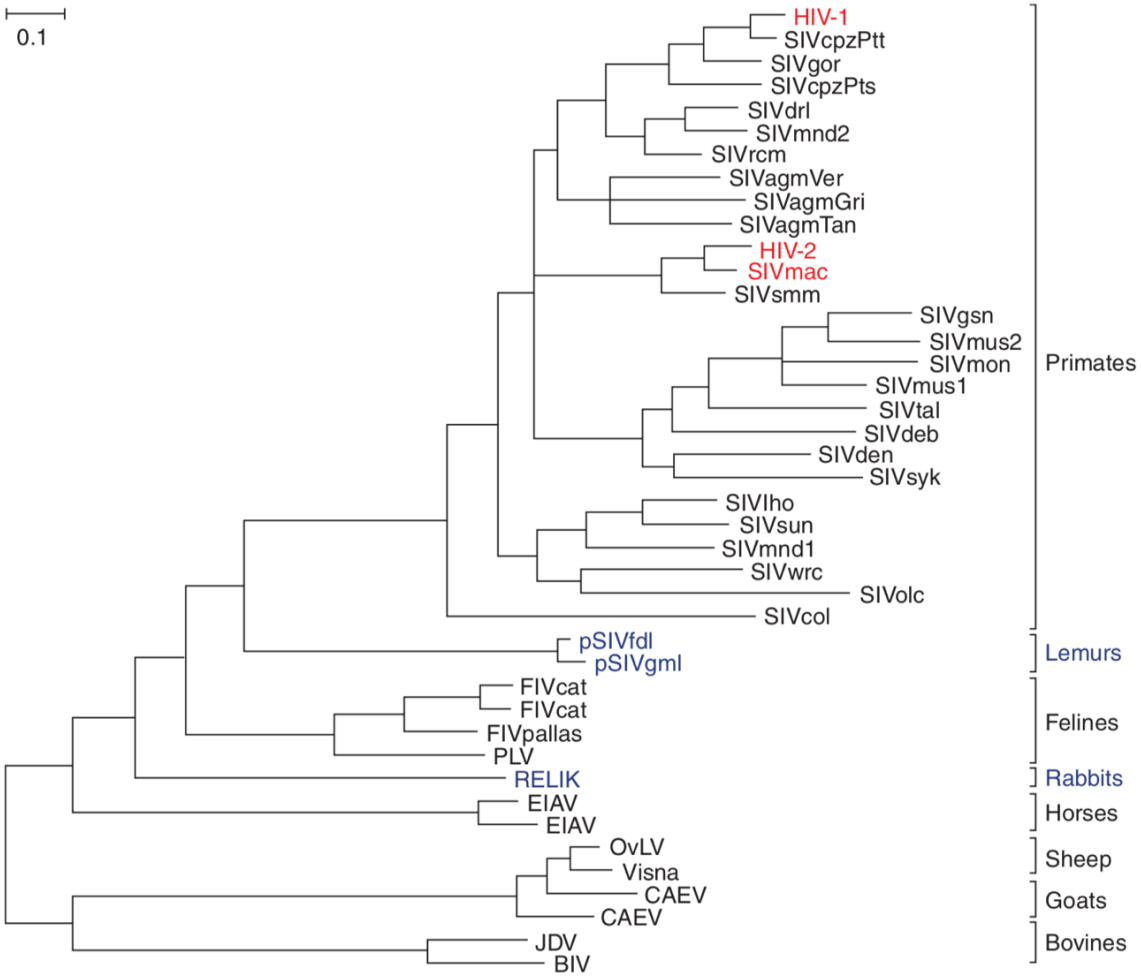


Figure 1.2 Phylogeny of lentiviruses.

Phylogeny of lentiviruses. The evolutionary relationships among *Pol* sequences (~770 amino acids) derived from various mammalian lentiviruses; host species are indicated at the right. Exogenous viruses are depicted in black, with HIV-1, HIV-2, and SIVmac highlighted in red; endogenous viruses are shown in purple. The phylogenetic tree was estimated using maximum likelihood methods (Guindon and Gascuel 2003). The scale bar represents 0.10 amino acid replacements per site. [Diagram and text reproduced with permission (refer to section 7.1.1)]

Lentivirus	Abbreviation	Species (English)	Species *(Latin)*
Human Immunodeficiency Virus 1	HIV-1	Human	*Homosapien*
Human Immunodeficiency Virus 2	HIV-2	Human	*Homosapien*
Simian Immunodeficiency Virus	SIVcpzPtt	Chimpanzee	*Pan troglodytes troglodytes*
Simian Immunodeficiency Virus	SIVcpzPts	Chimpanzee	*Pan troglodytes schweinfurthii*
Simian Immunodeficiency Virus	SIVmac	Rhesus Macaque	*Macaca Mulatta*
Simian Immunodeficiency Virus	SIVdrl	Drill	*Mandrillus leucophaeus*
Simian Immunodeficiency Virus	SIV/lho	L'hoest monkey	*Allochrocebus lhoesti*
Simian Immunodeficiency Virus	SIVmnd1-2	Mandrill	*Mandrillus sphinx*
Simian Immunodeficiency Virus	SIVmon	Campbell's mona monkey	*Cercopithecus mona*
Simian Immunodeficiency Virus	SIVrcm	Red-capped mangabey	*Cercocebus torquatus*
Simian Immunodeficiency Virus	SIVsun	Sun-tailed monkey	*Allochrocebus solatus*
Simian Immunodeficiency Virus	SIVsyk	Sykes' monkey	*Cercopithecus albogularis*
Simian Immunodeficiency Virus	SIVagm (SIVagm.tan)	Tantalus (African green) Monkey	*Chlorocebus tantalus*
Simian Immunodeficiency Virus	SIVagm (SIVagm.ver)	Vervet (African green) Monkey	*Chlorocebus pygerythrus*

Table 1.1 Primate Lentiviruses.

Lentivirus	Abbreviation	Species (English)	Species *(Latin)*
Simian Immunodeficiency Virus	SIVsm/smm	Sooty Mangabeys	*Cercocebus torquantus atys*
Simian Immunodeficiency Virus	SIVmus1-2	Mustached monkeys	*Saguinus imperator*
Simian Immunodeficiency Virus	SIVgsn	Greater spot-nosed monkey	*Cercopithecus nictitans*
Simian Immunodeficiency Virus	SIVden	Dent's mona monkey	*Cercopithecus denti*
Simian Immunodeficiency Virus	SIVcol	Eastern black-and-white colobus	*Colobus guereza*
Simian Immunodeficiency Virus	SIVdeb	De Brazza's monkey	*Cercopithecus neglectus*
Simian Immunodeficiency Virus	SIVwrc	Western red colobus	*Piliocolobus badius*
Simian Immunodeficiency Virus	SIVolc	Olive colobus monkey	*Procolobus verus*
Simian Immunodeficiency Virus	SIVgor	Gorilla	*Gorilla gorilla*

Table 1.1 Primate Lentiviruses – continued

Extensive sampling and phylogenetic analysis of SIV infecting captive and wild primates identified an SIV infecting the chimpanzee subspecies *Pan troglodytes troglodytes* (SIVcpz) as the immediate precursor to HIV-1 group M and N viruses [38]. The zoonosis of HIV-1 group M and N viruses were separate events theorised to have originated in a region bordering the Ngoko, Boumba, and Sangha rivers in the southeast corner of Cameroon [39] at the beginning of the 20th century, circa 1925 [40]. In this location, chimpanzees harbouring SIV most closely related to HIV-1 group M and N strains can be found [39]. HIV-1 group O and P viruses, also the products of separate zoonotic events, phylogenetically cluster closer with SIV infecting West African gorillas (SIVgor; *Gorilla gorilla gorilla*) than with SIV infecting chimpanzees which are suggestive of human-gorilla zoonosis, also originating in Cameroon [19, 34]. HIV-1 groups exhibit very different prevalence: while group M viruses are pandemic, group N viruses

have been identified in 16 individuals, two of which as recently as 2017 [41, 42], group O virus infections are estimated at 100,000 [43], and group P viruses have been identified in only two cases [19, 43].

The immediate precursor to HIV-2 is an SIV that naturally infects the sooty mangabey (SIVsm; *Cercocebus torquantus atys)*, an old-world monkey that is native to West Africa [29, 44]. The nine HIV-2 groups represent multiple zoonotic events evidenced by phylogenetic group interspersion among SIVsm lineages [22, 23], all of which appear to have originated in West Africa. Groups A and B are endemic in West Africa but can also be found at low prevalence in France, Portugal, India, Mozambique, French Guiana, Myanmar, and the US [26]. Theorised zoonosis dates for groups A and B are estimated at 1940 $\pm$ 16 years and 1945 $\pm$ 14 years, respectively [45]. Groups C-I represent separate transmission events in single individuals, except group F for which two distinct zoonotic events have been identified [22, 46-48]. The inability of group C-I viruses to spread beyond an individual host is most likely due to inadequate interspecies viral adaptation and thus represent 'dead-end' infections.

Primates are hunted in Africa for consumption, and thus one possible mode of primate to human virus transmission is exposure to bodily fluids during the butchering and preparation of monkeys and apes (bushmeat) for consumption. Indeed, in a study analysing bushmeat in Sierra Leone, 58% of samples tested positive for SIV [49]. Soft contact with baby monkeys which are often kept as pets, or bites and scratches from tame adults, may also represent transmission routes [48]. However, despite massive exposure to SIV in markets and to a lesser extent in the domestic environment, the prevalence of non-HIV-1 group M strains in West Africa is notably low [26], and in some regions, in decline [50]. Primate to human transmission of SIV is relatively rare in West Africa [51] as evidenced by i) HIV-1 group N, O and P, and HIV-2 groups C-I, successful zoonotic events primarily resulting in poor transmissibility (e.g. group HIV-1 group N) or no transmissibility at all (e.g. HIV-1 group p, HIV-2 groups C-I) i.e. 'dead-end' infections, and ii) lack of regular novel strain identification [41].

Taken together, this evidence appears to question whether zoonosis in isolation was sufficient to produce epidemic HIV-2 and pandemic HIV-1.

Estimates for the emergence of epidemic HIV coincides with colonial expansion in West Africa, a significant geopolitical and cultural change that may have provided the conditions necessary to enhance the viral fitness of an otherwise dead-end SIV-HIV zoonosis. Colonial expansion was associated with the destruction of small rural settlements, the construction of dense urban populations, and the physical abuse of the native populations - including mutilation, amputation, and rape. Colonial expansion also was responsible for the introduction and expansion of medical infrastructure, exposing individuals to reused syringes, invasive surgery using inadequately sterilised equipment [52], and blood transfusions unscreened for infectious elements [53].

Indeed it has been proposed that the colonial associated risk factors detailed above, in particular, the reuse of syringes in intravenous injections between 1950 and 1970 in Cameroon, may have provided the means for serial passage of an otherwise unfit and 'dead-end' HIV, enabling the acquisition of the necessary mutations to become pandemic [54]. Currently, in this region, economic stability, increasing public awareness, and a reduction in risk factor associated behaviours effectively negate the 'cultural catalyst' that is evidently required to produce novel HIV strains with sufficient virulence to become pandemic [55]. Nevertheless, given the long incubation period prior to AIDS manifestation, it may still be prudent to monitor for novel zoonotic events to ensure early detection should a more virulent HIV strain than HIV-1 group M, emerge.

1.1.2 HIV and SIV genome

HIV and SIV are of the family retroviridae and the genus lentivirus. A fundamental and unique feature of retroviruses is the transcription of the viral RNA genome into DNA using the virally encoded reverse transcriptase (RT) enzyme and insertion of this DNA copy into the host genome using the viral integrase (IN) enzyme. All retroviruses require cell division in order to enter the nucleus prior to integration

except lentiviruses, which can traverse the nuclear envelope of non-dividing cells. Retroviral genes are encoded on two, dimerised strands of positive-sense RNA. The lentiviral proviral DNA genome is comprised of 9-10 kilobase pairs, which translate into 15 proteins encoded by nine genes (8 genes and 14 proteins for some SIV strains) flanked by long terminal repeat sequences at both ends [56] (Figure 1.3). The long terminal repeat (LTR) is a grouping of three discrete units, untranslated region-3' (U3), Repeat region (R), and untranslated region -5' (U5) which are critical for viral gene expression, integration and therefore replication. Since the site of transcription initiation corresponds to the first base of the R (repeats) region, the viral RNA genomic sequence is not identical to the proviral DNA. The proviral DNA sequence reads U3-R-U5-genes-U3-R-U5, whereas the RNA genomic structure reads R-U5-genes-U3-R. This is because in genomic RNA, while the U3 and part of the R region are retained at the 3'-LTR, the U5 and R region is contained at the 5'-LTR.

The LTR encodes signals for transcription, RNA capping, and polyadenylation. Specifically, in the U3 region of the 5'-LTR are located enhancer, basal and distal promoter elements that drive transcription of proviral DNA by the cellular machinery. Additionally, the tat-activating region within the R region is important for tat-regulated transcription.

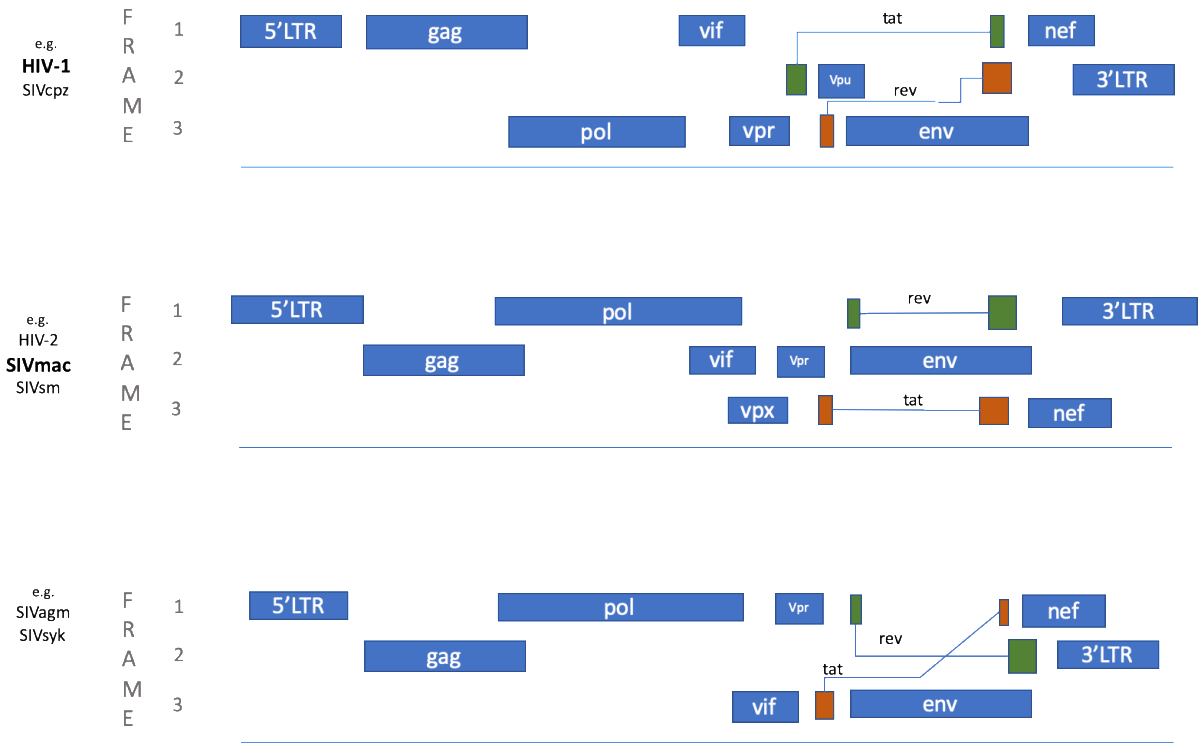


Figure 1.3 Primate lentiviral genomes.

1.1.3 HIV and SIV core proteins

1.1.3.1 Regulatory proteins

Rev and Tat are regulatory proteins 21kDa and 15kDa in size, respectively. Rev is required for the export of unspliced and singly spliced RNA from the nucleus [57]. This is accomplished via interaction with a sequence in the viral env region, the Rev Response Element (RRE), as well as cellular karyopherins such as importin-α1. Interaction of Rev with the RRE also neutralises the effects of instability elements in the lentiviral genome that would otherwise lead to the degradation of single and unspliced viral RNA. Doubly spliced mRNA usurps the cellular machinery to facilitate its export from the nucleus and, therefore, does not require Rev. Consequently, Rev is encoded on doubly spliced mRNA allowing its early translation [58]. Tat functions in transactivation during transcriptional elongation of viral RNA and is therefore critical for viral replication [59]. During transcription, Tat binds to the transactivating

response element (TAR) at the 5' end of viral RNA as well as several cellular factors that facilitate the function of Tat, including NFkB, cyclin-dependent kinase 9 (CDK9), and cyclin T1 [59, 60].

1.1.3.2 Structural proteins

For both HIV and SIV, expression of the gag and pol genes results in the polyprotein precursors p55 Gag and p160 Gagpol. Processing of p55 Gag creates matrix (MA, p17), implicated in several processes including cytoskeletal-mediated transport and viral entry/uncoating [61]; capsid (CA, p24), which forms the viral core; the viral RNA binding protein nucleocapsid (NC, p9); and p6 proteins which is vital for final fission and release of progeny virions and also contains packaging signals for the accessory proteins Vpr and Vpx. [62]. Processing of p160 Gag-pol produces all the proteins detailed above for p55 Gag processing as well as RT [63], viral IN, and a viral protease (PR)[64]. As previously described, RT is responsible for the generation of proviral DNA using the viral RNA genome as a template. IN cleaves the host genome and inserts the proviral DNA. Finally, the viral PR processes polyproteins within progeny virions, facilitating maturation. Envelope glycoproteins (env) are encoded by the env gene from which the 160kDa polyprotein is translated. Processing of this precursor polyprotein by cellular proteases creates a non-covalent complex of two glycosylated proteins: an external glycoprotein (gp120), and a transmembrane glycoprotein (gp41) which exist as gp120-gp41 trimers, located on the cell surface. Gp120 and gp41 recognise the cell surface molecules CD4 and chemokine receptors CCR5 and CXCR4, respectively mediating virus particle fusion and entry into cells (see Section 1.1.6 HIV and SIV life cycle).

1.1.4 HIV and SIV Accessory proteins

Accessory proteins alter the microenvironment to facilitate optimal replication. Accessory proteins are dispensable for viral infection and replication *in vitro* but critically required for sustained infection and pathogenesis *in vivo*.

1.1.4.1 Nef, Vif and Vpu

All HIV and SIV viruses encode Nef (Negative effector protein). Nef is a 27kD myristoylated protein that facilitates viral replication by multiple mechanisms, including cytoskeletal remodelling, signal transduction, and vesicular transport. Nef has been shown to modulate the expression of several molecules important to the lentiviral life cycle including CD4, the T-cell antigen receptor (TCR) and the major histocompatibility complex I (MHC-I). Nef is one of the earliest proteins translated from de novo proviral integration, is primarily cytoplasmic, and associated with plasma membranes. Nef also enhances virion penetration of cells by antagonisation of the host transmembrane protein SERINC5 [65]. Additionally, Nef enhances viral infectivity and growth and has been shown to contribute to the maintenance of high viral loads in primate models of SIV pathogenesis in old world monkeys [66, 67].

Vpu (Viral protein U) is a 16kD type I integral membrane protein that functions in the downmodulation of the CD4 molecule and antagonisation of the interferon (IFN) inducible restriction factor, Tetherin [68-70] (see section 1.1.5.3 Tetherin). Both functions serve to facilitate and enhance the egress of progeny virions from infected cells. HIV-1, SIVcpz, SIVgsn, SIVmus, SIVmon, and SIVden all encode Vpu. Vpu is not encoded by HIV-2, SIVsm lineage, or other SIVs, nor do these viruses encode a discernible homologue.

All primate lentiviruses encode Vif (Viral infectivity factor). Vif is an approximately 23kD protein that facilitates the production of infectious progeny by antagonisation of the cellular cytodine deaminase APOBEC3G [71, 72], in a cell type-dependent manner (see Section 1.1.5.1 APOBEC3G).

1.1.4.2 Vpr

Viral protein r (Vpr) is a small 15kD phosphorylated regulatory protein [73] encoded by all extant primate lentiviruses [74]. *In vitro,* Vpr is dispensable for replication in lymphocytes [75, 76] yet critically required for replication in primary monocytes [77] and monocyte-derived macrophages (MDM) [75, 76, 78, 79]. Vpr also appears to carry clinical significance and importance *in vivo* [80-82]. Vpr is packaged into viral

particles via interaction with p6 of the p55 Gag polyprotein [83-86] and influences early steps in the viral life cycle. Functions attributed to Vpr include initiation of G2/M cell cycle arrest [87-91], proviral genome fidelity stabilisation [92], rescue of infection in primary monocytes and MDMs [78, 93-95], and host restriction factor antagonisation in myeloid cells and lymphocytes [96].

Data derived from a combination of NMR and protein crystallization studies show that the central region of Vpr consists of a three α-helix bundle spanning residues 17–33, 38–50 and 55–77 flanked by flexible C and N terminal domains [97, 98] (Figure 1.4). Notable regions important for protein interactions are the α-helix 3 c-terminal region, the connecting loop of α-helix 1 and α-helix 2; a hydrophobic cleft structure comprising α-helix 1, α-helix 2 and the first turn of α-helix 3; and N-terminal coiled tail [98]. Vpr multimerization has been documented in several studies and appears to be dependent on α-helix 3 [99, 100]. Moreover, Vpr's α-helix 3 is the binding site for the DCAF1-DDB1-Cullin 4-RING E3 ubiquitin ligase (DCAF1-CLR4) complex, a cellular effector involved in degradation and ubiquitination [101] which appears central to several Vpr functions (see below).

In the early 1990s, Vpr was shown to interact with a cellular protein of approximately 180kDa, initially named VpR Interacting Protein (RIP) [102], which was later renamed to Vpr binding protein (VprBP) [103]. VprBP was subsequently identified as a substrate for the Cullin 4-RING E3 ligase (CRL4) and hence renamed DDB1-Cullin 4-Associated Factor 1 (DCAF1) [104]. Vpr binds to the DCAF1-CLR4 complex via interaction of α-helix 3 with a large cleft in the DCAF1 domain where residues R73, Q65, and R62 on α-helix 3 of Vpr form hydrogen bonds with T1138, S1136 and E1088 of DCAF1, respectively [98]. The N-terminal domain of Vpr also interacts with DCAF1 [98] (Figure 1.5). Interaction between Vpr and the DCAF1-CLR4 complex has been shown to be a requirement for Vpr-driven G2/M arrest in cycling CD4+ T-cells, a function highly conserved across primate lentiviruses [105, 106]. The mechanism appears to depend on Vpr-mediated premature activation of the SLX4-bound MUS81-EME1 complex, and the subsequent (and perhaps paradoxical) degradation of the SLX4-bound MUS81-EME1 complex by

association with CLR4-DCAF1, also mediated by Vpr protein [90, 107]. MUS81-EME1 is a structure-specific endonuclease that is regulated by SLX4, active in the resolution of DNA branched or multi-stranded structures which are intermediates of DNA replication and repair. Premature activation of the SLX4-bound MUS81-EME1 complex prior to G2/M translation is believed to result in replication stresses which trigger DNA damage responses and G2/M arrest [90, 107, 108].

Vpr has been shown to co-localise with viral DNA during reverse transcription and remains associated for over 10 hrs [109]. Interestingly, the SLX4-bound MUS81-EME1 complex has also been shown to localise with and degrade HIV-1 cDNA during reverse transcription in a manner dependent on Vpr [90]. Knockdown of the SLX4 complex results in an accumulation of HIV-1 cDNA, and HIV-1 infection in the absence of Vpr has been shown to result in increased production of IFNα and IFNβ, possibly due to sensing of the HIV-1 cDNA [90]. Thus, prior to Vpr induced reduction of SLX4-bound MUS81-EME1 complex levels, Vpr mediated activation of the MUS81-EME1 endonuclease and subsequent degradation of viral cDNA may aid viral replication by facilitating evasion of innate immune sensing [90]. However, persistent degradation of viral cDNA may be detrimental to viral replication, which may explain the otherwise counterintuitive Vpr-DCAF1-CLR4 mediated degradation of the SLX4-bound MUS81-EME1 complex. Furthermore, Vpr has also been shown to play a role in transcription of genes from unintegrated viral cDNA (e.g., 1-Long Terminal Repeat circles (1-LTR) and 2-Long Terminal Repeat Circles (2-LTR)) [110], a mechanism with peak efficiency likely prior to SLX4-bound MUS81-EME1 complex activation or after DCAF1-CLR4-mediated SLX4-bound MUS81-EME1 complex depletion.

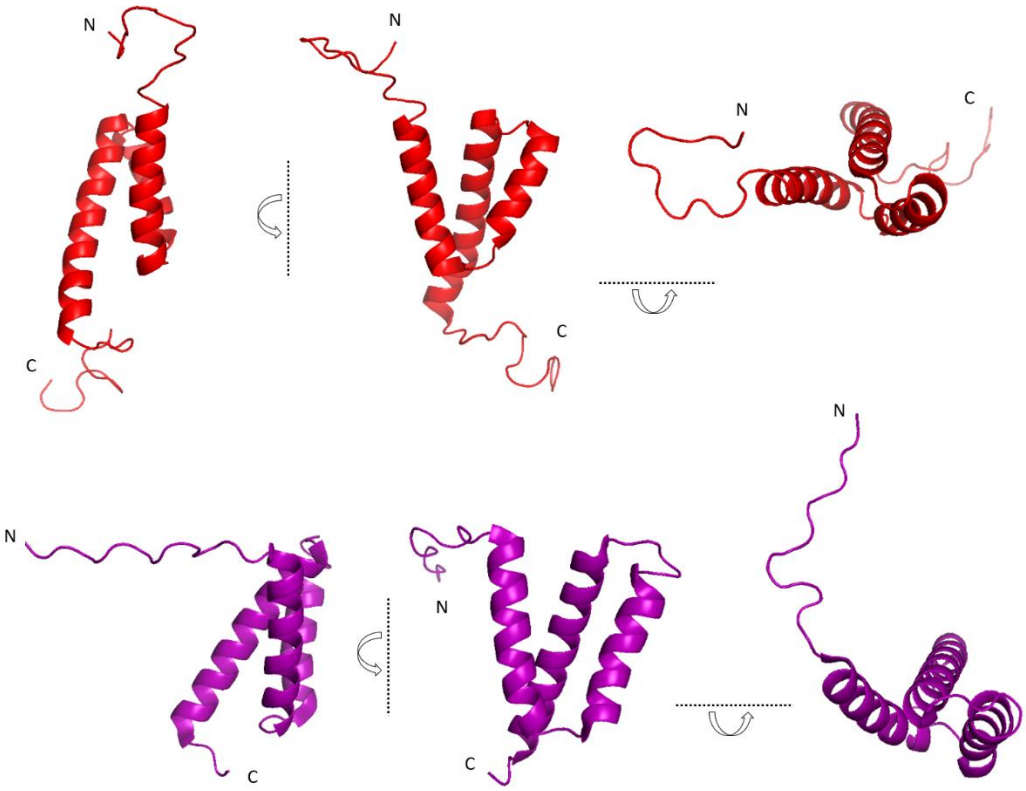


Figure 1.4 Structure of Vpx and Vpr proteins.

The structure of Vpr (red) and Vpx (purple) proteins are similar: both are comprised of an anti-parallel bundle of three alpha-helices. The Vpx protein is that encoded by SIVmnd-2 (from madrills) as depicted in the crystal structure of Vpx bound to mandrill SAMHD1 (amino acid residues 1-114) and human DCAF1 (amino acid residues 1058-1396) (SAMHD1 and DCAF1 not shown) [111] PD:5AJA. The Vpr protein is that encoded by HIV-1 [97] PD:1M8L. 'N' denoted N-terminal, 'C' denotes C-terminal. Cartoons generated using Pymol ™ 2.4.0 – Incentive Product.

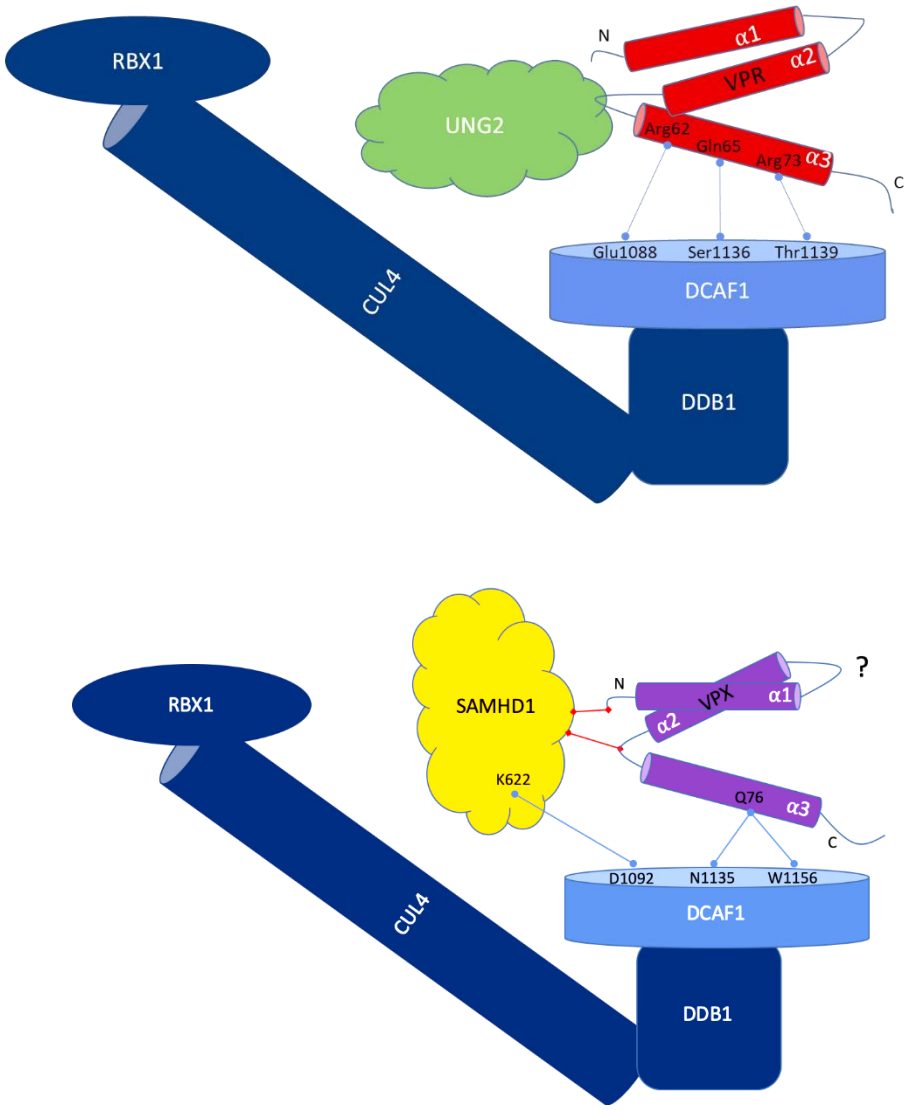


Figure 1.5 Comparative models for Vpx and Vpr interaction with DCAF1.

A schematic model showing Vpr (of HIV-1) and Vpx (of SIVsm) interaction with the DCAF1 sub-unit of the DCAF1-CLR4 ubiquitin ligase complex. Both Vpr and Vpx bind to DCAF1 via interaction with their third α-helix however the interacting residues differ: residues R62, Q65 and R73 on Vpr interact with residues E1088, S1136 and T1139 on DCAF1 respectively [98], whereas residue Q76 on Vpx interacts with residues N1135 and W1156 on DCAF1 [112]. The residues on DCAF1 used by Vpr and Vpx overlap prohibiting both binding to DCAF1 simultaneously. Vpr and Vpx use similar regions for binding known cellular substrates. Vpr binds UNG2 via the connecting loop region between α-helix 2 and α-helix 3 which functions in DNA molecular mimicry [98]. Vpx binds SAMHD1 via multiple residues in the unstructured N-terminus as well as residues of the connecting loop of α-helix 2 and α-helix 3 [112]. SAMHD1 residue K622 also interacts with DCAF1 at residue D1092 which is critically required for degradation of SAMHD1[112]. Binding partners for the connecting loop region between α-helix 1 and α-helix 2 for Vpx and Vpr remain to be identified. Adapted from [104]. DCAF1 - DDB1 & CUL4A-associated factor 1, CUL4A - cullin4A, RBX1 - RING H2 finger protein 1, and DDB1 - DNA damage–binding protein 1.

Similar to that described above for the SLX4-bound MUS81-EME1 complex, the host restriction factor SAMHD1 (see Section 1.1.5.4 SAMHD1) has also been shown to localise with HIV-1 DNA and hinder reverse transcription in a manner that may involve degradation of viral cDNA [113-116]. Vpr proteins of the SIVdeb, SIVmus, and SIVagm lineages (Figure 1.6) target SAMHD1 for DCAF1-CLR4 complex mediated degradation, in a cell type dependent and species-specific manner [96]. The perturbation of SAMHD1 has similarly been linked to the accumulation of viral cDNA and the production of type 1 IFNs [113, 117]. This mechanism of SAMHD1 antagonisation is not encoded by Vpr proteins of HIV-1 and related SIV lineages, nor has it been shown to be encoded by Vpr proteins of HIV-2 and related SIV lineages, which antagonise SAMHD1 via Vpx protein (see Section 1.1.4.3 Vpx). Components of HIV-1, however, have been implicated in SAMHD1 antagonisation as an indirect consequence of [DCAF1-CLR4]-[SLX4-MUS81-EME1] driven cell cycle manipulation, functions which, as previously discussed are also attributed to HIV-1 Vpr [118].

Vpr has also been shown to directly enhance the fidelity of reverse transcription products by interaction with uracil DNA glycosylase (UNG2), a nucleic acid repair enzyme that removes the RNA base uracil from DNA [119, 120]. Vpr facilitates the incorporation of UNG2 into virions and consequently limits the detrimental accumulation of uracil in proviral DNA, exerting a positive effect on viral replication. Vpr-induced UNG2-mediated enhancement of proviral fidelity has been directly linked to increased HIV-1 replication kinetics in MDMs and to a lesser extent in cycling CD4+T-cells [92]. More recently, however, the crystallization of HIV-1 Vpr-UNG2 in complex with the DCAF1-CLR4 complex presented compelling evidence for HIV-1 Vpr mediated antagonisation of UNG2, not only via E3 ligase driven proteasomal degradation but also by direct inactivity of the UNG2 active enzymatic site by interaction with HIV-1 Vpr [98]. Vpr-UNG2 interactions are dependent on the connecting loop of α-helix 2 and α-helix 3 and the 'molecular mimicry' of DNA [98]. Vpr antagonisation of UNG2 is a property well conserved in HIV-1 and SIVcpz lineages [98] and implies that UNG2 exerts a negative effect on viral replication (hence requiring Vpr mediated degradation) in contrast to the evidence detailed above. It is also possible that, as per

the duplicitous interaction of the SLX4-bound MUS81-EME1 complex on HIV-1 replication detailed above, both phenomena are true - and that UNG2 initially exerts a positive effect on viral replication but then exerts a negative effect later in the viral life cycle.

Vpr protein has been implicated as a component of the reverse transcription complex (RTC) [121], and may also function to mediate the nuclear import of the PIC [122-124]. Vpr localises to the perinuclear space independent of soluble assistance and is imported into the nucleus by means of a bona fide NLS located between residues 17 and 74 that interacts with importin-α [125]. Vpr mediated nuclear import of the PIC has been shown to be critically required in non-dividing cells [126].

Vpr initiates apoptosis in multiple cell types; however, several studies have presented evidence for additional antiapoptotic roles. The determining pro or anti apoptotic functions appear to depend on intracellular concentrations of Vpr, stage of HIV-1 infection, and the type of cell [127-131].

Several studies have proposed a role for Vpr in the activation of latent infection. Early reports showed that serum associated HIV-1 Vpr was functional in the reactivation of latent provirus in PBMCs isolated from HIV-1 infected individuals as well as several cell lines of lymphocyte and myeloid origin [132, 133]. In macrophages, the underlying mechanism is believed to involve transactivation of the LTR via depletion of histone deacetylase (HDAC) 1. Vpr proteins of SIVagm and SIVmnd1 lineages have also been shown to activate latent virus in human lymphocytic cell lines, however, the mechanism here involves the downregulation of a human silencing hub (HUSH) complex in a manner dependent on the DCAF1-CLR4 complex [134]. Interestingly, this function and mechanism are also encoded by Vpx proteins, among which it is highly conserved [134].

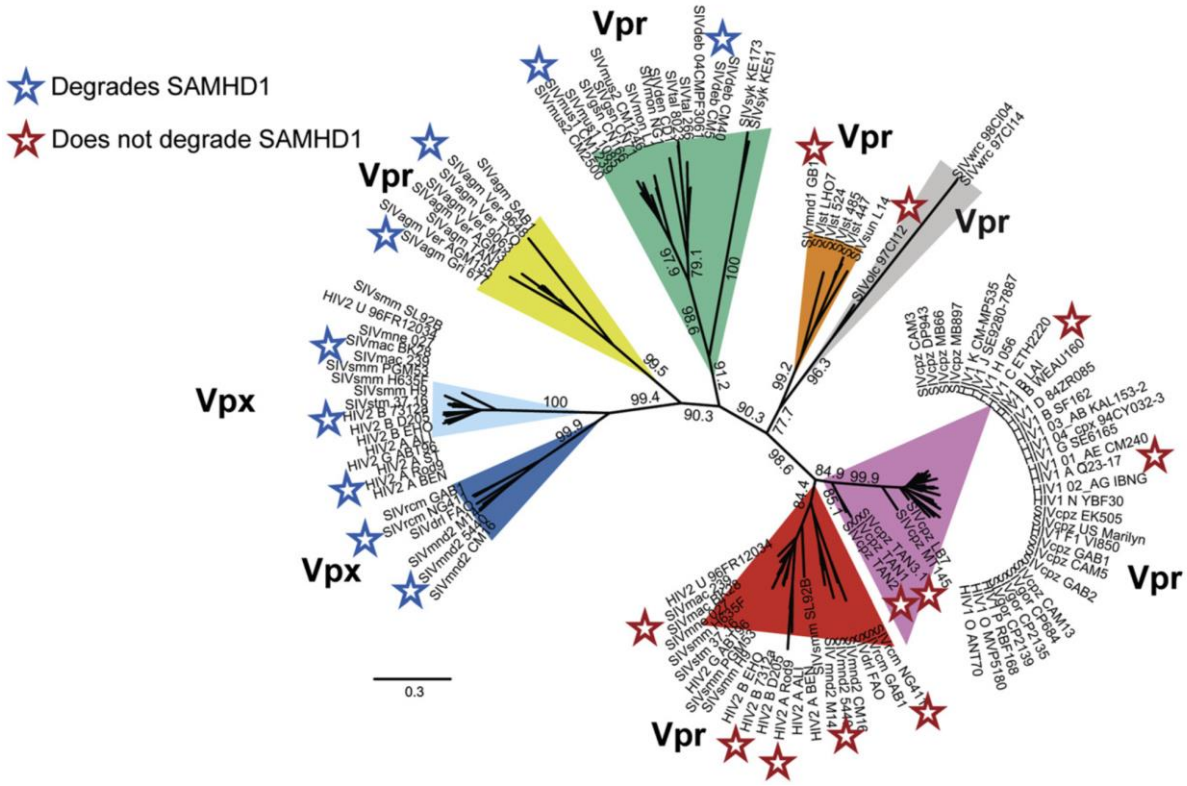


Figure 1.6 Some Vpr Proteins Degrade SAMHD1.

Unrooted phylogeny of 115 Vpr and Vpx sequences among diverse primate lentiviruses. Bootstrap values indicate maximum likelihood proportions that are highly supported by Bayesian inference. Seven phylogenetic clusters are shaded in colors (cutoff at ML bootstrap >75, Bayesian posterior probability >0.87). Vpx sequences form two clades (shaded in light blue and dark blue) that have strong support of monophyly from all other Vpr sequences. Functional phenotypes of Vpr and Vpx that degrade SAMHD1 (Blue stars) or do not degrade SAMHD1 (Red stars) are overlaid on the phylogeny. [Diagram and text reproduced with permission (refer to section 7.1.2) [96]]

1.1.4.3 Vpx

The Vpx gene is a homolog of the Vpr gene and codes for a 12-16kDa accessory protein [135]. Unlike Vpr, which is encoded by all extant primate lentiviruses, Vpx is encoded only by lentiviruses of the SIVsm/SIVmac/HIV-2 lineage and SIVrcm/SIVmnd2 lineage [136] (Figure 1.6). Vpx is present in mature virions and is packaged via interaction of residues 73 to 89 with residues 15 to 40 of Gag p6 [137]. Consequently, Vpx and Gag are present in mature virions in approximately equal quantities [138]. On entry into the cytoplasm, Vpx has been shown to localise to the nucleus by virtue of two non-canonical nuclear localization signals, spanning residues 65 to 72 at the C-terminus and 20 to 40 at the N-terminus

[139-141]. Vpx exhibits a strong cell type dependence and is dispensable *in vitro* for SIV replication in several lymphocytic and monocytic cell lines but is critically required in primary myeloid cells and resting primary lymphocytes [142].

Like Vpr, Vpx is composed of a three α-helix bundle flanked by flexible C and N terminal domains (Figure 1.4). Notable regions important for protein interactions are α-helix 3, the N-terminal region, and the connecting loop of α-helix 2 and α-helix 3 [111, 112]. Evidence for Vpx multimerization has also been documented, and again like Vpr, a key function of Vpx is determined by its interaction with the DCAF1-CLR4 complex, which is also mediated by the α-helix 3 region of Vpx (see below).

Investigations probing the usefulness of Vpx in the enhancement of lentivector transduction in MDDCs revealed that exogenous application of Vpx encoded by SIVmac resulted in the rescue of HIV-1 lentivector replication in human MDMs, MDDCs but not stimulated CD4+ T-cells [143-146]. The lentiviral species independence of Vpx functions in this observation implied that Vpx altered the cellular environment to facilitate viral replication. Vpx rescue of infection was consistently accompanied by accumulation of viral DNA. This implied that the potential Vpx-mediated modification of the microenvironment could involve the removal of a block to nuclear import (and hence integration) of viral genetic material. An investigation to identify this block neutralised by Vpx identified SAMHD1 by immunoprecipitation of HA-tagged Vpx in HEK293T cells [2, 3]. SAMHD1 is a deoxynucleotide triphosphate hydrolase (dNTPase) that inhibits successful completion of viral reverse transcription resulting in an accumulation of viral DNA and termination of infection [2] (see Section 1.1.5.4 SAMHD1). Vpx targets SAMHD1 for degradation by, like Vpr, usurping the degradative capacity of the DCAF1-CLR4 complex [147-149]. The binding of Vpx to DCAF1 induces a new adaptive molecular surface on DCAF1 which allows binding of the C-terminal domain of SAMHD1. SAMHD1 reside K622, and DCAF1 residue D1092 have been shown to be important in this regard [111, 112]. The Vpx-DCAF1-SAMHD1 interaction

renders SAMHD1 recognisable by the CLR4 ubiquitin ligase as a substrate, which marks SAMHD1 for proteasomal degradation [104, 150-152].

Although the DCAF1-binding motif of Vpx and Vpr is very similar, the two proteins interact via different residues with DCAF1. Vpx has been shown to interact via residue Q76 with residues N1135 and W1156 on DCAF1 (Figure 1.5), whereas Vpr residues engaged are E1088, S1136, and T1139 [98] (Figure 1.5)). Residue Q76 is crucial for functional binding, and indeed proximal mutations abolish binding of Vpx to DCAF1 [2, 104, 147, 148]. Interestingly, the DCAF1 residues used by Vpx and Vpr are overlapping, which implies that Vpx and Vpr would interact with DCAF1 in a competitive manner. Amino acids located in the N-terminal region of Vpx have also been shown to be vital for the rescue of HIV infection in myeloid cells [150, 153, 154].

Vpx-mediated degradation of SAMHD1 is dependent on nuclear localization of SAMHD1, with Vpx reportedly unable to antagonise SAMHD1 localised to the cytoplasm [155, 156]. All clades of Vpx proteins are active in SAMHD1 antagonisation with varying degrees of species specificity for any given Vpx gene [96] (see Table 1.2). Vpx proteins vary in recognition sites for binding SAMHD1. For example, SIVmnd-2 Vpx binds SAMHD1 at the N-terminus whereas HIV-2/SIVmac/SIVsm Vpx proteins recognise the SAMHD1 C-terminus [111]. This is believed to be driven by the head-to-tail dimer position of oligomerised SAMHD1 such that the C and N termini of individual monomers are in proximity (Figure 1.7). In the steady state, Vpx exhibits a strong affinity for one terminus and a weak affinity for the other. Consequently, there are strong signatures of positive selection at both the N and C termini of SAMHD1. Moreover, the strong evolutionary pressure presented by this mechanism may be a major contributing factor to the species specificity observed for SAMHD1 antagonisation by Vpx.

SAMHD1	HIV-2 Rod9 Vpx	HIV-2 7312a Vpx	SIVmac Vpx	SIVdeb Vpr	SIVmus Vpr	SIVagm.Gri Vpr	SIVagm.Ver Vpr	SIVrcm Vpx	SIVmnd2 Vpx
Human	+	+	+	+	+	-	-	-	-
Rhesus	-	+	+	+	+	-	+	+	+
Red-capped mangabey	-	+	+	+	+	-	+	+	+
Mandrill	-	+	+	+	+	-	+	+	+
African green monkey	-	+	+	+	+	+	+	+	-
De Brazza's	+	+	+	+	+	-	+	+	+
Sooty mangabey	-	+	+	+	+	-	+	-	+

Table 1.2 Species-Specific SAMHD1 Degradation by Vpr and Vpx.

The table summarises the results of western blot analyses of the SAMHD1 degradation phenotype by indicated Vpr and Vpx across a panel of primate SAMHD1. The host species SAMHD1 is listed in the left column, and the Vpx or Vpr proteins tested against SAMHD1 are listed in the top row. ''+'' indicates combinations that resulted in a greater than 90% decrease in SAMHD1 levels. ''–'' indicates combinations that had no significant changes in SAMHD1 levels. [Table and text reproduced with permission (refer to section 7.1.2) [96]].

Vpx has also been shown to enhance lentiviral infection in a SAMHD1 independent manner in cytokine stimulated myeloid cells and non-activated resting CD4+ T-cells [157, 158]. Potential Vpx interaction with the cytidine deaminase APOBEC3A has been proposed; however, the strong phenotype exerted by SAMHD1 has made attributing restrictive phenotypes to APOBEC3A in the presence of SAMHD1, problematic [158]. Vpx functions independent of binding to DCAF1 have also been proposed; however, whether these functions are also independent of SAMHD1 remains to be defined (see Section 1.1.5.4 SAMHD1). Potential additional functions encoded by Vpx are discussed in greater depth later in this thesis (see Section 3.3.7 – SAMHD1 independent function of Vpx in esYDMs and ipsYDMs).

As previously described, Vpx targets SAMHD1 for degradation resulting in a rescue of viral replication. This sequence of events implies a model in which proteasomal degradation of SAMHD1 is the immediate precursor to deactivation of SAMHD1 catalytic activity and hence rescue of viral infection. However, the solved crystal structure (of Vpx and SAMHD1 in the complex) from which these conclusions were partly drawn was unable to provide information on the original oligomerised state of Vpx bound SAMHD1. This is important since evidence exists suggesting binding of Vpx to oligomerised SAMHD1 may deactivate catalytic activity prior to SAMHD1 recognition by DCAF1-CLR4 [159]. This scenario thus

implies that SAMHD1 degradation may occur after deactivation of catalytic activity and, therefore, that SAMHD1 degradation may not necessarily be required for deactivation of SAMHD1 antiviral functions.

The two Vpx encoding primate lentiviral lineages, HIV-2/SIVsm/SIVmac and SIVrcm/SIVmnd-2 [160], infect hosts of the same primate family and form a monophylogentic cluster, that, interestingly, groups with SIVagm Vpr [160] (Figure 1.6). All Vpx encoding SIVs are endemic in their wild natural hosts except SIVmac, which is believed to have arisen via the cross-species transmission of SIVsm in captivity [44]. The most prominent current model explaining the origin of Vpx focuses on evolutionary pressure for antagonisation of SAMHD1 which, despite sequence variation of up to 40% between some Vpx genes (e.g., SIVrcm/SIVmnd-2lineage and HIV-2/SIVsm), is conserved across all Vpx encoding primate lentiviruses. As previously described, some Vpr proteins encoded by diverse SIVs are also functional in SAMHD1 antagonisation. Overlay of this function on a primate lentivirus Vpr and Vpx phylogenetic framework identified the neofunctionalization of SAMHD1 by an ancestral SIV Vpr protein as the event that directly drove the genesis of Vpx [96]. All Vpr proteins across extant primate lentivirus lineages initiate cell cycle arrest by a mechanism that is believed to be critically dependant on interaction with the DCAF1-CLR4 complex. The model suggests that at a point leading up to the split of SIVagm and SIVdeb/SIVmus/SIVmon lineages, Vpr neofunctionalises SAMHD1 antagonisation, crucially by a mechanism that also involves interaction with the DCAF1-CLR4 complex [96]. In some hosts, the competitive advantage that antagonisation of SAMHD1 conferred resulted in either the duplication of Vpr within a single lentiviral species or the recombination of Vpr proteins from separate lentiviral species (one able to antagonise SAMHD1 and one not), resulting in the birth of Vpx. The separation of cell cycle arrest and SAMHD1 antagonism to Vpr and Vpx proteins, respectively, in these SIV lineages, may have allowed for greater capacity to adapt and bind proteins that were rapidly evolving to evade antagonisation [96].

Conclusions drawn from phylogenetic analysis of SIVcpz, the immediate precursor to HIV-1, suggest that SIVcpz may be the result of recombination between SIVrcm and a common ancestor of SIVgsn/SIVmus/SIVmon [161]. Interestingly, all these viruses directly antagonise SAMHD1 via Vpx (SIVrcm) or Vpr (SIVgsn/SIVmus/SIVmon), yet SIVcpz (and HIV-1) Vpr does not antagonise SAMHD1. An early theory explaining this phenomenon proposed that SAMHD1 antagonism may have been dispensable for zoonosis from monkeys into chimpanzees, perhaps due to enhanced immune evasion resulting from a functional (non-antagonised) SAMHD1 [162]. However, a more recent report suggests that while Vpx and direct antagonisation of SAMHD1 by Vpr was not acquired by SIVcpz and therefore also HIV-1, the ability to antagonise SAMHD1 may have been conserved or perhaps arisen independently in these viruses. Cribier et al. [163] showed that HIV-1 did indeed downregulate SAMHD1 in macrophages but via indirect manipulation of the cell cycle rather than the direct interaction of a viral component with SAMHD1. Additional study is required to corroborate this finding but if confirmed it would certainly assist in explaining the enigma of the success of the HIV-1 (group M) pandemic independent of HIV-1 encoding a Vpx (or Vpr) gene functional in the antagonisation of such a potent HIV-1 restriction factor, as SAMHD1.

1.1.5 Restriction factors

Restriction factors are cellular antiviral agents and components of the innate immune system that have evolved to disrupt key points of viral replication cycles. Some restriction factors operate on viral components that are common amongst diverse viral families such as glycolipid constituents of env, and as such, are effective against a broad range of viruses (e.g., Tetherin, see below). Other restriction factors are highly specific, targeting viral components unique to individual viral species such as capsid lattices, and thus are effective against a very narrow range of viral species (e.g., TRIM5α, also discussed below). The successful evasion by HIV-1 of cellular restriction factors is a fundamental prerequisite for successful replication and pathogenesis in humans *in vivo*. Moreover, subversion of restriction factors is a key requirement for viruses to replicate in cells not of their natural host species, and thus these

factors can be considered vital regulators of zoonosis viability and host breadth. Currently, over a dozen mammalian restriction factors have been described – this section discusses the primate lentiviral focussed restriction factors that have been most extensively investigated to date: APOBEC3G, TRIM5α, Tetherin and SAMHD1.

1.1.5.1 APOBEC3G

Apolipoprotein B mRNA editing enzyme catalytic polypeptide-like 3G (APOBEC3G) was one of the first restriction factors identified as an interacting partner for HIV-1. APOBEC3G exhibits cytidine deaminase activity converting cytidine bases to uracil post synthetically and thus is restrictive to diverse retroviruses [164, 165]. In the absence of Vif, APOBEC3G is incorporated into viral particles where it corrupts the genetic integrity of the cDNA synthesised by reverse transcriptase. Integration of the mutated transcript may still occur; however, translated proteins are unable to assemble into infectious virions, thus inhibiting the spread of the virus to neighbouring cells. HIV-1 Vif targets APOBEC3G to the ubiquitin ligase complex, thus prohibiting APOBEC3G packaging into progeny virions [166]. Species specificity of primate lentiviral Vif proteins for APOBEC3G is, in part, conveyed by recognition of non-continuous elements within the Vif amino-terminal region by the APOBEC3G substrate. As such HIV-1 Vif proteins do not recognise APOBEC3G from non-human apes or monkeys, nor indeed do SIV Vif proteins recognise APOBEC3G proteins from species outside of their natural hosts [167].

1.1.5.2 TRIM5α

Tripartite-containing motif 5 (TRIM5) is a member of a large subgroup of RING E3 ubiquitin (Ub) ligases. Located in the cytoplasm, TRIM5 proteins assemble, via a layered process of self-association, into hexagonal lattices on retroviral cores [168]. The resulting structure creates a signalling platform which synchronises innate immune activation and proteasome recruitment enabling disassembly of the viral core, arrest of reverse transcription and hence termination of infection [168]. The alpha isoform of human TRIM5, TRIM5α, has been shown to restrict N-tropic murine leukaemia virus (N-MLV), equine

infectious anemia virus (EIAV), feline immunodeficiency virus (FIV), bovine immunodeficiency virus (BIV), and SIVmac [169]. However, despite recognition of the HIV-1 CA lattice, TRIM5α is poorly restrictive to HIV-1 in human cells [169, 170]. Extensive investigation revealed that a ubiquitous cellular protein, Cyclophilin A (CypA), benefits HIV-1 infection in a manner dependent on TRIM5α, and indeed, in the absence of CypA TRIM5α is potent in restriction of HIV-1 [170]. The mechanism underlying CypA interference of TRIM5α-mediated restriction is believed to involve inhibition of HIV-1 CA lattice conformation recognition by TRIM5α. However, whether inhibition is achieved sterically or via conformational changes to HIV-1 CA lattice induced by CypA, remains to be defined [170].

1.1.5.3 Tetherin

Tetherin inhibits the release of diverse enveloped viruses from the surface of infected cells by forming a 'Tether' between the virus membrane and plasma cell surface. Tetherin is an IFN-inducible (see Section 1.3.3 Macrophages and Immunity) type II transmembrane protein that possesses both a C-terminal glycophosphatidylinositol (GPI) lipid anchor and an N-terminal transmembrane anchor [171]. Diverse retroviruses have evolved multiple independent mechanisms to antagonise Tetherin, presumably due to Tetherin interacting with cellular components (cell membrane) rather than viral components. For example, HIV-1 antagonises Tetherin via the accessory protein Vpu, whereas SIVs that do not encode a Vpu protein antagonise Tetherin via the accessory protein Nef, furthermore in some cases primate lentiviral env proteins have been shown to antagonise Tetherin [172-174]. In addition to retroviruses, Tetherin has been shown to restrict several enveloped viruses, including the Ebola virus and Influenza A virus [175, 176].

1.1.5.4 SAMHD1

Sterile alpha domain and HD domain containing protein 1 (SAMHD1) was identified as a major factor inhibiting HIV-1 replication in monocyte-derived DCs that could be neutralised by Vpx encoded by HIV-2 and SIVmac. SAMHD1 is a deoxynucleotide triphosphate hydrolase that catalyses the hydrolysis of

deoxynucleotides into deoxynucleosides and inorganic triphosphates [177]. SAMHD1 is important to cell homeostasis and functions in regulation of dNTP concentrations within cells [178]. SAMHD1 is also an effector of the innate immune system and functions in the restriction of several viruses, including HIV-1 [3, 179].

Human SAMHD1 is a 6Kb gene located on chromosome 20 [180]. The dominant protein species translated is composed of 626 amino acids and comprises 19 α-helices and nine β-strands, arranged in a mixed α/β fold generating an N-terminus proxima sterile alpha motif domain (SAM), and a histidine aspartic acid containing domain (HD) [177, 181] (Figure 1.7). Comparison of SAMHD1 SAM and HD sequences from previously characterised proteins revealed that SAM domains are involved in protein-protein, DNA-protein, or RNA-protein interactions whereas HD domains indicate metal-dependent phosphohydrolase activity [177, 182]. The exact function of the human SAMHD1 SAM domain is currently unclear, however the HD domain has been identified by several studies as the location of the enzymatic active site for dNTP hydrolysis (residues 115-599 [182]) (Figure 1.7A) as well as elements essential for oligomerisation and functional regulation [183, 184]. An NLS defined as KRPR is situated prior to the SAM domain between residues 11 and 14 and is directly responsible for the nuclear residence of SAMHD1 [155] (Figure 1.7A). Minor species splice variants of human SAMDH1 have also been reported; however, these proteins are highly unstable and swiftly degraded [185].

SAMHD1 is localised primarily to the nucleus; however, some SAMHD1 protein is detectible in the cytoplasm of myeloid cells [155, 156, 186]. SAMDH1 exists in monomeric, dimeric, and tetrameric forms yet is only active in dNTP hydrolysis in a tetrameric state [187, 188] (Figure 1.7D). The formation and catalytic activation of tetrameric SAMHD1 is a multistep process driven by interaction between nucleotides and two distinct activating sites (AS1 and AS2) present on each monomer [189] (Figure 1.8). The initial step is dimerization, which is driven by binding of GTP or dGTP to AS1 [190, 191]. This is followed by tetramerisation, stabilisation, and catalytic activation, all determined by AS2. AS2 activation

is dependent on the prior occupation of AS1 and is driven by binding dATP, dCTP, dGTP or dTTP with positive bias towards dATP interaction. AS2 binds dNTPs with an estimated Kd of 1-20μM and thus is only occupied once physiological levels of dNTPs reach the required threshold. Occupation of AS1 and AS2 in all four SAMHD1 monomers induces conformational changes that stabilise the tetramer and activates the catalytic sites [189, 192]. Thus, dNTP concentrations are the major factor regulating SAMHD1 hydrolysis of dNTPs.

The deactivation and dissociation of SAMHD1 tetramers are, unfortunately, less well described. SAMHD1 interaction with the tetraspanin CD81 has been reported to induce SAMHD1 proteasomal turnover [193], as has interaction with cyclin L2 [118] and eukaryotic elongation faction 1A1 (eEF1A1) [194], the latter two by association with Cullin4A and hence E3 ubiquitin ligase. Vpx has been shown to drive SAMHD1 tetrameric disassociation, a process which also ultimately results in SAMHD1 degradation via the E3 ubiquitin ligase [195]. In non-cycling cells where phase-mediated turnover is absent, tetrameric catalytically active SAMHD1 may persist in the tetrameric state for extended periods even after dNTP concentrations have fallen below the activation threshold [196].

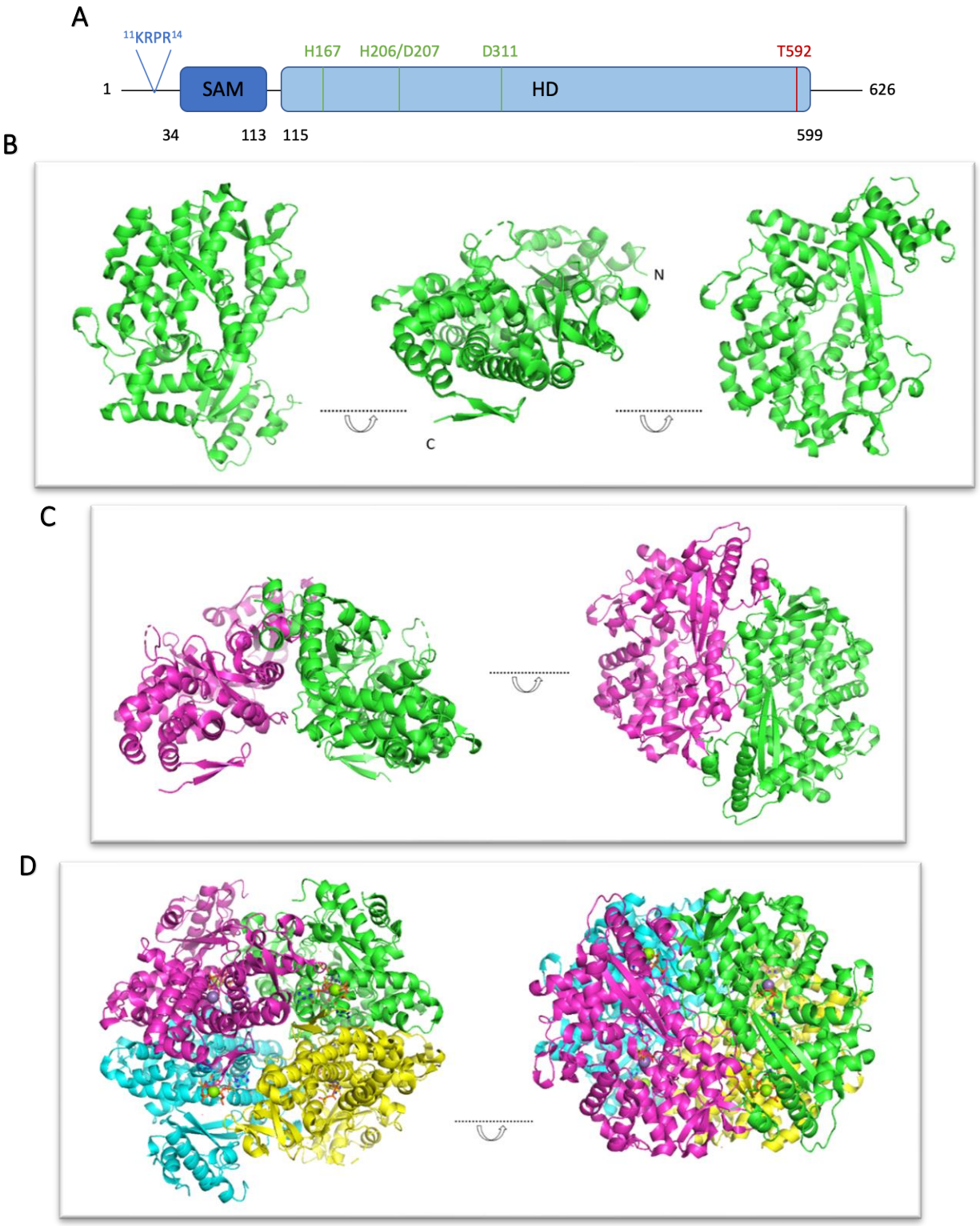


Figure 1.7 Structure of SAMHD1.

A schematic diagram of human SAMHD1 domain organisation. The NLS is shown just prior to the SAM domain and the phosphorylation site T592 is shown towards the C-terminus. Residues that if mutated abolish dNTPase activity are shown in green [197] **(A)**. Ribbon representation of the crystal structure of human SAMHD1 catalytic core (SAMHD1c2, residues 113–626 [192]) in monomeric **(B)**, dimeric **(C)** and tetrameric state **(D)**. The tetrameric representation shows activating dGTP-Mg^{2+}-dGTP bound to allosteric sites. PDB:4BZC [192] . 'N' denotes N-terminal, 'C' denotes C-terminal. Cartoons generated using Pymol ™ 2.4.0 – Incentive Product.

Several studies have reported nucleic acid binding properties for primarily monomeric and dimeric SAMHD1 forms [197-200]. SAMHD1 binds nucleic acids with the following binding preferences: ssRNA > ssDNA > RNA:DNA hybrid > dsDNA [197]. Nucleic acid binding induces dNTPase defective oligomeric states but does not prevent tetramerisation and dNTPase activation in the presence of high dNTP concentrations [197]. While the interaction with nucleic acids is almost indisputable, less certainty surrounds the proposed consequent effects. A recent proposition is the involvement of SAMHD1 nucleic acid binding in DNA repair [201]. In immortalised carcinogenic cell lines, SAMHD1 has been shown to localise to sites of DNA damage and associate with the endonuclease CtBP-interacting protein (CtIP) and the endo and 3' to 5' exonuclease MRE11-RAD50-NBS1 (MRN), resulting in homologous recombination (HR) [201]. SAMHD1 may also bind nucleic acids as an initiator for degradation.

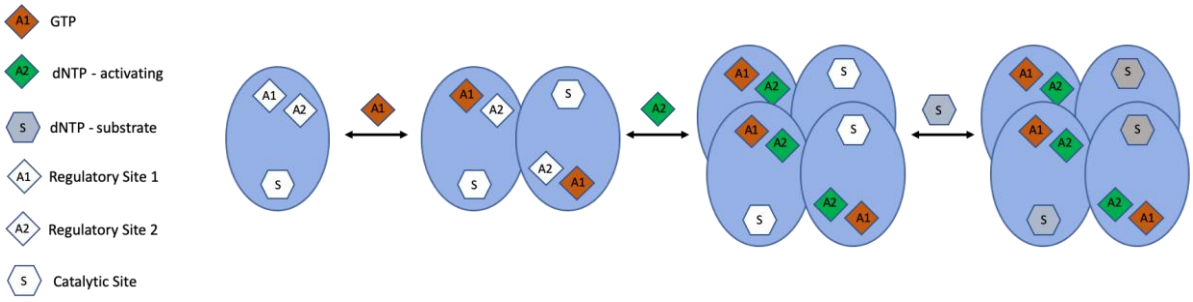


Figure 1.8 Regulation of SAMHD1 catalytic activity by nucleotide concentrations.

Schematic showing steps for activation of SAMHD1 catalytic activity. SAMHD1 exists as monomers and dimers in equilibrium when concentrations of dNTPs are low. GTP binding to Regulatory site 1 (A1) induces stable dimer formation. Binding of dNTPs to Regulatory site 2 (A2) as dNTP concentrations increase results in SAMHD1 tetramerisation and a conformational change which activates the catalytic site (s), allowing the hydrolysis of dNTP substrates. Adapted from [191].

Most human tissues express SAMHD1; however, expression level and functionality vary significantly in a cell type-dependent manner [202] (for additional description, see Section 3.3.2 SAMHD1 is phosphorylated and highly expressed in esYDM). At the transcriptional level, SAMHD1 can be silenced by methylation or upregulated by cytokines such as interleukin 12 (IL-12), interleukin 18 (IL-18), Tumor Necrosis Factor – alpha (TNFα) and type I IFNs [203-205]. SAMHD1 is post-translationally regulated by phosphorylation at T592 (Figure 1.7A), a modification regulated by cyclin-dependent kinase 1 (CDK1)

and cyclin-dependent kinase 2 (CDK2) in a cell cycle-dependent manner [118, 163]. In non-cycling cells, and to a lesser extent in cycling cells, phosphorylation of SAMHD1 at T592 is accompanied by an increase in dNTP concentrations [206]. In cycling cells, SAMHD1 is phosphorylated at T592 when cells enter G1 phase and start proliferating [207]; SAMHD1 is believed to be dephosphorylated during G2 phase by an undescribed mechanism that could involve a phosphatase or the cell cycle regulator p21/Waf1/Cip1 [163]. p21/Waf1/Cip1 is a cyclin-dependent kinase inhibitor that is believed to also function in the regulation of HIV-1 restriction in myeloid cells [208]. In non-cycling cells that remain in G1 phase, such as resting CD4+ T-cells and bone marrow-derived macrophages, SAMHD1 exists in a perpetually dephosphorylated state [207, 209]. Cascades involving extra-cell cycle interactors further regulate phosphorylation at T592. Treatment of cycling cells with IFN-I, differentiating monocytes with M-CSF, or indeed DNA damage results in dephosphorylation at T592 in a manner that may depend on p21/Waf1/Cip1 mediated cell cycle arrest [208, 210, 211]. Although an increase in dNTP concentrations is well documented to coincide with phosphorylation at T592, the direct effect of phosphorylation on the catalytic activity of SAMHD1 is unclear with several investigations reporting a positive regulatory effect [184, 206, 212] and several investigations reporting no effect at all [184, 209, 213, 214]. There appears to be a consensus that phosphorylation at T592 alters tetramerisation kinetics, but further study is required to deduce the ultimate consequence of such modifications. More certainty surrounds the post-translational regulation of SAMHD1 catalytic activity via redox signalling.

The tight, cell cycle-dependent regulation of SAMHD1 catalytic activity strongly implies a critical role for SAMHD1 (and hence control of dNTP concentrations) in cell homeostasis, and therefore potentially also in disease. Homeostatic imbalance, and particularly cellular growth dysfunction, are causative in important clinical diseases such as cancer, and indeed aberrant SAMHD1 function has been implicated in several oncogenic disorders including colon cancer and lung cancer [215-218].

SAMHD1 has also been implicated in autoimmunity [219]. Mutations in SAMHD1 are causative in Aicardi-Goutières syndrome (AGS), an autoimmune, genetic condition that mimics persistent viral infection [220]. AGS can be caused by mutations in SAMHD1 alone or in combination with mutated Three prime Repair EXonuclease 1 (TREX1) and Ribonuclease H enzyme 2 RNASEH2 (complex) genes [221]. AGS is characterised by high levels of IFN-α in blood and cerebral spinal fluid, encephalopathy, cerebral vasculopathy, leukodystrophy, arthropathy, and mitochondrial DNA deletions [222-226]. The mechanism underlying AGS is believed to involve triggering of innate immunity by sensing of accumulated host nucleic acids which would otherwise have been processed by SAMHD1 [116]. How AGS related SAMHD1 mutations perturb nucleic acid clearance is unclear; however, abnormal localisation to the cytosol may be involved [198]. The origin of the aberrant nucleic acids is also not entirely clear but could include retroelements [227] and remnants of normal DNA processing by the cellular machinery [198].

SAMHD1 was originally identified as the human homolog to *Mg11*, a murine IFN-inducible gene [228]. Mutations in SAMHD1 were identified in AGS patients and for several years the focus of SAMHD1 was in understanding the underlying mechanisms causative of the autoimmune disease [220, 222]. The research focus changed when SAMHD1 was co-immunoprecipitated with Vpx protein and shown to be active in HIV-1 restriction in MDDCs and later in primary monocytes, MDMs, and resting CD4+ T-cells [2, 3, 202, 229]. SAMHD1 is dephosphorylated at T592 and constitutively expressed at high levels in these cells; application of Vpx resulted in almost complete depletion of SAMHD1 protein, an increase in dNTP concentrations, and robust rescue of HIV-1 infection [2, 3]. The consistent observation of all three of these effects in multiple cell types resulted in the hypothesis that low dNTP concentrations were detrimental to successful HIV-1 replication, and therefore, the mechanism underlying SAMHD1-mediated HIV-1 restriction was dNTP hydrolysis [230]. Evidence in support of this hypothesis came from subsequent observations that external application of deoxynucleosides (dNs) to macrophages (in the absence of Vpx) resulted in rescue of HIV-1 infection [204, 229] and, moreover, that SAMHD1 was active

in restriction of divergent viruses including hepatitis B virus, herpes simplex virus type 1, vaccinia virus and α, β & γ retroviruses - implying a functionally generalised mechanism of restriction [115, 219]. However, subsequent observations detailed several incidences of active SAMHD1-mediated HIV-1 restriction in the presence of high dNTP concentrations [184, 209, 213, 214]. Furthermore, experiments using SAMHD1 truncation and phospho-mimetic mutants revealed that dephosphorylation at T592 was critically required for SAMHD1-mediated HIV-1 restriction in a manner independent of the dNTPase concentration [163, 209, 213].

Subsequently, a research group investigating SAMHD1:nucleic acid binding attributes proposed a role for a novel ribonuclease activity that functioned in restriction of HIV-1 by degrading incoming viral RNA prior to completion of reverse transcription [114, 115]. Importantly the nuclease activity was independent of the dNTPase and regulated by phosphorylation at T592. The observation proved controversial since subsequent researchers were unable to reproduce the results of the original investigation leading to the conclusion that the novel ribonuclease identified was, in fact, contamination of co-purified SAMHD1 independent nucleases [197, 231]. Moreover, closer scrutiny of the original model highlighted a discrepancy regarding the feasibility of SAMHD1 interaction with viral RNA prior to completion of reverse transcription. SAMHD1 is primarily localised to the nucleus, and current models define completion of RT within the RTC/PIC prior to nuclear entry [109, 121, 232-234]. The authors of the original manuscript proposed that differences in experimental procedures could be responsible for the discrepancies [235]. Another possible explanation is that SAMHD1 recruits a cellular nuclease [197], such as the previously mentioned CtIP/MRN (which has only recently been described). Recruitment of a DNA nuclease such as CtIP/MRN would enable degradation of cDNA in the nucleus, would restrict HIV-1 independently of the dNTPase, and, importantly, could co-purify with SAMHD1. In support of this notion, the original authors have since presented further evidence detailing the reduction of purified SAMHD1-nuclease activity on the application of Vpx [235]. The effect of Vpx on nuclease activity is intended to eliminate the notion of co-purified SAMHD1-independent nucleases, which would not be

affected by Vpx. This new observation does not eliminate the possibility of a SAMHD1-bound co-purified nuclease but does bolster the evidence supporting the existence of a nuclease function acting as part of, or in concert with, SAMHD1 [113].

The mechanics of the hypothetical nuclease dependent SAMHD1-mediated HIV-1 restriction is believed to involve the degradation of HIV-1 nucleic acids resulting in a block to integration and hence, the expression of viral genes [197, 231, 236] (refer to Chapter 5, Section 5.1 Introduction). Interestingly, this process has also been theorised to be beneficial to HIV-1 pathogenesis - by removing viral nucleic acids that would otherwise be detected by cytosolic sensors, triggering an innate immune response [162] (refer to Chapter 1, Section 1.1.4.2 Vpr).

In addition to antiviral properties, SAMHD1 has also been shown to be active in human endogenous retrotransposon LINE-1 restriction, yet the underlying mechanism is not entirely clear. There is, however, some evidence to suggest a mechanism dependent on phosphorylation at T592 and the HD enzymatic domain, yet independent of the dNTPase [237, 238]. This is almost identical to the mechanics of dNTPase independent HIV-1 restriction described above however while binding of LINE-1 nucleic acid is a requirement, a putative nuclease function is not implicated. SAMHD1-mediated LINE-1 inhibition has also been linked to the sequestering of nucleic acids to stress granules by a mechanism that also involves the binding of nucleic acids by SAMHD1 [239]. Absent or incorrect processing of LINE-1 nucleic acids is believed to result in innate immune activation by cytosolic sensing of LINE-1 products [239, 240] and an inflammatory response, and in support of this proposition disease mutations in SAMHD1 relating to AGS result in impaired LINE-1 restriction [227]. Taken together, these observations could imply a SAMHD1-mediated retroelement nucleic acid restriction that is nucleic acid binding dependent but nuclease independent.

SAMHD1 has also been implicated in cellular apoptosis with significant variations in phenotype that is dependent on cell type. For example, in T-cells, endogenous SAMHD1 appears to induce apoptosis upon

infection by HTLV-1 via the STING and IRF3-Bax apoptosis pathway [241], however exogenous SAMHD1 expression in HuT78 cells induces apoptosis via the extrinsic pathway including caspase 8, 3 & 7 [242]. Conversely, knockout of SAMHD1 in myeloid cells (THP-1) resulted in the inhibition of apoptosis in a manner that may be dependent on cyclin D3 [243]. SAMHD1 effects on cellular proliferation have also been shown to vary significantly in a cell type dependent manner. Both in T-Cells (HuT78) and myeloid cells (THP-1), faster proliferation is observed in the absence of SAMHD1 [242, 243], whereas in fibroblasts absence of SAMHD1 results in slower proliferation [178].

1.1.6 HIV and SIV lifecycle

Events in the HIV life cycle can be separated temporally into an early stage and a late stage. The early-stage encompasses virion attachment and fusion to the host cell, reverse transcription of viral RNA, uncoating of the viral core, transit of replication components to - and entry into the cell nucleus, and integration of the reverse-transcribed viral genome into the host chromosome. Late-stage events involve transcription of viral genes, nuclear export, and translation of viral RNA, trafficking of viral polyproteins and glycoproteins to the plasma membrane, and subsequent assembly, budding, and maturation of progeny virions (Figure 1.9).

HIV-1 entry is mediated by the env glycoproteins gp120 and gp41, which exist as trimers on the surface of virions [244]. The first step of a strictly sequential process involves the binding of gp120 to the cell surface mounted CD4 receptor molecule. Successful gp120 and CD4 coupling results in conformational changes in both gp120 and CD4. Conformational changes in gp120 expose additional co-receptor binding sites that recognise the chemokine co-receptors CCR5 and CXCR4 [244]. Conformational changes in CD4 bring the env glycoprotein complexes into sufficient proximity to facilitate gp120 and co-receptor coupling. Co-receptor binding triggers further conformational changes in the env glycoproteins resulting in the insertion of the gp41 fusion peptide into the cellular membrane. Insertion of gp41 initiates fusion between the virion and cell lipid membranes and drives the subsequent insertion

of the viral core and associated viral proteins (such as Vpr, Vpx, and Nef) into the host cell cytoplasm [245]. HIV-1 fuses with target cell membranes both at the cell surface and in early endosomes in a manner that depends on cell type, virus strain, and potentially HIV-1 co-receptor usage by virtue of differential sensitivity to IFN-induced transmembrane proteins (IFITMs) [246]. Macrophage entry of HIV-1 is predominantly via endocytosis and therefore fusion in early endosomes in a manner dependent on dynamin, Rac1 and Pak1 [247, 248]

The release of the viral core into the cytoplasm triggers reverse transcriptase; synthesis of a DNA copy of the RNA genome commences, and the reverse transcription complex (RTC) is formed [249]. Dissociation ('uncoating') of the RTC occurs at some point between delivery of the viral core into the cytoplasm and 'docking' of the core at the host cell nuclear pore. The spatiotemporal mechanics and nature of the components governing this process are a matter of controversy, however it is generally accepted that enough CA dissociates during transit to allow remodelling of the viral core vital for reverse transcription, while also retaining sufficient integrity to shelter viral RNA and DNA from host cytosolic sensors and (some) restriction factors [250].

The mechanics of reverse transcription are depicted in Figure 1.10 and are as follows: a primer binding site (PBS) located approximately 170 nucleotides from the 5' end of the viral genome is the location at which reverse transcription is initiated via the tRNALys3 primer. A short portion of the negative-sense strong stop DNA strand is initially synthesised by RT using the positive-sense RNA as a template resulting in a ±RNA/DNA hybrid. The RNase H activity of RT then degrades the viral RNA template bound in the RNA/DNA hybrid. The first strand switch then occurs in which the strong stop DNA subsequently translocates and hybridises to the 3' end of the viral RNA. Synthesis of the remaining portion of the negative sense strong stop DNA continues to completion during which time the RNase H activity of RT degrades the entirety of the copied viral RNA template except for the RNase H resistant central polypurine tract (cPPT) and 3' end polypurine tract (3'PPT). The cPPT and 3'PPT serve as a primer for

synthesis of the positive sense DNA strand, which remains bound to the negative sense strong stop DNA once synthesis is complete. Synthesis of the positive sense DNA strand commences up to and including a portion of the PBS, after which the positive DNA strand translocates to the complimentary 3' end of the negative sense strong stop DNA strand (second strand transfer). Reverse transcription continues culminating in the synthesis of complete double-stranded proviral DNA. The sequence for synthesis termination is located in the cPPT of the positive DNA strand by way of a central termination signal (CTS) at the 3' end. Concomitant with the termination of DNA synthesis, a 99nt central DNA flap is generated, which is believed to function in the facilitation of nuclear import [251].

Concurrent with RT, the RTC traffics to the nuclear membrane by hijacking the cellular microtubule network and the associated transport molecules dynein and kinesin [252, 253]. Completion of reverse transcription redefines the RTC as the pre-integration complex (PIC), which comprises two complete DNA copies of the RNA viral genome (referred to as cDNA), some remaining capsid (CA) protein, matrix protein (MA), IN, some Vpr or Vpx, and several cellular components. Nuclear import of the PIC has been shown to be enhanced by Vpr protein and facilitated by nucleoporins such as NUP153 [254].

Nuclear localization of the PIC activates the viral IN enzyme, which processes the viral DNA to create 3' recesses and 5' protruding ends. Proviral strand transfer is then catalysed by the IN processed 3' hydroxyl group, which attacks phosphodiester bonds in the host chromosomal DNA [251]. Insertion of the proviral DNA into the host chromosome creates a genetically independent cassette transcriptionally regulated by the HIV-1 promoter [255]. Transcription of the proviral DNA and subsequent extensive splicing yields four distinct RNA species: a full length (approx. 9.7kb) precursor mRNA (pre-mRNA), singly spliced mRNA of approx. 4kb, double spliced mRNA of approx. 2kb and finally doubly spliced mRNA of approx. 1kb. Singly spliced mRNA encodes Vpr, Vpu, and Vif; doubly spliced (2kb) mRNA encode Tat, Rev, and Nef; the gene encoded by the doubly-spliced 1kb species has yet to be defined [255]. Rev is required for nuclear export and stabilisation of un-spliced and singly spliced mRNA; hence, the doubly

spliced Rev encoding mRNA species is the first to be translated [255]. In addition to serving as a pre-mRNA for subsequent splice events the full-length transcript also encodes for p55 Gag precursor which contains nucleocapsid (NC), CA, MA, p6 domains and two spacer peptides, SP1 and SP2; and p160 Gagpol precursor polyprotein which contains the additional proteins: PR, RT and IN [251]. The alternative splicing of the full-length pre-mRNA delivers over 50 mRNA isoforms in proportions required for viral assembly with optimal efficiency [255].

Gag and Gagpol are targeted to the plasma membrane by sequences within MA and multimerises via interactions with CA as the virion assembles [256]. The process by which env glycoprotein complexes are incorporated is not entirely clear; however, env interactions with MA have been shown to be, at least in part, a requirement [256]. Vpr and Vpx accessory proteins are packaged by interaction with the p6 region of the Gag polyprotein, as previously described. Packaging of HIV-1 Vpr requires a L-X-X-L-F motif present at the C-terminus of p6 [257]. The L-X-X-L-F is conserved across primate lentiviral p6 proteins, and indeed, it has been shown that the ability to package HIV-1 Vpr can be conferred to heterologous Gag precursors by transfer of the amino acid sequence including the L-X-X-L-F motif [257]. Packaging of Vpx protein, however, requires the D-X-A-X-X-L-L motif located towards the N-terminus of p6, which is conserved among members of the HIV-2/SIVsm/SIVmac and SIVagm lineages [257]. The D-X-A-X-X-L-L motif is also required for the packaging of SIVmac Vpr protein; however, the L-X-X-L-F motif critically required for HIV-1 Vpr packaging, while conserved in the SIVmac genome, is dispensable for Vpx and SIVmac Vpr packaging [257]. The accessory proteins Nef and Vif, together with several cellular components, are also targeted to the site of particle assembly for packaging into progeny virions and execution of function, respectively (see Section 1.1.4.1 Nef, Vif, and Vpu). Viral genomic RNA is sequestered for packaging by NC, and finally, the budding process is completed by catalysis of membrane fission by the cellular endosomal sorting complex required for transport (ESCRT) machinery which is recruited also by p6 domains [256]. Completion of viral budding triggers maturation which involves proteolytic cleavage of Gag and Gagpol polyproteins into the virion's primary constituents: MA,

CA, NC, p6, RT, IN and PR. These proteins spontaneously reorganise resulting in the characteristic particle structure containing the fullerene (conical shaped) core [256].

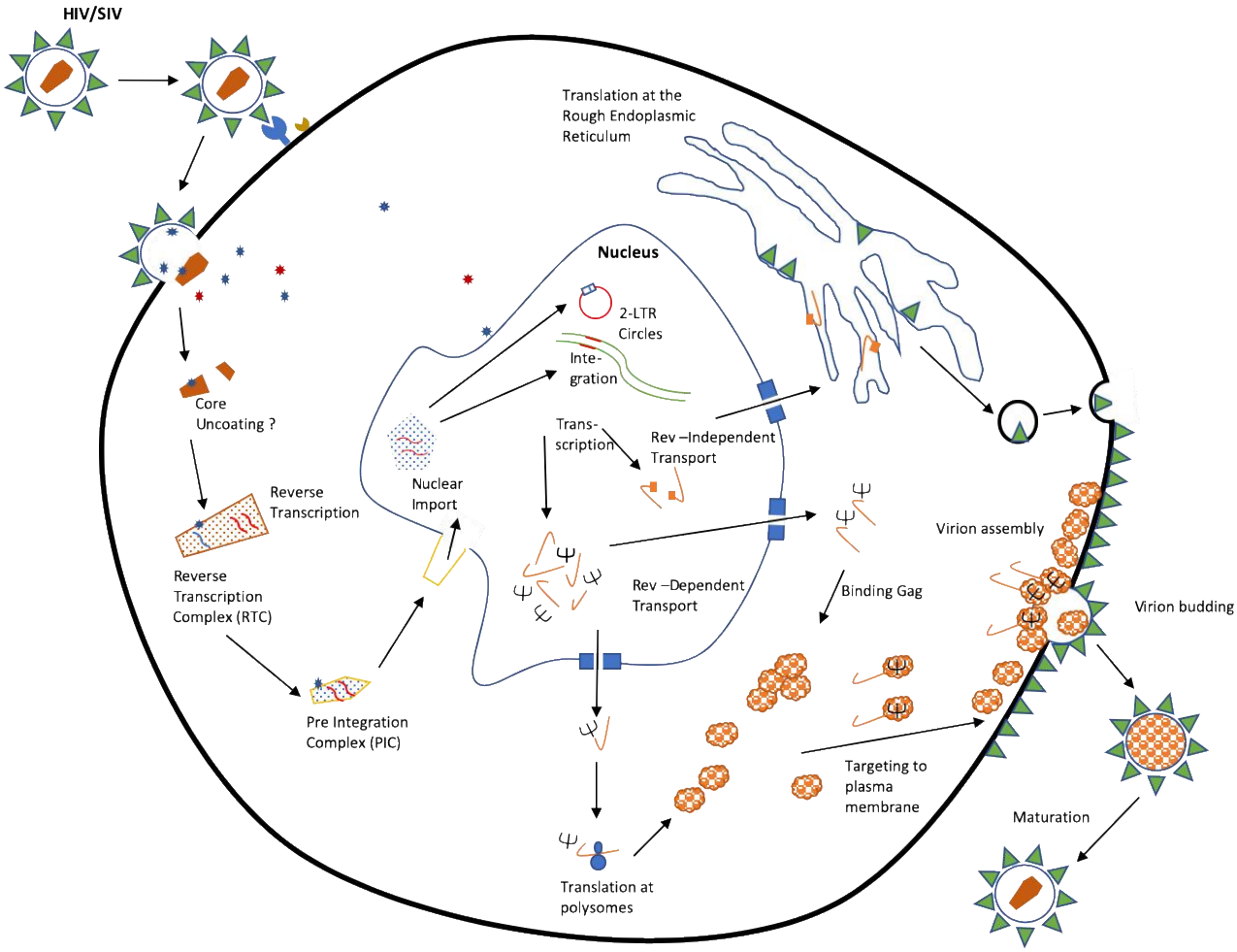


Figure 1.9 The HIV and SIV lifecycle.

Schematic showing the HIV and SIV life cycle in mammalian cells. A detailed description of the process can be found in Section 1.1.6 HIV and SIV lifecycle. Key: Viral RNA genome, viral DNA genome (cDNA), cellular DNA genome, Vpr or Vpx, Nef, packaging signal psi. Adapted from [258].

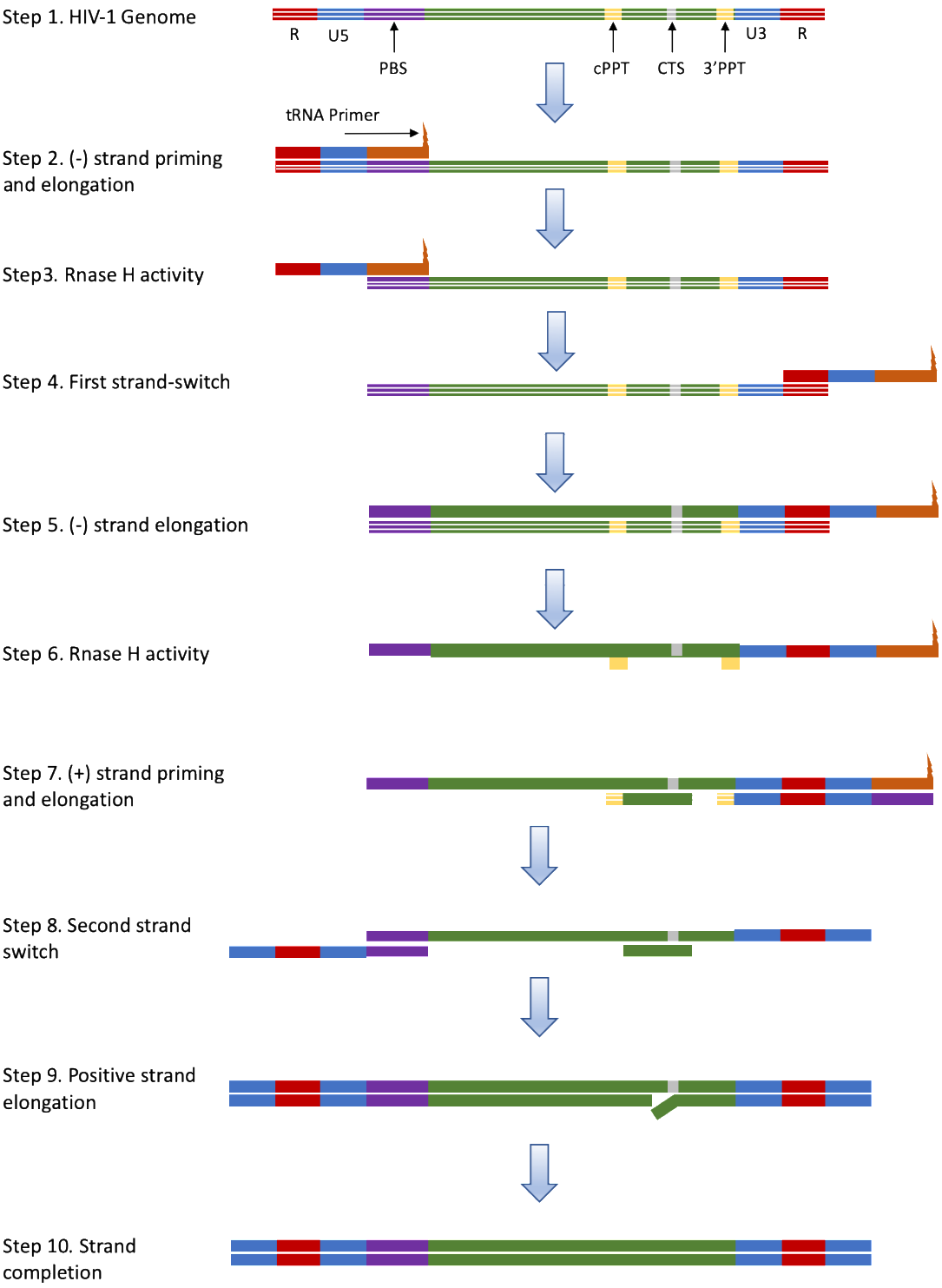


Figure 1.10 HIV and SIV Reverse transcription.

Schematic diagram showing the steps for reverse transcription of the viral RNA genome by the viral reverse transcriptase enzyme. Step 1 - Striped lines represent the positive sense viral genome. Step 2 – The solid line represents the synthesis of the first DNA copy (cDNA), which is negative sense. Bonded to the primer binding site (PBS) of the template RNA is the tRNALys3 (tRNA primer) molecule, which primes the negative sense DNA synthesis. Step 6 & 7 - RNase H activity at the polypurine tracts bordering the U3 region of the LTR (3' PPT) and the 3' end of the pol gene (cPPT) produces a short RNA fragment which serves as a primer for positive sense cDNA synthesis. A detailed description can be found in Section 1.1.6 HIV and SIV life cycle. CTS – central termination signal. Adapted from [258].

1.2 Lentiviral Vectors

The unique ability of members of the lentivirus family to insert a copy of viral genomic DNA into a host chromosome has resulted in their popular use as a stable gene delivery system in molecular biological research [259, 260]. Viral vectors can be defined as viruses that have been modified to encode a gene of interest as well as transcriptional elements required to enable expression. Viral vectors are genetically altered to ensure a lack of replication competency. This is achieved by the division of viral genes (refer to Table 1.3) amongst physically separate constructs that must all be expressed simultaneously in producer cells to enable viral production (see below) [261].

First-generation lentiviral vectors encoded lentiviral genes on three separate constructs (packaging-, transgene- and envelope constructs). The packaging construct encoded Gag, Pol, Rev, Tat, Vif, Vpu, Vpr, and Nef. The transgene construct encoded the cis-elements of the lentiviral genome (LTR, packaging signal, RRE), the transgene of interest, and optional genes such as the central polypurine tract sequence (cPPT) and the woodchuck post-regulatory element (WPRE) which enhance transduction efficiency and transcription stability, respectively. The envelope constructs allowed expression of native lentiviral env or those of other, more permissive viruses such as the vesicular stomatitis virus env (VSV.G). The lack of both packaging signal and LTR sequences in both the envelope and packaging constructs ensures that viral proteins were not expressed in target (transduced) cells [262].

Second generation lentiviral vectors were engineered to further reduce the likelihood of viral gene expression in target cells and thus increase safety. This was achieved by the removal of all viral accessory proteins from the plasmid that were not required for infection as well as additional modifications that rendered the integrated lentiviral vector self-inactivating (SIN). Self-inactivation was achieved by deletion of a portion of the 3'-LTR, which resulted in the incorporation of deleterious mutations in both the 5' and 3' LTR, and inactivation of LTR driven transcription [263].

Third-generation lentiviral vectors are engineered such that Rev is removed from the packaging construct and encoded on a separate plasmid, thus creating a four-construct expression system. Furthermore, by the addition of a hybrid LTR, which involves a partially deleted 5'LTR fused to a heterologous promoter such as those native to cytomegalovirus (CMV) in the transfer plasmid, the requirement for Tat is removed. These alterations render third-generation lentiviral vectors less likely to yield viral proteins enabling viral replication in transduced cells than first or second-generation systems [264].

The second-generation production system was used for the creation of Lentiviral Vectors (LV) and Viral Lentivector like Particles (VLPs) in this thesis.

Genetic Element	Function	Required in Vector?
	Cis Elements	
LTR	Codes for gene expression, integration, and reverse transcription	Yes
Ψ	"Psi" - RNA packaging signal	Yes
RRE	Important for viral mRNA transport; Rev interactor	Beneficial
3' PPT	Required for positive sense strand synthesis	Yes
	Trans Elements	
gag/pol	Encodes structural and enzymatic proteins	Yes
env	Encodes env	Yes
vif	Affects virion assembly and infectivity in certain cell types	No
vpu	Inhibits CD4 and MHC I surface expression and stimulates viral budding	No
vpr	Important for infectivity of non-dividing cells	No
tat	Enhances transcription from the LTR	No, (5' LTR+ vectors exception)
rev	Important for expression of singly spliced and unspliced viral mRNA	Required for RRE containing vectors
nef	Assists HIV-1 evade host restriction factors.	No

Table 1.3 The major genetic elements of HIV-1 and their role in lentiviral vectors.
Adapted from [265].

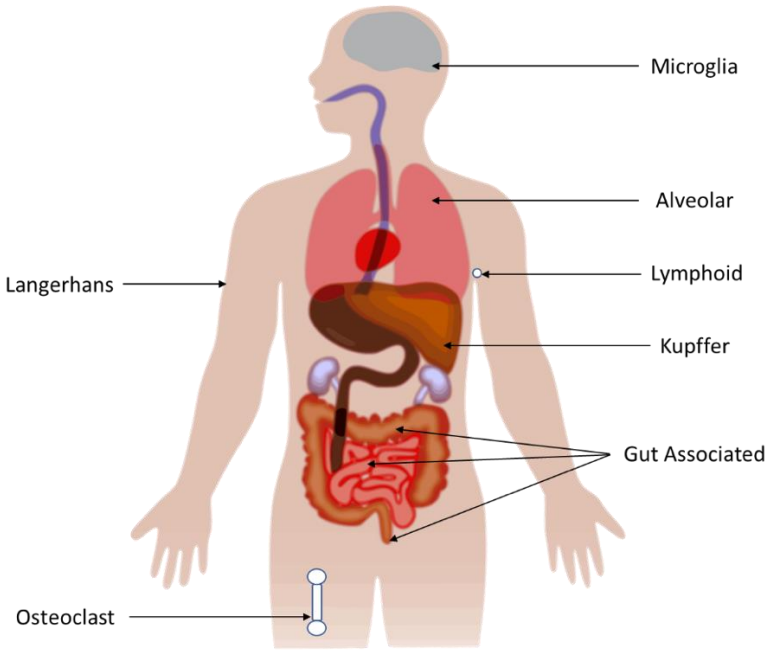
1.3 Macrophages

Macrophages are a heterogenous leukocyte subset of ancient origin that are present throughout mammalian anatomy. Macrophages are involved in tissue homeostasis, regulation of hematopoiesis, chronic inflammation, wound repair, tissue remodelling, and intimately involved in immunity (Figure 1.11). Macrophages are not terminally differentiated cells and hence macrophage functions are not terminally defined, but rather attenuate in response to stimulation from the microenvironment.

1.3.1 Development

During mammalian development and throughout adulthood, macrophages function in the structuring and remodelling of tissue, provide trophic support for cells of multiple lineages, and function in the clearance of debris and apoptotic cells [266-271]. The remodelling deficiency osteoporosis, for example, was observed in mice deficient in osteoclasts, a macrophage subset specialised in the reabsorption and remodelling of bone [272, 273]. Macrophages regulate erythropoiesis [274], mechanics of hematopoietic stem cell differentiation, and egress from the bone marrow [274, 275], and angiogenesis [276, 277]. Macrophages also play crucial roles in the development of the brain and the central nervous system (CNS). Microglia are macrophages of the CNS, and function to promote fasciculation, support neuronal survival and synapse maturation and remodelling in the prenatal, perinatal and postnatal mammalian organism, respectively [278]. In a study investigating foetal microglial depletion in mice, it was shown that microglial absence aberrates laminar positioning of subsets of neocortical interneurons and perturbs the progression of dopaminergic axons in the forebrain [279]. While behavioural abnormalities in these mice were muted, in humans, dysfunction of both cortical networks and dopamine innervation have been linked to neuropsychiatric disorders and hint at a link between macrophage-mediated developmental homeostasis and adult disease [280]. Observations of mice deficient in the colony-stimulating factor 1 (CSF1) ligand CSFR1, revealed heavy deficiencies in both microglia and a professional antigen-presenting tissue-resident macrophage subset termed Langerhans cells. These mice displayed cerebral structural development abnormalities but

intriguingly no behavioural aberrations. In addition, individuals were substantially more susceptible to productive viral infection than controls, highlighting the importance of macrophage-mediated immunity during development [281].



Type	Location	Function	Pathology
Microglia	Brain	Immunity, CNS homeostasis, support neuronal survival, synapse maturation	Neurodegenerative diseases
Alveolar	Lung	Immunity, lung homeostasis, inhaled debris clearance	Chronic obstructive pulmonary disease (COPD)
Lymphoid	Lymph nodes	Immunity, trans virus capture, and presentation	Cancer
Kupffer Cells	Liver	Immunity, glucose, lipid and iron homeostasis	Fibrosis
Gut Associated	Gut	Immunity, gut homeostasis	Irritable bowel disorder (IBD)
Langerhans cells	Skin	Immunity, tolerance induction, lymph node migration, and antigen presentation	Langerhans' cell histiocytosis;
Osteoclast	Bone	Bone remodeling and reabsorption; hematopoiesis	Osteoporosis; Leukemia

Figure 1.11 Macrophage heterogeneity in development, homeostasis, and disease.

Macrophage subpopulation locations in humans. Macrophages are vital in development, such as in the remodeling of bone and the maturation of synapses; in homeostases such as in the clearance of self and non-self debris; and in immunity via the direct termination of pathogens, the activation of cytokine signaling arrays and the bridging of innate and adaptive immunity. Aberrant macrophage behavior, however, is also central to several non-pathogen associated diseases such as cancer, inflammatory bowel disease (IBD), and osteoporosis [282-285]. Adapted from [282, 283].

1.3.2 Homeostasis

Macrophages have fundamental homeostatic functions in several tissues. In metabolism, for example, macrophages, together with parenchymal cells and stromal cells, are the primary constituents of important metabolic organs such as the liver, pancreas, and adipose tissue [286]. Metabolic regulation enables an organism to adapt to nutrient requirements that may fluctuate greatly in response to stimuli from the microenvironment such as viral or bacterial infection; and the macroenvironment, such as the requirement for increased locomotion during the fight or flight response. Macrophages govern the metabolic health of adipocytes, the primary effectors of nutrient storage and systemic metabolism regulation of adipose tissue [287, 288]. In mouse models of obesity, macrophages are crucial for maintaining insulin resistance [289, 290], and to a lesser degree facilitating the storage of excess nutrients in adipocytes [283, 291]. Macrophages have been shown to function directly in the regulation of thermogenic homeostasis by triggering of adaptive thermogenesis in response to environmental declines from normal body temperature [292]. This is achieved by the adoption of alternative activation states, which in turn induce thermogenic genes and effect lipolysis of stored triglycerides, cascades vital for the maintenance of core body temperature in the cold [283, 292]. Mouse models of obesity have also highlighted the importance of Kupfer cells, macrophages of the liver, in support of glucose and lipid homeostasis. Kupfer cells provide trophic support to hepatocytes, effector cells of the liver, whereby stabilising the uptake, synthesis, and oxidation of fatty acids, the imbalance of which is the hallmark of obesity [271, 289].

In contrast to the beneficial roles detailed above, macrophages are central to the pathology of several non-pathogen associated diseases. In cancer, for example, macrophages have been shown to directly stimulate tumorigenesis by several mechanisms, including the production of inflammatory cytokines such as interferon-gamma (IFNγ) and tumor necrosis factor-alpha (TNFα), and alteration of the microbiome [293-295]. Tumor-associated macrophages (TAM) regulate the angiogenic switch of tumors to the malignant state [296], simulate invasion and intravasion [297] and are involved in

metastasis both in the liberation of tumor cells into the bloodstream [298, 299] and in preparation of tumor cell receiving sites termed pre-metastatic niches [300]. Macrophages have also been identified as causal in rheumatoid arthritis [301], inflammatory bowel disease [302], multiple sclerosis [303], fibrosis [304], atherosclerosis [305], systemic lupus erythematosus [306], asthma [307] as well as neurological [308], cardiovascular [309] and osteolytic [310] complications resulting from HIV-1 pathogenesis. In each of these diseases, macrophage contributions and functions are highly diverse, dependent on the stage of the disease, as well as the milieu of stimulation from the microenvironment. The presence and prominence of macrophages in almost all human diseases have made these cells highly attractive targets for therapeutic design [311-314].

1.3.3 Macrophages and Immunity

Macrophages, dendritic cells, and neutrophils are fundamental components of the mammalian immune system and function to identify, neutralise and remove pathogens such as bacteria [315], fungi [316], viruses [317, 318] and parasites [316, 319]. The systemic distribution of macrophages with particularly high density at sites of pathogen abundance, such as the skin and the gut, make it highly probable that macrophages are the primary cells of the immune system that invading microbes initially encounter. Pathogens are recognised via numerous pattern recognition receptors (PRR) specific for unique pathogen-associated molecular patterns (PAMP) [320]. The macrophage mannose receptor, for example, recognises certain sugars found on the surface of many bacteria and viruses [321]; Toll-like receptors (TLR) recognise bacterial lipopeptides and peptidoglycans such as bacterial lipopolysaccharide (LPS) [322]; and RIG-I like receptors (RLR) recognise cytosolic antigen such as viral double-stranded RNA [320, 323]. Stimulation of PRRs can trigger phagocytosis (the process of particle internalisation by a cell) directly or can activate signalling cascades that trigger gene expression and production of cytokines and chemokines that tailor the host immune response specificity to that of the pathogenic threat [324]. Phagocytosed microbes are internalised and destroyed using a repertoire of anti-microbial effector mechanisms, including oxidation and enzymatic degradation [325]. The antigen is presented in both

soluble and digested form to B-cells [326] and T-cells [327, 328], respectively, which in the presence of additional cytokine stimulation, amplifies the adaptive immune response.

Macrophages are central effectors of the IFN system, a major cytokine defence array of the innate immune system vital to the control of diverse viral pathogens [329]. The system is activated by PAMPs that trigger intracellular or cell surface PRRs resulting in a signalling cascade that comprises the stimulation of interferon regulatory factors (IRF) and, ultimately, the expression of IFNs [330]. IFN proteins are effective in both autocrine and paracrine capacities [329]. Activation of the IFN receptor triggers a further signalling cascade involving activation of the JAK-STAT signalling pathway and, consequently, the transcription of interferon-stimulated genes (ISG). ISG transcription can result both in the de novo production of proteins, the upregulation of constitutively expressed antiviral factors as well as the expression of IFNs, the latter thus expanding the immune response [329-331]. In HIV-1 infection, ISG induction has been reported to be dual-phasic, with an initial phase 0-24 hrs post-infection due primarily to non-pathogen associated extracellular vesicle constituents, and a subsequent phase >48 hrs post-infection intimately associated with de novo synthesis of HIV-1 mRNA [332]. ISGs can function broadly, for example, by regulation of cellular growth or apoptosis and thus affecting a range or potential viral families or with high specificities, such as the recognition of protein lattices of individual species viral cores [333].

A subset of ISGs, known as restriction factors, have been shown to have very specific and potent antagonistic activity against several viruses, including HIV. In response, some viruses encode proteins that specifically neutralise restriction factors in addition to the core viral replicative machinery, termed accessory proteins [174, 334]. As previously discussed, the most extensively studied restriction factors to date are Tetherin, APOBEG3G, Trim5α and SAMHD1 (refer to Section 1.1.5 Restriction factors).

1.3.4 Ontogenesis

In the mouse, macrophages arise from three distinct lineages that are temporally segregated during development (Figure 1.12). The initial stage is primitive hematopoiesis and the production of macrophages that develop both from an uncommitted progenitor and without an immediate monocyte precursor, in blood islands of the yolk sac at approximately day 7 [335, 336]. Yolk sac derived macrophage progenitors migrate to populate the brain and throughout embryonic tissues where they expand, differentiate, and mature, maintained into adult life via continual self-renewal [337-342]. Seeding of the foetal liver (FL) by yolk sac derived committed myeloid progenitors initiates the production of a second lineage of macrophages, a definitive hematopoiesis. The liver is then the source of definitive hematopoiesis for macrophages destined for residence in the endothelium and for monocytes during embryogenesis. FL derived macrophage precursors migrate and become resident in all tissues where they expand and differentiate into macrophages [343, 344]. The third lineage of macrophages arises from the bone marrow via definitive hematopoiesis of hematopoietic stem cells seeded from the aorta-gonadal-mesonephros embryonic region. Bone marrow definitive hematopoiesis replaces that of the liver and is the source of many macrophage subsets, most dendritic cells, and all circulating blood monocytes. In contrast to yolk sack and liver-derived macrophages, bone marrow lineage macrophages are derived from monocyte precursors. These macrophages expand to populate all tissues with particularly high densities in areas of high turnover, such as the gut. Bone marrow-derived macrophages subsequently provide a constant supply via circulating monocytes to replace or reinforce macrophages of all lineages in response to structural damage or disease [283, 344, 345].

The accuracy with which the murine macrophage ontogenic system maps onto that observed in humans has been difficult to evaluate due to the operational and moral challenges surrounding experimentation with human embryos. However, macrophage self-renewal has been observed *in vivo* in a study

investigating human hand allograph where Langerhans cells were shown to be of donor origin over ten years post-transplant [346].

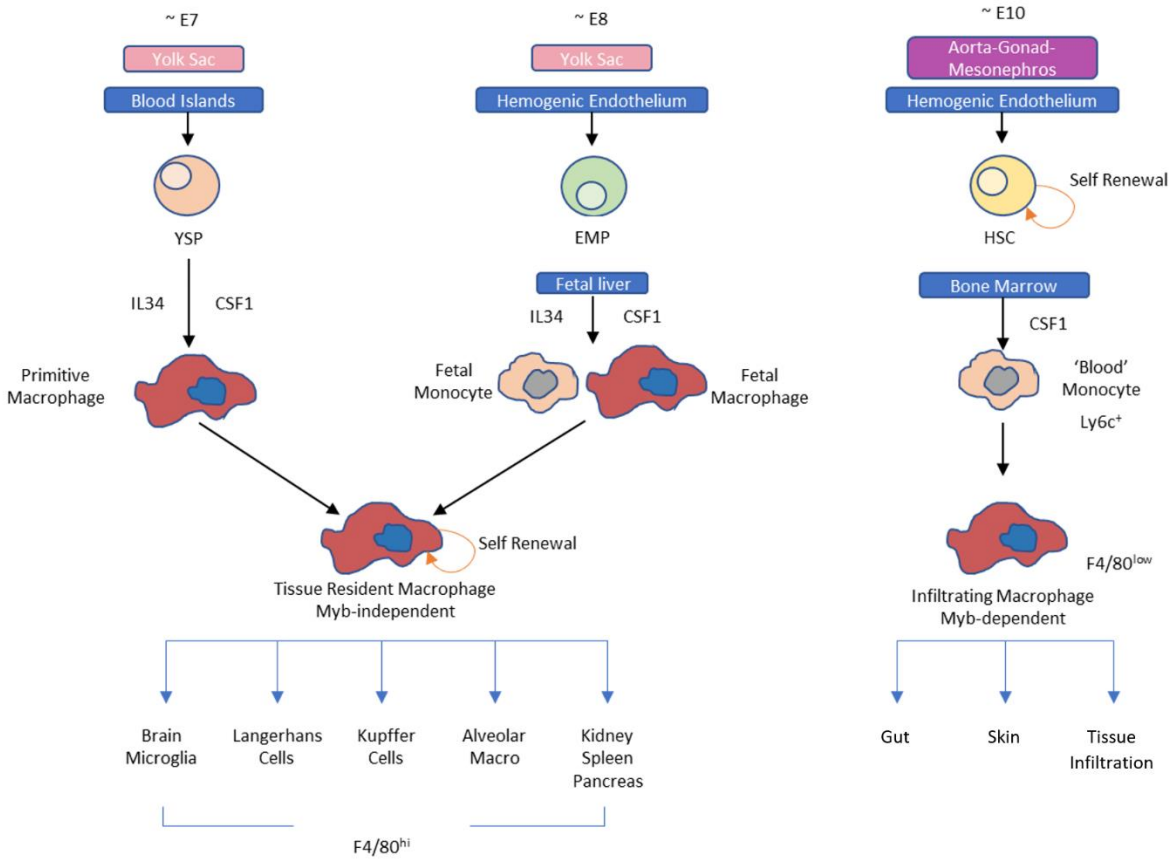


Figure 1.12 Myeloid lineages in the mouse.

Macrophages arise from three distinct, temporally segregated lineages. The first lineage arises from yolk sac progenitors (YSP) that emerge from extraembryonic membranes at E7 days post coitum. These primitive macrophages migrate to populate the brain and other tissues where they mature into tissue-resident macrophages. A second lineage arises from the foetal liver, which is seeded by erythroid-myeloid progenitors (EMP), also derived from the yolk sac. Monocytes, in addition to macrophages, emerge from this lineage. Descendants migrate and become resident self-renewing macrophages in multiple tissues. The third wave of hematopoiesis results in the emergence of hematopoietic stem cells (HSC) from the aorta-gonad-mesonephros (AGM), which subsequently seed the bone marrow. HSCs differentiate into monocytes and, ultimately, macrophages. This lineage subsequently becomes the sole replenishment source for sites devoid of self-renewing macrophages such as the gut or to replace self-renewing macrophages depleted due to injury or disease. Adapted from [282, 283]

1.3.5 Differentiation

In humans and the mouse, three main growth factors regulate macrophage differentiation: Macrophage colony-stimulating factor (M-CSF; also known as CSF1), Granular Macrophage colony-stimulating factor (GM-CSF; also known as CSF2), and interleukin-3 (IL-3) [283, 347-349]. M-CSF is produced constitutively by a wide range of cells, including macrophages, and in the steady-state circulates at approximately 10ng/mL [350]. Studies examining circulating M-CSF rescue in M-CSF knockout mice have revealed that circulating M-CSF exclusively regulates cells bearing the murine macrophage marker F4/F8 in the liver, kidney, and spleen and partially regulates these cells in the bone marrow, salivary gland, bladder, dermis and a macrophage subset in the gut [351]. Circulating M-CSF is, however, dispensable for several subsets of tissue-resident macrophages, including those of the gut epithelia, adrenals, synovial membrane, periosteum, tendon, and muscle which are instead sustained by M-CSF produced locally [352]. M-CSF stimulates the migration of blood monocytes from the bone marrow [353], regulates tissue-resident macrophage numbers by control of macrophage survival [350], and supports self-renewal of some tissue-resident cells [354-356]. M-CSF stimulated macrophages display an anti-inflammatory activation signature characterised in part by the expression of IL-10 at high levels.

Langerhans cells, microglia, and alveolar macrophages differentiate and are sustained in the steady-state, independently of both circulating and locally produced M-CSF. Instead, Langerhans cells and microglia are stimulated by the alternative ligand of CSFR1 interaction with interleukin 34 (IL-34), which is delivered to these cells via secretion from keratinocytes and neurons, respectively [281, 357]. Alveolar macrophages in both humans and mice are dependent on GM-CSF for maturation and differentiation [358, 359]. GM-CSF is a key regulator of granulocyte and subsets of macrophage differentiation [360]. In the steady-state, GM-CSF circulates at low levels, is produced by a number of cells in response to inflammation, and can be induced by cytokines such as IL-1B, IL-23, and IL-12 or suppressed by IL-4, and IFNγ [361-367]. GM-CSF has a proinflammatory activating signature, enhancing the survival of myeloid lineage cells recruited to sites of trauma and infection [358, 368].

In vitro, both M-CSF and GM-CSF are able to effect the differentiation of bone marrow-derived monocytes into macrophages [369] termed monocyte-derived macrophages (MDM). Phenotypic investigation of MDMs differentiated *in vitro* using M-CSF exhibit functional characteristics observed in peritoneal anti-inflammatory polarised macrophages *in vivo* [370]. In a comparison of human-derived peritoneal macrophages and MDMs, it was shown that both have the ability to produce large amounts of IL-10 on stimulation with LPS and are active in endocytosis and phagocytosis of early apoptotic cells [370, 371]. Furthermore, human peritoneal macrophages show high and comparable levels of CD14 and CD16 expression as well as CD163, which is not expressed on pro-inflammatory polarised macrophages [371]. Peritoneal macrophages and MDMs also exhibit comparable activity in allogenic T-cell activation [371].

In contrast, the phenotype of GM-CSF MDMs maps more accurately to that observed with human alveolar macrophages, a macrophage subset with a defined pro-inflammatory phenotype [372]. Alveolar macrophages and GM-CSF differentiated MDMs express similar levels of CD14 and CD71, are morphologically spherical with a domed central region, and are resistant to H_2O_2 [372]. Both M-CSF and GM-CSF MDMs express CD14, CD16, and CD11b and mediate antibody-dependent cellular cytotoxicity [369] (Table 1.4). Due to the high degree of phenotypic similarity between *in vitro* produced M-CSF and GM-CSF dependent macrophages and *in vivo* anti-inflammatory and pro-inflammatory macrophages, respectively, MDMs are generally regarded as a good tool for investigative microbiological research and have thus been used extensively in molecular experimental research in multiple fields.

Recent refinements of stem cell differentiation protocols now allow the efficient production of macrophages *in vitro* from embryonic stem (es) cells or induced pluripotent stem (iPS) cells. Es cells are derived from undifferentiated inner mass pluripotent cells of a human blastocyst (embryo) [373, 374]. iPS cells are created *in vitro* by expressing pluripotency inducing transcription factors in human fibroblasts, usually from transient viral vectors [375, 376]. The stem cell-derived macrophage

differentiation protocol involves the induction of macrophage precursor differentiation using M-CSF and IL3 from embryogenic embryoid body aggregates composed of all three germ layers, that emerge from stem cell precursors. M-CSF is then applied in isolation to stimulate macrophage-precursor differentiation into macrophages [5, 377]. Elegant work using CRISPR-Cas9 knockout of the differentiation transcription factor Myb has shown that these cells differentiate in a manner independent of Myb [4, 282]. Our understanding of macrophage ontology in the mouse has revealed that Myb-independent macrophage differentiation is a feature of tissue-resident, self-renewing macrophages such as Langerhans cells, Kupfer cells and microglia derived from the yolk sac [339, 378]. These cells are therefore defined in this thesis as stem cell origin yolk sac derived-like macrophages (scYDM) in general, esYDMs if originated from es cells or ipsYDMs if originated from iPs cells. scYDMs have been extensively characterised and shown to express similar levels of CD14, CD16, and CD168 to blood MDMs [377] (Table 1.4). The developmental similarity of esYDMs and ipsYDMs to tissue-resident macrophages suggests they may represent a good model for molecular investigations that have historically proved challenging due to the technical barriers in accessing sufficient quantities of primary cells (e.g., macrophages of the liver (Kupfer cells) and the brain (microglia)).

Phenotype	Monocyte	Inflammatory Macrophage	Intestinal Macrophage	Microglia	scYDM
CD14	+	+	Low	+	+
CD16	- (subset)	+	-	+	+
CD45	+	+	+	+	+
CD11b	+	+	-	+	+
CD4	+	+	Low	+	+
CCR5	+	+	-	+	+
CXCR4	+	+	-	+	+

Table 1.4 Comparison of monocyte and multi-lineage macrophage cell surface receptors.

Table showing receptor expression of monocytes and macrophage subsets. Monocytes can be divided into two groups, of which 85-90% stain negative for CD16 and 10-15% stain positive for CD16. [265, 282, 377, 379-386].

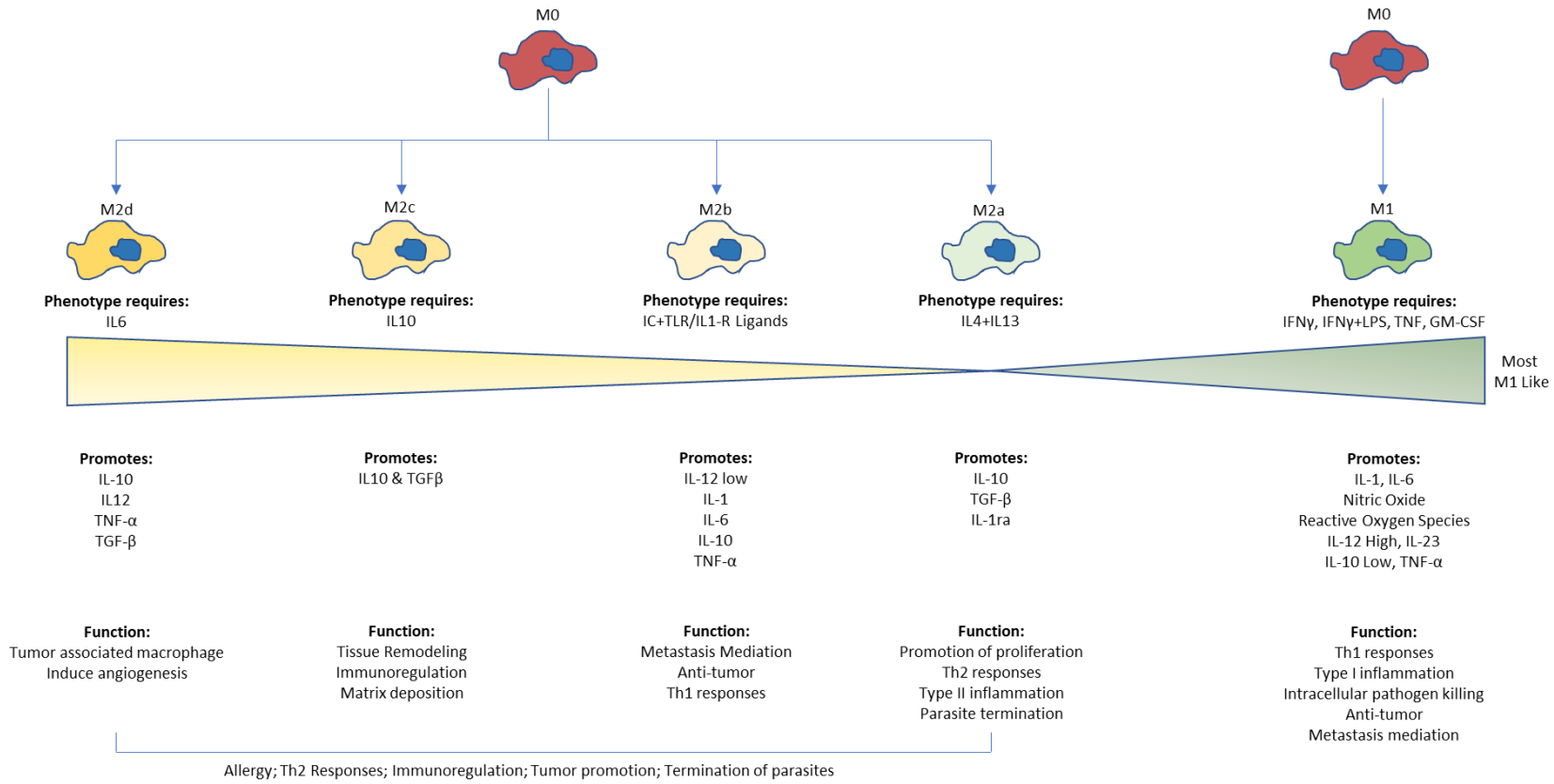


Figure 1.13 Macrophage polarisation continuum

Schematic diagram showing categorisation of macrophage subsets in relation to polarisation and activation phenotypes. A detailed description can be found in Section 1.3.6 Activation and polarisation. Adapted from [6, 7].

1.3.6 Activation and polarisation

Macrophages display a vast array of phenotypes and functions which are acquired and specialised in response to the surrounding environment in a lineage independent manner [387]. Macrophage activation occurs in response to PAMPs, damage-associated molecular patterns (DAMPs), or in response to cytokines, such as type I IFNs, secreted from immune effector cells intrinsic to the amplification of an adaptive immune response [319]. The generally accepted approach to discrete categorisation of activated macrophage subpopulations is the M0, M1, and M2 polarisation nomenclature, which represent 'un-activated,' 'classically activated,' and 'alternatively activated' macrophages, respectively [388, 389] (Figure 1.13). M1 activation occurs upon stimulation with IFNγ in isolation, IFNγ combined with microbial activators (e.g., LPS) or cytokines (e.g., TNFα, GM-CSF). M1 macrophages characteristically display enhanced phagocytosis, an increased capacity for antigen presentation, and secrete high levels of IL-12, the latter stimulating Th1 polarisation of CD4+ T cells. M1 polarised macrophages secrete high levels of pro-inflammatory cytokines such as IL-23, IL-15, IL-1β, and TNFα and have a high capacity for the production of reactive oxygen intermediates (ROS) and nitric oxide synthase (NOS) [389-392]. M1 macrophages, therefore, constitute a potent anti-microbial defence, either directly via the phagocytosis of microbes or indirectly via the priming of additional innate and adaptive immune system effectors.

M2 macrophages differentiate in response to multiple stimuli, including IL-4, IL-13, immunoglobulin complexes, and glucocorticoids [391, 392]. The M2 phenotype is anti-inflammatory, defined by secretion of large amounts of IL-10, downregulation of IL-12 and IL-23 expression, and mediation of adaptive Th2 polarisation of CD4+ T cells. M2 macrophages also mediate extracellular matrix tissue remodelling and are functional in angiogenesis and tumour progression. M2 macrophages can subsequently be subdivided into four further groups M2a, M2b, M2c, and M2d. M2a subtype macrophages differentiate in response to IL-4 and IL-13 and are characterised by reduced production of pro-inflammatory cytokines such as IL-12 and IFNγ, downregulation of surface receptors such as CD4

and CCR5, mediation of fibrogenesis and tissue repair, and promotion of proliferation [391, 392]. M2b subtype macrophages differentiate in response to immunogens plus LPS or IL-1R and are characterised by a Th2 skewed secretion profile, high expression of IL-10, and low expression of IL-12 [393, 394]. M2c subtype macrophages differentiate in response to TGF-β, IL-10 or glucocorticoids and are defined by increased phagocytosis and reduced production of pro-inflammatory cytokines [392, 395, 396]. M2d subtype macrophages are TAMs, which secrete IL-10, IL-12, TNFα, and TGFβ. This macrophage subtype actively supports tumor growth and progression [6].

1.3.7 Macrophages and HIV

In keeping with the vast array of macrophage subtypes and phenotypes found within the mammalian organism, dynamics of HIV-1 infection of macrophages is a complex phenomenon dependent not only on the location and polarisation of macrophage subsets but also on the systemic effects of disease progression at any given point in time. For example, in the steady-state, gut-associated macrophages of the colon are relatively resistant to HIV-1 infection, whereas macrophages of the rectum, also of the gut, are permissive [397]. Gut-associated macrophages are of bone marrow-derived blood monocyte origin, and additional studies of these cells have indicated that steady-state permissiveness can be reduced by subsequent M1 and M2 polarisation, states often observed in response to tissue damage or infection [398]. Furthermore, macrophage subsets that are inherently refractory to HIV-1 infection during the acute disease phase, such as lymphoid macrophages, may then become sites of major virus production during late-stage disease [399]. The complexity of macrophage-HIV dynamics has been a major hindrance to investigative microbiological research further exacerbated by the difficulty in obtaining tissue samples from key locations such as the CNS, from HIV-1 infected or uninfected individuals. Study of HIV-1 dynamics in tissue-resident macrophages is important since, as previously discussed, recent advances in our understanding of macrophage ontology have revealed the existence of two distinct macrophage lineages in addition to macrophages of bone marrow-derived blood lineage that has historically been used for the majority of primary cell focussed HIV investigations to date.

Macrophages harbouring HIV-1 DNA or RNA and thus deemed 'infected' have been isolated at various stages of disease in the brain [400], lungs [401, 402], skin [403-406], liver [407], gut [408] and lymphoid tissue [399]. Infected macrophages are relatively resistant to not only cytotoxic effects of viral replication [409] but also to CD8+ T-cell mediated killing [410]. In addition, HIV-1 has evolved mechanisms to enhance the longevity of infected macrophages [409] as well as induce the production of chemokines designed to attract CD4+T-cells and other macrophages [411], thus increasing the probability of infection and viral spread. During the acute and chronic phases of HIV-1 disease, macrophages appear sparsely infected, which persists in the presence of highly active antiretroviral therapy (HAART) [412-414]. However, analysis of tissue extracted pre and post mortem from AIDS patients shows that macrophages become a major source of productive infection during this stage of the disease [400], which can, in turn, be further amplified in the presence of opportunistic infections [399].

1.3.7.1 Tropism

The adaptation of HIV-1 to successfully enter and replicate within a given cell population, defined as tropism, is determined in part by post-entry blocks to infection but primarily by HIV-1 env mediated attachment and fusion events with target cells [415-418]. Macrophage cell surface CD4 density is far lower than that observed with CD4+ T-cells, and thus, the most significant adaptation macrophage-tropic HIV-1 strains evolve is an enhanced ability to use low CD4 density to facilitate fusion [419-421]. Hence, the CD4 density requirement for infection can be considered an unequivocal indicator of HIV-1 cellular tropism [418]. Multiple studies have mapped HIV-1 tropicity to polymorphic affinity adaptations and interactions of the HIV-1 env glycoprotein gp120 [422, 423] for the host receptor CD4 [415] and chemokine co-receptor CCR5 [415, 416]. Several positions within the V3 loop of gp120 have been implicated in dictating tropism in this regard [424], and more recently, accessibility of a key antibody binding motif within the V4 region has been proposed as a major driver toward macrophage tropism [415]. Macrophage tropic (M-Tropic) strains appear to have this region exposed, whereas CD4+ T-cell

tropic (T-Tropic) strains do not, thus implicating antibody escape as a potential evolutionary pressure [415]. Indeed, in acute and chronic infection, M-Tropic HIV-1 is largely confined to the CNS, an immune-privileged niche exhibiting notable reduced immune activation and antibody concentrations compared to all other anatomical sites [420, 425]. Furthermore, evidence suggests that whilst CD4+ T-cell tropism is driven by selective pressures unique to a given individual, macrophage tropism associated polymorphisms are homogenous across individuals [417], which can be interpreted as the existence and absence of antibody-mediated evolutionary pressure, respectively.

HIV-1 isolates that require CCR5, CXCR4, or can use either, have been identified for both M-tropic and T-tropic viruses, and thus, coreceptor usage is deemed an unreliable predictor of tropism [410, 411, 415-420, 422, 426-428]. However, while M-tropic CXCR4 viruses have been identified, the vast majority of M-tropic HIV-1 isolates use CCR5 [429, 430]. Evidence from *in vitro* infection of primary MDMs implies that so-called transmitter-founder viruses are weakly macrophage-tropic, suggesting that plasma membrane fusion mediated infection of macrophages is not the primary objective for HIV-1 during initial infection [431]. Macrophage tropism then appears to evolve via several intermediary 'dual tropic' steps [418] from T-tropic CCR5 viruses, most likely within the CNS [425]. During AIDS, M-Tropic HIV-1 strains have been isolated throughout the body [11, 421, 432, 433]; however, the details of the evolutionary pathway permitting the emergence of these species remain to be defined.

1.3.7.2 HIV-1 Infection of macrophages

Compared to cycling CD4+ T-cells (the primary HIV-1 target cell), macrophages (and monocytes) are refractory to HIV-1 infection, requiring high titres of laboratory-adapted HIV-1 to establish infection *in vitro* (unpublished lab data)[434]. Observations *in vivo* suggest that both monocytes [435] and macrophages harbour replication-competent provirus, and furthermore that macrophages are major sites of viral production during AIDS [11]. This implies that *in vivo* high titres of HIV-1 may be necessary to establish infection. The low efficiency of cell-free HIV-1 infection of macrophages observed *in vitro*

is likely exacerbated *in vivo* by the presence of innate and adaptive immunity, with the humoral derivative of the latter presenting physical barriers, by way of antibodies, between infectious virions and target cells. It is possible that these challenges can partly be overcome by tropic adaptations as detailed above but only in subservience to humoral immunity. A strategic adaptation that negates these pressures entirely is infection transmission, cell-to-cell.

An obvious cellular candidate to infect macrophages is CD4+ T-cells, and indeed, recent investigations have provided evidence supporting cell-to-cell spread from CD4+ T-cells to MDMs [436]. Transmission in this regard is dependent on HIV-1 env, requiring the expression of CD4 and CCR5 on target cells. Contact between infected CD4+ T-cell and non-infected MDMs is succeeded by membrane fusion and swift relocation of viral replication components to the MDM cytoplasm. Transmission via this method is rapid and extremely potent, indeed MDMs infected in this manner can begin producing viable virions as early as 6 hrs post CD4+ T-cell fusion [436].

In addition to cell-to-cell fusion mediated HIV-1 infection, macrophages can also be infected via phagocytosis of HIV-1 infected dead or dying CD4+ T-cells [437]. Interestingly, this interaction is also dependent on HIV-1 env, and CCR5, since CCR5 negative MDMs were resistant to infection by this route and phagocytosed CD4+ T-cells infected with HIV-1 CXCR4 using virus, was unable to initiate infection in MDMs. Discovery of this mechanism raised the fundamental question of whether macrophages *in vivo* are indeed infected with replication-competent virus at all since any macrophage associated HIV-1 DNA detected may be remnants from phagocytosed HIV-1 infected CD4+ T-cells. Certainly, in AIDS, macrophages are associated with high virion densities, and virions have consistently been imaged (via electron microscopy) budding from macrophage membranes into apparently intracellular vesicular structures [11, 399, 438]. Recent advances in the assays used to interrogate the nature of HIV-1 proviral DNA are certainly assisting in answering this question [387, 439]. However, at present, during the acute and chronic phases of disease at least, insufficient data exists from which to draw a definitive conclusion.

1.3.7.3 HIV-1 Infection from macrophages

Evidence from investigations of macrophages productively infected *in vitro* shows that when macrophages *are* infected, viral replication mediated cytopathic effects are diminished, and cells can produce infectious virus for a significant period [409]. Maturing virions bud almost exclusively from the plasma membrane and are either released into the extracellular medium or collect in intracellular plasma membrane-connected compartments (IPMC), also referred to as virus-containing compartments (VCC), within which virus can remain viable for several weeks [440-442]. VCCs were previously thought to be endosomal entities; however, the current consensus is that VCCs are contiguous with the cell surface membrane [440, 443-445]. VCCs are believed to be the driving force underlying cell-to-cell MDM to CD4+ T-cell transfer of HIV-1 by virtue of being a major constituent of the virological synapse (VS) [442, 446]. The VS is a junction between infected MDMs and uninfected CD4+ T-cells at which mature HIV-1 virions aggregate [442, 445, 447-449]. CD4+ T-cells have been shown to preferentially bind to macrophages at sites close to VCCs. CD4+ T-cell attachment triggers the rapid migration of the VCCs to the attachment site, virion release, and subsequent infection of the CD4+ T-cell [446]. Macrophages are potent transmitters of virus to CD4+ T-cells, and a large body of evidence suggests that cell-to-cell transmission is significantly more effective than cell-free transmission [440-443, 445, 447-453]. In addition to the VS, nanotubule mediated dissemination has also been implicated in facilitating MDM cell-to-cell transfer of HIV-1 [454]. HIV-1 infected macrophages have been shown to produce long tubules that connect with neighbouring cells within which HIV can pass via a mechanism that appears to involve HIV-1 Nef and the cellular protein M-sec [451]. Whist all macrophages produce such tubules; a greater incidence is reported to occur with HIV-1 infected cells [451, 454].

1.3.7.4 Macrophages as reservoirs

In the context of HIV-1 infection, the term viral reservoir is used to describe a population of cells that harbour HIV-1 provirus in a transcriptionally silent, latent state from which progeny can emerge after a protracted period. The silent nature of the provirus genome masks the infected status of the host cell

from extracellular immune surveillance as well as the diminishing effects of pharmacological inhibitors [455]. Viral reservoirs persist in the face of innate immunity, adaptive immunity, and HAART and are vital for sustained viral persistence *in vivo* [456]; however, the entirety and scope of this phenomenon has yet to be described. Hence, viral reservoirs represent a major frustration in the development of HIV curative strategies [456-458].

There are many attributes of HIV-1-macrophage biology that implicate macrophages as a reservoir cell type for HIV-1. For example, latency, by definition, requires host cell longevity, and in a non-infected state, macrophages, particularly of the CNS, can be very long-lived [459]. Moreover, and as previously described, in infected macrophages, HIV-1 has evolved mechanisms to prolong the lifespan of these cells [409]. These factors, combined with the reported resistance of infected macrophages to the cytopathic effects of viral replication [409], cytotoxic CD8+ T-cell mediated killing [460], and the colonisation of pharmacological sanctuaries [461], suggest that macrophages can be sites of sustained viral production for extended periods in an infected host. Indeed, proviral DNA has been isolated from blood monocytes and macrophages [435, 462], macrophages of the CNS [463], the lungs [401, 464], the gut [465], and lymphoid tissue [465], extracted from patients receiving long term HAART. However, whether these instances of integrated proviruses are from a previously latent (of significant duration) myeloid source and thus constitute a true myeloid viral reservoir, or whether they represent fresh infections from other cell types or viral reservoirs, remains to be defined [445]. Certainly, *in vitro,* HIV-1 infection, establishment of latency, and reactivation of latent provirus in human primary foetal microglia and MDMs [409] has been observed, and in AIDS, in the absence of CD4+ T-cells, macrophages are well established as the source of high titre virus production, as previously described [11]. However, data from clinical observations show that, for the CNS at least, in the absence of continual reseeding, CNS macrophages are functional in clearance of HIV-1 infection, even after a significant period of active viral replication in the absence of HAART [466, 467]. This observation argues against macrophages constituting a viral reservoir and offers potential clues to the conditions required for viremic resolution.

1.4 Gene Editing

Targeted genetic sequence manipulation (gene editing) is a rapidly evolving toolkit that facilitates the alteration of essentially any sequence coded within DNA. Current techniques rely mainly on engineered nucleases, which once targeted to the sequence of interest cleave single or both strands of DNA. In eukaryotes, double-stranded DNA breaks are repaired by one of two pathways: non-homologous end joining (NHEJ) [468] or homology-directed repair (HDR) [469-471]; exploitation of these pathways allows the introduction of targeted genome alterations of potentially any cell type or organism [472]. HDR driven gene editing can facilitate the introduction of unique sequences, for example, the addition of a reporter protein to an endogenously expressed gene [473] or repair of genetic defects [474]. HDR driven gene-editing utilises a 'donor template' which can be either single-stranded DNA (ssDNA) or double-stranded DNA (dsDNA), exogenously applied, to direct recombination at the desired locus [475]. In contrast, ligation of DNA strands by NHEJ occurs irrespective of strand sequence homology; consequently, insertions or deletions (indels) of varying sizes can be introduced at the cut site. Larger indels can also be induced by NHEJ directed repair of simultaneous cleavage by multiple nucleases at a given locus [476]. Both small and large indels can disrupt translation by translocating the sequence downstream of the indels, out of frame. This results in the destruction of the translated mRNA via non-sense mediated decay (NMD), knocking-out (knockout) the gene of interest [477-479].

1.4.1. Meganucleases

Nuclease mediated targeted genetic engineering originated with the use of meganucleases, restriction enzymes engineered to recognise larger DNA sequences (14-40bp) than WT counterparts. [480-482]. The dynamics of meganucleases are such that active and recognition sites are closely associated [483]. Retargeting, hence, is extremely challenging, and thus, target variability is limited [484]. Nevertheless, meganucleases were used successfully for gene editing in yeast [480], fish [485-488], frogs [489, 490], and the sea urchin [491].

Second-generation gene-editing nucleases, Zinc-finger nucleases (ZFN), and Transcription activator-like effectors nucleases (TALENs) are engineered fusions between a protein-based-DNA targeting domain and the bacterial type IIS restriction endonuclease FokI [492, 493]. Separation of the DNA binding (TALE or ZF-protein) and the nuclease domain (FokI) permitted greater flexibility in the manipulation of either domain [494, 495]. This, combined with the modularity of protein-based arrays for DNA recognition [495-497], effectively made the targeting of any DNA sequence possible.

1.4.2 Zinc finger nucleases and Transcription activator-like effectors nucleases

Zinc-finger nucleases (ZFN) are engineered such that the Zinc-finger protein (ZFP), a eukaryotic transcription factor, is fused to the FokI restriction enzyme [498]. The ZFP constitutes a tandem array of Cys_2-His_2 fingers; each finger recognises approximately 3bp of DNA [499]. Thus, a combination of 4 fingers would allow targeting of a sequence 12bp long. Similar to ZFP, TALEN's are transcription regulator proteins, which are fused to the FokI restriction enzyme [500, 501]. TALE's are of bacterial origin, and function to manipulate gene transcription in the bacteria's plant hosts such that it is more favourable for colonisation [502]. Structurally, TALEs constitute a highly conserved array of repeat domains, each repeat unit of 33-35 amino acids recognising a single base pair of DNA [503]. A simple cypher, determined by the relationship between a TALE's preferred target base and its successive repeat variable di-residue, allows the construction of TALE arrays for the targeting of novel DNA sequences [495, 503].

FokI enzymes must dimerise in order to become catalytically active[504]. Dimerization is dependent on the presence of sequence-specific DNA, which drives the correct alignment of the monomeric FokI catalytic cores [504]. The requirement of two DNA binding events enables targeting of longer sequences, which, combined with heterodimer dependent cleavage of FokI mutants [505, 506], enhances the specificity of both ZFN and TALEN's for their target sequences. Sequence specificity, unrestricted targeting, and the ability to be expressed in the vast majority of organisms are clear

advantages of ZFP and TALENs. As a result, ZFP and TALENs have been used to alter genomes of bacteria [507, 508], yeast [509, 510], insects [511], amphibians [512, 513], fish [514, 515], lower mammals [516, 517] and humans [518, 519].

Construction of the DNA binding domains for both ZFP and TALENs, whilst optimised and streamlined by several groups, is still financially and technically challenging and, therefore, a barrier to widespread adoption of the techniques. Third-generation gene-editing toolkits, such as the CRISPR- Cas9 system, have overcome this problem via the use of RNA as the DNA targeting mechanism [520]. RNA based DNA binding modules are very simple to synthesise, reducing both the complexity of the experimental procedure required and financial burdens.

1.4.3 CRISPR- Cas9

CRISPR (Clustered Regularly Interspaced Short Palindromic Repeat) is a nucleic-acid based system of acquired immunity to defend against viruses, bacteriophages and plasmids, and other mobile genetic elements, found in bacteria and most archaea [521-523]. CRISPR *loci* tend to be located next to *cas* genes (CRISPR-associated) and are typically structured such that stretches of variable sequences (of viral and plasmid origin) are separated by regular non-contiguous direct repeats. Combined CRISPR and Cas proteins result in the CRISPR- Cas system [524].

CRISPR- Cas immunity functions mechanistically by recognising and degrading DNA and RNA encoded by exogenous or endogenous alien entities [525]. Invading or mobile nucleic elements are recognised, processed into short DNA sequences, joined to a non-contiguous sequence of direct repeats, and incorporated into the CRISPR array at the leader end [525, 526]. The CRISPR array thus represents a working immunological 'memory' where a combination of all the incorporated variable sequences corresponds to a history of the alien elements that the microbe has encountered [527]. The array does not grow indefinitely, and while it is clear that alien elements can be removed from the array, it is as yet unclear whether this is the only mechanism available to restrict the size of the array [526].

Transcription from the CRISPR promoter results in a single RNA (pre-crRNA) containing all spacers and repeats (representing the CRISPR array), mRNAs transcribed from the adjacent (or sometimes flanking) *cas* genes and CRISPR associated effector RNAs (e.g., transactivation CRISPR RNA - tracrRNA) [528]. Translation of the *cas* genes results in effector CRISPR associated proteins tasked with surveillance and interference, such as the nuclease Cas9 [529]. In type II systems, mature CRISPR RNAs (crRNAs), consist of a spacer region flanked by repeat derived sequences (protospacer), and are produced by processing of the pre-crRNA by host ribonucleases [530]. The processed crRNA hybridises to the tracrRNA and is loaded into the Cas9 complex, causing a conformational change in Cas9 that produces a groove capable of scanning genomic DNA [529]. The hybridised crRNA & tracrRNA recognise target sequences via complementary Watson-Crick base pairing [531]. The Cas9 enzyme will only cleave DNA if the target sequence is located immediately 5' of a protospacer adjacent motif (PAM), which, for the Cas9 enzyme of *Streptococcus pyogenes* is 5'NNG [531]. The PAM motif assists the CRISPR- Cas machinery in distinguishing self from non-self, lack of the PAM motif in the CRISPR array (which would have spacer sequences identical to those targeted by the protospacer crRNA) ensures the host genome is not cleaved. Once recognised, the foreign genetic material is cleaved by the Cas9 nuclease and ultimately degraded [531-533].

Two independent endonuclease domains, HNH and RucV, make up the Cas9 protein, each cleaving one strand of DNA only. The HNH-like homologous endonuclease cleaves the strand complementary to the crRNA, while the RucV-like domain bearing nuclease cleaves the non-complementary DNA strand [527, 532].

The system detailed above for the type II CRISPR system from *S. pyrogenes* has been adapted for genome engineering [531] and further optimised for gene editing in human cells [534]. The process requires duel expression of only two elements: the Cas9 protein and a guide RNA (gRNA), which is a fusion of 20nt of the protospacer and a truncated form of a fixed tracrRNA. This system can, therefore,

target any nucleotide sequence of the form N20-NGG and can be re-targeted simply by altering the first 20nt of the gRNA [535]. In addition to gene editing in human cells [474, 535-544], this system has been used to successfully edit the genomes of tobacco [545], rice [546], fish [545, 547-554], flies [555], mice [556-558] and rats [559].

When the CRISPR- Cas9 system is used in its native form, the non-specific nature of CRISPR- Cas9 manifests as unwanted off-target effects [560]. Early investigations determined that off-target effects arise primarily from the pairing of the guide RNA to other loci in the genome with close homology to the target sequence [561]. Thus, bioinformatics tools were developed to predict the location of off-target effects. The genome of the organism in question would be compared to the target sequence, and homologous sequences scored depending on the number of mismatched nucleotides [562]. It has since been shown that Cas9 can bind and cleave with up to six mismatched bases [563], greatly increasing the number of potential off-target cleavage events.

Among the several approaches that have arisen to address the issue of Cas9 specificity, protein engineering of the Cas9 enzyme was among the first to be developed. Structural information of the two enzyme domains of Cas9 identified a single point mutation D10A, which resulted in deactivation of the RuvC domain. D10A mutants are only able to cleave a single strand of DNA complementary to gRNA and hence were termed 'nickases'. Nickase pairs cleaving at appropriate distances and orientation execute efficient indel formation, and the requirement for paired guides facilitated improvements in specificity in the order of 1,500 fold compared to wild type Cas9 nucleases [476, 564, 565]. Alternatively, catalytically inactive Cas9, facilitated by mutation of the Huv domain, have been fused with FokI nucleases, thus inferring the increased specificity associated with FokI dimerization, inherent with ZFNs and TALENs, to the Cas9 system [566]. More recently, 'high specificity' Cas9 proteins have been developed by manipulation of residues in the non-targeting DNA strand groove and later, residues

that interact with the phosphate backbone of the targeted DNA strand. The approaches show large reductions in off-target effects with only minor detriment to binding at the target sites.

1.5 Thesis Propositum

The main objective of this thesis is to investigate the activity of the HIV-1 restriction factor SAMHD1 in human stem cell-derived macrophages. These macrophages have been shown to represent a good model for tissue-resident macrophages by virtue of similarities in developmental characteristics. The activity of SAMHD1 retroviral restriction in primary tissue-resident macrophages such as microglia and kidney macrophages is not well described primarily due to difficulties in obtaining primary samples in significant quantities. Since the phenotype of HIV-1 restriction in macrophages has been shown to vary depending on the macrophage subpopulation and resident microenvironment, it is possible that phenotypes in tissue-resident macrophages may differ to those documented for blood macrophages which are of a different development lineage. Understanding HIV-1 dynamics in such a large and yet distinct population as tissue-resident macrophages may reveal novel insights that can assist in addressing some of the unanswered questions regarding HIV-1 pathogenesis. The working hypothesis of this thesis is that esYDMs will exhibit a SAMHD1-dependent HIV-1 restrictive phenotype that is less sensitive than that observed in blood MDMs, as has been documented in other yolk sac origin macrophages, such as microglia [567]. SAMHD1 is first characterised in human stem cell-derived macrophages, then I use a loss of function strategy where SAMHD1 is knocked down by shRNA, knocked out by CRISPR- Cas9 gene editing, or degraded by the SIV accessory protein Vpx. Loss of function is quantified by the resulting dNTP concentration levels and frequency of HIV-1 infection.

Chapter 2

Chapter 2: General Materials and Methods

2.1 Cell Culture

2.1.1 Cell Lines

THP-1 Blue CD14 cells were cultured in RPMI 1640 supplemented with 10% foetal calf serum (FCS, Gibco), 100U/mL penicillin and 100µg/mL streptomycin (PAA/ Invitrogen). Human embryonic kidney 293T (HEK293T) cells were cultured in DMEM supplemented with 10% foetal calf serum (FCS, Gibco), 100U/mL penicillin and 100µg/mL streptomycin (PAA/ Invitrogen). THP-1 Blue CD14 cells were passaged by cell dilution. HEK293T and TZM-bl cells were passaged by enzymatic dissociation using 0.25% Trypsin-EDTA solution (Sigma). HEK293T cells were first washed with phosphate-buffered saline (PBS) (PAA, Invitrogen, SIGMA) and then treated with 0.25% Trypsin-EDTA solution followed by incubation at 37^{o}C with 5% CO_2 for 5 mins at room temperature. Detached cells were then diluted at a ratio of 1:10 cell suspension to PBS (PAA, Invitrogen, Sigma) and centrifuged at 400 x g for 3 mins before being re-suspended in fresh DMEM supplemented with 10% FCS. Cells were cultured in 6-well plates (Corning), 12-well plates (Greiner Bio-One), 24-well plates (Corning), 48-well plates (Corning), 96 well plates (Corning), T-25 flasks (Corning), T-75 flasks (Corning) and T-175 flasks (Corning).

2.1.2 Human es cell and iPS cell culture

The HUES-2 human es cell line (originally obtained from Douglas Melton at Harvard University) was approved for use by the UK Stem Cell Bank Steering committee [568]. The originator's gender was male. The NHDF-1 iPS cell line was generated from a dermal fibroblast, of a female donor, by retroviral reprogramming at the James Martin Stem Cell Facility, Sir William Dunn School of Pathology [282].

Es cells and iPS cells were cultured in mTesR™ (StemCell™ Technologies) supplemented with 100U/mL penicillin and 100µg/mL streptomycin (PAA/ Invitrogen) using a feeder-free system of tissue culture

plates coated with Matrigel® Matrix (Corning) diluted in Knockout DMEM® (Gibco) (KODMEM) to a concentration of 3mg/mL.

Es and iPS cells were passaged by either enzymatic dissociation or EDTA assisted dissociation. One hour or more before es and iPS cells passage, 1mL of Matrigel®/KODMEM was applied to tissue culture quality plates (Corning® Costar®). For passage by enzymatic dissociation, es and iPS cells were incubated with pre-warmed TrypLE Express (Gibco) at 37°C, 5% CO_2 for 5 mins after being washed with PBS (PAA, Invitrogen, Sigma). Dissociated cells were triturated into a single cell suspension followed by further dilution of 1:10, cell suspension to PBS (PAA, Invitrogen, Sigma) and centrifuged at 400 x g for 5 mins at room temperature. Cells were then gently resuspended in fresh mTesR™ supplemented with 100U/mL penicillin and 100µg/mL streptomycin (PAA/ Invitrogen) and Rock Inhibitor (Rocki) (Y27632; Calbiochem) 10µM FC. For passage by EDTA assisted dissociation, es and iPS cells were first washed with PBS, 0.5mM EDTA/PBS was then applied and allowed to incubate at room temperature for 15 sec before being removed and discarded. Fresh 0.5mM EDTA/PBS was then applied after which the es and iPS cells were incubated for 5 mins at 37°C, 5% CO_2. Post incubation es and iPS cells were detached from the tissue culture plates (Corning® Costar®) by dispensing mTesR™ medium supplemented with 100U/mL penicillin and 100µg/mL streptomycin (PAA/ Invitrogen) through a p1000 pipette. Es and iPS cell suspensions were then gently transferred to new, Matrigel® coated tissue culture plates (Corning® Costar®) using a 25mL serological pipette.

2.1.3 Es and iPS macrophage differentiation

2.1.3.1 Embryoid Body (EB) formation – Aggrewell™ 800

Aggrewell™ 800 plates (Stem Cell Technologies) was prepared as follows: Each well of the plate to be used was washed with PBS (PAA, Invitrogen, Sigma). 1mL of mTesR® medium supplemented with Rock Inhibitor (Rocki) (Y27632; Calbiochem) 10µM FC and 100U/mL penicillin and 100µg/mL streptomycin (PAA/ Invitrogen) was added to each well to be used. The plate was then centrifuged at 3000 x g for 2

mins at room temperature and subsequently placed at 37°C, 5% CO_2 in preparation for the application of the es or iPS cells. 4 x 10^6 stem cells were used per well of the Aggrewell™ 800 plate (Stem Cell Technologies). Es cells were dissociated into a single-cell suspension by initially washing with PBS (PAA, Invitrogen, Sigma), then incubation at 37°C, 5% CO_2 for 5 mins with TrypLE Express, trituration with a p1000 pipette and finally dilution at a 1:10 ration, cell suspension to PBS (PAA, Invitrogen, Sigma). Es cells were then centrifuged at 400 x g for 5 mins at room temperature, then re-suspended in 1mL Embryoid Body Formation media, consisting of mTesR™ medium supplemented with Rock Inhibitor (Rocki) (Y27632; Calbiochem) 10µM FC, 100ng/mL Bone morphogenetic protein 4 (BMP4)(Peprotech), 100ng/mL Vascular Endothelial Growth Factor (VEGF) (Peprotech) and 40ng/mL stem cell factor (SCF) (Peprotech). The cell suspension was then gently added to one well of the Aggrewell™ 800 plate containing 1mL of mTesR Rock Inhibitor (Rocki) (Y27632; Calbiochem) 10µM FC and 100U/mL penicillin and 100µg/mL streptomycin (PAA/ Invitrogen) to give a final concentration of 50ng/mL BMP4, 50ng/mL VEGF and 20ng/mL Stem cell factor SCF. The Aggrewell™ 800 was then centrifuged at 100 x g for 5 mins, followed by incubation at 37°C, 5% CO_2. 75% of media was replaced daily with EB culture media consisting of mTesR™ medium supplemented with 50ng/mL BMP4, 50ng/mL VEGF, and 20ng/mL SCF.

2.1.3.2 Directed differentiation of Embryoid Bodies into Stem Cell origin Yolk sac Derived-like Macrophage Precursors (scYDMPs)

Ten to fifteen EBs were transferred to one well of a six-well tissue culture plate, or 150 EBs were transferred to a T175 tissue culture flask and cultured in 4mL or 40mL of monocyte differentiation medium, respectively. Macrophage precursor differentiation medium contained X-Vivo15™ (Lonza) supplemented with 100U/mL penicillin and 100 µg/mL streptomycin (Invitrogen), 100 ng/mL M-CSF (Invitrogen), 25 ng/mL IL-3 (R&D), 2 mM glutamax (Invitrogen), and 0.055 mM β-mercaptoethanol (Invitrogen). Fifty percent of the medium was replaced every seven days until the cultures began producing macrophage precursor cells (typically 3-5 weeks), after which the percentage replacement medium was increased to 80%. Es derived macrophage precursor cells were harvested during medium changes from the supernatant on a weekly basis.

2.1.3.3 Differentiation of Stem Cell origin Yolk sac Derived-like Macrophages (scYDMs)

Previous characterisations have shown close to complete CD14+ macrophage precursor homogeneity in harvested cells [265, 282, 377, 569]. For differentiation into macrophages, harvested esYDMPs were plated in 6 well tissue culture plates at a density of 1.5×10^6 cells per well in macrophage differentiation media. Macrophage differentiation media consisted of X-Vivo15^{TM} (Lonza) supplemented with 100 U/mL penicillin and 100 µg/mL streptomycin (Invitrogen), 100 ng/mL M-CSF (Invitrogen), and 2 mM glutamax (Invitrogen). Plated cells were incubated at 37°C, 5% CO_2 for 7 days.

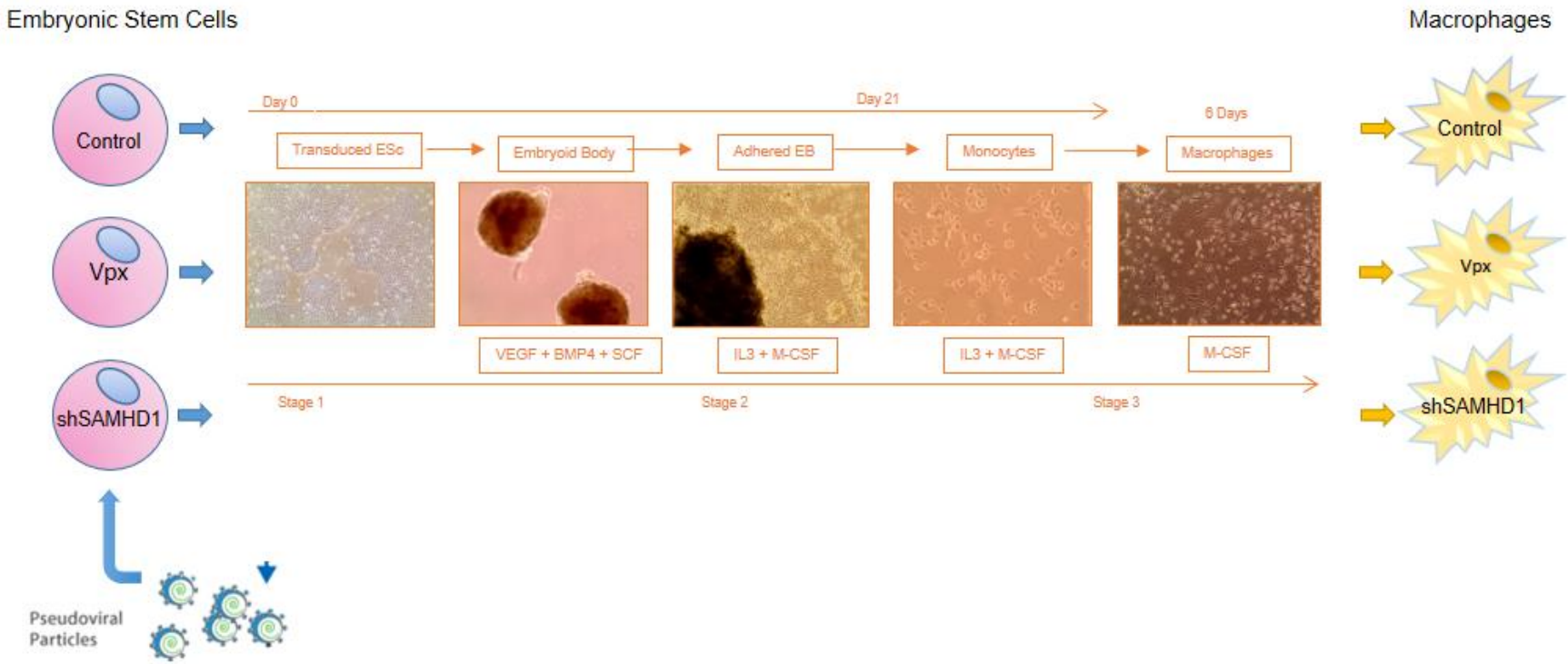


Figure 2.1 Directed differentiation of embryonic stem cells.

Schematic detailing the directed differentiation of genetically modified macrophages from es cells. Human es cells (HUES2) and iPS cells (NHDF1) were transduced with lentiviral vector particles encoding SIVmac251 Vpx (Vpx), SIVmac251 VpxQ76A (VpxQ76A), shRNA targeting SAMHD1 (shSAM [also defined as shSAMHD1]) or controls. Successfully transduced stem cells were selected with puromycin and cultured for expansion. Selected cells were dissociated into single cells, applied to an Aggrewell™ and spun to create embryoid bodies (EBs) of uniform size. EB differentiation was initially directed via culturing in stem cell media (mTesR®) supplemented with BMP4, VEGF and SCF for 4 days. Myeloid differentiation was then induced by culture of the EBs in X-Vivo15 supplemented with M-CSF and IL3. Approximately 3 weeks post myeloid differentiation induction, monocyte-like macrophage precursor cells (esYDMPs & ipsYDMPs) are produced by the EBs. The precursor cells are harvested and differentiated into macrophages (esYDMs) by culturing in X-vivo15™ supplemented with M-CSF, for 6 days. Monocytes = esYDMPs ; Macrophages = esYDMs

2.1.4 Freezing and thawing of cell lines

HEK293T and THP-1 cells were centrifuged at 500 x g for 5 mins and re-suspended in 1 x freezing medium (70% culture medium (RPMI or DMEM), 20% FCS and 10% DMSO) at a density of 1 x 10^6 cells/mL. Suspensions were then aliquoted into 1.8mL cryovials (Starlab) and subsequently transferred to cryo-bombs (Nalgene). Cryo-bombs were then placed at -80^{o}C for 24 hrs. Frozen cells were then transferred to liquid nitrogen for long term storage. In order to thaw cells, frozen vials were removed from liquid nitrogen storage and placed on dry ice. Vials were then transferred quickly from dry ice to a water bath at 37^{o}C. Thawed cells were re-suspended in PBS (PAA, Invitrogen, Sigma), centrifuged at 500 x g for 5 mins then re-suspended in the relevant cell culture medium (see Section 2.1.1 Cell lines).

2.1.5 Freezing and thawing of stem cells

Es cells (HUES2) were enzymatically lifted from tissue culture plates (refer to Section 2.1.2 Human es cell and iPS cell culture) and re-suspended in mTesR® medium at a density of 2.5 x 10^6 cells/mL. Cells were transferred to a 1.8mL cryovial (Starlab) in a volume of 500µL. An equal volume of stem cell freeze medium (20% DMSO, 60% es cell knockout FCS (Stem cell technologies), 20% knockout DMEM) was added to the cryovial. Cryovials were then transferred to freeze-bombs and placed at -80^{o}C overnight before being transferred to liquid nitrogen for long term storage. In order to thaw cells, frozen vials were removed from liquid nitrogen storage and placed on dry ice. Vials were then transferred quickly from dry ice to a water bath at 37^{o}C. Thawed cells were re-suspended in PBS (PAA, Invitrogen, Sigma), centrifuged at 500 x g for 5 mins then re-suspended in the relevant cell culture medium (refer to Section 2.1.2 Human es cell and iPS cell culture).

2.1.6 Cell counts and viability

The NucleoCounter® NC-3000™ full-spectrum fluorescence microscope (Chemometec), was used for determining cell count and viability. Cells to be counted were harvested and re-suspended in media or PBS (PAA, Invitrogen, Sigma). 19µL of the cell suspension was then mixed with 1µL of Solution13

(Chemometec) containing acridine orange (AO) and 4',6-diamidino-2-phenylindole (DAPI)) in a single well of a 96 well plate. The suspension was then transferred to a chamber of an A8-slide (Chemometec).

2.1.7 Microscopy

Fluorescence of HIV-1 infected GFP expressing cells were acquired using a Zeiss Axiovert 40 inverted microscope. The EVOS® XL Core Cell Imaging System (Life Technologies) was utilised for capturing Phase contrast and bright-field images.

2.1.8 Electroporation

HUES2 es cells were cultured to 70%-80% confluence in one well of a 6 well tissue culture plate (Corning® Costar®). Cells were then enzymatically detached (refer to Section 2.1.2 Human es cell and iPS cell culture), re-suspended in PBS (PAA, Invitrogen, SIGMA) and centrifuged at 500 x g for 5 mins. Cells were then re-suspended in NeonTransfection® Resuspension Buffer R at a final density of 1 x 10^7 cells/mL. Twenty four well plates were then prepared containing 500µL of mTesR without antibiotics. Neon®Tube with 3mL Electrolytic Buffer E2 was loaded into the Neon® Pipette Station. Cells were combined with DNA in a 1.5mL Eppendorf tube. Neon® Tip was then inserted into the Neon® Pipette, into which the cell/DNA mix was applied. The Neon® Pipette was then inserted into the Neon® Pipette Station and a current applied with the following conditions: 1400volts, 20mA, and 2 pulses. Electroporated cells were then transferred to a single well of a 24 well plate and incubated at 37°C, 5% CO_2.

2.1.9 Staining for cell surface receptor expression levels

Culture media was removed from fully differentiated scYDMs and blood MDMs, and replaced with macrophage detachment buffer (5mM EDTA (Sigma), 12mM Lidocaine (Sigma)). Cells were then incubated at 37°C for between 10 and 20 mins, after which a pipette was used to detach macrophages. Cells were transferred to coned bottomed 96 well plates (Corning® Costar®), then centrifuged at 500 x

g for 5 mins. Cells were then re-suspended in 50µL fluorophore-conjugated monoclonal antibody (mAb) or isotype control, diluted in FACS buffer (for flow cytometry). FACS buffer consisted of 1% FCS, 0.01% sodium azide and 10ug/mL human IgG (Sigma). Following dilution in FACS buffer cells were incubated at 4°C for 1 hour. Post incubation, 100µL of FACS buffer was added to each well (already containing cells, antibody in FACS buffer) followed by centrifugation at 500 x g for 5 mins. Cells were then re-suspended in 1% formaldehyde.

2.1.10 Flow cytometry

Fluorescence was measured using the FACSCalibur (Beckton-Dickinson) and data analysed using FlowJo® FACS analytical software.

2.1.11 Co-transfection of HEK293T cells

HEK293T cells were plated in tissue culture plates to achieve 70% confluence on the day of transfection in culture medium as previously described (refer to Section 2.1 Cell culture). The transfection mixture was created as follows: Plasmid DNA was prepared in Optimem (GIBCO) to which 12µl of transfection reagent was added at a ratio of 3:1 transfection reagent to DNA. The transfection reagents used were FuGENE HD Transfection Reagent (Roche), TurboFect Transfection Reagent (Fermentas) or Lipofectamine 2000 (Invitrogen), according to the manufacturer's instructions. The transfection mixture was vortexed for 3 mins and allowed to incubate at room temperature for approximately 30 mins. The transfection mixture was then applied to the cells in a dropwise fashion. The cells were incubated at 37°C, 5% CO_2 for 4 hrs, after which the media was changed completely. If puromycin selection was required, this was done using a concentration of (0.4 µg/mL; MP Biomedicals) 24 hrs after the complete media change.

2.2 Quantification assays

2.2.1 SIV p27 antigen ELISA

SIV p27 was quantified using the SIV p27 antigen ELISA supplied by ZeptoMetrix Corporation (RETROtex). 450µL of viral preparation was mixed with 50µL of ZeptoMetrix proprietary Lysis Buffer. Samples were then transferred to a ZeptoMetrix proprietary microplate and incubated at 37°C 5% CO_2 for a duration of 2 hrs to overnight. Post incubation, the supernatant was removed, and wells were washed with ZeptoMetrix proprietary wash solution 6 times. ZeptoMetrix proprietary SIV p27 antibody detector was then applied at 100µL per well; microplates were then sealed and incubated at 37°C 5% CO_2 for 1 hour. Post incubation, the supernatant was removed, and wells were washed with ZeptoMetrix proprietary wash solution 6 times. Streptavidin Peroxidase Working Solution was then applied at 100µL per well; microplates were then sealed and incubated at 37°C, 5% CO_2 for 1 hour. Post incubation, the supernatant was removed, and wells were washed with ZeptoMetrix proprietary wash solution 6 times. ZeptoMetrix proprietary Substrate Working Solution was then applied at 100µL per well; the microplate was then incubated at 18-25°C (room temperature) for 30 mins. Post incubation, ZeptoMetrix proprietary Stop Solution was then applied at 100µL per well. Optical density at 450nm was then measured using the SpectraMax M5 with SoftmaxPro version 5.0 software.

2.2.2 Western Blot

Approximately 1 x 10^6 scYDMs were harvested and centrifuged at 1200 x g for 5 mins. Cell pellets were then re-suspended in 100µL RIPA buffer (150 mM Sodium Chloride (Sigma), 1% Triton® X-100 (Sigma), 0.5 % Sodium deoxycholate (Sigma), 50 mM Tris (Sigma) dissolved in distilled water and brought to pH 8.0) containing cOmplete® Protease Inhibitor Cocktail (Roche) (tablets dissolved as per manufacturer's instructions) and agitated on a rotator plate for 30 mins. Cell lysates were then centrifuged at 16,000 x g for 20 mins, after which the supernatant was transferred to a new receptacle. Specimens were stored at -80°C.

Protein concentrations were quantified using the Bradford quantification assay (Pierce) according to the manufacturer's instructions. Cell lysates were then mixed with 4x proprietary NuPage® LDS Sample buffer, 10x proprietary NuPAGE® reducing agent, and made up to 10µL with deionised water. Mixtures were then heated to 70°C for 10 mins. Denatured protein lysates were then loaded into a 4-12% Bis-Tris precast polyacrylamide gel allowing the proteins to be separated by electrophoresis in proprietary NuPAGE® SDS running buffer at 200v. Proteins were then transferred from the polyacrylamide gel to a nitrocellulose membrane or PVDF membrane via electroblotting at 45v overnight in Transfer buffer (0.192M Glycine, 25mM Tris base, 20% methanol). The membranes were then blocked using Blocking buffer (5% BSA or 5% low fat dried milk dissolved in Tris Buffered Saline Solution (TBS)) and agitated on a roller machine or rocking machine for 3 hrs to overnight. Membranes were then incubated with primary antibody diluted in Blocking Buffer overnight (refer to Table 2.2). Membranes were then washed three times with Tris Buffered Saline Solution with 0.1% Tween (TBST), after which membranes were incubated with the secondary antibody, also diluted in Blocking Buffer for approximately 1hr. Post incubation, membranes were washed three times with TBST and assessed using the LI-COR Odyssey western blotting imaging system.

2.2.3 ATP (Adenosine 5'-triphosphate) determination

Samples for which ATP was to be quantified were taken from the dNTP containing H_2O suspension resulting from the methanolic extraction. ATP was quantified using the Molecular Probes™ ATP Determination Kit (A22066) according to the manufacturer's instructions.

2.3 Cloning Techniques

2.3.1 Bacterial transformation

Chemically Competent Escherichia coli (E.Coli) bacteria were removed from -80°C storage and allowed to thaw on ice. Plasmid DNA in solution as then added gently to the E.Coli cells. The transformation mix was then incubated at room temperature for 20 mins, after which bacteria were heat-shocked by

incubating at 42°C for 50 sec using a pre-heated water bath, then immediately placed on ice for 2 mins. 450µL of S.O.C medium (Super Optimal broth with Catabolite repression) was then added to the transfection mix and subsequently incubated on a shaker at 37°C for 1 hour. Post incubation, 100µL of the mixture was spread onto pre-warmed Lysogeny broth (LB)-Agar containing 100 µg/mL Ampicillin (Sigma) and incubated at 37°C overnight.

2.3.2 Restriction enzyme digest of DNA

Restriction enzymes purchased from Roche or New England Biolabs were used for digestion and cutting of DNA for molecular cloning. Annealed oligonucleotides (refer Section 2.3.6 Preparation of oligonucleotides for cloning) for PCR amplified DNA (refer to Section 2.3.3 DNA amplification using the polymerase chain reaction (PCR)) was digested for durations up to 20 hrs while plasmid DNA was digested for 30 mins to 5 hrs. All restriction enzyme digestions were executed at 37°C and according to the manufacturer's instructions.

2.3.3 DNA amplification using the polymerase chain reaction (PCR)

The polymerase chain reaction (PCR) was used to amplify DNA for molecular cloning purposed. A typical reaction mix contained the following: 1µM forward DNA primer, 1µM reverse DNA primer, 1 unit Taq enzyme (New England Biolabs), 1 x Taq buffer (New England Biolabs), 1.5mM magnesium chloride and H_20 up to a total volume of 50µL. Mixtures were then applied to a thermal cycler; a typical PCR cycle is as follows: Initial denaturation 95°C for 5 mins, 25-35 cycles of denaturation at 95°C for 15 sec, primer annealing at 55°C-70°C for 30-90 sec, extension at 72°C for 30-90 sec per 1Kbase pairs to be amplified.

2.3.4 Agarose gel purification and separation of DNA in solution

Electrophoresis using 1% Tris-acetate EDTA buffer (TAE) agarose gels were used to separate DNA in solution resulting from PCR amplification or ligation reactions. A sample of the DNA in solution was combined with 1 x DNA loading buffer (Bioline) and applied to the agarose gel. SYBR® Safe DNA Gel

Stain (Invitrogen) and a UV transilluminator were used to visualise the bands. To separate the DNA and gel required bands were excised and the DNA extracted using the gel extraction kit QIAquick (Qiagen) according to the manufacturer's instructions.

2.3.5 DNA ligation

Ligation reactions were required to insert (normally PCR amplified) DNA fragments into a plasmid backbone. A typical ligation reaction consisted of 1 unit of T4 DNA ligase (Promega), 2x rapid ligation buffer (Promega), and 2-6µL of fragment DNA in a total volume of 20µL. Mixtures were incubated at room temperature for 20 mins. When necessary, 3'dATP overhangs were introduced to fragments using Taq polymerase (New England Biolabs) or 5' and 3' phosphate groups were removed using Fast Alkaline Phosphatase (Fermentas) to prevent re-ligation.

2.3.6 Preparation of oligonucleotides for cloning

The double-stranded DNA template in which radiolabelled dNTPs were incorporated as part of the dNTP assay (refer to Section 3.2.2 Tritium based enzymatic assay for the determination of intracellular dNTP concentrations) were constructed by the annealing of single-stranded oligonucleotides which were ordered from Sigma. The annealing reaction was as follows: (10 mM Tris pH 7.5, 1 mM EDTA, 50 mM NaCl) in a total volume of 50µL. Conditions for the reaction are as follows: 4 mins at 95^{o}C, 10 mins at 72^{o}C, slow decline to room temperature by leaving at room temperature, finally cooling to 4^{o}C by placing on ice.

Annealing of single-stranded DNA sequences is also required for the insertion of linker sequences into plasmid DNA digested by restriction enzymes. A typical annealing reaction consists of the following: 16 µM mix of complementary oligonucleotides in annealing buffer [10mM Tris pH 7.5-8.0 (Sigma), 50mM sodium chloride (Sigma), 1 mM EDTA(Sigma)] in a 50 µL volume. The reaction conditions were as follows: 3 mins at 95 °C, 10 mins at 70.5 °C, cooling to room temperature followed by cooling to 4 °C on ice. T4

Polynucleotide Kinase was used (as per manufacturer's instructions, New England Biolabs) to phosphorylate the ends of annealed oligonucleotides at 37°C for 30 mins followed by a 20-minute incubation at 65°C to inactivate the T4 Polynucleotide Kinase. Annealed oligonucleotides were stored at -20 °C.

2.3.7 Vector design and sequence analysis

Bioinformatics relating to vector design was performed using Snapgene™ and DNAdynamo™ software packages.

Antibody	Conjugate	Host	mAb/ pAb	Manufacturer
CD4	Allophycocyanin (APC)	Mouse	Monoclonal	R&D Systems
IgG2a isotype for CD4 staining	Allophycocyanin (APC)	Mouse	Monoclonal	R&D Systems
CCR5	Fluorescein isothiocyanate (FITC)	Mouse	Monoclonal	R&D Systems
IgG2b isotype for CCR5 staining	Fluorescein isothiocyanate (FITC)	Mouse	Monoclonal	R&D Systems
CD14	Allophycocyanin (APC)	Mouse	Monoclonal	Immunotools
IgG1 isotype for CD14 staining	Allophycocyanin (APC)	Mouse	Monoclonal	Immunotools
CXCR4	Allophycocyanin (APC)	Mouse	Monoclonal	Immunotools
IgG1 isotype for CXCR4 staining	Allophycocyanin (APC)	Mouse	Monoclonal	Immunotools
CD45	Fluorescein isothiocyanate (FITC)	Mouse	Monoclonal	Immunotools
IgG1 isotype for CD45 staining	Fluorescein isothiocyanate (FITC)	Mouse	Monoclonal	Immunotools
CD16	Allophycocyanin (APC)	Mouse	Monoclonal	Immunotools
IgG1 isotype for CD16 staining	Allophycocyanin (APC)	Mouse	Monoclonal	Immunotools
CD11b	Allophycocyanin (APC)	Mouse	Monoclonal	Biolegend
IgG1 isotype for CD11b staining	Allophycocyanin (APC)	Mouse	Monoclonal	Biolegend

Table 2.1 Antibodies for detection of surface CD4, CCR5, CD14, CXCR4, CD45, CD16 and CD11b.

Primary Antibody	Dilution	Host	mAb/ pAb	Manufacturer
SAMHD1	1 in 1000	Mouse	Monoclonal	Invitrogen
Tubulin	1 in 2000	Rabbit	Monoclonal	Sigma
Phosphorylated (T592) SAMHD1	1 in 1000	Mouse	Monoclonal	Sigma
GAPDH	1 in 5000	Rabbit	Monoclonal	Sigma
p21(Waf1/Cip1) (DCS60)	1 in 2000	Mouse	Monoclonal	Sigma

Table 2.2 Antibodies used for western blotting.

Primer	Sequence (5'-3')
EF1α forward	TCAAGCCTCAGACAGTG
IREStartRev	CATATAGACAAACGCAC
CMV Forward	CGCAAATGGGCGGTAGGCGTG
DPW-20	CACCGTGTATCAATGATTCGGACG
DPW-21	AAACCGTCCGAATCATTGATACAC
DPW-22	CACCGCGATACATCAAACAGCTGGG
DPW-23	AAACCCCAGCTGTTTGATGTATCGC
DPW-24	CACCGCGTTCACTTATCTGCAGCTC
DPW-25	AAACGAGCTGCAGATAAGTGAACGC
DPW-26	CACCGGATGTCTAGTTCACGCACT
DPW-27	AAACAGTGCGTGAACTAGACATCC
DW39 HRMex4FWD	ATGATCCTATCCATGGCCACAT
DW40 HRMex4REV	CCCATTCCCTTCTTACCCTAGACT
DW41 HRMex5FWD	AGAACTATCACTCCTCTTGCAAACAG
DW42 HRMex5REV	GATCATGACAAAGTCCAGCAATCT
dxTP-PartnerPrimer	CCGCCTCCACCGCC
dTTP (for 3H dATP)	TTATTATTATTATTATTAGGCGGTGGAGGCGG
dCTP (for 3H dATP)	TTTGTTTGTTTGTTTGTTTGGGCGGTGGAGGCGG
dGTP (for 3H dATP)	TTTCTTTCTTTCTTTCTTTCGGCGGTGGAGGCGG
dATP (for 3H dTTP)	AAATAAATAAATAAATAAATGGCGGTGGAGGCGG
dCTP (for 3H dTTP)	AAAGAAAGAAAGAAAGAAAGGGCGGTGGAGGCGG
dGTP (for 3H dTTP)	AAACAAACAAACAAACAAACGGCGGTGGAGGCGG
SIVmac251 Vpx (Fwd)	ATGTCAGATCCCAGGGAGAGAATCC
SIVmac251 Vpx (Rev)	TTATGCTAGTCCTGGAGGGGGAGGAGG
SIVmac251 Vpr (Fwd)	ATGGAAGAAAGACCTCCAGAAAATG
SIVmac251 Vpr (Rev)	TCAAGAGGGCGGTATAGTTGAGAG

Table 2.3 Sequences of primers*.

shRNA	Sequence (5'-3')
shSAM	GCAGATGACTACATAGAGATT [156]
shCTRL	ATCATCCCCGACTCGTTTA

Table 2.4 Sequences for the generation of shRNA*.

*primers and oligonucleotides used in this thesis were ordered from Sigma.

Plasmid	Description	Source
pCMVdR 8.91	HIV-1 gag-pol expressing plasmid deleted for *env, vif, vpu, vpr,* and *nef*	Didier Trono Laboratory, Global Health Institute, School of Life Sciences, EPFL, Laussane, Switzerland.
pEF1-IRES-PuroR	2nd generation self-inactivating lentiviral vector where the EF1α promoter drives constitutive expression of the desired transgene and the IRES enables constitutive expression of the puromycin resistance gene.	Salman Bodla, William James' laboratory, Sir William Dunn School of Pathology, University of Oxford.
pVpr(HIV-1)	Vectors based on pEF1-IRES-PuroR where the EF1α promoter drives constitutive expression of HIV-1 Vpr and the IRES enable constitutive expression of the puromycin resistance gene.	Kenny Moore, William James' laboratory, Sir William Dunn School of Pathology, University of Oxford.
pEF1-Vpx-IRES-PuroR	Vectors based on pEF1-IRES-PuroR where the EF1α promoter drives constitutive expression of SIVmac251 Vpx and the IRES enable constitutive expression of the puromycin resistance gene.	Damien Warner, William James' laboratory, Sir William Dunn School of Pathology, University of Oxford.
pEF1-SVpr-IRES-PuroR	Vectors based on pEF1-IRES-PuroR where the EF1α promoter drives constitutive expression of SIVmac251 Vpr and the IRES enables constitutive expression of the puromycin resistance gene.	Damien Warner, William James' laboratory, Sir William Dunn School of Pathology, University of Oxford.
pJRFL	Plasmid encoding HIV-1 R5 tropic JRFL envelope based on the pcDNA3.1/Zeo (+) plasmid from Invitrogen	NIH AIDS Research and Reference Reagent Program, Division of AIDS, NIAID, NIH
pNL4-3.Luc.R-.E-	HIV-1 virus not expressing the env and the accessory protein Vpr; has luciferase gene inserted into the *nef* gene	from Dr. Nathaniel Landau; NIH AIDS Research and Reference Reagent Program, Division of AIDS, NIAID, NIH
pMD2.G	VSV-G glycoprotein expressing plasmid	Didier Trono Laboratory, Global Health Institute, School of Life Sciences, EPFL, Laussane, Switzerland.

Table 2.5 Plasmid DNA constructs used in this thesis.

Plasmid	Description	Source
pSIV3+	Vector derived from SIVmac251 deleted for env, nef, 5'LTR and 3'LTR	(a gift from Francois Lacose) [145]
pSIV4+	Vector derived from pSIV3+ deleted for env, nef, 5'LTR and 3'LTR, Vif, Vpr and Vpx	(a gift from Ravindra Gupta)
px462	Vector based on the pSpCas9n(BB)-2A-Puro (pX462) V2.0	(a gift from Feng Zhang (Addgene plasmid #48141)) [560],
px462-gRNAsamEx4+	Vector based on pX462 plus positive sense guide RNA targeting SAMHD1 Exon 4	Damien Warner, William James' laboratory, Sir William Dunn School of Pathology, University of Oxford.
px462-gRNAsamEx4-	Vector based on pX462 plus positive sense guide RNA targeting SAMHD1 Exon 4	Damien Warner, William James' laboratory, Sir William Dunn School of Pathology, University of Oxford.
px462-gRNAsamEx5+	Vector based on pX462 plus positive sense guide RNA targeting SAMHD1 Exon 5	Damien Warner, William James' laboratory, Sir William Dunn School of Pathology, University of Oxford.
px462-gRNAsamEx5-	Vector based on pX462 plus positive sense guide RNA targeting SAMHD1 Exon 5	Damien Warner, William James' laboratory, Sir William Dunn School of Pathology, University of Oxford.

Table 2.5 Plasmid DNA constructs used in this thesis (continued).

2.4 HIV-1 assays

2.4.1 Viruses used in this thesis

2.4.1.1 HIV-1.GIP (EF1-GFP-Ires-Puro-SIN)

EF1-GFP-Ires-Puro-SIN is a replication defective 2nd generation self-inactivating viral vector that comprises the HIV-1 genome devoid of env, and the accessory proteins, Vif, Vpu, Vpr, and Nef. EF1-GFP-Ires-Puro-SIN is capable of single-cycle infection only. A green fluorescent protein (GFP) reporter gene is encoded within a bicistronic RNA consisting of GFP-IRES-Puro, driven by a constitutively active EF1α promoter. In this thesis, the EF1-GFP-Ires-Puro-SIN viral vector was pseudotyped with VSV.G env and HIV-1 R5-tropic JRFL env. This virus was used in HIV-1 infection experiments in Chapter 3 and Chapter 5, where transductions with this viral vector are referred to as infections.

2.4.1.2 HIV-1.NLU (NL4-3.Luc.R-E)

NL4-3.Luc.R-E- is a replication defective virus that comprises the HIV-1 genome devoid of env, the accessory protein Vpr, and the accessory protein Nef. NL4-3.Luc.R-E- is capable of single-cycle infection only. A firefly luciferase reporter gene (LUC) has been inserted in place of the Nef gene, thus enabling the quantification of successful infection. In this thesis, the NL4-3.Luc.R-E- virus was pseudotyped with the HIV-1 R5-tropic JRFL virus env. This virus was used in HIV-1 infection experiments in Chapter 5, where transductions with this viral vector are referred to as infections.

2.4.2 Viral lentivector like particles (VLP)

2.4.2.1 Vpx-VLP (CMV-SIV4+Vpx)

CMV-SIV4+ is a replication defective packaging construct that comprises the SIVmac251 genome devoid of env, and the accessory proteins, Vif, Vpu, Vpr, and Nef but packages SIVmac251 Vpx which is supplied in *trans*. CMV-SIV4+ was pseudotyped with VSV.G env. This VLP was used to deliver SIV Vpx to target cells.

2.4.2.2 Vpr-VLP (CMV-SIV4+Vpr)

CMV-SIV4+ is a replication defective packaging construct that comprises the SIVmac251 genome devoid of env, and the accessory proteins, Vif, Vpu, Vpx, and Nef but packages SIVmac251 Vpr which is supplied in *trans*. CMV-SIV4+ was pseudotyped with VSV.G env. This VLP was used to deliver SIV Vpr to target cells.

2.4.2.3 Empty-VLPs (CMV-SIV4+CTRL)

CMV-SIV4+ is a replication defective packaging construct that comprises the SIVmac251 genome devoid of env, and the accessory proteins, Vif, Vpu, Vpr, Vpx, and Nef (see Section 2.5.2 Viral Lentivector Like Particles (VLPs)). CMV-SIV4+ was pseudotyped with VSV.G env. This empty VLP was used as a control for the accessory protein packaging VLPs detailed above (see section 2.4.2.1 to 2.4.2.2).

2.4.2.4 Vpr_{HIV-1}-VLP (CMV-HIV-1+Vpr)

CMVdR 8.91 (pCMVdR 8.91) is a replication defective packaging construct that comprises the HIV-1 genome devoid of env, and the accessory proteins, Vif, Vpu, and Nef but packages HIV-1 Vpr. CMVdR 8.91 was pseudotyped with VSV.G env. This VLP was used to deliver HIV-1 Vpr to target cells.

2.4.3 HIV-1 Infection assays

2.4.3.1 HIV-1 Infection assay (GFP)

esYDMPs were differentiated into esYDMs (refer to Section 2.1.3 Es and iPS macrophage differentiation) in 96 well tissue culture plates (Corning® Costar®) at a density of 5 x 10^4 cells per well in 100µL of cell media (X-Vivo15™ (Lonza) supplemented with 100 U/mL penicillin and 100 µg/mL streptomycin (Invitrogen), 100 ng/mL M-CSF (Invitrogen), and 2 mM glutamax (Invitrogen)). At the time of infection, 50µL of the media was removed from each well and replaced with 49µL of fresh media and 1µL of HIV-1.GIP virus. Infected cultures were then incubated at 37°C, 5% CO_2, for 3.5 days. Following incubation,

cells were lifted, CD14 stained (see Section 2.1.9 Staining for cell surface receptor expression levels), and infection quantified by flow cytometry (see Section 2.1.10 Flow cytometry).

2.4.3.2 HIV-1 Infection assay (GFP) with VLPs

esYDMPs were differentiated into esYDMs (refer to Section 2.1.3 Es and iPS macrophage differentiation) in 96 well tissue culture plates (Corning® Costar®) at a density of 5 x 10^4 cells per well in 100µL of cell media (X-Vivo15™ (Lonza) supplemented with 100 U/mL penicillin and 100 µg/mL streptomycin (Invitrogen), 100 ng/mL M-CSF (Invitrogen), and 2 mM glutamax (Invitrogen)). VLPs (Vpx-VLP, Vpr-VLP or Vpr_{HIV-1}-VLP, Empty-VLP) as required were added to cell-containing media at a volume of 1µL of VLPs per well. VLP treated esYDMs were incubated at 37°C, 5% CO_2, for 2hrs. Post incubation, 50µL of the VLP containing media was removed and replaced with 49µL of fresh media and 1µL of HIV-1.GIP virus. Infected cultures were then incubated at 37°C, 5% CO_2, for 3.5 days. Following incubation, cells were lifted, CD14 stained (see Section 2.1.9 Staining for cell surface receptor expression levels), and infection quantified by flow cytometry (see Section 2.1.10 Flow cytometry).

2.4.3.3 HIV-1 Infection assay (Luciferase)

esYDMPs were differentiated into esYDMs (refer to Section 2.1.3 Es and iPS macrophage differentiation) in 96 well tissue culture plates (Corning® Costar®) at a density of 5 x 10^4 cells per well in 100µL of cell media (X-Vivo15™ (Lonza) supplemented with 100 U/mL penicillin and 100 µg/mL streptomycin (Invitrogen), 100 ng/mL M-CSF (Invitrogen), and 2 mM glutamax (Invitrogen)). At the time of infection, 50µL of the media was removed from each well and replaced with 49µL of fresh media and 1µL of HIV-1.NLU virus. Infected cultures were then incubated at 37°C, 5% CO_2, for 3.5 days. Following incubation, the 96 well plate containing the cells was removed from the incubator and allowed to equilibrate with room temperature for approximately 15 mins. 100µL of Thermo Scientific® Firefly Luciferase One-Step Glow Assay Working Solution was added to each well, and the whole plate subsequently placed on a plate shaker at medium speed for 3 mins. After 11 mins of incubation at room temperature, 75uL of

lysed cells were transferred into a black/white 96 well plate. Luciferase expression from the viral genome was measured by detecting luminescence (in relative light units; RLU) using the SpectraMax M5 with SoftmaxPro version 5.0 software.

2.4.3.4 HIV-1 Infection assay (Luciferase) with VLPs

esYDMPs were differentiated into esYDMs (refer to Section 2.1.3 Es and iPS macrophage differentiation) in 96 well tissue culture plates (Corning® Costar®) at a density of 5 x 10^4 cells per well in 100µL of cell media (X-Vivo15™ (Lonza) supplemented with 100 U/mL penicillin and 100 µg/mL streptomycin (Invitrogen), 100 ng/mL M-CSF (Invitrogen), and 2 mM glutamax (Invitrogen)). VLPs (Vpx-VLP, Vpr-VLP, or Vpr_{HIV-1}-VLP, Empty-VLP) as required were added to cell-containing media at a volume of 1µL of VLPs per well. VLP treated esYDMs were incubated at 37°C, 5% CO_2, for 2hrs. Post incubation 50µL of the VLP containing media was removed from each well and replaced with 49µL of fresh media and 1µL of HIV-1.NLU virus. Infected cultures were then incubated at 37°C, 5% CO_2, for 3.5 days. Following incubation, the 96 well plate containing the cells was removed from the incubator and allowed to equilibrate with room temperature for approximately 15 mins. 100µL of Thermo Scientific® Firefly Luciferase One-Step Glow Assay Working Solution was added to each well, and the whole plate subsequently placed on a plate shaker at medium speed for 3 mins. After 11 mins incubation at room temperature, 75µl of lysed cells were transferred into a black/white 96 well plate. Luciferase expression from the viral genome was measured by detecting luminescence (in relative light units; RLU) using the SpectraMax® M5 with SoftmaxPro® version 5.0 software.

2.5 Lentiviral Particle Production

2.5.1 HIV-1 virus

HEK293T cells were cultured in T175 flasks until 70-80% confluent. A transfection mixture was then established in three stages. Firstly, plasmid DNA was combined with DMEM (without additives) and vortexed for 20 sec. For HIV-1.GIP Virus, this comprised 6 µg transgene lentivector DNA (pEF1-GFP-IRES-

Puro), 9 µg of gag-pol expressing packaging plasmid DNA (pCMVdR 8.91), and 4.5 µg of envelope expressing plasmid DNA (pMD2.G or pJRFL). For HIV-1.NLU Virus, this comprised 6 µg Gag-pol+lentivectorgene (NL4-3.Luc.R-E-) DNA and 4 µg of envelope expressing plasmid (pJRFL). In the second stage, 0.24 µM polyethyleneimine (PEI) was combined with DMEM (without additives) and vortexed for 20 sec, finally, in stage three, the DNA and PEI mixtures were combined by vortexing the tube containing the DNA whilst slowly adding the PEI mixture in a dropwise fashion. The transfectant was then incubated at room temperature for 20 mins. Post incubation, the media was removed from HEK293T cells, which were then washed once with PBS (PAA, Invitrogen, Sigma). PBS was then aspirated and replaced with the transfectant. Transfected cells were then incubated for 48 hrs at 37°C, 5% CO_2. Post incubation virus-containing media was carefully removed and passed through a 0.45µm filter. LentiX® was used to concentrate viral preparations. Virus containing media was mixed at a ratio of 3:1 with LentiX® (Virus:LentiX®) centrifuged at 1400 x g for 30 mins and incubated at 4°C for a duration of 30 mins to overnight. Post incubation, the supernatant was removed, and the virus-containing pellet re-suspended in PBS (PAA, Invitrogen, Sigma), mTesR™, or Xvivo15™. Concentrated virus preps were then aliquoted in single-use volumes and stored at -80°C.

2.5.2 Viral Lentivector Like Particles (VLPs)

HEK293T cells were cultured in T175 flasks until 70-80% confluent. A transfection mixture was then established in three stages. Firstly, plasmid DNA was combined with DMEM (without additives) and vortexed for 20 sec. For empty VLPs, Vpx-VLPs, and Vpr-VLPs, this comprised 6µg lentivector DNA (e.g., pEF1-Vpx-IRES-Puro), 9µg of gag-pol expressing packaging plasmid DNA (pSIV4+), and 4.5µg of VSV.G envelope expressing plasmid DNA (pMD2.G). For HIV-1 Vpr-VLPs, this comprised 6µg lentivector DNA (pVpr(HIV-1)), 9µg of gag-pol expressing packaging plasmid DNA (pCMVdR 8.91), and 4.5µg of VSV.G envelope expressing plasmid DNA (pMD2.G). In the second stage, 0.24 µM polyethyleneimine (PEI) was combined with DMEM (without additives) and vortexed for 20 sec, finally, in stage three, the DNA and PEI mixtures were combined by vortexing the tube containing the DNA whilst slowly adding the PEI

mixture in a dropwise fashion. The transfectant was then incubated at room temperature for 20 mins. Post incubation, the media was removed from HEK293T cells, which were then washed once with PBS (PAA, Invitrogen, Sigma). PBS was then aspirated and replaced with the transfectant. Transfected cells were then incubated for 48 hrs at 37°C, 5% CO_2. Post incubation VLP containing media was carefully removed and passed through a 0.45µm filter.

VLPs were then concentrated via Ultracentrifugation as follows: VLP containing media (VLP prep) was placed into a washed Ultraclear® ultracentrifuge tubes 25mm x 99mm (Beckman 344058) and made up to 30mL volume. A 2mL layer of 7% Optiprep® in PBS (PAA, Invitrogen, Sigma) was then pipetted to the bottom of the tube, forming a clear layer below the VLP prep. Using the SW28 rotor, spin for 1.5hr @4°C @25,000RPM, spin down to 800rpm, then slowed to stop by gravity. Resulting VLP pellet was resuspended in 1mL PBS (PAA, Invitrogen, Sigma), and further split into 100µL aliquots and stored at -80°C. The efficiency of production was assessed using the SIV p27 Antigen ELISA (ZeptoMetrix Corporation (RETROtex)) according to the manufacturer's instructions.

2.6 Lentivector transduction of THP-1 cells

THP-1 monocytes were cultured in T75 tissue culture flasks (refer to Section 2.1 Cell culture) until approximately 5 x 10^6 cells were present. 1µL of lentivector viral prep was added to the existing culture media, and cultures were incubated at 37°C for 6 hrs. Lentivector containing media was then completely removed, and cells were gently washed once with PBS (PAA, Invitrogen, Sigma). Cultures were then incubated at 37°C ,5% CO_2 for 24 hrs after which growth medium was supplemented with 2µg/µL (final concentration) of puromycin (Invitrogen). Surviving cells were subsequently expanded.

2.7 Statistical Analysis

Statistical analysis was performed by one or two-tailed unpaired t-test using GraphPad® Prism version 8. Stars indicate p values; *p<0.05, **p<0.01, ***p<0.001, and ****p<0.0001.

Chapter 3

Chapter 3: SAMHD1 activity in stem cell-derived macrophages

3.1 Introduction

Macrophages are an important component of HIV-1 pathogenesis, and although cell-free infection of macrophages *in vivo* is still a matter of controversy [387], it is widely accepted that macrophages harbour integrated provirus and are active in virus production at all stages of disease (refer to Section 1.3.7 Macrophages and HIV). The magnitude of macrophage-associated viral production appears to be dependent on the stage of HIV-1 infection. During the acute and chronic disease phases, virus production is low, evidenced primarily by the low density of infected macrophages extracted from infected individuals [445]. However, during AIDS, macrophages have been shown to produce large quantities of infectious virus [11, 399]. The myeloid associated mechanisms underlying this change in viral production kinetics are not entirely clear. Certainly, CD4+ T-cell depletion appears to be a pre-requisite, and so a switch to macrophage tropism of circulating HIV-1 to increase the efficiency of macrophage entry may be involved. However, given the intrinsic low efficiency of macrophage tropic cell free HIV-1 infection in the steady state, it seems that this adaptation in isolation may be insufficient to drive the increase in macrophage-associated virus production observed. A novel line of inquiry in this regard has stemmed from the identification of multiple macrophage lineages as previously described (refer to Section 1.3.4 Ontogenesis) and seeks to investigate whether lineage specific attributes are involved. For example, tissue-resident macrophages such as alveolar macrophages are of yolk sac origin, however when substantially depleted (e.g., due to trauma or disease) are replaced by monocyte-derived macrophages of bone marrow origin. Stimulation from the microenvironment renders infiltrating macrophages phenotypically identical to yolk sac derived macrophages already resident; however, they remain transcriptionally distinct [387]. In these circumstances, a lineage-specific transcriptional attribute unique to yolk sac derived alveolar macrophages would be lost due to a lack of expression in infiltrating bone marrow lineage macrophages. Such lineage-specific attributes have been hinted at when considering macrophages in the context of HIV-1 infection. Bone marrow-derived MDMs such as

those located in the intestines can be highly refractory to HIV-1 entry and replication [397], however once infected are unable to manage or terminate viral replication (permanent gene silencing). In contrast, yolk sac derived microglia are relatively permissive to HIV-1 [567], yet *in vivo* appear functional in the clearance of productive infection [466, 467]. Evidence for lineage-specific macrophage attributes involvement in occurrences such as microglia self-clearance or the amplification of macrophage-associated virus production mentioned above is lacking, primarily due to the challenges in obtaining tissue-resident macrophages (for experimental use) from key locations such as the brain and lymph nodes from HIV-1 infected individuals [387].

An efficient and simple solution to the challenges surrounding the acquisition of primary tissue-resident macrophages is the differentiation of macrophages from stems cells. The robust and long-term production of macrophages from es and iPS cells is well described and the recent characterisation of their differentiation as myb-independent (and hence developmental similarity to yolk sac derived myeloid like cells) [4, 282], suggests that these cells may represent a good model for the study of yolk sac derived tissue-resident macrophage biology. The technique enables the production of genetically homogenous macrophages and precursors, which are easily harvested and purified for a period of up to 12 months [377]. The stem cell origin of the macrophages used in this protocol presents an efficient point to apply genetic modification strategies, which, if applied at the macrophage stage, would have met significant natural immunological resistance. Once modified, stem cells can be rapidly expanded and stored long term for use in future experiments.

In blood monocytes and MDMs, SAMHD1 is highly expressed and functional in HIV-1 restriction; however, the dynamics of SAMHD1 expression and HIV-1 restriction in scYDMs have yet to be described. In this Chapter, the activity of SAMHD1 in isolation, and in relation to HIV-1 infection and facilitation by Vpx protein is investigated in scYDMs. The investigative strategy employs loss of function experiments where the activity of SAMHD1 is silenced by RNA interference using short hairpin RNA (shRNA) or

depletion via application of SIVmac251 Vpx protein (herein referred to as Vpx). Lentiviral vectors are used to induce the stable endogenous expression in stem cells of shRNA targeting SAMHD1 (shSAM), an shRNA control (shCtrl), Vpx (Vpx), a Vpx mutant control unable to bind DCAF1, (VpxQ76A) (refer to Section 1.1.4.3 Vpx), and a lentivector control encoding an empty transgene expression cassette (IresPuro [IRP]). Stably transduced stem cells are then differentiated into esYDMs or ipsYDMs. The SAMHD1 protein expression profile is determined, and a tritium-based dNTP quantification assay established and optimised in order to determine dNTP concentrations in scYDMs. SAMHD1 and Vpx infectivity dynamics were subsequently investigated in the transduced scYDM cell lines using single-round HIV-1 infection assays.

3.2 Methods and Materials

3.2.1 Generation of scYDMs expressing Vpx and shRNA targeting SAMHD1

3.2.1.1 Lentivector particles for transduction of stem cells

Purified lentivector viral particles for the expression of Vpx, VpxQ76A, transgene control (IRP), shRNA targeting SAMHD1 (shSAM) and an shRNA control (shCTRL) were obtained from Dr. Michael (Kenny) Moore, James Laboratory, University of Oxford, and were constructed as follows:

3.2.1.1.1 Expression of transgenes Vpx, VpxQ76A and transgene control (IRP) from lentiviral integrant

SIVmac251 Vpx was amplified from the pSIV3+ plasmid and VpxQ76A generated via site-directed mutagenesis of the SIVmac251 Vpx sequence. Amplified transgene sequences were cloned into the pEF1-IRES-PuroR self-inactivating (SIN) lentiviral vector. Transgene containing plasmids were co-transfected in HEK293T cells together with suitable helper plasmids to generate VSV.G pseudotyped lentivector viral-like particles (Figure 3.1).

3.2.1.1.2 Expression of shRNA targeting SAMHD1 from lentiviral integrant

A published shRNA sequence was used for RNA interference of SAMHD1 (shSAM) (GCAGATGACTACATAGAGATT) [156], which had been further validated in the laboratory. The control shRNA, shCTRL, was a scramble sequence (ATCATCCCCGACTCGTTTA) also already established in the laboratory [569]. Both shRNA sequences were cloned into the pSIREN-RetroQ construct. shRNA containing plasmids were co-transfected in HEK293T cells together with suitable helper plasmids to generate VSV.G pseudotyped lentivector viral-like particles (Figure 3.1).

Lentiviral particles were concentrated such that 1μL of virus resulted in 10% lentiviral transduction of es or iPS cells and therefore a 99.5% probability that any given transfected cell contains a single lentiviral integrant [282].

3.2.1.2 Transduction of stem cells

Es or iPS cells were plated to obtain 50% confluence on the day of transduction in 12 well tissue culture plates. 1μl of lentivector viral prep was added to the existing culture media (see Section 2.1.2 Human es cell and iPS cell culture) and cultures were incubated at 37°C for 6 hrs. Lentivector containing media was then completely removed, and cells were gently washed once with PBS (PAA, Invitrogen, Sigma). Cultures were then incubated at 37°C ,5% CO_2 for 24 hrs after which growth medium was supplemented with 2μg/μL (final concentration) of puromycin (Invitrogen). Surviving cells were subsequently expanded.

3.2.1.3 Differentiation of transduced scYDMs

Transduced stem cell lines expressing shRNA or transgenes were differentiated to esYDM as previously described (refer to 2.1.3 Es and iPS macrophage differentiation). Puromycin was constantly applied to cell media throughout the differentiation process to ensure that only integrant containing cells survived.

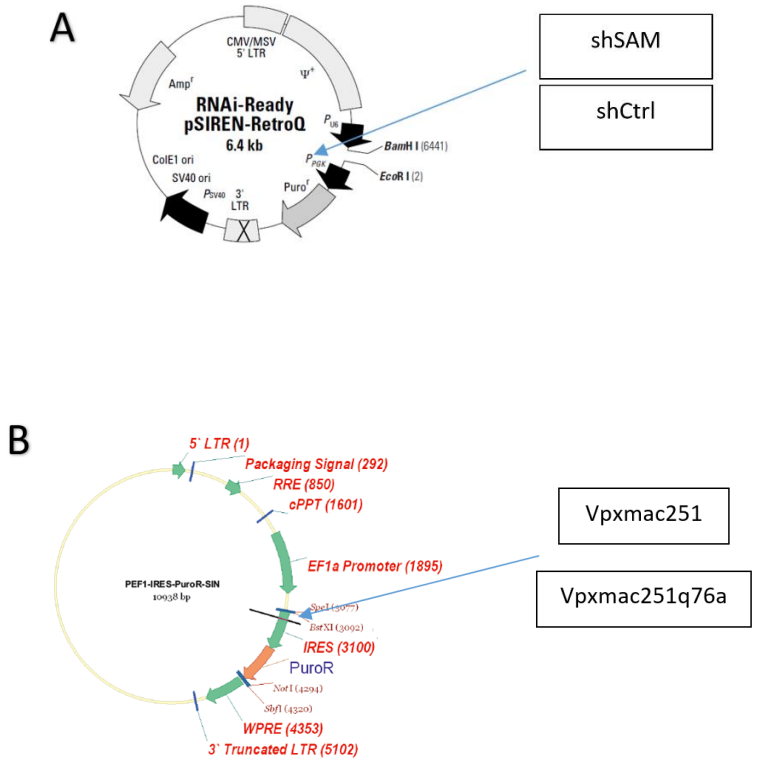


Figure 3.1 Lentiviral vectors for constitutive expression of Vpx, VpxQ76A, and shRNA.

Transgene and shRNA expressing lentiviral vectors were a gift from Dr. Michael (Kenny) Moore and were constructed as follows: pSIREN-RetroQ-RNAi-Ready self-inactivating (SIN) vector plasmid map. Coding sequences complementary to those found in the SAMHD1 gene (shSAM) and a control gene (shCTRL) were inserted at the BamHI EcoRI cloning site resulting in two new lentiviral vectors: pSIREN-shSAM & pSIREN-shCTRL, **(A)**. pEF1-IRES-Puro self-inactivating (SIN) lentiviral vector plasmid map. Coding sequences for SIVmac251 Vpx or SIVmac251 VpxQ76A were inserted at the SpeI BstXI cloning site resulting in two new lentiviral vectors: pEF1-Vpxmac251-IRES-Puro & pEF1-Vpxmac251Q76A-IRES-Puro, **(B)**. Generation of lentiviral vector particles involved the co-transfection of VSV.G expression plasmid (pMD2.G), a *gag-pol* expression plasmid (pCMVdR 8.91) and the lentivector encoding the transgene of choice at a ratio of 3:6:4 into HEK293T cells. Supernatant containing the lentiviral particles was harvested 48 hrs post-transfection, **(C)**.

3.2.2 Tritium based enzymatic assay for the determination of intracellular dNTP concentrations

Given SAMHD1 functions in dNTP hydrolysis, data regarding cellular dNTP concentrations would be a valuable component of any investigation into the nature of SAMHD1. However, quantification of intracellular dNTP concentrations within the department was not possible as an assay had not been established. It was possible to send samples to external researchers specialising in the quantification of dNTPs, however large cell numbers per sample were required (e.g., 1 x 10^7). This made the option unworkable due to the relatively low numbers of esYDMs generated by an economically viable differentiation protocol (e.g., 5 x 10^6 per week, per cell line). Thus, an assay for the quantification of dNTPs was researched and established.

Two main independent techniques are currently employed for the determination of dNTP concentrations: determination via high-performance liquid chromatography (HPLC), or determination by an enzymatic assay using a DNA polymerase [570]. Enzymatic assays require low cell numbers (as low as 1 x 10^5 cells per sample) but incorporate the use of radiolabelling (phosphorous-32 (^{32}p) or tritiated dNTP (^{3}H)). The advantage of HPLC was the lack of radioisotope usage; however, it required large numbers of cells per sample. The assay eventually implemented determined dNTP concentrations via quantification of radiolabelled ^{3}H enzymatically incorporated into short primer pairs [570]. This assay was chosen because of the low cell number requirement per sample, the greater flexibility in working environments inherent in the use of an isotope with low radioactivity, and the existence of apparatus and well-established procedures for experiments involving radioisotopes, within the department. Thus, the assay for determining dNTPs via enzymatic incorporation of ^{3}H, hereafter referred to as the 'dNTP assay', was established.

The dNTP assay is based on the fundamental biochemistry that all four dNTPs must be present for continued enzymatic incorporation of any given dNTP into a growing DNA strand [571]. If a single dNTP is limiting, and the remaining three dNTPs are in excess, the reaction will continue until the limiting

dNTP is exhausted. If one of the dNTPs in excess is radiolabelled, and if primers are designed such that incorporation of the limiting dNTP (to be quantified) and the radiolabelled dNTP are at a known ratio, then the signal emitted by the incorporated radiolabelled dNTPs will be directly proportional to the quantity of incorporated dNTP being measured (Figure 3.2).

Cells containing dNTPs to be quantified were cultured in 6 well plates (approximately 1 x 10^6 cells per well) and were detached by replacing media with 1.5mL of 0.5mM Ethylenediaminetetraacetic acid (EDTA), 12mM Lidocaine solution followed by incubation at 37°C for 15 mins. Rounded cells were lifted using jets from a p1000 pipette and transferred to 1.8mL Eppendorf tubes. Cells were then counted, centrifuged at 5,000 x g for 2 mins, after which the supernatant was removed and discarded. Cell pellets were then re-suspended in 500µL of 60% methanol solution and vortexed vigorously for 2 mins at room temperature. Tubes were incubated at 95°C for 3 mins, followed by centrifugation at 16,000 x g for 5 mins. The resulting supernatant was transferred to a separate Eppendorf tube and spun in a heated SpeedVac™ dryer for 5 hrs. Lyophilised residue containing dNTPs was re-suspended in 100µL ddH_2O or a volume required for a concentration of 10,000 cells/µL. One well of a 96 well plate was used per sample for enzymatic incorporation. The reaction mixture contained, in a volume of 50µL, 6.5µL of the dNTP containing sample or 0.125-8pM of the dNTP Standard to be determined, 2µM dNTPs in excess, 1µM ^{3}HdTTP (or ^{3}HdATP for dTTP determination), 0.125µM oligonucleotide, 10µM $MgCL_2$, 40mM Tris-HCL, 2 units DNA polymerase (Taq Neb® cat M0273S). 96 well plates were incubated at 37°C for 1 hour. Reactions were stopped by placing the 96 well plate on ice or at 4°C. Reaction mixtures were transferred to a semi-permeable glass-fibre membrane (Perkin Elmer ® Filtermat A Cat 1450-421), and washed once with 20% Na_2HPO_4, once with ddH_2O and once with 99% EtOH using an automated cell harvester (Skantron™ Micro96 Cell Harvester). Oligo containing membranes were then air-dried and subsequently saturated with liquid scintillant (Perkin Elmer® Ultima Gold™ Cat 6013321) and radioactivity quantified using a scintillation counter (Perkin Elmer® MicroBeta® 1450LSC Trilux 1450-021) (Figure 3.2). The scintillation counter measures emitted tritium in counts per minute.

Anomalous results, which will be detailed in Section 3.3.4, prompted further optimisation of the protocol by increasing the accuracy of sample normalisation. The change was to normalise cell samples based on intracellular ATP levels rather than cell count. Aliquots for ATP for determination were taken from the re-suspended extracted dNTP-H_2O solution. This was advantageous since it did not require additional steps being added to the protocol and removed any error incorporated in previous steps of the assay (e.g., due to spillages or inaccurate pipetting, etc.). ATP was quantified using the Molecular Probes™ ATP Determination Kit according to the manufacturer's instructions (refer to Section 2.2.3 ATP (Adenosine 5′-triphosphate) determination). Raw dNTP sample values were then normalised using the corresponding value for ATP for any given sample.

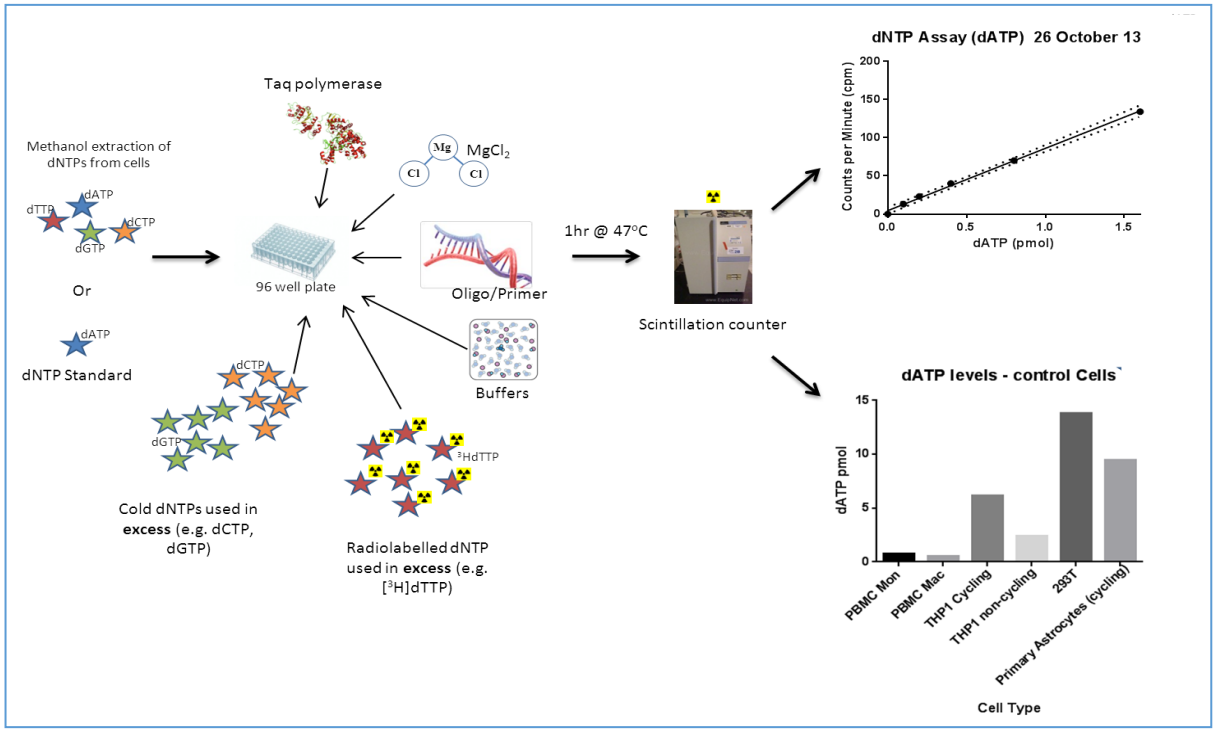


Figure 3.2 Tritium based enzymatic assay for the quantification of dNTPs (dNTP assay).

dNTPs were extracted from cell lysates via methanoic extraction and combined with the reaction reagents in one well of a 96 well plate. Each well-represented quantification of a single dNTP and one technical repeat, thus 12 wells were required for quantification of all four dNTPs (dATP, dCTP, dGTP, and dTTP) in triplicate. Reactions were incubated at 47°C for 1hr, after which incorporated ^3H was determined using a scintillation counter. A standard curve was used to extrapolate dNTP concentrations from the scintillation counter output (counts per minute). dATP pmol per 1 x 10^6 cells.

3.3 Results

3.3.1 Successful differentiation of es cells and iPS cells into macrophages

Tight regulation of intracellular dNTP concentrations reduces the emergence of detrimental genetic mutations and is thus important to normal human development [202]. Indeed, as previously described, natural mutations in the SAMHD1 gene can lead to AGS characterised by significant infantile associated growth abnormalities. However, in humans, and in the mouse, SAMHD1 aberration does not hinder foetal growth, and this, therefore, implies that SAMHD1 is dispensable during this crucial stage of cellular differentiation and organism development [572]. The impact of SAMHD1 depletion via Vpx or shRNA on *in vitro* stem cell differentiation has not been described, nor has the effects of constitutive expression of Vpx or Vpx mutants throughout the differentiation process. In this thesis, both es and iPS cells were used to generate macrophages. iPS cells, in addition to es cells, were used in order to determine iPS derived macrophage suitability for use in HIV-1 investigative experiments, but also to probe for any phenotypic end stage differences compared to es derived macrophages. Lentivector transduction of stem cells did not alter stem cell survival or morphology and all cell lines produced embryoid bodies that were morphologically uniform (Figure 3.3A, B & C). Wild type (non-transduced), IRP and VpxQ76A expressing cell lines produced macrophage precursor cells at approximately the same time point (2 weeks). Vpx expressing cells produced macrophage precursor cells after approximately 3 weeks, whereas SAMHD1-KD and shCTRL expressing cells produced cells approximately 5 weeks after EB plating (Figure 3.4). This production timing phenomenon of Vpx and shRNA expressing cells was observed with both es and iPS derived cell lines (Figure 3.4).

Macrophages produced using the protocol and stem cell lines detailed in this thesis have been extensively characterised elsewhere [377]. These reports showed that esYDMs phenotypically resemble bone marrow-derived blood MDMs differentiated *in vitro* with M-CSF in terms of surface marker expression, functionality, and morphology [282, 569]. Hence, surface markers of esYDMs were not probed in these experiments, (however, this data can be found for subsequent differentiations using

the same protocol later in this thesis (refer to Chapter 4, Figure 4.12)). The morphology of macrophages produced here matched that described in these reports. esYDMs are of a similar size to blood MDMs, and phorbol 12-myristate 13-acetate (PMA) treated THP-1 cells, however, are spindle-shaped rather than the classical 'fried egg' shape observed with blood MDMs and PMA treated THP-1 cells (Figure 3.3D).

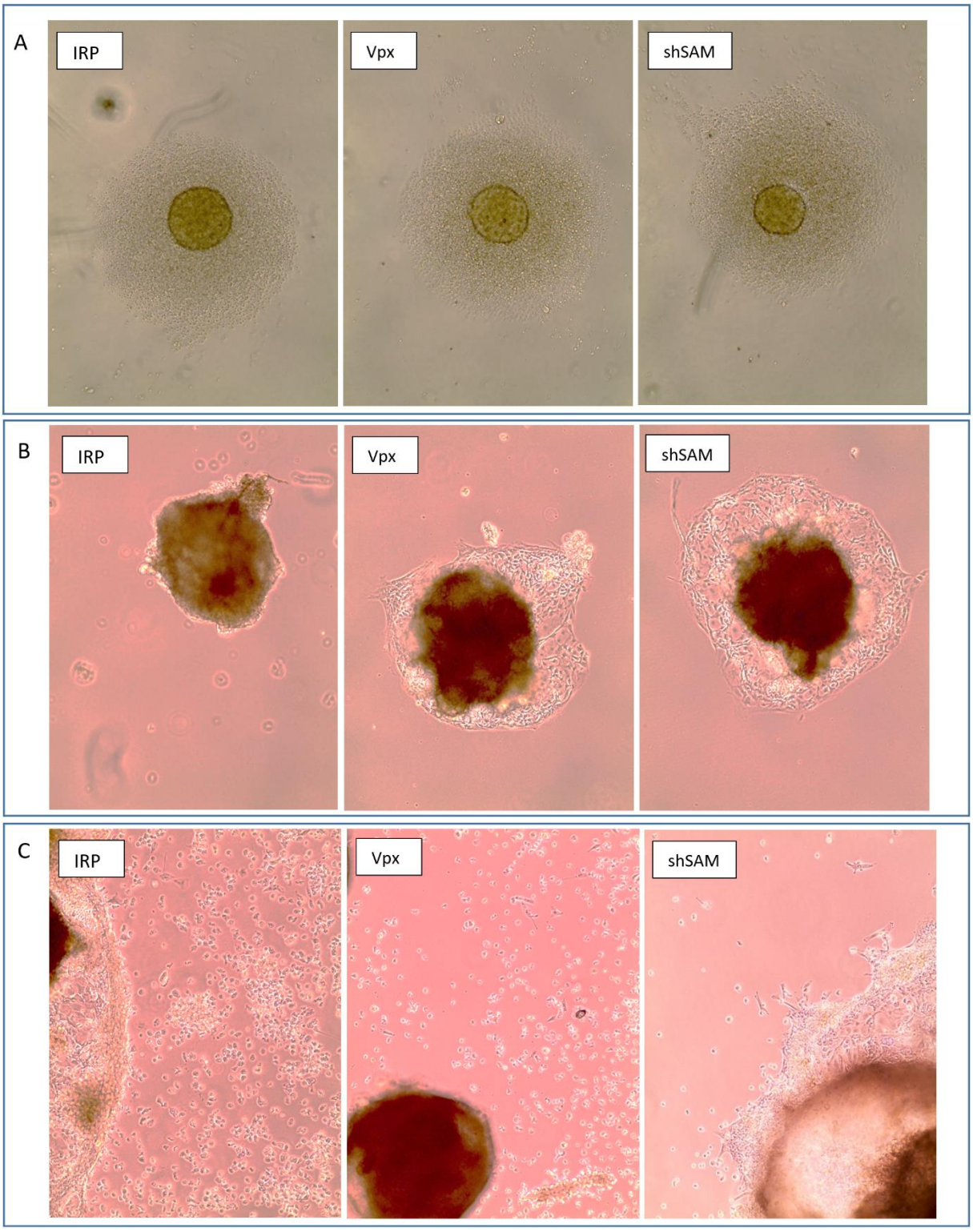


Figure 3.3 Embryoid body (EB), esYDMP and esYDM morphology.

Es-derived embryoid body (EB), esYDMP and esYDM morphology. Expression of Vpx, shRNA to SAMHD1 (shSAM) and control transgene (IRP) does not alter morphology of newly created EBs (**A**), EBs after 7 days incubation (**B**), nor the production of macrophage precursor cells (esYDMPs) (**C**). esYDM morphology in comparison to blood MDMs (DA77) and PMA differentiated THP-1 cells (**D**).

D

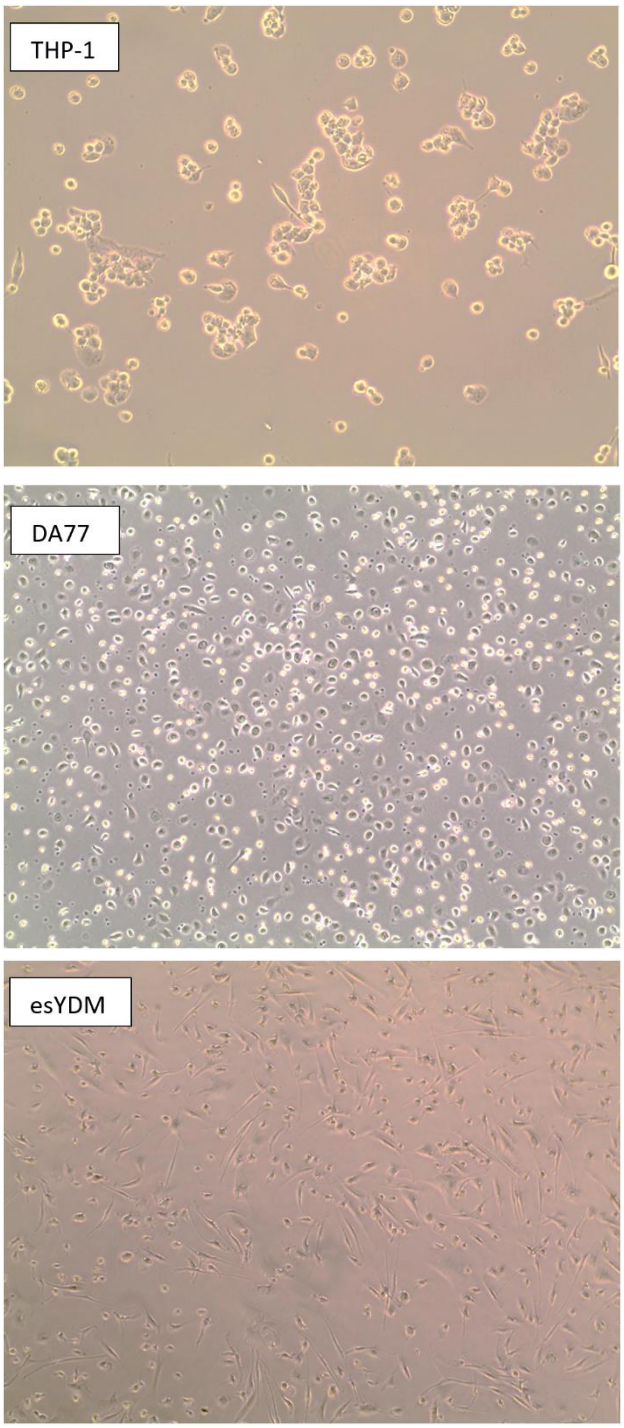


Figure 3.3 - Continued

Es-derived embryoid body (EB), esYDMP and esYDM morphology. Expression of Vpx, shRNA to SAMHD1 (shSAM) and control transgene (IRP) does not alter morphology of newly created EBs (**A**), EBs after 7 days incubation (**B**), nor the production of macrophage precursor cells (esYDMPs) (**C**). esYDM morphology in comparison to blood MDMs (DA77) and PMA differentiated THP-1 cells (**D**).

HUES-2	24/02/2014	31/02/14	10/03/2014	17/03/2014	24/03/2014	31/03/2014	07/04/2014	14/04/2014	21/04/2014	28/04/2014	05/05/2014
WT	EBs Plated		yes	2.32E+06	yes	1.70E+06	2.16E+06	2.00E+06	3.40E+06	1.45E+06	2.05E+06
IRP	EBs Plated		yes	2.00E+06	yes	2.20E+06	1.93E+06	2.40E+06	3.72E+06	1.21E+06	3.21E+06
Vpx	EBs Plated			1.99E+06	yes	2.00E+06	1.55E+06	1.05E+06	1.71E+06	5.00E+05	3.30E+06
VpxQ76A	EBs Plated		yes	1.00E+06	yes	6.43E+05	1.00E+06	6.00E+05	1.28E+06	1.60E+05	7.30E+05
shSAM	EBs Plated					5.00E+05	1.57E+05	5.25E+05	2.50E+05	9.40E+05	1.50E+05
shCTRL	EBs Plated					3.00E+05	3.00E+05	2.50E+05	6.00E+05	1.78E+06	2.30E+05

NHDF1	24/02/2014	31/02/14	10/03/2014	17/03/2014	24/03/2014	31/03/2014	07/04/2014	14/04/2014	21/04/2014	28/04/2014	05/05/2014
WT	EBs Plated			3.51E+05	yes	2.80E+05	1.73E+06	1.30E+06	2.21E+06	2.00E+05	1.71E+06
IRP	EBs Plated		yes	2.00E+06	yes	3.67E+06	4.71E+06	2.43E+06	3.53E+06	2.00E+05	3.71E+06
Vpx	EBs Plated			1.98E+06	yes	4.00E+06	4.58E+06	1.70E+06	3.00E+06	2.50E+05	2.72E+06
VpxQ76A	EBs Plated		yes	3.80E+05	yes	5.00E+04	3.33E+05	1.65E+06	1.80E+05	6.20E+05	4.00E+05
shSAM	EBs Plated					2.50E+05	3.30E+05	4.00E+05	3.50E+05	1.10E+06	1.50E+05
shCTRL	EBs Plated					2.00E+05	7.14E+05	4.50E+05	6.00E+05	4.75E+04	2.60E+05

Figure 3.4 Production timing of stem cell-derived factories.

The expanded embryoid bodies (factories) produce macrophage precursors (esYDMPs) at different time points, and there is synergy between the production timing of es (HUES2) and iPS (NHDF1) derived cell lines with the same transgenic phenotype. For example, Vpx expressing cells produce esYDMPs approx. 1 week later than cells transduced with a lentivector control (IRP – IresPuor) and the Vpx control construct (VpxQ76A), for both es and iPS derived esYDMP cell lines. Also, the SAMHD1-KD cell line (shSAM) and the shRNA control cell line (shCTRL) produce esYDMPs approximately 2 weeks after Vpx expressing cell lines. Wild Type (WT) cells are a non-transduced control cell line differentiated in the absence of puromycin. "Yes" refers to the presence of cells at a given time point in the culture vessel. These cells may not have been counted due to low numbers or to synchronise harvesting of cells with other factories. Cells were counted using the NucleoCounter® NC-3000™ (refer to Chapter 2, Section 2.1.6 Cell counts and viability).

3.3.2 SAMHD1 is phosphorylated and highly expressed in esYDMs

Since the initial discovery of SAMHD1 in MDDCs [228], SAMHD1 has been identified in a variety of cell types including CD4+ T-cells, blood monocytes, MDMs, microglia, HEK293T cells, human stem cells, and THP-1 cells [2, 96, 204, 229, 567, 573]. SAMHD1 is believed to be expressed in almost all mammalian cells; however, expression levels vary greatly in a manner partly dependent on cell type. For example, SAMHD1 is highly expressed in blood monocytes, MDMs, MDDCs, CD4+ T-cells, THP-1 cells and HEK293T cells, and expressed at relatively low levels in es cells and human fibroblasts [2, 96, 204, 229, 567, 574]. SAMHD1 expression levels are also governed by the cell cycle, and hence in cycling cells, such as HEK293T cells, SAMDH1 expression has been shown to fluctuate, synchronised with phases of cell division [202, 207, 243]. Similarly, in non-cycling cells, such as blood monocytes, MDMs, MDDCs and resting CD4+ T-cells, SAMHD1 expression remains relatively constant [202, 207, 243]. SAMHD1 is an IFN-stimulated gene, and thus, SAMHD1 expression can be upregulated by type I IFNs such as IFNα and IFNγ in a cell type dependent manner [204, 575]. For example, IFN stimulation robustly increases SAMHD1 expression in HEK293T cells and fibroblasts, whereas IFN stimulation of blood monocytes, MDMs, MDDCs, and THP-1 cells does not alter the expression of SAMHD1 significantly from steady-state levels, which are comparable in these types of cell [204, 575-578].

In primary yolk sac derived tissue-resident macrophages such as microglia and alveolar macrophages, SAMHD1 expression is comparable to that observed in blood macrophages [567]. Immunoblot of SAMHD1 in esYDMs revealed robust expression at levels comparable to those observed for the total fraction of SAMHD1 in PMA treated THP-1 cells (Figure 3.5A). This could indicate similar SAMHD1 expression levels to blood MDMs since, as just discussed, SAMHD1 levels in PMA treated THP-1 cells, and blood MDMs have been shown to be comparable.

SAMHD1 expression levels alone do not determine the HIV-1 restrictive capacity of a cell. For example, although SAMHD1 is expressed at comparable levels in macrophages and activated (cycling) CD4+ T-

cells, SAMHD1 is restrictive to HIV-1 in the former but permissive in the latter [229]. As previously described, posttranslational modification of SAMHD1 via phosphorylation at T592 has been shown to modulate HIV-1 antiviral activity [163, 209]; unphosphorylated SAMHD1 is restrictive to HIV-1 whereas phosphorylated SAMHD1 is permissive. Moreover, the degree of phosphorylated SAMHD1 positively correlates with the potency of HIV-1 restriction. SAMHD1 is phosphorylated at T592 by the cyclin-dependent kinase CDK1, which in turn is modulated by the cell cycle in addition to type I and II IFNs [163, 579].

SAMHD1 has been shown to be partially unphosphorylated at T592 in PMA treated THP-1 cells and U937 cells, and completely unphosphorylated in blood MDMs [209]. The phosphorylation phenotype in yolk sac derived tissue-resident macrophages and esYDMs, however, is less well defined. Immunoblot of phosphorylated SAMHD1 (pSAMHD1) did not identify any phosphorylated SAMHD1 confirming a similar phenotype to that reported for blood MDMs. In contrast, in PMA treated THP-1 cells and cycling CD4+ T-cells, SAMHD1 exists in partially and predominantly phosphorylated states, respectively (Figure 3.5A).

These results show that in esYDMs, the SAMHD1 expression and phosphorylation phenotype is like that reported for bone marrow-derived blood macrophages.

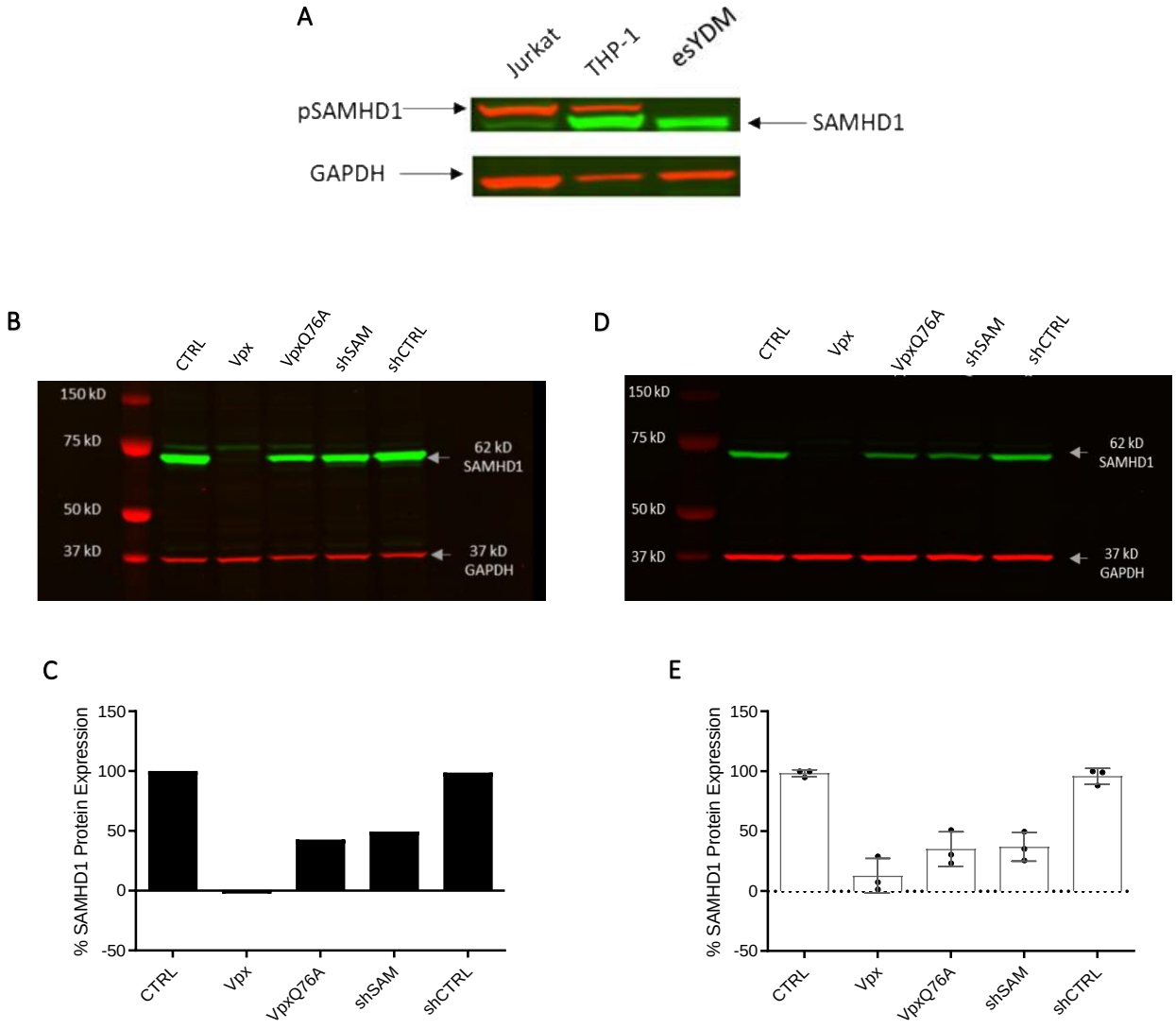


Figure 3.5 SAMHD1 protein expression profile.

Immunoblot of Jurkat cells, THP-1 cells, and esYDMs; stained with α-SAMHD1, α-phosphorylated SAMHD1, and α-GAPDH antibodies (**A**). Immunoblot of esYDMPs expressing a transgene control (CTRL), Vpx (Vpx), VpxQ76A (VpxQ76A), shRNA targeting SAMHD1 (shSAM) or an shRNA control (shCTRL), stained with α-SAMHD1 and α-GAPDH antibodies (**B**). Quantification (using LICOR software) of (B) - graphical representation of SAMHD1 protein levels in esYDMPs. Each sample has been internally normalised to GAPDH levels, relative quantity is expressed compared to the respective control (CTRL) (n=1) (**C**). Immunoblot of esYDMs expressing a transgene control (CTRL), Vpx (Vpx), VpxQ76A (VpxQ76A), shRNA targeting SAMHD1 (shSAM) or an shRNA control (shCTRL), stained with α-SAMHD1 and α-GAPDH antibodies (**D**). Relative expression quantification (using LICOR software) of (D) - graphical representation of SAMHD1 protein levels in esYDMs, mean with SD. Each sample has been internally normalised to GAPDH protein levels, relative quantity is expressed compared to the respective control (CTRL) (n=3) (**E**).

3.3.3 Vpx degrades SAMHD1 in esYDMs and ipsYDMs

In human cells, the efficiency of SAMHD1 antagonisation by Vpx is primarily dependent on cell type but also cellular differentiation and polarisation state. For example, in MDMs and MDDCs, Vpx degrades SAMHD1; however, in es cells, SAMHD1 is resistant to Vpx-mediated degradation [573]. Variability also exists in cells of the same lineage. In bone marrow-derived myeloid cells, for example, Vpx-mediated SAMHD1 antagonisation is more efficient in MDMs and MDDCs than in blood monocytes. Furthermore in primary DC cell subsets (mDCs), and particularly plasmacytoid DCs (pDC), SAMHD1 is relatively resistant to Vpx mediated degradation [580]. Components of the IFN system may be involved since blocking IFN signalling in mDCs and pDCs partially rescued SAMHD1 degradation by Vpx, and application of exogenous IFN to MDDCs rendered SAMHD1 resistant to antagonisation [580]. IFN expression does not, however, explain the block to Vpx-mediated SAMHD1 degradation in HEK293T cells or es cells, or indeed the portion of SAMHD1 protein remaining in mDCs and pDCs post silencing of IFN signalling. As such, cell lineage, or indeed polarisation of a given cell type subset, is not a reliable predictor of the efficiency of Vpx-mediated SAMHD1 degradation.

In primary yolk sac derived tissue-resident macrophages such as alveolar macrophages and microglia, Vpx potently degrades SAMHD1 [567]. Immunoblot of protein extracted from esYDMPs and esYDMs expressing Vpx showed that in these cells, Vpx efficiently degrades SAMHD1; however, degradation is not 100% efficient, and a small amount of SAMHD1 protein remained (Figure 3.5B, C, D, and E). Unexpectedly, the Vpx control mutant, VpxQ76A, was also able to degrade SAMHD1 in these cells. This is unexpected since the mutation at residue 76 from glutamine (Q) to alanine (A) is purported to destroy interaction with the DCAF1-CLR4 complex and hence, degradation of SAMHD1 [2, 148]. Thus, in esYDMs, Vpx may modulate SAMHD1 protein concentrations via multiple mechanisms. These results show that in esYDMPs and esYDMs, SAMHD1 is degraded by Vpx.

3.3.4 Quantification of dNTPs using the Tritiated (^{3}H) dNTP enzymatic assay (dNTP assay)

As previously discussed, SAMHD1 is a dNTPase, and therefore, a thorough investigation into the activity of SAMHD1 in scYDMs required the ability to quantify dNTPs in cells. In order to do this, I established and optimised the dNTP assay (refer to Section 3.2.2 Tritium based enzymatic assay for the determination of intracellular dNTP concentrations). Quantification of dNTPs required separation from other cell constituents. Once extracted, lyophilised dNTPs were resuspended to a concentration of 1 x 10^4 cells (equivalent) per µL. Between 6.5µL and 13µL of each sample was used per reaction (per experimental repeat); thus, a minimum of 65,000 cells were required to determine dNTP concentrations using this assay. Samples were diluted further if required in order to keep nucleotide measurements within the linear range 0.01-8pmol per 1 x 10^6 cells. Linear standard curves were established for all four dNTPs (Figure 3.6A) for each run of the assay. dATP concentrations were then quantified in es cells, HEK293T cells, Astrocytes, blood MDMs, PMA treated THP-1 cells, untreated THP-1 cells, and esYDM (Figure 3.6B & C), and all four dNTPs were quantified in blood MDMs (Figure 3.6D). esYDM and MDM dATP concentrations were within the range of dATP concentrations reported for blood MDMs (Table 3.1), and the expected high dNTP concentrations in HEK293T cells (compared to myeloid cells), was observed (Figure 3.6B). dATP concentrations in PMA treated THP-1 cells were higher than reported elsewhere (Table 3.1). That said, dATP concentrations in PMA treated THP-1 cells were substantially lower than those observed in non-PMA treated THP-1 cells and showed that the assay is sensitive enough to quantify the differences in dATP between cycling (monocytic) and non-cycling (macrophage-like) THP-1 cells (Figure 3.6C). Taken together, these results confirmed the sufficient quantification of intracellular dNTPs via use of the dNTP assay.

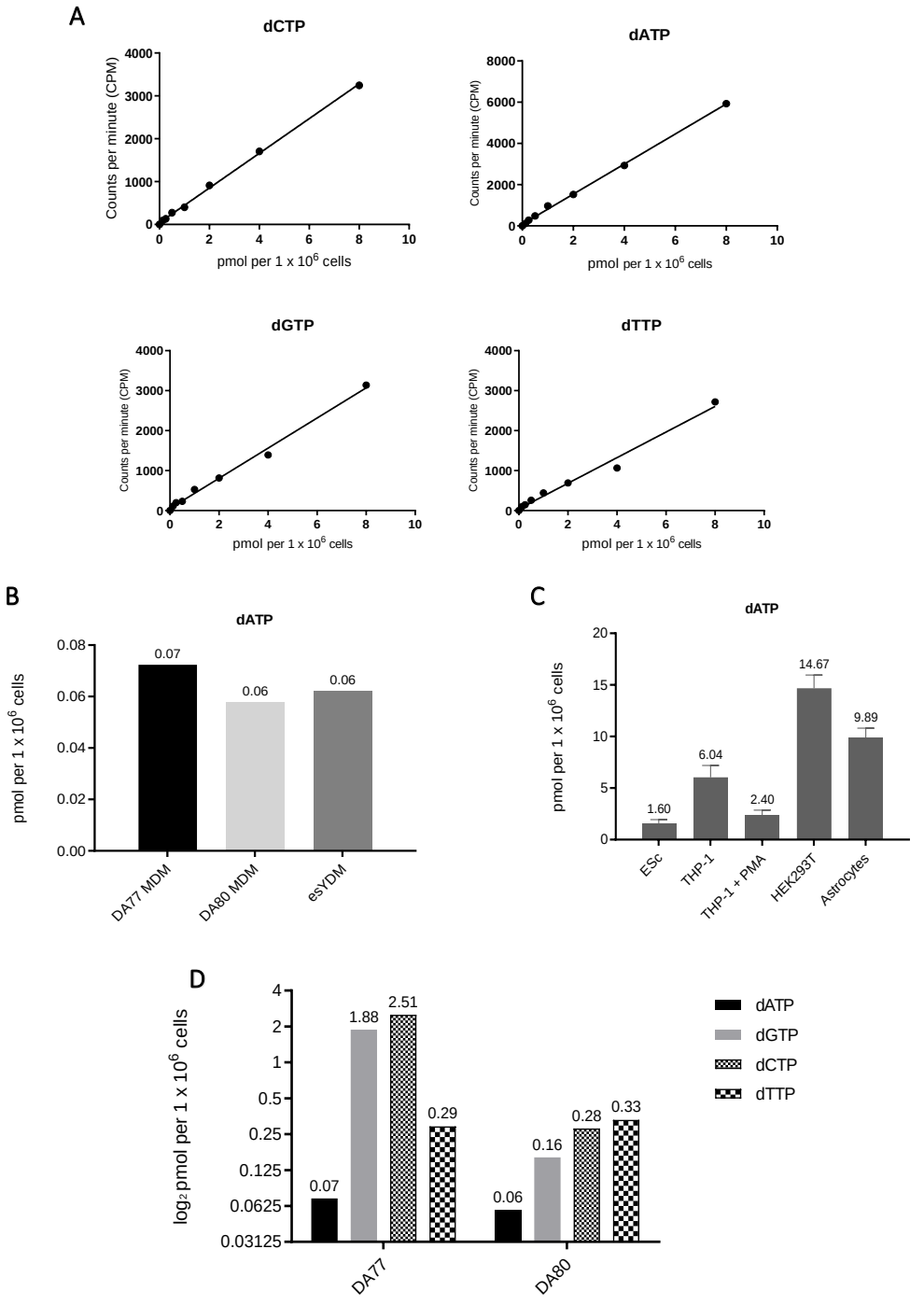


Figure 3.6 dNTP quantification by enzymatic incorporation of tritiated dNTPs.

dNTPs were extracted from 1 x 10^6 cells and quantified using the dNTP assay (for a detailed protocol refer to 3.2.2 Tritium based enzymatic assay for the determination of intracellular dNTP concentrations). A new standard for dATP, dCTP, dGTP, and dTTP was used for each run of the dNTP assay. Data are representative of a single experiment, (**A**). A 'run' ends after the decontamination procedure of the assay equipment. dATP levels are comparable in blood MDMs and esYDMs. Data is representative of a single sample point, (**B**). dATP levels were determined for es cells, THP-1 cycling cells, PMA treated THP-1 cells, HEK293T cells, and Astrocytes. Data are representative of the mean +/- SEM of a single experiment in technical triplicate (**C**). dATP, dCTP, dGTP and dTTP concentration determinations for blood MDMs from two donors. Data is representative of one sample point, (**D**).

Cell type	Desc.	Unit	dATP	dCTP	dGTP	dTTP	dNTP Assay	Ref.
MDM	MDM	μM	0.1	0.1	0.1	0.1	PE	[581]
MDM	MDM	μM	0.035	0.035	0.05	0.055	PE	[582]
MDM	MDM	nM	100	375	100	60	PE	[583]
MDM	MDM	pmol per 10^6 cells	0.062	0.081	0.051	0.084	PE	[584]
MDM	MDM	fmol per 10^6 cells	237	-	-	56	PE	[585]
MDM	MDM	fmol per 10^{-3} cells	0.2	-	-	-	PE	[204]
U937	PMA+ SAMHD1+	pmol per 10^6 cells	8	-	-	-	^{32}p Enzymatic	[586]
U937	SAMHD1+	nM	-	95	-	-	PE	[114]
U937	PMA+ SAMHD1+	pmol per 10^6 cells	0.6	-	-	-	HPLC	[188]
U937	PMA+ SAMHD1+	pmol per 10^6 cells	0.4	-	-	-	HPLC	[182]
U937	SAMHD1+ PMA+	fmol per 10^6 cells	50	-	-	100	PE	[156]
U937	SAMHD1+ PMA+	pmol	10	2.5	8	4	HPLC	[183]
U937	PMA+	fmol	2700	5000	-	500	PE	[209]
THP-1	PMA+	fmol per 10^6 cells	22	-	-	25	PE	[587]
MDDC	MDDC	nM	100	240	240	125	PE	[575]
CD4+ T-cells	Resting	pmol per 10^6 cells	0.32	0.35	0.28	0.31	PE	[584]
CD4+ T-cells	Activated	pmol per 10^6 cells	1.63	1.89	1.45	2.53	PE	[584]
HeLa	Hela	pmol per 10^6 cells	34	-	-	-	^{32}p Enzymatic	[586]
Fibroblast	Fibroblast	pmol per 10^6 cells	1.1	1.6	0.2	0.9	Enzymatic	[588]

Table 3.1 Reported dNTP concentrations for several cell types.

Table showing dNTP concentrations for various cell types. All data are extracted from published reports. MDM – monocyte-derived macrophage; PE - Primer Extension assay (Single nucleotide incorporation assay) [584]; HPLC - High performance liquid chromatography [570]; ^{32}p – Phosphorus-32 [570]; SAMHD1+ –Stable transgene expression of wild type SAMHD1; PMA+ –Differentiated using PMA.

3.3.5 SAMHD1 hydrolyses dNTPs in esYDMs and ipsYDMs

The relationship between SAMHD1 activity, presence of Vpx and dNTP concentrations is relatively uniform across cell types and polarisation states: in cells where SAMHD1 is catalytically active in suppression of dNTPs, such as blood monocytes, MDMs, MDDCs, resting CD4+ T-cells and THP-1 cells, antagonisation of SAMHD1 via gene silencing or application of Vpx, is concomitant with an increase in dNTP concentrations. Similarly, in cells where SAMHD1 is not catalytically active, such as cycling CD4+ T-cells, antagonisation of SAMHD1 via gene silencing or Vpx does not significantly alter dNTP concentrations [229, 230, 582, 589]. An isolated exception has been reported in LPS matured MDDCs, where, although the application of Vpx resulted in the degradation of SAMHD1, no associated increase in dNTP concentrations was observed [590].

Expression of Vpx in PMA treated THP-1 cells coincided with significant increases in dATP and dGTP, over wild type controls (Figure 3.7A). No increases in dATP or dCTP concentrations were observed, however, in THP-1 cells expressing VpxQ76A or in SAMHD1 knockdown (SAMHD1-KD) THP-1 cells (Figure 3.7B & C). Analysis of dNTP concentrations in esYDMs did not reveal notable Vpx-mediated increases in dATP, dCTP, dGTP or dTTP (Figure 3.8A). Furthermore, no notable increases in dATP, dCTP, dGTP, or dTTP were observed in esYDMs expressing VpxQ76A or in SAMHD1-KD esYDMs, compared to controls (Figure 3.8A). After optimising the dNTP quantification assay sample normalisation procedure (refer to Section 3.2.2 Tritium based enzymatic assay for the determination of intracellular dNTP concentrations), the dATP concentrations in esYDMs were re-assessed using the same samples. Analysis of post-optimisation dATP concentrations revealed a 7.6-fold increase in dATP concentrations in cells expressing Vpx compared to controls, a magnitude increase approximately half that reported in blood MDMs (Table 3.2). In addition, a 2.5-fold increase in dATP concentrations in SAMHD1-KD cells was observed, whereas no increase in dATP was observed in cells expressing VpxQ76A (Figure 3.8B, C, E, & F), all compared to controls. Interestingly, the Vpx mediated increase in dATP was 2.7-fold larger than dATP increases observed in SAMHD1-KD cells (Figure 3.8D).

These results imply that SAMHD1 is active in dATP hydrolysis in esYDMs. Furthermore, these data imply that the application of Vpx results in an increase in dATP in esYDMs and PMA treated THP-1 cells, and moreover that Vpx mediated increases in dATPs may be larger than those observed for increases consequent of SAMHD1-KD in esYDMs. Interestingly, the Vpx effect on dATP concentrations appears proportionally related to the effect of Vpx on SAMHD1 protein expression levels (Figure 3.5E and Figure 3.8B). Similarly, the effect SAMHD1-KD on dATP concentrations appears proportionally related to the effect of SAMHD1-KD on SAMHD1 protein expression levels (Figure 3.5E and Figure 3.8C). Finally, expression of the VpxQ76A mutant was not concomitant with a rise in dATP in esYDMs or PMA treated THP-1 cells, and thus the effect of VpxQ76A on dATP concentrations does not appear proportionally related to the effect of VpxQ76A on SAMHD1 expression levels in esYDMs (Figure 3.5E and Figure 3.8E).

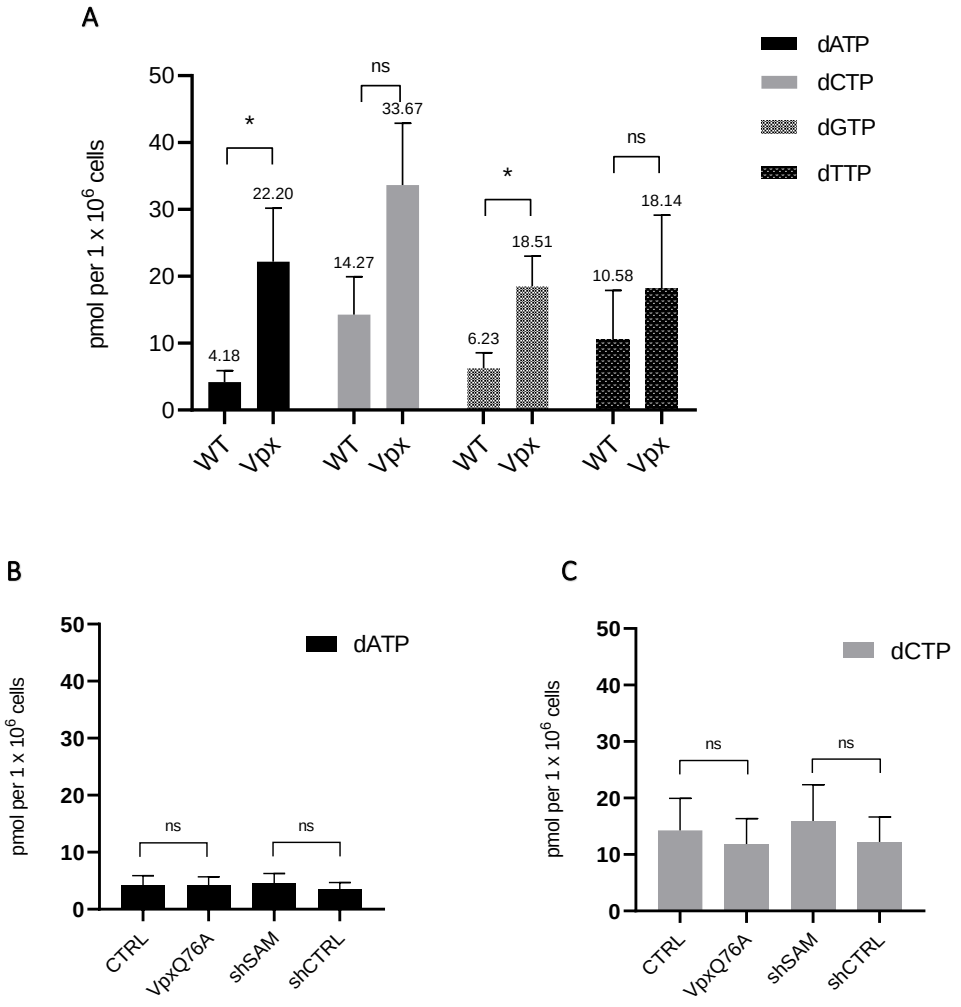


Figure 3.7 dNTP concentrations in relation to Vpx and SAMHD1 in PMA treated THP-1 cells.

dNTPs were extracted from 1 x 10^6 cells and quantified using the dNTP assay (for a detailed protocol refer to 3.2.2 Tritium based enzymatic assay for the determination of intracellular dNTP concentrations). Endogenous lentivector transgene expression of Vpx protein results in a significant increase in dATP and dGTP, but not dCTP or dTTP, (**A**). Neither expression of short hairpin RNA targeting SAMHD1 (shSAM) or the Vpx mutant Q76A resulted in an increase in dATP or dCTP, (**B**). Data are presented as the mean +\- SEM and is representative of three independent experiments (n=3); one-tailed, unpaired, parametric t-test. ns=non-significant, *p<0.05.

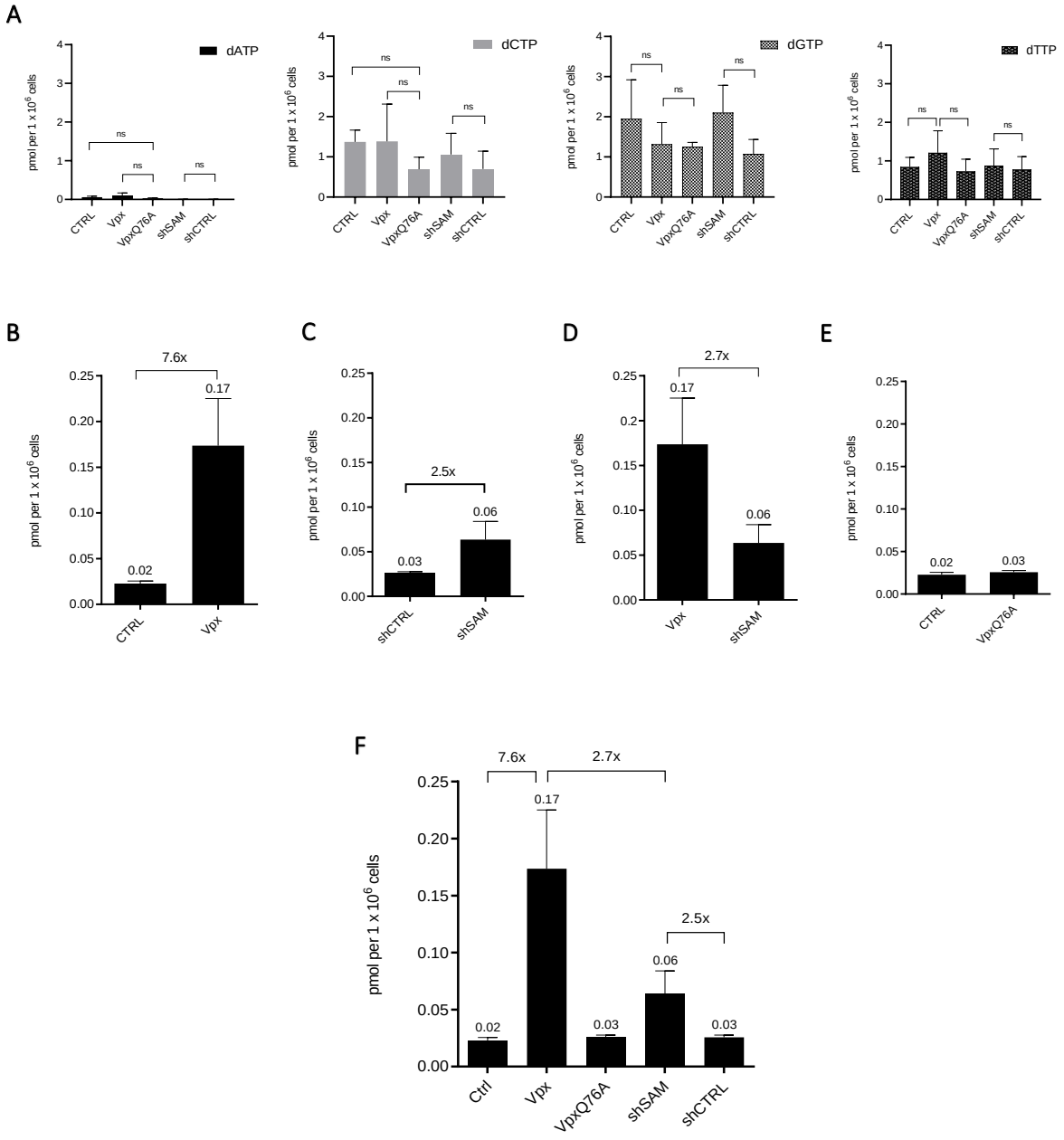


Figure 3.8 dNTP concentrations in relation to Vpx and SAMHD1 in esYDMs.

dNTPs were extracted from 1 x 10^6 cells and quantified using the dNTP assay (for a detailed protocol refer to 3.2.2 Tritium based enzymatic assay for the determination of intracellular dNTP concentrations). Expression of Vpx, shSAM, or VpxQ76A does not significantly alter the concentration of dNTPs in esYDMs; data are presented as the mean +\- SEM and is representative of three independent experiments (n=3); one-tailed, unpaired, parametric t-test; ns=non-significant, (**A**). The same samples run in (A) were re-run after assay optimisation switching to normalisation using intracellular ATP concentrations (**B - F**). Here expression of both Vpx and shSAM result in 7.6-fold and 2.5-fold increases in dATP over controls, respectively (**B & C**), furthermore, dATP increases in Vpx expressing cells were 2.7-fold higher than dATP concentrations in shSAM expressing cells, (**D**). There was no increase in dATP concentration in cells expressing VpxQ76A or shCTRL, (**E & F**). For **B,C,D, E and F**, data are presented as the mean +\- SEM and is representative of a single experiment executed in technical triplicate (n=1).

Cell Type	Desc.	Unit	dATP (+Vpx Fold Change)	dCTP (+Vpx Fold Change)	dGTP (+Vpx Fold Change)	dTTP (+Vpx Fold Change)	dNTP Assay	Ref.
MDM	MDM	logμM	0.035 (-vpx) (0.55) (+vpx) [15fold]	0.035 (-vpx) (1) (+vpx) [29fold]	0.05 (-vpx) (0.56) (+vpx) [11fold]	0.055 (-vpx) (0.25) (+vpx) [4.5fold]	PE	[582]
MDM	MDM	fmol per 10^6 cells	237 (-vpx) 3561 (+vpx) [15fold]	-	-	56 (-vpx) 304 (+vpx) [5.4fold]	PE	[585]

Table 3.2 Reported change in dNTPs for the addition of Vpx.

Table showing Vpx effect on dNTP concentrations in MDMs. All data are extracted from published reports. MDM – monocyte derived macrophage; PE - Primer Extension assay (Single nucleotide incorporation assay) [584] (-vpx) dNTP concentrations in absence of Vpx; (+vpx) dNTP concentration in the presence of Vpx.

3.3.6 SAMHD1 restricts HIV-1 in esYDMs and ipsYDMs

SAMHD1 restricts HIV-1 in non-cycling cells such as blood monocytes, MDMs, MDDCs, resting (non-cycling) CD4+ T-cells, but is non-restrictive to HIV-1 in cycling cells, such as activated (cycling) CD4+ T-cells, HEK293T cells and es cells [155, 229, 230, 243, 567, 573, 574]. A notable exception to this is the immortalised monocytic cell line THP-1. PMA treatment of these cells stimulates exit from the cell cycle to a non-cycling reversibly differentiated state that phenotypically mimics macrophages. In non-cycling THP-1 cells, SAMHD1 is restrictive to HIV; however, in cycling THP-1 cells, SAMHD1 is also restrictive to HIV-1 albeit to a lesser extent than in non-cycling THP-1 cells [113, 243]. This exception is likely a result of the immortalised state of these cells and therefore is not representative of a myeloid phenotype found *in vivo*. SAMHD1-mediated restriction of HIV-1 is, therefore, independent of SAMHD1 expression levels (e.g., cycling CD4+T cells where SAMHD1 is highly expressed yet non-restrictive to HIV-1) and instead modulated in part by posttranslational modifications such as phosphorylation at T592 (refer to Chapter 1, Section 1.1.5.4 SAMHD1; refer to Chapter 3, Section 3.3.2 SAMHD1 is phosphorylated and highly expressed in esYDMs). However, even in non-cycling cells of the same lineage, such as monocytes, MDMs, and MDDCs, where SAMHD1 is expressed and phosphorylated to similar levels, there is variation in the potency of SAMHD1-mediated HIV-1 restriction [143, 567]. Ergo SAMHD1-mediated HIV-1 restriction is determined by several factors, including cell type, cell cycling status, cell activation or polarisation, and posttranslational modification of SAMHD1.

The phenotype of SAMHD1 mediated HIV-1 restriction in yolk sac derived tissue-resident macrophages is less well described than for blood macrophages of bone marrow lineage. Yolk sac derived macrophages self-renew and thus will require periods of elevated dNTP concentrations for mitosis. A long-lived myeloid self-renewing cell subset that is similarly restrictive to HIV-1 has yet to be described, and this, when considered with the cell cycle dependence of SAMHD1 activity detailed above, implies that yolk sac derived macrophages may have intermittent periods when SAMHD1-mediated HIV-1 restriction is diminished. In support of this, SAMHD1 has been shown to be variably restrictive in primary yolk sac derived tissue-resident macrophages such as microglia and alveolar macrophages [567].

In order to investigate SAMHD1 mediated HIV-1 restriction in esYDMs, a single round HIV-1 infection assay using pseudotyped HIV-1 replication-defective virus encoding the luminescent reporter genes green fluorescent protein (GFP) or luciferase (LUC)), were used (refer to Section 2.4.3 HIV-1 Infection assays). Successful HIV-1 infection is defined by the integration of the viral genome into that of the hosts and expression of viral genes. Hence, quantification of luminescence was used to determine LTR driven viral gene expression and was thus confirmation that the early stages of infection were complete.

HIV-1 infection dynamics in transduced esYDMs and ipsYDMs were investigated using the HIV-1 infection assay (GFP) (refer to Section 2.4.3.1 HIV-1 Infection Assay (GFP)). esYDMs and ipsYDMs exposed to HIV-1.GIP alone resulted in HIV-1 infection of approximately ~7% of cells (Figure 3.9). Knockdown of SAMHD1 in esYDMs and ipsYDMs resulted in 4.2-fold and 5.1-fold rescue of HIV-1 infection, versus HIV-1 infection cells expressing the shRNA control (shCTRL), respectively (Figure 3.9A & B). Furthermore, in both esYDMs and ipsYDMs antagonisation of SAMHD1 via endogenous expression of Vpx resulted in a 4-fold and 3.2-fold rescue of HIV-1 infection versus controls, respectively (Figure 3.9E & F). These fold changes are similar to those reported in blood MDMs (Table 3.3). Taken together, these results indicate that SAMHD1 is active in restricting HIV-1 in esYDMs and ipsYDMs. Moreover,

these results show that the expression of Vpx protein rescues HIV-1 infection in esYDMs and ipsYDMs (Figure 3.9E & F). Finally, there was no significant difference in the rescue of HIV-1 infection in isolation, in the presence of Vpx, or in SAMHD1 KD cells, between esYDMs and ipsYDMs (Figure 3.9I). This could indicate that induced pluripotency does not alter HIV-1 infection dynamics in differentiated macrophages from that observed in macrophages differentiated from es cells. (Figure 3.9I).

Cell Type	Description	Addition of Vpx	Reference
MDM	MDM	3-33-fold	[582]
MDM	MDM	3-fold	[210]
MDM	MDM	30-40-fold	[585]
MDM	MDM	9-fold	[587]
MDM	MDM	10-fold	[567]
AM	AM	15-fold	[567]
PM	PM	20-fold	[567]
Microglia	Microglia	19-fold	[567]
MDDC	MDDC	30-fold	[580]
MDDC	MDDC	12-fold	[3]
pDC	pDC	5-fold	[580]
mDC	mDC	2-fold	[580]
THP-1	THP-1	9-fold	[3]
THP-1	PMA+	4-fold	[587]
U937	SAMHD1+	6-fold	[155]

Table 3.3 Reported rescue of HIV-1 infection by Vpx.

Table showing Vpx effect on dNTP concentrations for various cell types. All data are extracted from published reports. MDM – monocyte-derived macrophage; MDDC – monocyte-derived dendritic cell; pDC- plasmacytoid dendritic cell, mDC myeloid dendritic cell; AM – Alveolar macrophage; PM – Peritoneal macrophage; SAMHD1+ –Stable transgene expression of wild type SAMHD1; PMA+ –Differentiated using PMA.

3.3.7 SAMHD1 independent functions of Vpx in esYDMs and ipsYDM

All primate lentiviral accessory proteins, including Vpx, are multifunctional, active in assisting viral replication at various steps in the life cycle (See Chapter 1, Section 1.1.4 HIV and SIV Accessory proteins). For example, (and as previously mentioned) in addition to SAMHD1 antagonisation, Vpx has also been implicated in nuclear import of the PIC in MDMs, as well as in antagonisation of APOBEC3A, also in MDMs (see Chapter 1, Section 1.1.4.3 Vpx protein). Evidence has also been mounting for additional functions of Vpx, where both interacting partners and underlying mechanics are not so well defined. For example, a Vpx mutant lacking the n-terminal SAMHD1 binding domain was still able to initiate the

degradation of SAMHD1 and rescue HIV-1 infection in MDDCs, although it was unable to rescue HIV-2 infection in MDMs and MDDCs [591]. This hints at a potentially novel mechanism of Vpx-mediated SAMHD1 degradation. Additionally, several studies have provided evidence for a Vpx-mediated but DCAF1 independent (and therefore potentially by extension, SAMHD1 independent) mechanism to rescue HIV-1 infection [153, 592]. In both PMA treated THP-1 cells and IFN (endogenous) activated MDDCs the Vpx interaction with DCAF1 was dispensable for rescue of HIV-1 infection (refer to Section 1.1.4.3 Vpx) [576, 590]. However, DCAF1 binding is critically required for the depletion of SAMHD1 in MDMs, potentially indicating cell type and activation state dependence of some proposed additional Vpx functions [2]. In resting CD4+ T-cells, diverse Vpx (and Vpr) proteins have been shown to increase proviral transcription by targeting the host silencing factor HUSH for degradation in a DCAF1 dependent but SAMHD1 independent manner [134]. Finally, an unknown cryptic block to HIV-1 infection has been identified in resting CD4+ T cells that can be antagonised by Vpx proteins of the SIVrcm/SIVmnd-2 lineage but not of the HIV-2/SIVsm/SIVmac lineage [593]. Antagonisation was dependent on DCAF1 binding since VpxQ76A mutants were unable to rescue HIV-1 infection. Interestingly, this block was absent in MDMs. Taken together these observations further underscore the intimate link between Vpx alleles and the cell type-dependent nature of HIV-1 restriction.

In order to investigate potential Vpx-mediated SAMHD1 independent mechanisms in scYDMs, HIV-1 rescue was compared in esYDMs and ipsYDMs expressing Vpx versus SAMHD1-KD esYDMs and ipsYDMs using the HIV-1 infection assay (GFP) (refer to Section 2.4.3.1). The Vpx mediated rescue of HIV-1 infection in these cells was significantly greater than that observed with SAMHD1-KD cells (Figure 3.10A & B).

Interestingly, cell lines expressing the Vpx mutant Q76A did not show rescue of HIV infection over controls despite a reduction in SAMHD1 protein concentrations to similar levels observed in SAMHD1-KD cells (Figure 3.5D & E; Figure 3.10E & F). In order to investigate activities of VpxQ76A further, a

SAMHD1-KD ipsYDM cell line was created, which also expressed VpxQ76A via a lentiviral integrant. This, theoretically, enabled the probing of VpxQ76A behaviour in the absence of translated SAMHD1. ipsYDMs expressing Vpx, VpxQ76A, SAMHD1-KD cells, SAMHD1-KD-VpxQ76A cells, or controls were subjected to the HIV-1 infection assay (GFP) (refer to Section 2.4.3.1). Intriguingly, HIV-1 rescue in SAMHD1-KD-VpxQ76A cells was significantly higher than HIV-1 rescue in SAMHD1-KD cells alone (Figure 3.10I). In order to investigate any cell type specificity inherent in the behaviour of the VpxQ76A mutant, endogenously expressed VpxQ76A-mediated HIV-1 infection was first investigated in PMA treated THP-1 cells since several studies have reported VpxQ76A rescue of HIV-1 infection in these cells, as previously described. Actively dividing THP-1 monocytes were transduced with lentivectors expressing Vpx, VpxQ76A, shSAM, or controls and selected with puromycin (refer to Section 2.6 Lentivector transduction of THP-1 cells). Selected THP-1 monocytes were then differentiated into macrophage-like cells by supplementing media with 50ng/mL PMA for 24 hrs, after which cells were probed using the HIV-1 infection assay (GFP) (refer to Section 2.4.3.1). As expected, expression of VpxQ76A rescued HIV-1 infection in these cells (Figure 3.10H), and to a greater degree than the expression of Vpx (Figure 3.10J). Interestingly, however, Vpx and SAMHD1-KD mediated rescues were muted compared to that observed in esYDMs (refer to Section 3.3.6 SAMHD1 restricts HIV-1 in esYDMs and ipsYDMs) at 1.8-fold and 1.3-fold respectively (Figure 3.9D & H). The cell type-dependent nature of the effects of Vpx on HIV-1 infection dynamics was next investigated in esYDMPs, the monocyte-like macrophage precursor cells. Transduced esYDMP cell lines expressing Vpx, SAMHD1-KD cells, or controls were harvested from factories, incubated for 6 hrs at 37^{o}C, 5% CO_2, and were then probed with the HIV-1 infection assay (GFP) (refer to Section 2.4.3.1). Curiously, in esYDMPs, VpxQ76A rescued HIV-1 infection over 5-fold compared to controls (Figure 3.10G & Figure 3.11). Vpx and SAMHD1-KD rescue of HIV-1 infection in esYDMPs was over double the fold increases seen in esYDMs (Figure 3.9B, C, F, & G), and in contrast to esYDMs, ipsYDMs and to a certain extent PMA treated THP-1 cells, Vpx mediated rescue of HIV-1 infection was not more potent than knockdown of SAMHD1 (Figure 3.10A, B, C, and D). In summary, these results show that VpxQ76A is functional in the rescue of HIV-1 infection in PMA treated THP-1

cells, esYDMPs, and SAMHD1-KD ipsYDMs. Furthermore, the mechanism involved is independent of coupling with DCAF1 and, therefore, may also be independent of SAMHD1 degradation. Finally, the potency of VpxQ76A rescue of HIV-1 infection diminishes in cells on differentiation from esYDMPs to esYDMs.

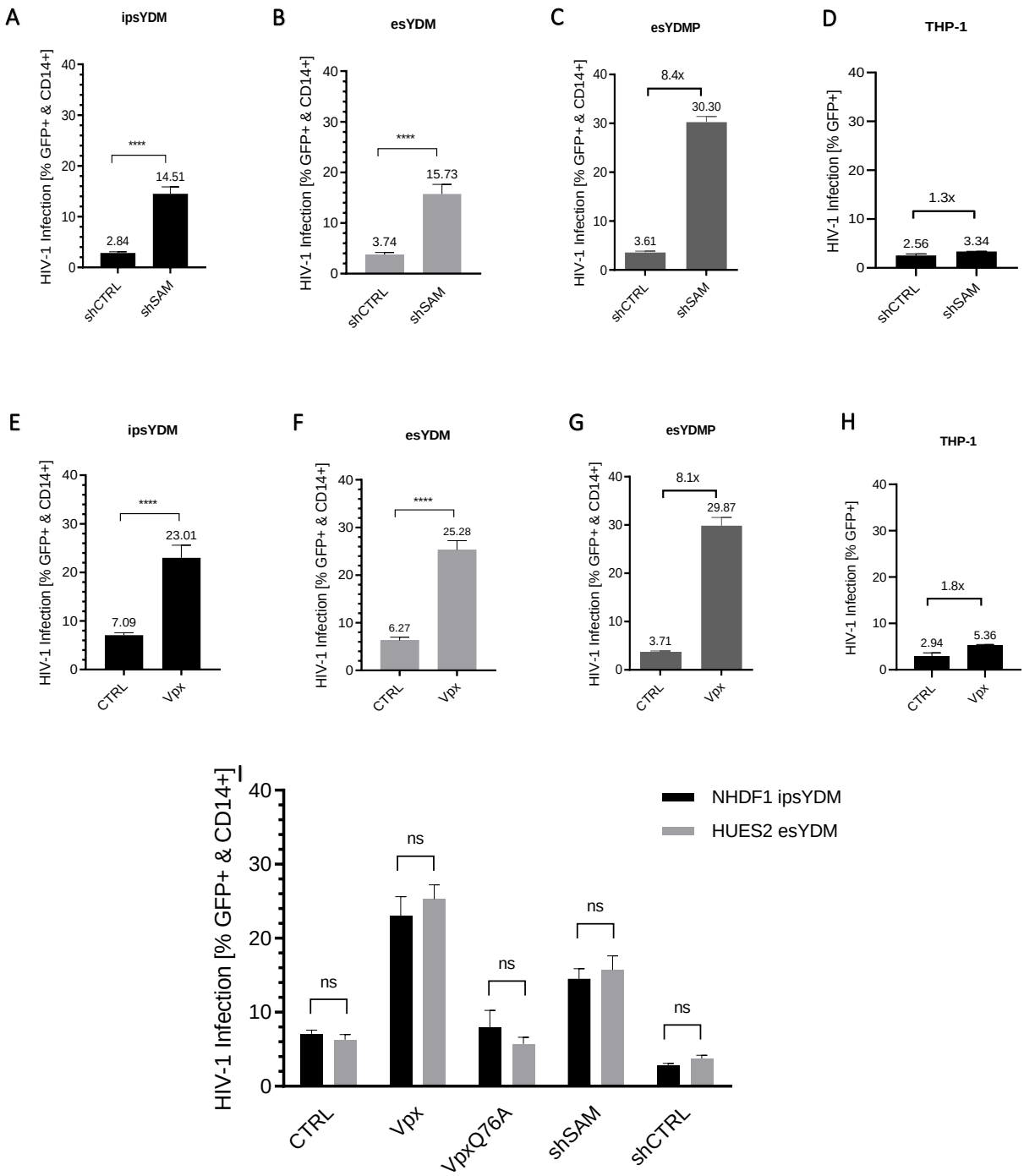


Figure 3.9 HIV-1 infection dynamics in relation to Vpx and SAMHD1.

Cells were cultured at a density of 5 x 10^4 cells per well in 96 well tissue culture plates. Cells were then infected with HIV-1.GIP virus and allowed to incubate for 3.5 days after which cells were lifted and CD14 stained. HIV-1 infection was quantified via flow cytometry. Knockdown of SAMHD1 substantially increases HIV-1 infection in ipsYDMs (**A**), esYDMs (**B**), esYDMPs (**C**), but not in PMA treated THP-1 cells (**D**). Endogenous expression of Vpx substantially increases HIV-1 infection in ipsYDMs (**E**), esYDMs (**F**), esYDMPs (**G**), and PMA treated THP-1 cells (**H**). HIV-1 infection of es cells and iPS cell-derived macrophages are comparable (**I**). Data for esYDMs and ipsYDMs are presented as the mean +\- SEM and is representative of the four independent experiments (n=4). Data for esYDMPs and PMA treated THP-1 cells represents the mean +/- SEM of a single experiment executed in technical triplicate. One-tailed, unpaired, parametric t-test. ns=non-significant, **** p<0.0001.

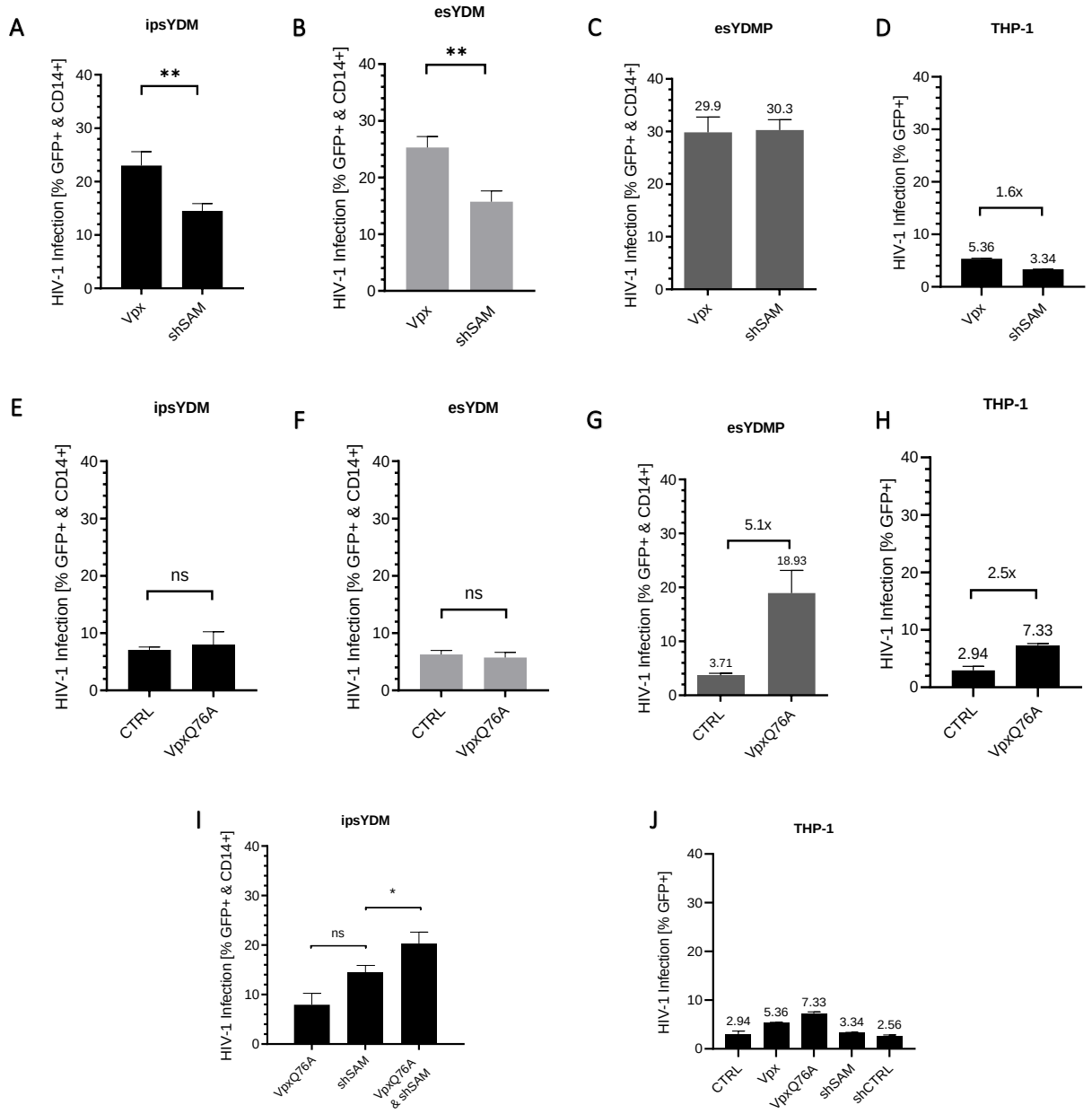


Figure 3.10 Potential SAMHD1 independent Vpx functions.

Cells were cultured at a density of 5 x 10^4 cells per well in 96 well tissue culture plates. Cells were then infected with HIV-1.GIP virus and allowed to incubate for 3.5 days after which cells were lifted and CD14 stained. HIV-1 infection was quantified by flow cytometry. Expression of Vpx rescues HIV-1 infection to a greater degree than knockdown with shSAM in ipsYDMs (**A**) and esYDMs (**B**) but not in esYDMPs (**C**) or PMA treated THP-1 cells (**D**). The Vpx mutant Q76A is unable to bind DCAF1 and cannot rescue HIV-1 infection in ipsYDMs (**E**) or esYDMs (**F**) but can rescue HIV-1 infection in esYDMPs (**G**) and PMA treated THP-1 cells (**H**). Co-expression of VpxQ76A and shSAM in esYDMs resulted in the rescue of HIV-1 infection that was greater than HIV-1 infection rescue via expression of shSAM alone (**I**). HIV-1 infection profile in relation to Vpx, VpxQ76A, and shSAM in THP-1 cells (**J**). Data for esYDMs and ipsYDMs are presented as the mean +\- SEM and is representative of four independent experiments (n=4). Data for esYDMPs and PMA treated THP-1 cells is representative of the mean +/- SEM of a single experiment consisting of three technical repeats (n=1). Statistical test used for **A**, **B**, **E**, **F** and **I** is one-tailed, unpaired, parametric t-test; ns=non-significant, *p<0.05, **p<0.01.

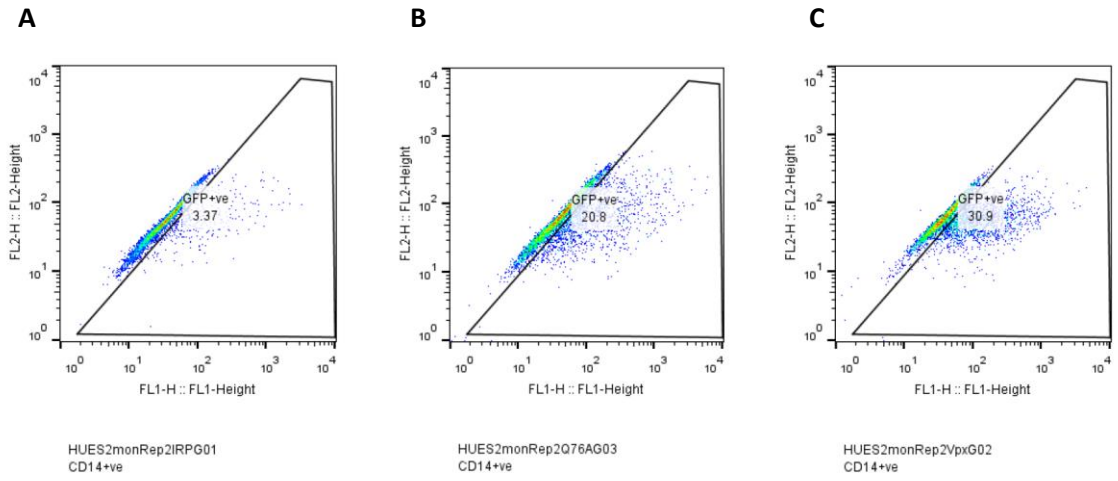


Figure 3.11 Rescue of HIV-1 infection by VpxQ76A in esYDMPs.

EsYDMPs were cultured at a density of 5 x 10^4 cells per well in 96 well tissue culture plates. Cells were then infected with HIV-1.GIP virus and allowed to incubate for 3.5 days after which cells were lifted and CD14 stained. HIV-1 infection was quantified by flow cytometry. Representative dot plots for one donor, where blue dots represent stained CD14+ esYDMPs expressing a control construct (IRP) (**A**), VpxQ76A (**B**) and Vpx (**C**). The gate represents cells expressing green fluorescent protein (GFP) and hence are infected with HIV-1 (n=1).

3.4 Discussion

In humans, HIV-1 infects macrophages of all lineages, however difficulty in obtaining primary tissue-resident macrophages, particularly from sensitive anatomical locations such as the brain, has meant that most studies to date have used bone marrow-derived blood monocyte-derived macrophages. Cellular-HIV-1 dynamics vary greatly even within terminally differentiated cells from a single lineage, such as blood MDMs and MDDCs. Thus, it follows that yolk sac derived tissue-resident macrophages and precursors, which are transcriptionally distinct from bone marrow-derived macrophages, may exhibit unique HIV-1 infection dynamics. The ability to differentiate yolk sac derived tissue resident-like macrophages from es cells and iPs cells provided a simple procedure for the continual production of scYDMPs and scYDMs in order to investigate HIV-1 dynamics in isolation, in relation to the host restriction factor SAMHD1, and in relation to the SIVmac251 accessory protein, Vpx.

Both es and iPS cell lines differentiated into macrophages that were morphologically homogenous; however, there were temporal differences in scYDMP production between the different cell lines. Knockdown of SAMHD1 via shRNA (SAMHD1-KD cells) appeared to delay eventual macrophage precursor production by approximately three weeks compared to control cell lines (Wild type (WT) and IRP). The delay in SAMHD1-KD cells is a possible consequence of cellular adjustments to modulate dNTPs in the absence of SAMHD1, which thus results in homeostasis and hence differentiation with lower overall efficiency. However, this delay was also observed in shCTRL expressing cells, so it is also possible that this was a consequence of the RNA interference system. Interestingly, although the expression of Vpx resulted in lower SAMHD1 protein expression levels than in SAMHD1-KD cells, macrophage precursors were produced approximately 2 weeks prior to SAMHD1-KD (and shCRTL expressing) cells. The mechanism underlying this Vpx-mediated effect is unclear. It is possible that the cytoplasmic fraction of SAMHD1 (which is resistant to Vpx degradation but not to shRNA silencing) may be involved. If so, this would require a larger fraction to exist in Vpx expressing cells than SAMHD1-KD cells despite the larger overall protein levels of SAMHD1 in SAMHD1-KD cells. Abolishing Vpx binding to DCAF1 (VpxQ76A expressing cells) appears to rescue differentiation to timeframes observed in control cells (e.g., WT and IRP). This suggests a dependence on SAMHD1 for this phenotype; however, it is also possible that this phenotype is a result of other, perhaps as yet undescribed, binding partners of DCAF1. A probe of SAMHD1 localisation or the use of SAMHD1 knockout cells in repeats of this experiment would be required to gain a greater understanding of this phenomenon.

Protein expression levels of SAMHD1 were probed by immunoblot (see Chapter 2, Section 2.2.2 Western Blots). In wild type esYDMs, SAMHD1 is robustly expressed, and unphosphorylated (Figure 3.5A). These data are like that observed elsewhere for blood MDMs and primary tissue-resident macrophages, adding further credence to the myeloid associated phenotype of SAMHD1 in stem cell-derived macrophages [2, 567]. In Vpx expressing esYDMs, SAMHD1 was potently degraded to a mean of 13% protein expression. Curiously, the standard deviation of the sample points for the Vpx expressing cell

lines (approx. 30%) was mirrored in the SAMHD1-KD cells and VpxQ76A expressing cell lines, but not the control cell lines. The lack of this error in the control cell lines implies that it was not caused by anomalous cell counting, which would have affected all cell lines similarly. Instead, the source of the error is specific to a factor shared by SAMHD1-KD cells, Vpx, and VpxQ76A expressing cell lines, which is hypothesised to be (SAMHD1 targeted) transgene expression. Therefore, the large standard deviation seen may be a manifestation of differing transfection efficiencies (and hence transgene expression) since data from cells produced from two separate differentiations were used in this thesis. Alternatively, the large standard deviation may represent differences in differentiation or polarisation state of esYDMs at the time of harvest. This may, in turn, be a consequence of slight concentration differences of growth factors and cytokines used during the differentiation process or the HIV-1 infection assay.

Published data for dNTP levels in blood MDMs reports a range of concentrations (Table 3.1). The lack of uniformity is probably due to differences in experimental procedure and to donor-derived differences inherent with primary sourced cells such as blood MDMs. Quantification of dNTPs in blood MDMs using the dNTP assay showed that in the steady-state dNTP concentrations fall within the range for blood MDMs shown in Table 3.1, as did dATP concentrations for esYDMs. That said, dCTP, dGTP and dTTP concentrations for the blood MDM sample DA77 were higher (compared to dATP of the same sample) than those published. This anomaly was not observed with the DA80 blood MDM sample and thus may be representative of donor-derived differences, or perhaps a requirement for additional quantification repeats. Irrespective of this anomaly, these data served as a preliminary validation of the dNTP assay, which was established specifically to produce data for this thesis. Experimental repeats are required before a dNTP concentration phenotype for all four dNTPs can be concluded for esYDMs. Further experiments should include concurrent quantification of dNTPs in blood MDMs and primary tissue-resident macrophages in order to determine any shared phenotype between these cells and esYDMs.

Initial investigations of dNTP concentrations in esYDMs did not reveal any notable increases in Vpx expressing cells, VpxQ76A expressing cells, or in SAMHD1-KD cells. However, after optimisation of the dNTP assay protocol replacing sample normalisation by cell count with sample normalisation by cellular ATP concentration, reassessment of dATP levels using the same samples revealed notable increases in dATP, for both Vpx expressing cells and SAMHD1-KD cells. The result of this optimisation highlights the sensitivity of the dNTP assay, and observation of the expected elevation of dATP by Vpx can be taken as further validation of the assay's correct functionality. Interestingly, Vpx mediated increases in dATP (7.6-fold) were approximately half that detailed in published reports (~15-fold) (Table 3.2). The deviation of these data (7.6-fold) from that observed in published reports may be due to experimental differences between the investigation in this work and published reports, such as the type of HIV-1 infection assays used, incubation times implemented, HIV-1 virus strains used, or Vpx application method. It is also possible that this is a phenotype specific to esYDMs. Experiments involving both esYDMs and blood MDMs would be required before conclusions can be drawn, as would the inclusion of primary tissue-resident macrophages in order to determine whether this is a phenotype specific to esYDMs. It was also observed that dATP increases in Vpx expressing cells were larger than those observed in SAMHD1-KD cells. This may be a consequence of the differences in SAMHD1 antagonisation efficiencies inherent with Vpx versus shRNA such that the higher levels of SAMHD1 protein available in SAMHD1-KD cells (also referred to in this thesis as residual knockdown protein - RKP) can suppress dNTP concentrations. Alternatively, Vpx may employ an additional, SAMHD1 independent mechanism to increase dNTP concentrations. Such a mechanism would require either the antagonisation of a novel dNTPase or the stimulation of dNTP synthesis, possibly via the upregulation of proteins involved in dNTP synthesis such as ribonucleotide reductase. Due to a lack of quantity of the original sample and overall time constraints prohibiting a fresh experiment, neither dCTP, dGTP, or dTTP concentrations were probed using optimised normalisation by ATP concentrations, and therefore, it is not possible to conclude what effect Vpx or SAMHD1-KD had on these nucleotides in esYDMs.

In THP-1 cells, the expression of Vpx resulted in robust increases in concentrations of all four dNTPs. The knockdown of SAMHD1, however, did not result in an increase in dNTPs. This may be a result of reduced shRNA knockdown efficiency in PMA treated THP-1 cells. Alternatively, the use of cell number to normalise samples may have allowed error to be incorporated into the assay such that significant increases in dNTPs were masked, as was observed in esYDM prior to using ATP concentrations for normalisation.

The steady-state dNTP concentrations in PMA treated THP-1 cells were all substantially higher than those observed in esYDM (dATP 72x, dCTP 10.4x, dGTP 3.2x, dTTP 12.6x). Interestingly, this is in contrast to published reports which have documented dNTP levels in PMA-treated THP-1 cells that are lower than in blood MDMs (Table 3.1). It is possible this anomaly is a result of different experimental procedures or perhaps different subclones of THP-1 cells used. It is also possible that the data presented here represent a mixture of cycling and non-cycling cells, perhaps due to inadequate concentrations (or quality) of PMA used to simulate differentiation to macrophage-like cells. Alternatively, these findings may reflect differences in the SAMHD1 activation threshold in these cells, requiring higher concentrations of dNTPs to trigger tetramerisation, and hence, hydrolysis in PMA treated THP-1 cells than in esYDMs (refer to Section 1.1.5.4 SAMHD1). Another possible explanation of the higher levels of dNTPs in PMA treated THP-1 cells compared to esYDMs might involve additional mechanisms for dNTP hydrolysis active in esYDMs, which, when combined with SAMHD1-mediated dNTP hydrolysis results in the lower overall levels seen in these cells.

HIV-1 infection dynamics in esYDM and ipsYDM cell lines were very similar. In both esYDMs and ipsYDMs, expression of Vpx rescued HIV-1 infection significantly (~4-fold) compared to HIV-1 infection in control scYDMs. This lies within, but at the bottom of, the range detailed in published reports for HIV-1 infection in blood MDMs and peripheral tissue macrophages (3-40-fold) (Table 3.3). As with the observation for dNTP concentrations in esYDMs versus primary macrophages, these differences may

reflect a phenotype specific to scYDMs; however, it could also be a consequence of experimental and donor-derived differences (inherent with blood MDMs and primary macrophages). Similarly, additional experiments probing HIV-1 infection of scYDMs and primary macrophages concurrently would be required to conclude on this subject further.

In both esYDMs and ipsYDMs expression of Vpx and SAMHD1-KD rescued HIV-1 infection significantly compared to HIV-1 infection in control cell lines; HIV-1 rescue was also more potent in Vpx expressing cells compared to SAMHD1-KD cells. Furthermore, in both esYDMs and ipsYDMs, frequency of HIV-1 infection in the control cell lines (IRP, shCTRL, and VpxQ76A) were also comparable. The similarity in HIV-1 infection dynamics between esYDM and ipsYDM suggests that artificially induced pluripotency does not affect the cellular HIV-1 restrictive phenotype at the terminally differentiated macrophage stage (i.e., compared to the natural pluripotency of es cells). Moreover, the differences often observed between donors with HIV-1 infection dynamics in primary MDMs is not observed between HUES2 and NHDF1 macrophages, which are from different donors (and different genders) (refer to Section 2.1.2 Human es cell and iPS cell culture). This may be a result of the *in vitro* differentiation lacking a factor(s) that determines the donor-derived differences observed in primary MDMs. It is also possible that this may be a phenotype specific to scYDMs.

In esYDMs, the SAMHD1 knockdown resulted in higher protein levels, lower dNTP concentrations and less potent rescue of HIV-1 infection compared to that observed with Vpx expressing esYDMs. The minimum concentration of SAMHD1 protein required for HIV-1 restriction has not been described, and thus, it is possible that this phenomenon was due to the activity of the higher concentrations of SAMHD1 protein present in SAMHD1-KD cells (residual knockdown protein - RKP). Alternatively, this may be an effect of a novel function encoded by Vpx that is SAMHD1 independent, and that may be separate from the mechanism by which Vpx is hypothesised to increase dNTPs. Antagonisation of APOBEC3A is a potential candidate; however, (and as concluded in other studies) investigations into APOBEC3A-Vpx

interactions are difficult in SAMHD1 expressing cells due to unknown contribution of SAMHD1 expression levels to HIV-1 restriction [594].

Vpx targets SAMHD1 for degradation by acting as a tether between SAMHD1 and the DDB1-DCAF1-CLR4-E3-Ubiquitin ligase complex. Vpx binds to human SAMHD1 via multiple interactions on its n-terminus and the connecting loop of α-helix 2 and α-helix 3. α-helix 3 is also the site of Vpx interaction with DCAF1, specifically at residue 76 and therefore Vpx interaction with DCAF1 can be abolished by a point mutation at this residue from glutamine (Q) to, for example, alanine (A). Such a Vpx mutant is defined as VpxQ76A (see Chapter 1, Section 1.1.4.3 Vpx). The inability of VpxQ76A to degrade SAMHD1 has been documented for several cell types, including MDMs [2], MDDCs [590] and resting CD4+T-cells [595]. However, expression of VpxQ76A in esYDM resulted in the unexpected fall in SAMHD1 protein concentrations to levels observed in SAMHD1-KD cells (refer to Figure 3.5E). The spread of sample points was of a similar magnitude to that observed with Vpx and shSAM (see above) and thus may also be a consequence of differing transfection efficiencies. Reduced SAMHD1 expression in VpxQ76A expressing cells implies that VpxQ76A employs an alternative DCAF1-independent mechanism for the degradation of SAMHD1. Such an alternative degradation pathway may involve an alternative (and as yet undescribed) ubiquitin ligase complex with which VpxQ76A acts as an adaptor. Alternatively, VpxQ76A binding to SAMHD1 may inhibit SAMHD1 function which may result in premature degradation. Certainly, Vpx has been shown to destabilise tetramerisation of SAMHD1 (as previously described), which presents at least the possibility that VpxQ76A may do the same. Intriguingly, an alternative degradation pathway has also been proposed for SIVdeb Vpr, which, like VpxQ76A, is active in SAMHD1 depletion yet did not interact with Cul4 ubiquitin ligase complex proteins, DDB1 [96] or DCAF1 [89].

Although SAMHD1 protein levels were comparable in SAMHD1-KD cells and VpxQ76A expressing cells, dNTP concentrations in SAMHD1-KD cells increased, whereas dNTP concentrations in VpxQ76A expressing cells remained unaltered compared to controls. This implies that effects on SAMHD1

hydrolysis by inhibited translation (SAMHD1-KD) are different from effects consequent of destabilisation or degradation by Vpx (or VpxQ76A). Interestingly a similar scenario has been detailed elsewhere: Reinhard et al. showed that in LPS treated MDDCs, Vpx mediated degradation of SAMHD1 was not accompanied by an increase in dNTP concentrations [590]. However, further investigation is required to determine the nature of the mechanism underlying this phenomenon.

As shown by others [153], and now also in this thesis, in PMA differentiated THP-1 cells, the interaction between DCAF1 and Vpx is dispensable for Vpx-mediated rescue of HIV-1. This was shown by the rescue of HIV-1 infection by VpxQ76A in these cells. This activity of VpxQ76A has also been observed in LPS treated MDDCs, and to a lesser extent in MDMs, elsewhere [590]. In this thesis expression of VpxQ76A rescued HIV-1 infection in esYDMPs, the monocyte-like macrophage-precursor cells freshly harvested from factories. Initially, this phenotype did not appear to extend to esYDMs since HIV-1 infection in VpxQ76A expressing esYDMs was not significantly higher than controls and no increase in dNTPs were observed. However, expression of VpxQ76A in SAMHD1-KD ipsYDMs revealed rescue of HIV-1 infection that was significantly higher than that observed in SAMHD1-KD cells not expressing VpxQ76A. This implied that VpxQ76A did have a restrictive phenotype in these cells and, moreover that it may be independent of SAMHD1. Notably, the magnitude of restriction was lower than that observed in esYDMPs, requiring co-expression of VpxQ76A and shSAM (SAMHD1-KD) before it became quantifiable. The myeloid differentiation state dependence of this observation is analogous to reports elsewhere. For example Vpx has been shown to rescue HIV-1 infection in IFNα treated PMA differentiated THP-1 cells but not IFNα treated actively dividing THP-1 monocytes [204]. Similarly, Vpx-mediated rescue of HIV-1 infection in LPS stimulated cells is far more potent in MDDCs than MDMs [590]. These data presented here imply a DCAF1 and potentially SAMHD1 independent mechanism of HIV-1 restriction that can be counteracted by Vpx in ipsYDMs and esYDMPs. The difference in potency of the unknown restriction factor in esYDMPs and ipsYDMs may be due to higher expression of the unknown factor in esYDMPs compared to ipsYDMs. Whether this is the same factor active in restriction in PMA treated

THP-1 cells or LPS treated MDDCs is unclear. Certainly, the cell type variability of the effect on HIV-1 restriction is analogous, as is the lack of increase in dNTPs even in a background of the concurrent rescue of HIV-1 infection [590]. The lack of required stimulation, whether via PMA, IFN, or LPS in esYDMPs and ipsYDMs, however, is notable. A possible explanation for this is that the novel factor is expressed constitutively in yolk sac derived tissue-resident macrophages but requires cytokine-mediated induction or posttranslational modification in bone marrow-derived MDMs, such as the activity of SAMHD1 in cycling CD4+ T-cells versus resting CD4+ T-cells (phosphorylation at T592) (refer to Section 1.1.5.4 SAMHD1). Vpx has been implicated in suppressing the IFN response [592]. If mutation at residue 76 (Q76A) destroyed this function (via binding to DCAF1, for example), then an IFN-induced antiviral response may have ensued. In such a scenario, it is possible that VpxQ76A may then have functioned in the rescue of HIV-1 infection in the background of an IFN-induced antiviral response, as has been reported elsewhere in MDDCs [576]. Intermittent testing of scYDM supernatants did not detect IFNα or IFNβ (data not shown), however the intermittent nature of the testing as well as the lack of IFNγ probing means that the possibility of this scenario cannot be completely dismissed.

In summary, in esYDMs SAMHD1 expression, phosphorylation at T592, dNTP hydrolysis, and restriction of HIV-1 are like those detailed in published reports for blood MDMs, which have been shown to behave (with regards to HIV-1 infection dynamics) like peripheral tissue-resident macrophages [567]. Vpx potently degrades SAMHD1, amplifies dNTP concentrations and rescues HIV-1 restriction in esYDMs. However, the interdependence of these phenotypes was not tested since separate cell cultures were used for SAMHD1 expression quantification, dNTP quantification, and HIV-1 infection experiments. SAMHD1 degradation, dNTP hydrolysis, and HIV-1 restriction are more potent in Vpx expressing cells than in SAMHD1-KD cells, which may be due to the lower efficiency of SAMHD1 antagonisation by shRNA (resulting in higher levels of SAMHD1 protein – residual knockdown protein) versus Vpx. Alternatively, Vpx may facilitate SAMHD1 degradation by a DCAF1 independent mechanism and facilitate dNTP hydrolysis and rescue HIV-1 infection by a DCAF1 *and* SAMHD1 independent mechanisms. HIV-1

infection kinetics in ipsYDMs were very similar to esYDMs. This showed that the induced pluripotency reprogramming procedure was not detrimental to the target cell retroviral restrictive phenotype. It was also indicative that the donor-derived differences often observed in HIV-1 infection assays using blood MDMs may not be transcriptionally native to the cells in question.

Chapter 4

Chapter 4: CRISPR- Cas9 Gene Editing of SAMHD1

4.1 Introduction

In Chapter 3, a 2nd generation self-inactivating lentivector based transgene expression system was used to genetically modify es and iPS cells to either express Vpx, shRNA targeting SAMHD1 (shSAM) or relevant controls. The gene of interest (GOI) was encoded within a bicistronic RNA consisting of GOI-IRES-PuroR, driven by a constitutively active EF1α promoter. Genetically modified es cells were successfully differentiated into scYDMs. Genetically modified scYDMs and control scYDMs were similar in terms of morphology.

Genetic modification via lentivector transgene expression is a reliable and reproducible system; however, some limitations do exist, particularly with regards to the expression of toxic genes or genes that may interfere with the differentiation process. None of the lentivectors constitutively expressed transgenes used in this thesis appear toxic to either iPS cells or macrophages derived from these cells; however, it was observed that both shRNA expressing cells lines (shSAM and shCTRL) produced macrophages approximately 3 weeks after control cell lines. If this was observed in shSAM cell lines alone, it could be attributed to the depletion of SAMHD1; however, it was also observed in shCRTL expressing cell lines which raised questions regarding the integrity of the RNAi system used. In addition, Vpx expressing factories consistently produced cells at earlier time points than shSAM and shCTRL cells but later than wild type (non-transduced), IRP, and VpxQ76A expressing cells. As previously discussed, this could be due to SAMHD1 localisation but could also be due to a Vpx mediated effect on differentiation that may be SAMHD1 independent (given the earlier production timing compared to shSAM expressing cells). In support of this, several reports have implicated SAMHD1 independent functions for Vpx, such as a DCAF1 (and hence SAMHD1) independent mechanism for rescue of HIV-1 infection (refer to Chapter 3, Section 3.3.7 SAMHD1 independent functions of Vpx in esYDMs and ipsYDMs), and [576]), nuclear import of the PIC [589] and regulation of IFN production [592]. Moreover,

it is unknown whether constitutive expression of Vpx (and hence engagement of additional functions of Vpx) may alter the phenotype of macrophages produced generally, or more specifically, in relation to the infection and replicative capacity of HIV-1.

In order to eliminate the potential unknown effects of RNA interference using shRNA or constitutive expression of Vpx on the macrophage differentiation process or the dynamics of HIV-1 infection in scYDMs, the CRISPR- Cas9 gene editing system (refer to Section 1.4.3 CRISPR- Cas9: Genetic modification in es cells) was used to render the SAMHD1 gene non-functional (knocked-out) at the stem cell stage. This chapter details the design, implementation, and testing of the CRISPR- Cas9 mediated gene editing of SAMHD1 in es cells. The SAMHD1 knock-out es cells (SAMHD1-KO) were then differentiated to macrophages and characterised.

4.2 Methods and Materials

4.2.1 CRISPR Design Considerations

In order to increase the likelihood of producing a successful gene knockout, several parameters were taken into consideration when determining which exon to target. Firstly, it was important that a potential exon target should be present in all isoforms of the gene. Also, where gene knockouts were required, in order to control for situations of <100% non-sense mediated decay (NMD) efficiency, exons prior to any enzymatic domains or protein binding sites were preferable. Furthermore, in order to avoid transcription of truncated proteins, exons located at the very start or end of the gene were avoided. This is because out of frame indels at the start of a gene may not inhibit transcription from later alternative start sites, and out of frame indels at the end of a gene may not result in NMD. The bioinformatics tool 'CRISPR Design'[596] was used to identify possible cutting sequences for a given exon. Optimal cleavage efficiency was encouraged by the selection of nicking pairs 5-10bp apart,

ensuring gRNA binding sequences do not overlap, and a low off-target score, the latter an indication of the genome-wide number of similar sequences where a given guide RNA might bind in error.

4.2.2 High-Resolution Melt Analysis (HRM) primer design

High-resolution melt analysis (HRM) is a PCR based technique that facilitates the identification and characterisation of mutations in nucleic acid sequences [597] (refer to 4.2.7 Identification of SAMHD1 mutants using High-Resolution Melt Analysis (HRM)). Primer express® software using the TaqMan® quantification default settings was used to design the HRM primers. In order to prevent the destruction of the HRM primer binding sites by slightly off-target cutting by Cas9, sites were chosen 30-70bp outside of the CRISPR gRNA binding sequence (Figure 4.1).

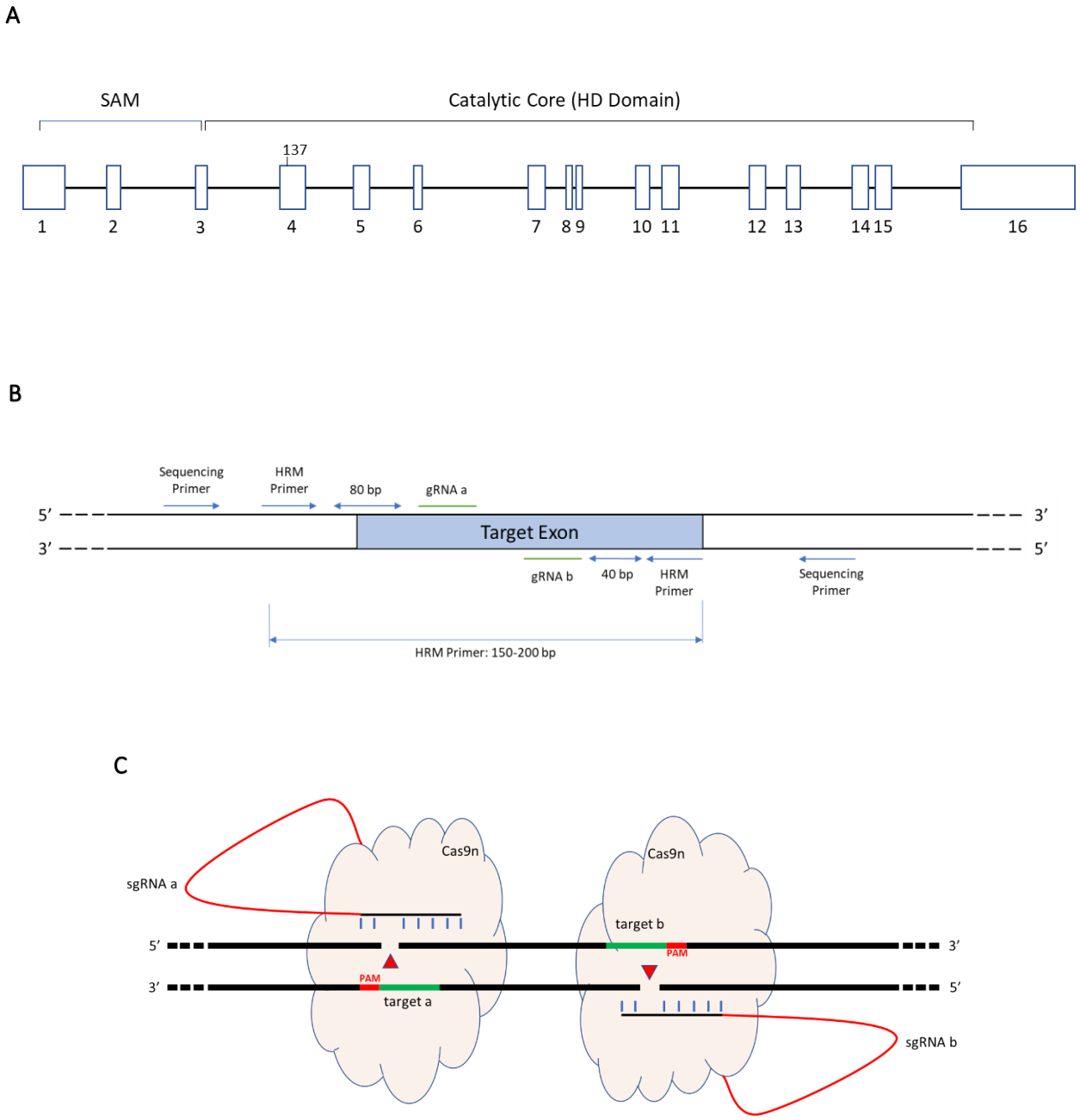


Figure 4.1 CRISPR- Cas9 Primer and target RNA design.

The schematic shows the SAMHD1 gene and spliced exons. In this example, Exon 4 was chosen for targeting CRISPR- Cas9 gRNA as close to reside 137 as possible. Residue 137 has been shown to be important for a functional dNTPase (refer to Section 4.3.2), (**A**). gRNAs are targeted within the exon determined by the location of suitable PAM sites, using sequences on the complementary strand to that being cut, (**B**) & (**C**). Two sets of primers are required for downstream analysis, a sequencing set both located outside of the chosen exon, and an HRM primer set located between 40 and 80nt from the start of a gRNA target sequence, B). Adapted from [282].

4.2.3 Vector cloning

The vector for expression of Cas9n (double-nicking) and full gRNA targeting SAMDH1 was created using the pSpCas9n(BB)-2A-Puro (pX462) V2.0 vector [560], (a gift from Feng Zhang (Addgene plasmid #48141)). The dsDNA (tgRNA) was inserted into the px462 backbone using the BbsI cloning site located immediately 5' of the sequence encoding the scaffolding guide RNA (sgRNA). Cloning was performed as previously described [560] using oligonucleotides DPW-20 (5' – CACCGTGTATCAATGATTCGGACG – 3') and DPW-21 (5' – AAACCGTCCGAATCATTGATACAC – 3') with pX462 to create pX462-gRNAsamEx4+, DPW-22 (5' – CACCGCGATACATCAAACAGCTGGG – 3') and DPW-23 (5' – AAACCCCAGCTGTTTGATGTATCGC – 3') with pX462 to create pX462-gRNAsamEx4-. DPW-24 (5' – CACCGCGTTCACTTATCTGCAGCTC – 3') and DPW-25 (5' – AAACGAGCTGCAGATAAGTGAACGC – 3') with pX462 to create pX462-gRNAsamEx5+, DPW-26 (5' – CACCGGATGTCTAGTTCACGCACT – 3') and DPW-27 (5' – AAACAGTGCGTGAACTAGACATCC – 3') with pX462 to create pX462-gRNAsamEx5-. Transcription from the U6 promoter results in a full gRNA, which is a combination of the tgRNA and the sgRNA with Cas9n expression driven by a synthetic CAG promoter. Ligated vectors were transformed into E. coli and subsequently analysed using the Source BioScience Sanger Sequencing Service to confirm error-free inserts.

4.2.4 CRISPR- Cas9: Validations of gRNAs activity in HEK293T cells using T7 Endonuclease 1

Cas9 activity is not equally efficient throughout the genome [524]. In order to determine whether the gRNAs designed were effective at targeting Cas9, the T7 endonuclease 1 assay (Neb M0302) for determining genome targeting efficiency was used. T7 Endonuclease 1 assay identifies and cuts imperfectly matched DNA, Holiday junctions or structures, heteroduplex DNA, and nicked dsDNA [598, 599].

In preparation for the T7 Endonuclease 1 assay, CRISPR- Cas9 pairs (e.g., pX462-gRNAsamEx4+, pX462-gRNAsamEx4-) were transfected into HEK293T cells (refer to 2.1.11 Co-transfection of HEK293T cells)

and selected with puromycin (0.4 µg/mL; MP Biomedicals) 24 hrs after transfection. Twenty-four hrs after puromycin selection, genomic DNA was extracted and used to amplify a small PCR product spanning the region targeted by the gRNA. These products were subjected to a hybridization reaction, consisting of the following reagents: NEB Buffer2, 2µL; Purified PCR product 200ng, 2µL; H_2O, 15µL (total 19µL); this was performed in a PCR cycler: 5min, 95°C; ramp down to 85°C at -2C/s; ramp down to 25°C at -0.1°C/s; hold at 4°C. 1µL (10U) NEB T7 endonuclease I was then added to the 19µL from the above hybridization reaction and incubated at 37°C for 15 mins. The mixture was then immediately loaded on a 2% agarose gel.

Lack of cleavage by T7 Endonuclease 1 results in a single band of identical size to the PCR product. Cleavage results in the appearance of a smaller band or multiple bands (depending on the cleavage site), in addition to the PCR product. All gRNAs tested resulted in the appearance of smaller bands and were therefore validated for targeting and nuclease cleavage in HEK293T cells (Figure 4.2).

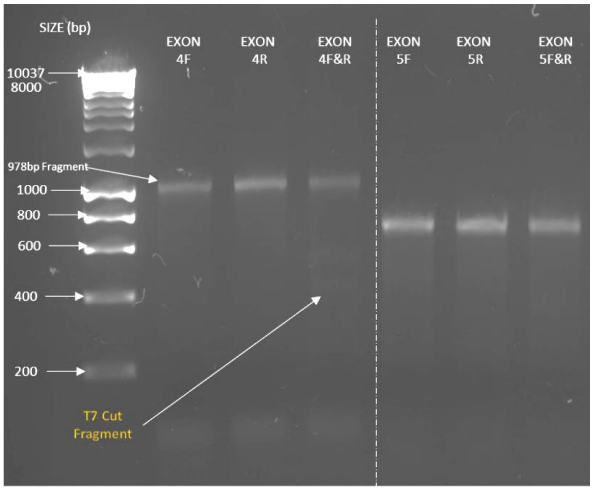


Figure 4.2 Gel separation for the T7 Endonuclease I Assay.

Separation of T7 Endonuclease fragments run on a 2% polyacrylamide gel. Cleavage by T7 Endonuclease I occur at areas of mismatched DNA and indicate mutated sequences. Exon 4F, Exon 4R, Exon 5F, and Exon 5R are PCR products amplified from HEK293T cells transfected with only one gRNA expressing plasmid (e.g., pX462-gRNAsamEx4+) and are used as controls. Exon4F&R and Exon5F&R are PCR products amplified from HEK293T cells transfected with both forward and reverse gRNA plasmids (e.g., pX462-gRNAsamEx4+, pX462-gRNAsamEx4-) which will allow Cas9 to cut and hence produce mutated sequences. The emergence of one or more (very faint) bands of a smaller size to the PCR product is indicative of T7 Endonuclease I cleavage and, therefore, that the CRISPR guide RNA pairs are successful in producing indels.

4.2.5 Electroporation of stem cells, selection, and expansion of potential SAMHD1 KO clones

A flow diagram for the CRISPR- Cas9 protocol used in this thesis can be found in Figure 4.3. Validated px462gRNA constructs were delivered to HUES2 es cells using the Neo-transfection® electroporation system (Neon® transfection system, Invitrogen). Using a 100µL transfection tip, and a single electroporation pulse at 1000 V and 40 ms, a maximum of 10µL of DNA (5µL of each plasmid) was transfected into 1 x 10^6 es cells. Transfected cells were subsequently transferred to a 12 well tissue culture plates (Corning® Costar®) coated with Matrigel® and cultured in mTeSR™ (StemCell™ technologies), supplemented with 10 µmol/LY-27632 (Abcam) without antibiotics. Cells were cultured for 48hrs after which successful transfections were selected for by the addition of puromycin (MP Biomedicals) at a concentration of 0.4µg/mL.

Surviving cells were plated at a density of 1 x10^4 on mitotically inactivated mouse embryonic fibroblast feeder cells (MEFs; outbred Swiss mice established and maintained at the Department of Pathology, Oxford Gardner (1982); Chia et al. (2005)) on gelatin-coated 10cm tissue culture plates (Corning® Costar®). Cells were cultured in hESC medium (KO-DMEM, 2 mmol/L L-Glutamine, 100 mmol/L non-essential amino acids, 20% serum replacement, and 8 ng/mL basic fibroblastic growth factor (FGF2)), supplemented with 10 µmol/L Y27632. After approximately 10 days, individual colonies were picked using a 1000µL pipette tip and transferred to Matrigel-coated 96 well plates and cultured in mTeSR™ (StemCell™ technologies). Colonies were then cultured to confluence and subsequently split 1:2. One population (96 well plate) was cultured for further expansion, whilst the second population was used as a source of DNA for subsequent validation steps.

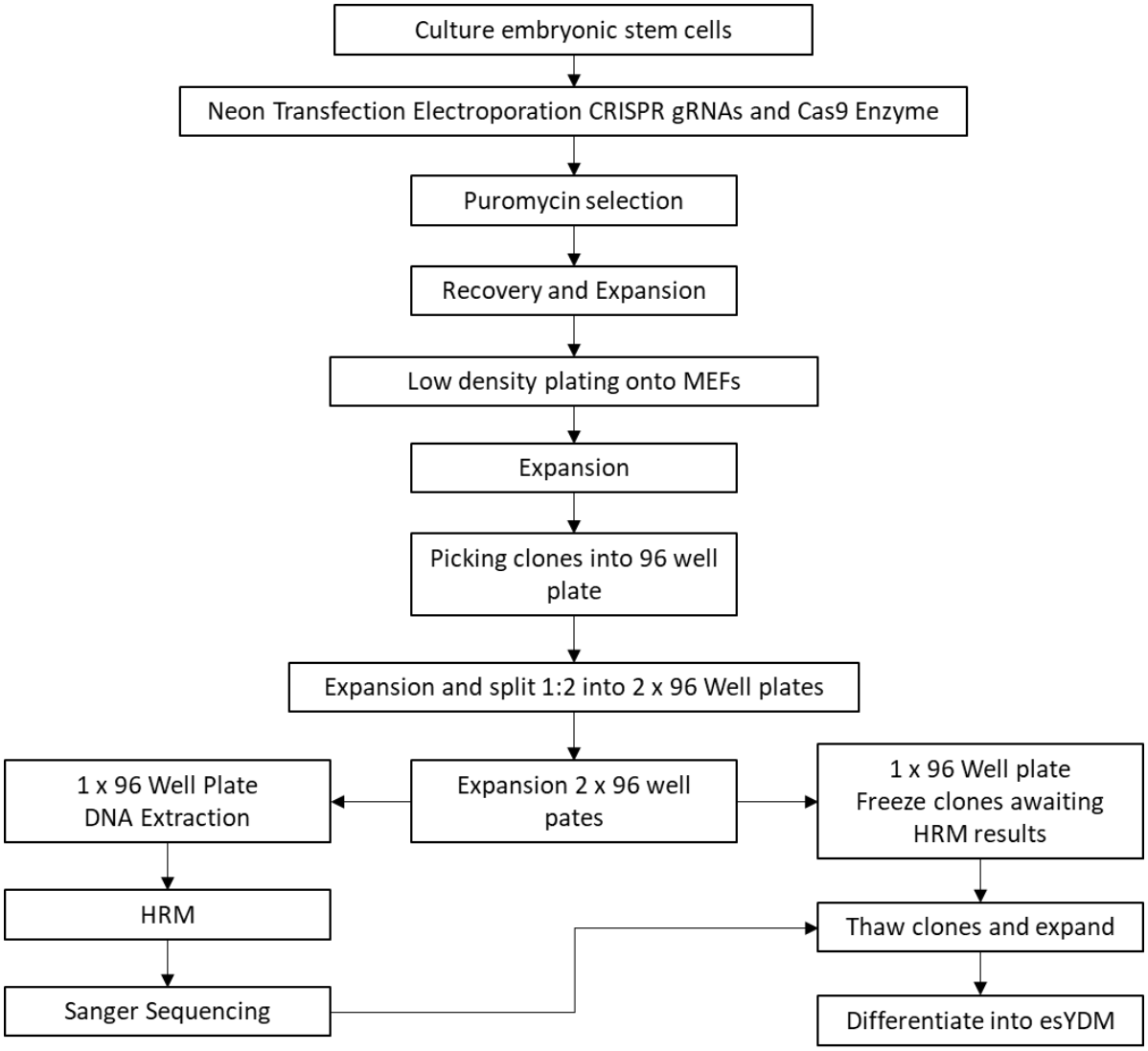


Figure 4.3 Flow diagram of CRISPR- Cas9 gene editing protocol.

Plasmids encoding the Cas9 enzyme and CRISPR gRNAs were transfected via electroporation into es cells. Successful transfections were selected for using puromycin. Transfected cells were expanded and then plated at single-cell density onto MEFs. Once single cells had grown into colonies, they were transferred ('picked') to feeder-free cultures using Matrigel® and mTeSR® in 96 well tissue culture plates. Colonies were expanded and then split into 1:2 to 96 well tissue culture plates. The colonies on one plate were used to source DNA for mutation analysis via HRM. The second plate was cultured further (or frozen at -80°C) and served as a source of cells for expansion and differentiation into esYDMPs once SAMHD1 knock-out clones had been identified. Adapted from [282]

4.2.6 DNA Extraction for HRM

Cells were lysed overnight at 55°C using lysis buffer (10mM tris pH 7.5, 10mM Ethylenediaminetetraacetic acid (EDTA), 10mM NaCl, 0.25% Triton X100, 1mg/mL proteinase K) and then precipitated using precipitation solution (75mM NaCl in 100% EtOH), at -80°C for 2 hrs. The precipitate was then washed in 100% EtOH three times, allowed to air dry, and then re-suspended in distilled water.

4.2.7 Identification of SAMHD1 mutants using HRM

HRM was used for the screening of CRISPR- Cas9 transfected cell lines for cuts in the exon of choice (positive hit), and therefore the elimination of negative (or wild type) clones.

A region spanning the gRNA target sites was amplified by PCR using LCGreen Plus (Idaho Technology via Clent Life Sciences) and Amplitaq Gold 360 Mastermix (Applied Biosystems, cat. 4398881). Using primers DW39 HRMex4FWD (5'- ATGATCCTATCCATGGCCACAT – 3'), DW40 HRMex4REV (5' – CCCATTCCCTTCTTACCCTAGACT – 3'), DW41 HRMex5FWD (5' – AGAACTATCACTCCTCTTGCAAACAG – 3'), DW42 HRMex5REV (5' – GATCATGACAAAGTCCAGCAATCT – 3') the reaction was set up as follows: LCGreen Plus, 1µL, Amplitaq Gold 5µL, Primer A (2.5 µM) 1µL, Primer B (2.5µM) 1µL. Using the following plates: MicroAmp Fast Optical 96-Well (ref: 4346906) and Applied Biosystems MicroAmp Optical Adhesive Film (ref: 4311971) Applied Biosystems, 8µL of reaction mix and 2µL of 10ng/µL gDNA was transferred to each well. The machine setup took the following parameters: Quantification:Standard Curve, Reagent:Other, +MeltCurve, Standard Sun (2h+), Passive reference: None, Reporter:LCGreen, Quencher:None, Volume: 10µL. The qPCR cycle parameters were as follows: Initial denaturation 95°C for 10min, 40x cycles Denaturation 95°C 15 Sec, primer annealing 60°C for 1 minute, Melt curve: Continues and 0.3% Ramp, denaturation 95°C 15 sec, 60°C 1 minute, 95°C 15 sec.

The result was analysed using the HRM native software. A melt curve was generated from which positive hits were identified. A melt curve is a graphical representation of the kinetics with which the dye incorporated into DNA strands is released as the temperate increases. These kinetics are quantifiably different for unaltered (wild type) and altered (mutated) DNA (Figure 4.4).

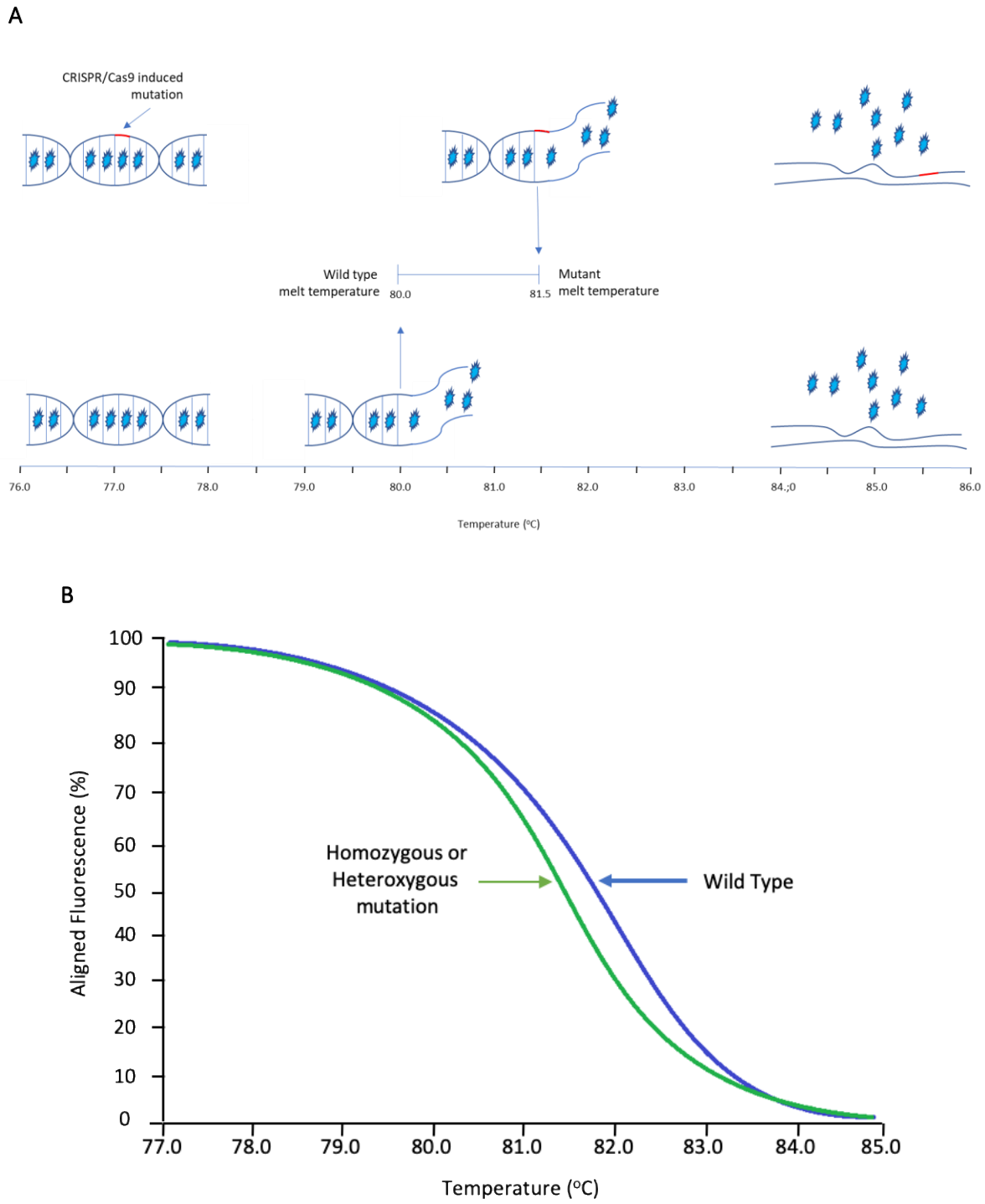


Figure 4.4 High resolution melt analysis (HRM).

A luminescent dye is mixed with PCR reaction mix, which then incorporates into the PCR products. As the temperature increases in the HRM reaction, the DNA denatures, and the dye is released. This is then detected by the HRM apparatus. Mutations in the PCR product sequence caused by Cas9 cutting alter the denaturing temperature and hence the temperature at which the dye is released, (**A**). The collective term for the graphical representation of this process is a 'melt curve' (**B**). Melt curves derived from PCR fragments with mutated sequences are adjusted compared to melt curves derived from control sequences. Melt curves that deviate significantly from the control can thus be considered to represent mutated sequences (**B**). Adapted from [282].

4.2.8 DNA Extraction and Illumina SNP array

DNA was extracted from 2.5 x 10^6 WT or SAMHD1 knockout stem cells, using the DNeasy Blood & Tissue Kit (QIAGEN) according to the manufacturer's instructions. Extracted DNA was resuspended at a concentration of 100ng/µL. Single nucleotide polymorphisms (SNP) analysis was performed on an OmniExpress24 chip covering 700,000 markers by the high-throughput genomics group at the Wellcome Trust Centre for Human Genetics.

4.3 Results

4.3.1 Genomic structure of SAMHD1

The SAMHD1 gene is located on Chromosome 20. The pre-mRNA is 62kb from which a 3.2kb mRNA is post-transcriptionally derived, which contains 16 exons. Three splice variants have been identified for SAMHD1: a mutation located in the splice acceptor site of exon 12 which resulted in the skipping of exon 13 (Δ13) [600]; a splice variant lacking exons 8 and 9 (Δ8-9), and a splice variant lacking exon 14 (Δ14) [185]. The expression of variant Δ13 was undetectable, indicating instability. Splice variants Δ8-9 and Δ14 were shown to be expressed in several cell types, including THP-1 cells, and while both splice variants localised to the nucleus and could bind Vpx, they were also catalytically inactive in dNTPase activity and were quickly degraded [185].

With consideration of the target selection criterion previously mentioned (Section 4.2.1 CRISPR Design Considerations), exon 4 and exon 5 were chosen as targets for CRISPR- Cas9. Exon 4 was the primary target since it was also the location of the catalytically active site for the dNTPase [601] and thus presented the possibility of producing dNTPase defective mutants in the event of in-frame indels at this site. Exon 5 was targeted to add redundancy and variability, and potentially increase the probability of a gene knockout in the event of unforeseen complications resulting in an out-of-frame deletion in Exon 4 but a functional protein.

4.3.2 Genotypic characterisation of SAMHD1 knockout ESCs

HRM identified seventeen clones carrying mutations (Figure 4.5, 4.7, 4.8 & 4.9) from a tissue culture plate of 96 clones tested. Of these, seven clones were identified as containing homozygous out of frame indels in exon 4 (potential knockouts: cell lines E1, E2, E7, F4, F8, G9, and G10), and two potentially heterozygous knockouts in exon 4 (A1 and H5), as evidenced by immunoblot (Figure 4.6). The sequences of cell lines E2 and G9 were extrapolated from sequencing data received using the Source Bioscience Sanger Sequencing Service. Cell line E2 contained two out of frame deletions in the region targeted by the CRISPR gRNA and thus are confirmed as complete SAMHD1 knockouts (Figure 4.7). The sequencing of cell line G9, however, revealed that it contained an out of frame deletion in one allele and an in-frame deletion on the second allele; the in-frame deletion also spanned the dNTPase active domain (Figure 4.8). Previous studies have shown that mutations in this region, specifically locations 137, 145, 167, 206, 207, and 311, abolish dNTPase activity [114, 177, 188, 197]. CRISPR- Cas9 gene editing of SAMHD1 exon 5 in HUES2 stem cells produced one potential SAMHD1 KO from 96 tested clones, as evidenced by the associated melt curve (Figure 4.9). The sequence was determined for this clone. Homozygous and heterozygous cell lines showed stem cell-like morphology and were absent of visible differentiation.

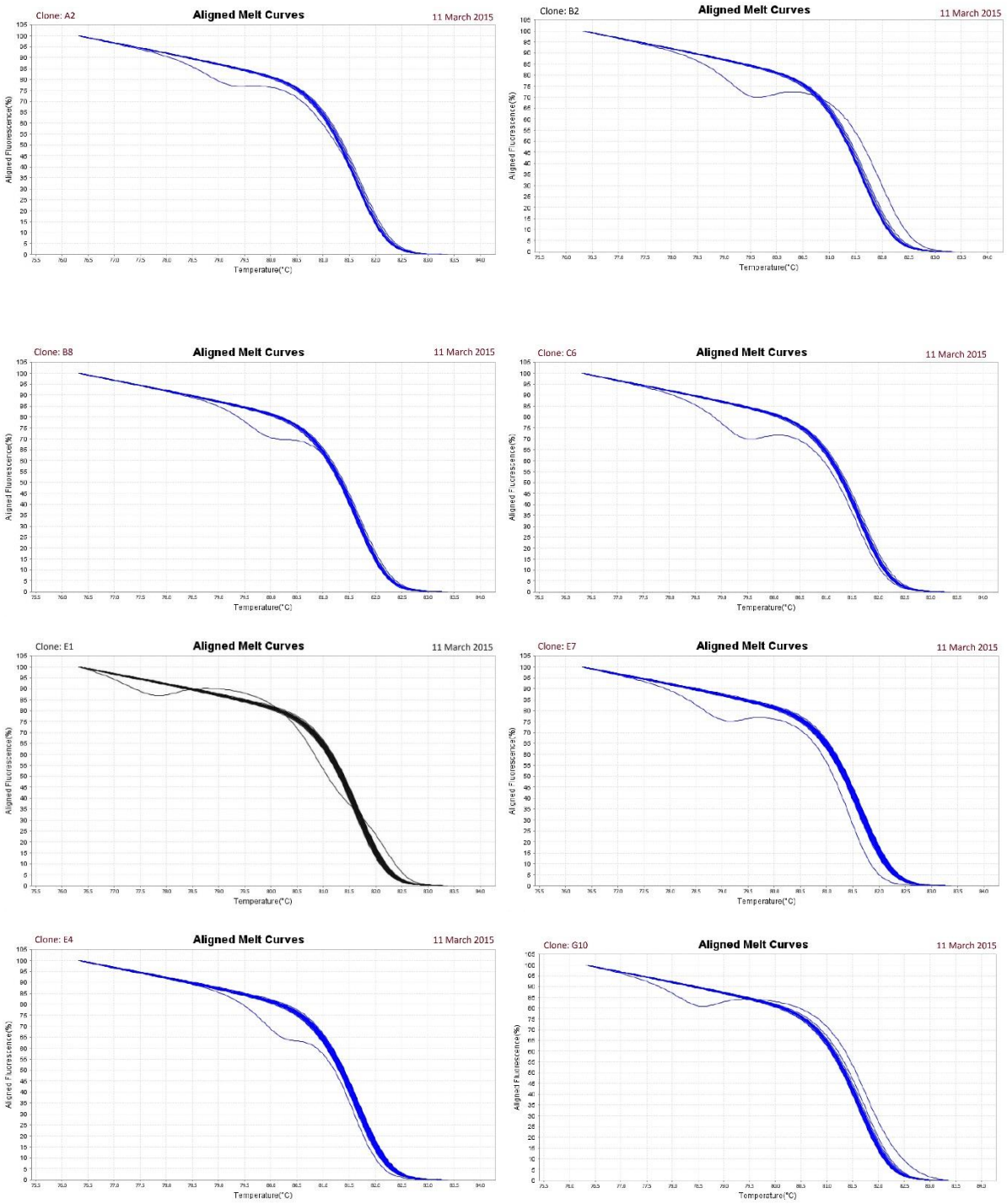


Figure 4.5 HRM Melt curves.

Examples of melt curves for potential SAMHD1 knockouts identified via HRM from a single 96 well plate. It was not possible to tell from these melt curves whether the mutation is heterozygous, homozygous, or in the correct location. This figure simply shows the different graphical representations of a 'mutation' for a given clone as well as all of the clones identified in this HRM run (except the three detailed in the following Figures). All graphs contain a melt curve of non-mutated sequences (DNA from cells that were not exposed to CRISPR- Cas9 – [WT]) for comparison. The WT curve represents a separate well of a 96 well plate and is superimposed onto the melt curve of the potentially mutant clone. The WT curve is the gradient that all the graph curves follow except the mutant curve (see Figure 4.4 for a schematic representation of this concept).

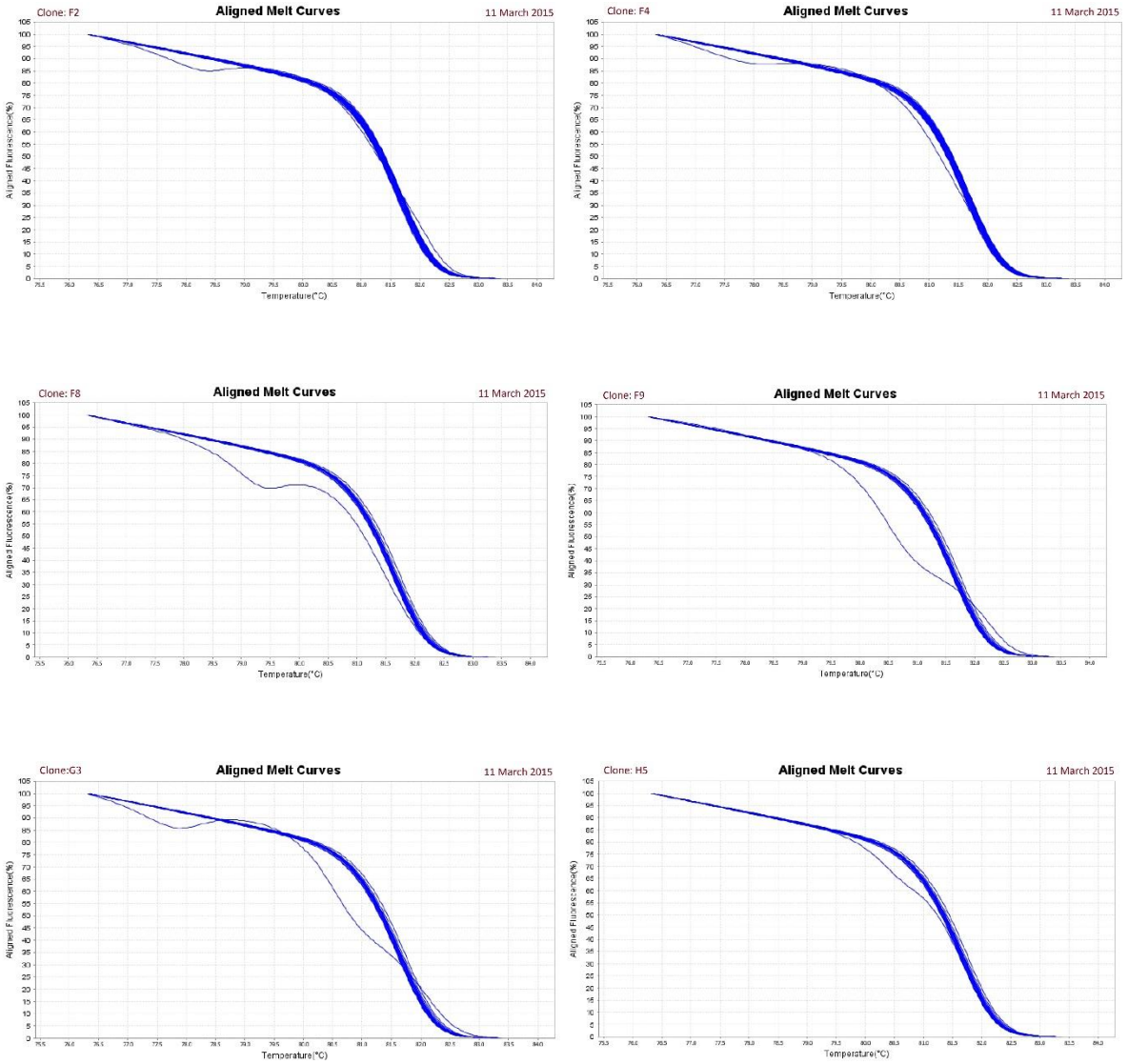


Figure 4.5 HRM Melt curves (continued).

Examples of melt curves for potential SAMHD1 knockouts identified via HRM from a single 96 well plate. It was not possible to tell from these melt curves whether the mutation is heterozygous, homozygous, or in the correct location. This figure simply shows the different graphical representations of a 'mutation' for a given clone as well as all of the clones identified in this HRM run (except the three detailed below). All graphs contain a melt curve of non-mutated sequences (DNA from cells that were not exposed to CRISPR- Cas9 – [WT]) for comparison. The WT curve represents a separate well of a 96 well plate and is superimposed onto the melt curve of the potentially mutant clone by the HRM software. The WT curve is the gradient that all the graph curves follow except the mutant curve (see Figure 4.4 for a schematic representation of this concept).

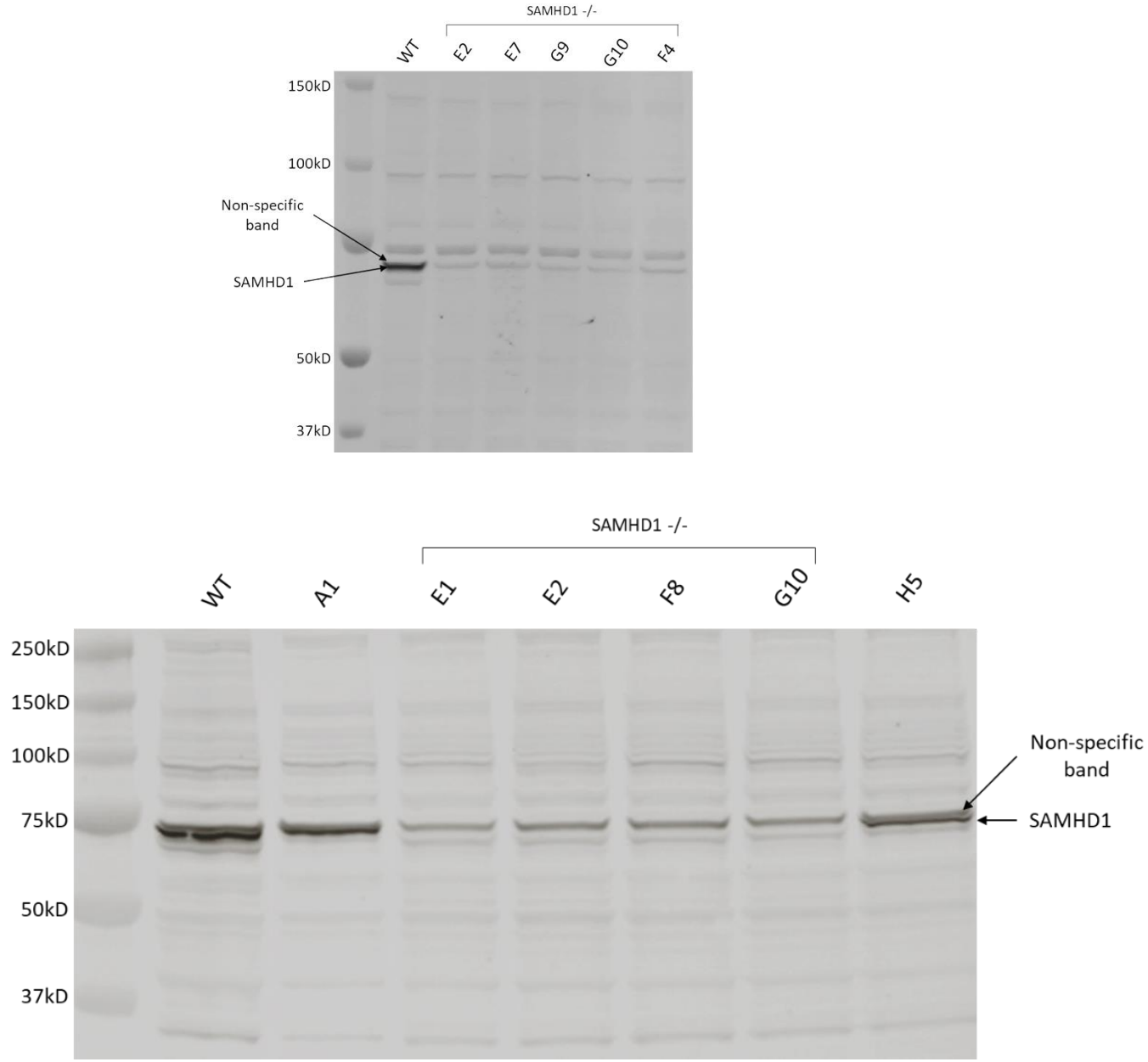


Figure 4.6 Immunoblot of SAMHD1 in es cells.

The expression of SAMHD1 was determined in wild type esYDMs and SAMHD1 knockout esYDMs by immunoblot using α-SAMHD1 and α-GAPDH antibodies. 'SAMHD1-/-' = SAMHD1 homozygous knockout.

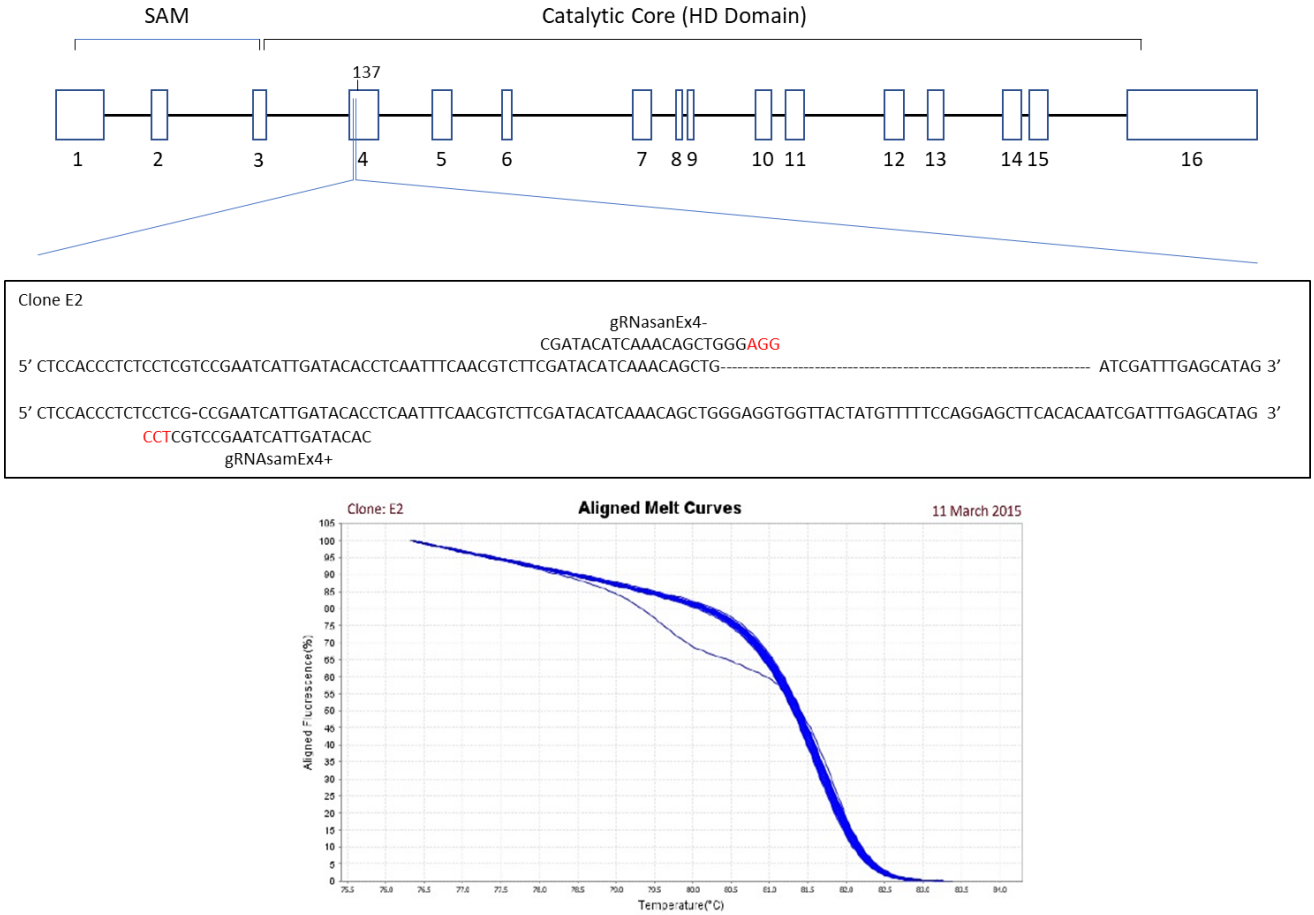


Figure 4.7 SAMHD1 knockout (E2) via targeting of exon 4.

Graphical representation of the SAMHD1 gene showing the functional SAM and HD domains, and the gRNA target in exon 4. Cas9 cutting resulted in two out of frame deletions, also represented as a melt cure from the HRM analysis. Adapted from [282].

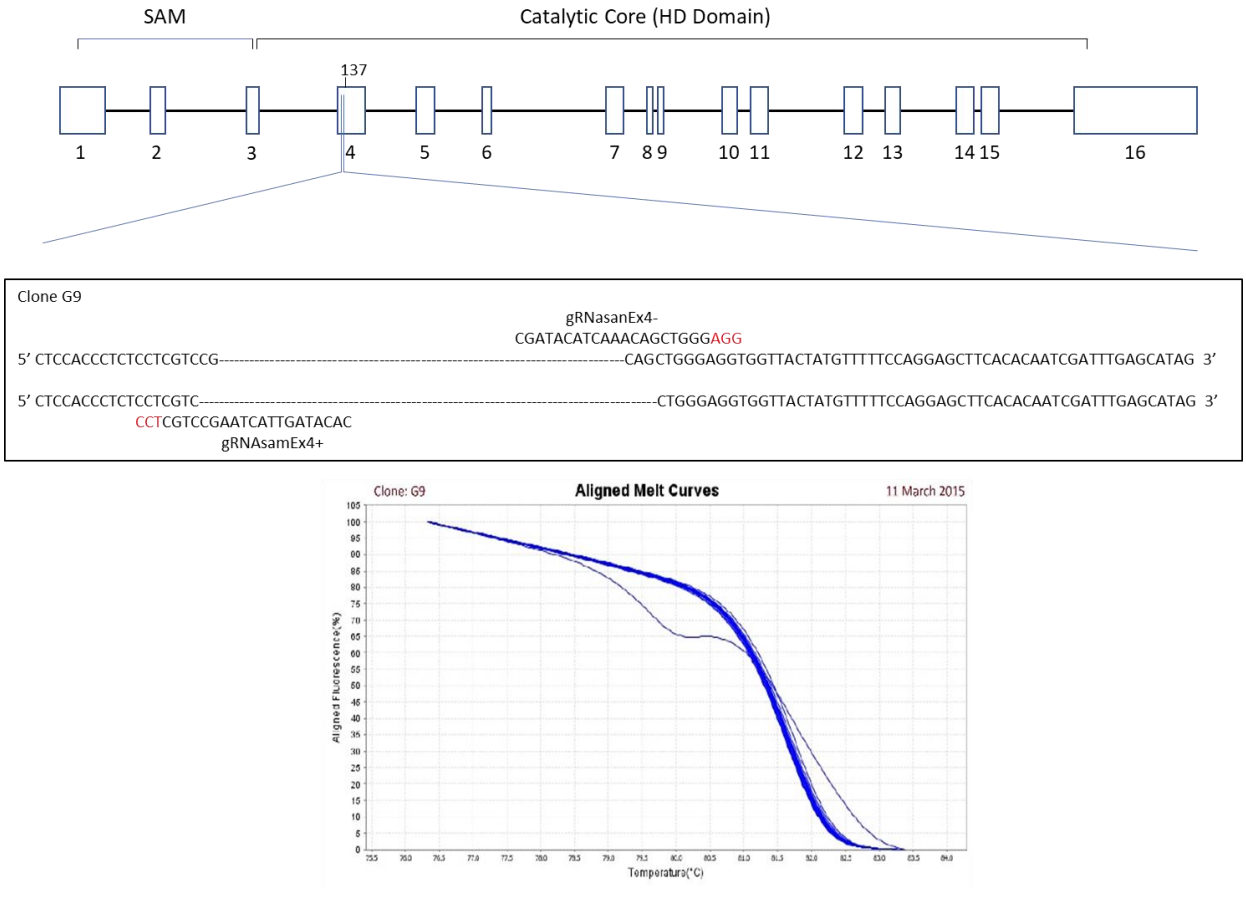


Figure 4.8 SAMHD1 dNTPase null mutant (G9) via targeting of exon 4.

Graphical representation of the SAMHD1 gene showing the functional SAM and HD domains, and the gRNA target in exon 4. Cas9 cutting resulted in one out of frame deletion and one in-frame deletion, the latter spanning the region encoding the dNTPase active site, also represented as a melt cure from the HRM analysis. Adapted from [282].

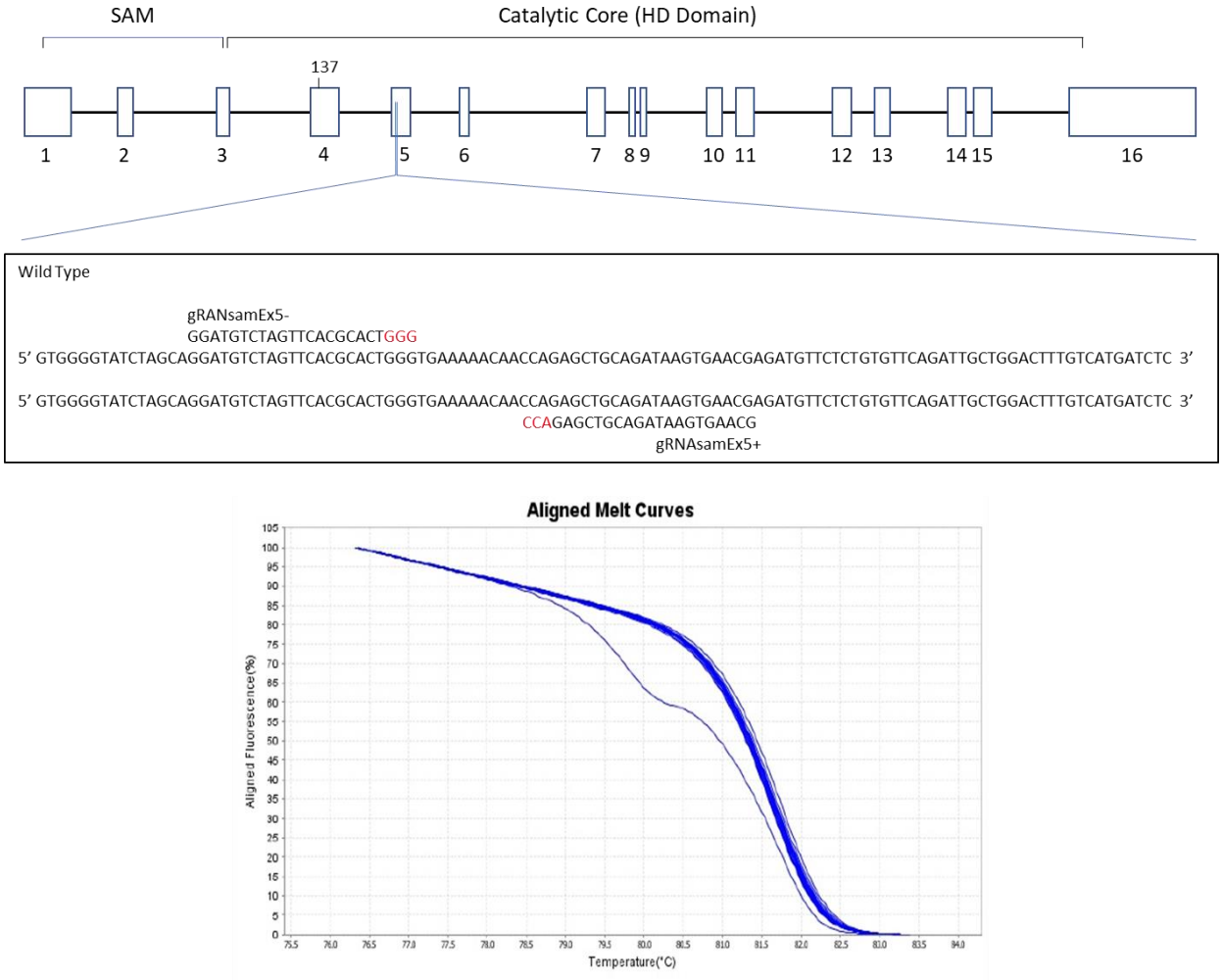


Figure 4.9 SAMHD1 mutant via targeting of exon 5.

Graphical representation of the SAMHD1 gene showing the functional SAM and HD domains, and the gRNA targets in exon 5, represented as a melt cure from the HRM analysis. The sequence for this clone was never determined. Adapted from [282].

4.3.3 Macrophage differentiation of SAMHD1 knockout ESCs

HUES2 stem cell lines E2, G9, and G10 were chosen as source cells for differentiation into esYDMs as these cell lines were absent of differentiation on thawing. The contribution of SAMHD1 to the regulation of dNTPs in cells is well established; however, the effect of the total absence of this regulation on the differentiation process remains to be described. Certainly, shRNA mediated knockdown of SAMHD1 does not critically disrupt stem cell differentiation into esYDMs as shown in Chapter 3; however it is possible that the residual SAMHD1 protein remaining was sufficient to function in this regard and while differentiation was successful, there was a marked delay in SAMHD1-KD esYDM precursor production

(Figure 3.4). However, gene-edited cell lines successfully produced esYDMs; hence, neither dNTPase defectivity or, indeed, the complete knockout of SAMHD1 terminated the differentiation of stem cells to esYDMPs and esYDMs. At all stages of the differentiation protocol, CRISPR- Cas9 mutated cell lines behaved like and were morphologically similar to, wild type cells (data not shown). Cell lines E2 and G9 were further probed for single nucleotide polymorphisms and the presence of monocyte and macrophage receptors. For both E2 and G9 cell lines, no single nucleotide polymorphisms were detected (Figure 4.11). Neither were there any significant variations in the expression of common myeloid markers or HIV receptors, compared to wild type cells (Figure 4.12). This showed that the lack of SAMHD1 or a functional dNTPase (and hence high dNTP concentrations) did not increase incidents of natural genetic mutation or alter receptor expression. However, as observed with shRNA knockdown, the mutant cell lines (SAMHD1-KO and SAMHD1-MUT) produced esYDMPs at later time points (approximately 2 weeks) compared to the WT cells (Figure 4.10). This serves as additional evidence that while it appears SAMHD1 is dispensable for homeostasis and hence differentiation, its absence may reduce the overall efficiency of the differentiation process.

HUES-2	26/04/2015	03/05/2015	10/05/2015	17/05/2015	24/05/2015
WT	EBs Plated		yes	yes	yes
E2	EBs Plated				yes
G9	EBs Plated				yes

Figure 4.10 SAMHD1-KO esYDMPs are produced later than wild type esYDMPs.

The expanded embryoid bodies (factories) produce macrophage precursors (esYDMPs) at different time points. Both the SAMHD1 knockout cell line (SAMHD1-KO, E2) and the SAMHD1 dNTPase mutant cell line (SAMHD1-MUT, G9) produced esYDMPs approximately two weeks after the wild type (WT). WT refers to esYDMPs that have not been genetically modified, differentiated in the absence of puromycin. "yes" refers to the presence of cells at a given time point in the culture vessel. These cells were not counted primarily due to low numbers but also in order to synchronise the harvesting of cells with other factories.

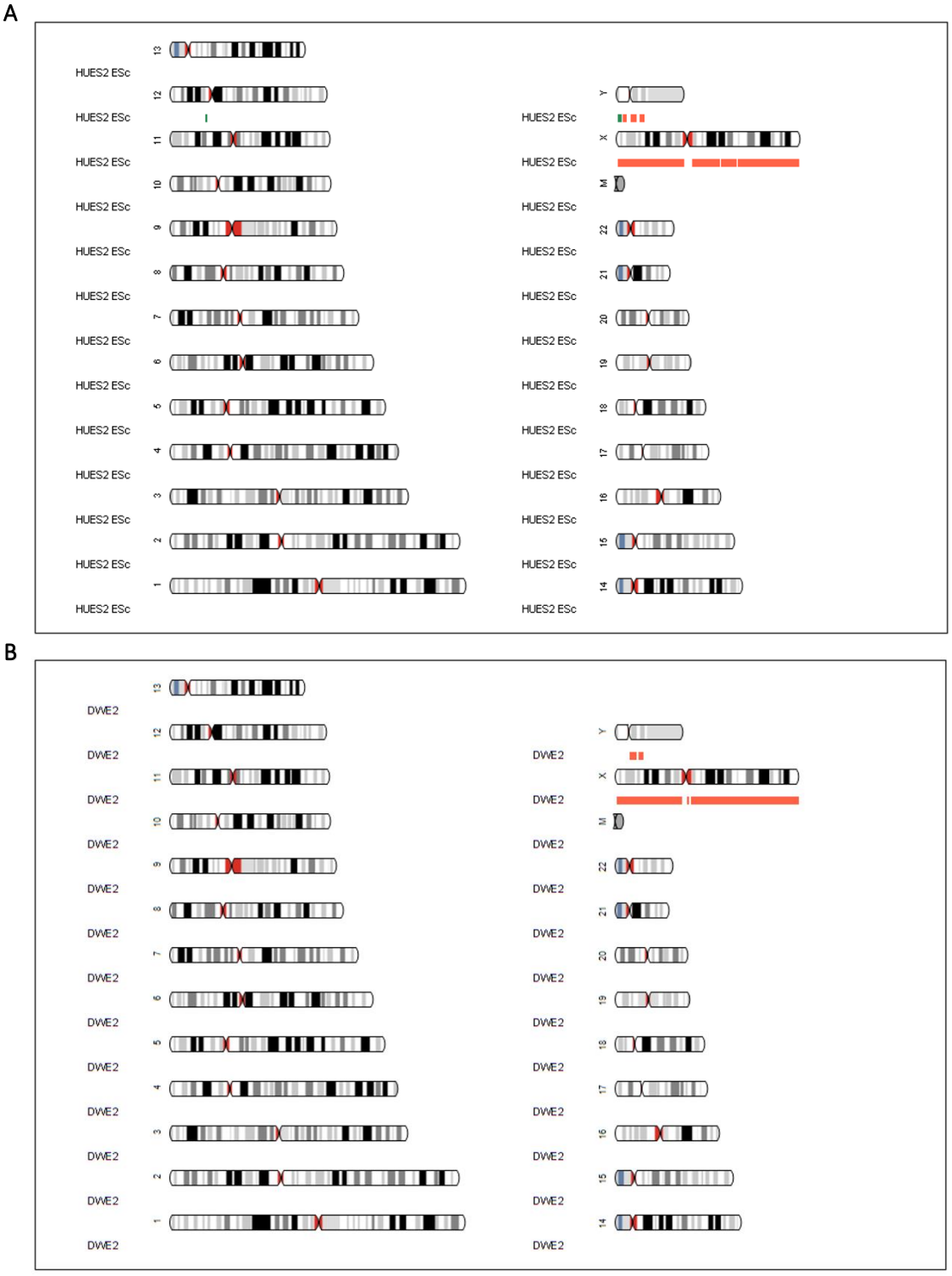


Figure 4.11 SAMHD1 knockout esYDM maintains karyotype.

Single nucleotide polymorphisms (SNP) analysis of wild type (**A**), knockout E2 (**B**), and dNTPase null mutant G9 (**C**) in HUES2 esYDMs. Karyotype integrity was probed using a Single Nucleotide Polymorphism (SNP) array (Illumina OmniExpress24 chip covering 700,000 markers) and analysed using KaryoStudio (Illumina) in order to identify copy number variations and aberrant chromosome amplifications and deletions across the genome. A loss of heterozygosity is indicated by grey markers under the chromosome. A single copy of a SNP is indicated by a red marker (e.g., identification of a single X chromosome in this genome; the donor is male). DNA duplications are indicated by a green marker.

C

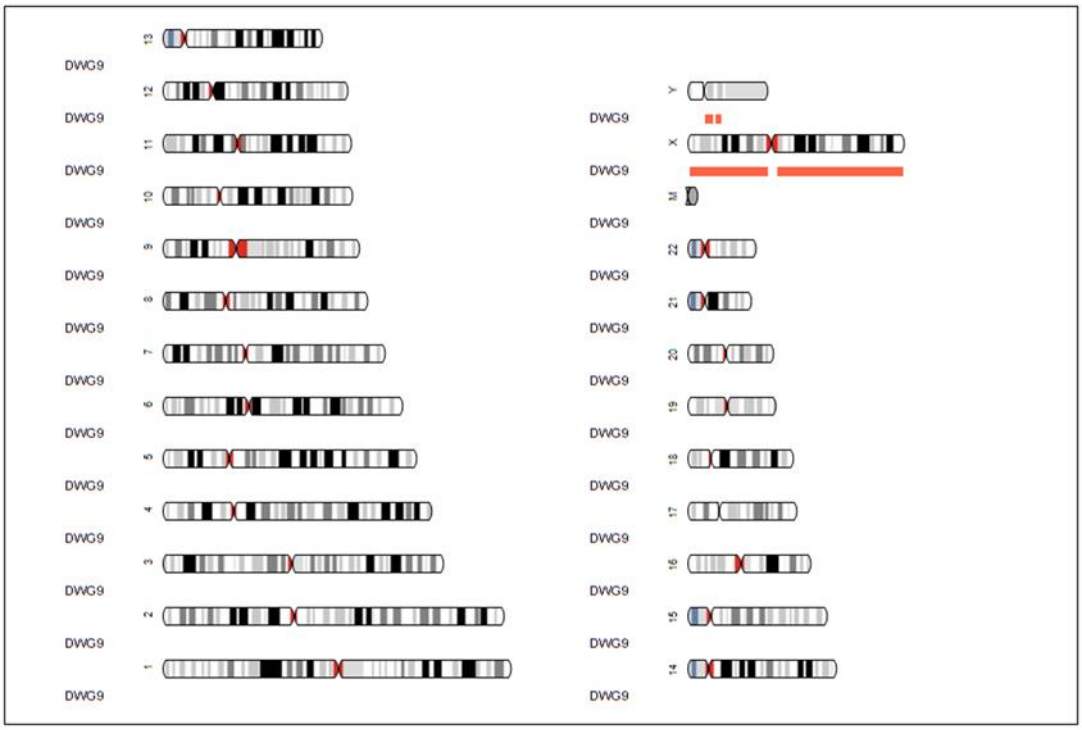


Figure 4.11 SAMHD1 knockout esYDM maintains karyotype. Continued.

Single nucleotide polymorphisms (SNP) analysis of wild type (**A**), knockout E2 (**B**), and dNTPase null mutant G9 (**C**) in HUES2 esYDMs. Karyotype integrity was probed using a Single Nucleotide Polymorphism (SNP) array (Illumina OmniExpress24 chip covering 700,000 markers) and analysed using KaryoStudio (Illumina) in order to identify copy number variations and aberrant chromosome amplifications and deletions across the genome. A loss of heterozygosity is indicated by grey markers under the chromosome. A single copy of a SNP is indicated by a red marker (e.g., identification of a single X chromosome in this genome; the donor is male). DNA duplications are indicated by a green marker.

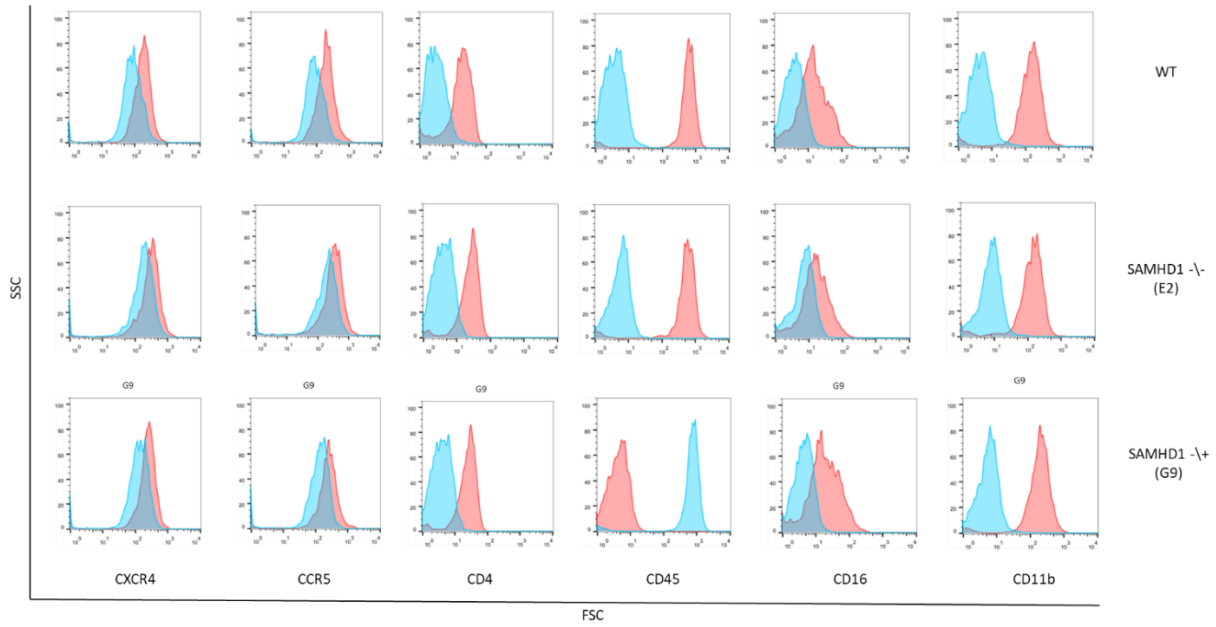


Figure 4.12 esYDM SAMHD1 mutant and esYDM WT markers are comparable.

Histogram plots quantifying flow cytometry staining of esYDMs for myeloid cell surface markers and HIV-1 receptors. For all series red peaks represent antibody staining, blue peaks represent isotype staining except for CD45 staining of SAMHD1 -/+ (G9) where the blue peak represents antibody staining, and the red peak represents isotype staining. Antibodies and isotypes used can be found in Table 2.1.

4.3.4 Phenotypic characterisation of SAMHD1 knockout esYDMs

SAMHD1 protein expression was undetectable in SAMHD1 mutant esYDM cell lines E2 and G10 showing that the mutations introduced in exon 4 of SAMHD1 in these cells were sufficient to sustain NMD throughout differentiation (Figure 4.13). SAMHD1 protein expression was, however, detected in SAMHD1 mutant esYDM cell line (SAMHD1 -/+ (G9)) (Figure 4.8), albeit at a very low level, indicating that the in-frame single allele indel spanning the dNTPase active site resulted either in sufficient mRNA instability to enhance NMD or sufficient protein instability to enhance degradation (Figure 4.13). SAMHD1 dNTPase absence was also confirmed by analysis of dNTP concentrations (Figure 4.14). dNTP concentrations were significantly higher for all dNTPs except dCTP, compared to wild type cells (Figure 4.14). This also potentially implies the lack of a redundancy mechanism (such as an alternative dNTP hydrolayse) to degrade dNTPs in the absence of SAMHD1 in esYDMs.

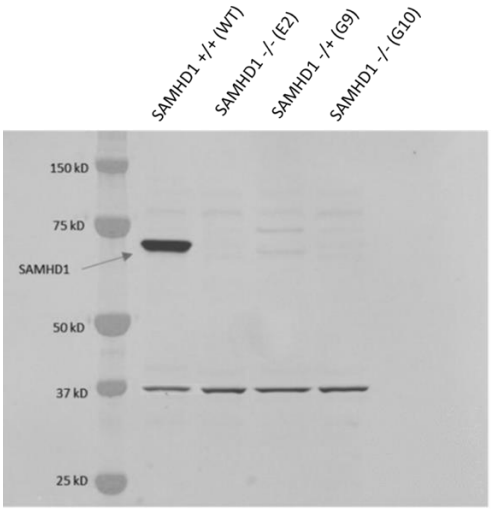


Figure 4.13 Immunoblot of SAMHD1 in esYDMs.

The expression of SAMHD1 was determined in wild type esYDMs and SAMHD1 knockout esYDMs by immunoblot using α-SAMHD1 and α-GAPDH antibodies.

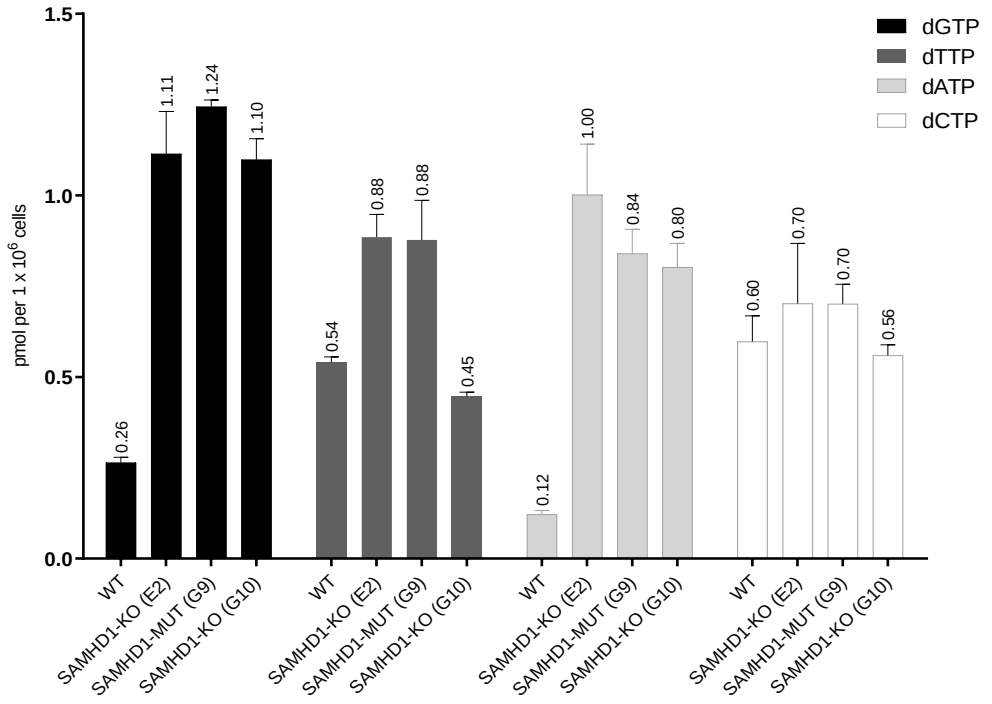


Figure 4.14 dNTP levels in SAMHD1 KO cells.

dNTPs were extracted from 1 x 10^6 cells and quantified using the dNTP assay (for a detailed protocol refer to 3.2.2 Tritium based enzymatic assay for the determination of intracellular dNTP concentrations). Data is representative of the mean +/- SEM of a single experiment comprised of three technical repeats (triplicate).

4.4 Discussion

The unusual temporal anomaly exhibited by Vpx expressing esYDMP producing factories prompted concern over the effects that constitutive expression of Vpx throughout the differentiation process may be having on the phenotype of end-stage esYDMs. A common alternative strategy is RNA interference via siRNA or shRNA, and indeed, shRNA-mediated SAMHD1-KD cells were produced, which did display markedly different temporal production kinetics to Vpx expressing cells. However, a similar delay in esYDMP production observed in SAMHD1-KD (shSAM) cells was also observed in shCTRL expressing cells, which questioned the integrity of the RNA interference system being used. Furthermore, uncertainty surrounding the effect of SAMHD1 residual knockdown protein (RKP) raised by data detailed in Chapter 3 challenged the use of RNA interference as a loss of function tool due to the potential inefficiency of shRNA mediated SAMHD1 depletion. Hence the decision was made to abolish SAMHD1 activity at the genomic level using CRISPR- Cas9 mediated gene editing.

By using a CRISPR- Cas9 gene editing protocol (that had been extensively optimised by members of the laboratory), several edited es cell clones were identified with heterozygous or homozygous out of frame indels in exon 4 of the SAMHD1 gene. One clone was identified with a heterozygous out of frame indel on one allele and an in-frame indel on the second allele that spanned the dNTPase catalytic site (G9 – [SAMHD1-MUT]). This clone and two homozygous out-of-frame indel containing clones (E2 – [SAMHD1-KO], and G10 – [SAMHD1-KO]) were then successfully differentiated into esYDMs. SAMHD1 protein concentrations at the macrophage stage were probed via immunoblot, which confirmed SAMHD1 ablation in the homozygous out of frame indel containing clones (E2 and G10), and very low-level SAMHD1 expression for the SAMHD1-MUT. dNTP concentrations for all four dNTPs in both SAMHD1-KO cells and SAMHD1-MUT cells were comparable, indicating that the activity of the dNTPase had been abolished in SAMHD1-MUT cells. Of note, no significant increase was observed for dCTP in any of the SAMHD1 mutant cell lines versus wild type controls. A review of data presented in Chapter 3 shows that no significant increase was observed in THP-1 cells or transgene expressing esYDMs for dCTP. Given

this consistent lack of significant change in dNTP concentrations in contrast to that reported in the literature, it is possible that dCTP levels in this report may be erroneous. A potential cause of these errors may be aberrant oligonucleotide sequences, which would inhibit the proportional incorporation of radiolabeled nucleotides.

SAMHD1 mutant esYDMs were indistinguishable from wild type esYDMs in terms of morphology and expression of common macrophage markers and HIV-1 entry receptors, showing that the deletion of SAMHD1 did not affect these components. Potential off-target cutting of the Cas9 enzyme was investigated using a single nucleotide polymorphism (SNP) analysis. No significant karyotypic mutations were detected except for a small SNP deletion and additional DNA duplication on the Y chromosome. The genes documented in the regions containing the SNPs encode primarily testis related functions. No genes in these regions have been identified to code for functions governing myeloid differentiation, macrophage polarisation, or antiviral defence [602].

As observed with the SAMHD1-KD cell lines, SAMHD1 knockout (SAMHD1-KO) and the SAMHD1 dNTPase mutant (SAMHD1-MUT) cell lines produced esYDMPs at a later time point (approximately 4 weeks post-EB plating) compared to wild type cells (2 weeks post-EB plating). These data imply that the factor delaying esYDMP production was depletion of SAMHD1. The fact that SAMHD1-KO cells produced esYDMPs 1 week earlier than SAMHD1-KD cells may further indicate detrimental effects on differentiation exerted by the RNAi system, however, the differences could also be due simply to the proximity of cell production to harvest dates. These data also present the possibility that the SAMHD1 function active in this regard is the dNTPase; however, repeats of these experiments using cells encoding a dNTPase defective SAMHD1 mutant that is expressed to levels comparable to that found in wild type cells would be required before full conclusions can be drawn.

Given that the delay in esYDMP production in SAMHD1-KD (shSAM) cells have been mapped to SAMHD1, the mechanism underlying the same production dynamics in shCTRL expressing cells is

unclear. One possibility is that shCTRL is targeting a cellular factor that is also functional in homeostatic and hence, differentiation regulation. However, a search for shCTRL sequence matches in the human genome did not return any hits known to be involved in dNTP regulation.

This observation, however, does not clarify the mechanism underlying the production kinetics observed in Vpx expressing cells which produced approximately 1 week (+/- 3.5 days) before SAMHD1-KD, SAMHD1-KO and SAMHD1-MUT cells but is confirmatory of the ~1 week lag between production kinetics in SAMHD1 deleted cells (SAMHD1-KD – confirmed in SAMHD1-KO) and Vpx expressing cells (refer to Chapter 3, Section 3.4 Discussion).

A common phenotype quality control for gene knockdown studies is reintroduction and expression of the knocked-out gene via, for example, lentiviral transgene expression of SAMHD1. Unfortunately, this important step was not completed, and thus, it was not possible to determine whether the phenotype observed was completely due to the knockout of SAMHD1.

In contrast to the multiple positive CRISPR- Cas9 cuts in exon 4, no SAMHD1-KOs were confirmed for gRNA targeting exon 5. This may be due to the close proximity of the cut sites since such proximity may have disrupted the DNA binding of complementary Cas9s. Exon 5 is a small gene, and CRISPR cut sites are driven by the availability of PAM sites in the genome. A possible solution for future experiments may be in choosing large exons with multiple PAM sequences.

Finally, the speed and efficiency of the CRISPR- Cas9 protocol used in this thesis, combined with the permissive nature of es cells and the production of macrophages via *in vitro* differentiation makes this system an extremely powerful tool for loss of function studies in non-permissive cells (such as macrophages) and cells in difficult to reach locations (such as neurons).

This chapter documents the successful creation of a SAMHD1 knockout cell line, designated E2 (SAMHD1-KO), and an esYDM cell line expressing SAMHD1 with a non-functional dNTPase, designated G9 (SAMHD1-MUT). These two-cell lines, combined with a wild type (CTRL), were then used to probe the activity of SAMHD1 in esYDMs further.

Chapter 5

Chapter 5: Vpx and Vpr antagonisation of SAMHD1

5.1 Introduction

In Chapter 3, it was shown that SAMHD1 expression profile, dNTP hydrolysis, and HIV-1 restriction seen in scYDMs is like that reported in blood MDMs (refer to Chapter 3, Section 3.3 Results). Interestingly, a phenotype observed in scYDMs but not blood MDMs [2] is the rescue of HIV-1 infection by VpxQ76A. Published reports have shown that VpxQ76A-mediated rescue of HIV-1 in MDDCs requires the existence of an antiviral state established by IFN [576], and therefore the lack of IFN required for VpxQ76A-mediated HIV-1 rescue in both scYDMs and scYDMPs in this thesis was intriguing. This potentially indicated a cell type dependence of the requirement for IFN to produce this phenotype in these cells. Existing reports detailing the dynamics of IFN production in macrophages in relation to SAMHD1 and Vpx are conflicting. *In vivo,* SAMHD1 knockout mice exhibit elevated levels of IFN [603], and chronic IFNα production is associated with SAMHD1 mutations in AGS in humans [220]. This is hypothesised to be a consequence of an additional nuclease function of SAMHD1 independent of dNTP hydrolysis and active in the digestion of nucleic acids, which would otherwise be sensed by cGAS or IFI16 resulting in the production of type I IFNs [116, 197, 231, 236]. However, *in vitro*, Vpx-mediated depletion of SAMHD1 in macrophages does not result in IFN production, neither does SAMHD1-KO in PMA differentiated THP-1 cells [113, 117]. That said, application of Vpx to macrophages *in vitro* in conjunction with HIV-1 has been shown to result in the production of IFN via an IFI16 dependent but a cGAS independent pathway [117, 604] yet evidence also exists for Vpx mediated suppression of type I IFN production via interaction with IRF5 [592]. HIV-1 Vpr has also been implicated in the modulation of IFN production in myeloid cells [605], a function that has been linked to, but also reported as dispensable for, enhancement of infection in macrophages [606]. In the HIV-2/SIVmac/SIVsm and SIVrcm/SIVmnd2 lineages, the functions of infection enhancement in macrophages (mediated by SAMHD1 and DCAF1) and G2 arrest (mediated by DCAF1) is split between Vpx and Vpr respectively [607], in SIVdeb, SIVmus and SIVagm lineages both functions are attributed to Vpr (mediated by SAMHD1 and DCAF1), whereas

in HIV-1 and SIVcpz lineages, although both functions are attributed to Vpr [607], the macrophage infectivity enhancements are believed to be independent of direct interaction with SAMHD1 (since HIV-1 and SIVcpz Vprs' do not antagonise SAMHD1) [96]. It is unclear to what extent IFN modulation is encoded by Vpr proteins of non-HIV-1 lineage primate lentiviruses, a question further complicated by the lineage-specific dependence of function division between Vpr (and Vpx) proteins just described.

The effects of LPS stimulation in macrophages with regards to HIV-1 replication is similarly opaque. LPS is a potent stimulating PAMP that polarises myeloid cells into an antimicrobial state [590]. Initial observations of LPS-mediated anti-HIV-1 effects revealed that the application of LPS restricted HIV-1 replication in primary macrophages [608] and in MDDCs [576], but curiously that overall HIV-1 restriction in MDMs was preceded by an LPS-mediated increase in viral entry [609, 610]. In the myeloid cell lines U937 and THP-1, the application of LPS has been shown to stimulate integrated provirus gene expression by activation of the HIV-1 LTR [611]. Provirus reactivation has also been observed with *in vitro* application of LPS to monocytes extracted from HIV-1 positive patients on long term HAART [435]. However, constant stimulation by LPS *in vitro* appears to result in a restrictive phenotype since repeated LPS exposure inhibited HIV-1 LTR transactivation and HIV-1 replication in THP-1 cells and MDMs, respectively [612]. That said, post mortem examination of lymph node tissue from AIDS patients revealed that tissue-resident macrophage-mediated HIV-1 production is amplified in the presence of opportunistic infections such as *Mycobacterium avium* complex and *Pneumocystis carinii* [399], implicating a pro-replication role for pathogen components in these cells.

It is possible, therefore, that the dynamics of SAMHD1 mediated HIV-1 restriction in macrophages in relation to IFN production or stimulation by IFN or LPS may involve cell type determinants which in the steady-state may influence HIV-1 infection but may also influence SAMHD1 independent functions of Vpx. Two lines of evidence presented in Chapter 3 supported potential SAMHD1 independent functions encoded by Vpx for HIV-1 infection enhancement and/or regulation of dNTP concentrations in esYDMs.

The first is the differential effects on SAMHD1 protein expression, dNTP concentrations, and HIV-1 infection of Vpx expressing cells versus SAMHD1-KD cells. The second is the VpxQ76A-mediated rescue of HIV-1 infection in esYDMPs, and PMA treated THP-1 cells, and to a lesser extent, in ipsYDMs. Alternative explanations for these two observations are the contribution of RKP in the former and a SAMHD1 dependent but DCAF1 independent mechanism for the latter. In both cases, experimental delineation required the use of cells totally devoid of SAMHD1 (and hence RKP), and thus, the SAMHD1-KO cells were used to investigate in this regard.

In this chapter, the SAMHD1-KO esYDMs generated in Chapter 4 were used to determine what effects residual levels of SAMHD1 protein remaining after knockdown or Vpx-mediated antagonisation may have on intracellular dNTP concentrations and HIV-1 restriction. Subsequent experiments used the esYDM cell line expressing the SAMHD1 mutant devoid of a functional dNTPase in determining the phenotype of any dNTPase independent HIV-1 restriction in esYDMs. Next, Vpx mediated SAMHD1 independent interacting partners are investigated via immunoprecipitations utilising the SAMHD1-KO cell line. This chapter concludes by investigating the dynamics of Vpr proteins encoded by SIVmac251 and HIV-1, the influence of env, and stimulation by IFN, LPS, and PMA, in relation to HIV-1 infection in esYDMs.

5.2 Methods and Materials

5.2.1 Immunoprecipitation & Mass Spectrometry Analysis

Immunoprecipitations were performed using the anti-HA Immunoprecipitation Kit (Sigma-Aldrich® Cat No IP0010). The manufacturer's protocol was used and expanded as follows. THP-1 cells were transduced with lentiviral vectors encoding HA-Vpx (HA-Vpx) or an empty cassette (IResPuro - IRP). 2 x 10^7 WT cells were cultured as previously described (refer to Chapter 2, Section 2.1 Cell Culture). HA-Vpx, IRP cell lines were also cultured as previously described (refer to Chapter 2, Section 2.1 Cell Culture) with the addition of puromycin (MP Biomedicals) at a concentration of 0.4μg/mL. Cells were then

harvested in a 50mL tube, centrifuged at 400 x g for 5 mins, resuspended in 1.5mL of PBS (PAA, Invitrogen, Sigma), and transferred to a 1.5mL Eppendorf. Cells were then centrifuged for 3 mins at 450g, after which time the supernatant was removed. In preparation, 1/8th of a cOmplete® EDTA-free Protease Inhibitor Cocktail tablet (Roche Cat No 46933132001) was added to 1mL of CelLytic solution® – CelLytic+P®. Cells were then resuspended in 200mL of CelLytic+P® lysis solution and agitated on a rotator for 25 mins at 4^{o}C. The suspension was then centrifuged at 17,000 x g for 20 mins at 4^{o}C. For IRP cells, protein-containing supernatant was removed and transferred to a 1.5mL Eppendorf previously chilled to 4^{o}C. For HA-Vpx and WT cells, protein-containing supernatant was removed and transferred to the same 1.5mL Eppendorf tube previously chilled to 4^{o}C. N.B. This step was to allow the interreacting partner abundant in WT cells to bind to HA-Vpx expressed in HA-Vpx cells. 400µL of 1 x IP buffer® added to IRP protein-containing supernatant (200µL) to total 600µL. 200µL of 1 x IP buffer® was added to Vpx+WT protein-containing supernatant (400µL) to total 600µL. For IRP, 10µL of HA beads were added to a spin column followed by the addition of 600µL of protein-containing supernatant plus 1 x IP buffer® was added to a column and mixed with a pipette. For the HA-Vpx+WT sample, 10µL of HA beads were added to a spin column followed by the addition of 600µL of protein-containing supernatant plus 1 x IP buffer® was added to a column and mixed with a pipette. Spin columns were then sealed with Parafilm® and placed on a rotator at 4^{o}C overnight. Spin columns were then washed six times at 4^{o}C. 300µL of 1 x IP buffer® was added to each spin column, followed by centrifugation at 12,000 x g for 15 sec. Flow-through was collected in 1.5mL Eppendorf tubes and stored. Spin columns were then washed a 7th and final time with 0.1 x IP buffer®. HA-Vpx bound proteins were then eluted in 1 x LDS sample buffer (NuPage®). 50µL of 1 x LDS sample buffer was added to each column. Spin columns were then heated at 95^{o}C for 5 mins. Spin columns were then placed in new 1.5mL Eppendorf tubes and centrifuged at 12,000 x g for 15 sec. Eluates of HA-Vpx and IRP/WT precipitations were then run on a 8-12% polyacrylamide gel along with relevant controls which consisted of a prewash sample of HA-Vpx (Vpx-input), first wash of HA-Vpx sample (Vpx flow-through), the prewash sample of IRP/WT (IRP input) and the first wash flow-through of IRP/WT (IRP flow-through).

The proteins separated in the polyacrylamide gel were then silver stained using the basic protocol of the SilverQuest™ Silver Staining Kit (Cat No: LC6070) according to the manufacturers' instructions. Protein bands requiring further processing were excised using a sharp metal scalpel and placed in a 1.5mL Eppendorf tube.

Protein containing gel fragments were then de-stained us a de-staining solution of 100mM $Na_2O_3S_2 \cdot 5H_2O$ & 30mM $K_3Fe(CN)_6$. Protein containing get fragment was then cut into small pieces and placed into a PCR tube to which 300µL of the de-staining solution was added. The PCR tubes were then placed on a shaker at 400rpm, 56°C for 5 mins. This was repeated until the gel fragments were completely de-stained. 300µL of acetonitrile solution was added to each tube. Tubes were then agitated at 700rpm, 37°C for 5 mins. This was repeated until the fragments turned white and brittle. The acetonitrile was then removed, and 300µL of 50mM TCEP was added to each tube. Tubes were then allowed to incubate at 37°C for 30-60 mins. TCEP supernatant was then discarded and replaced with 2-Chloroactamide and placed in the dark for 60 mins at room temperature. The 2-Chloroacetamide was then removed, and the contents were washed twice by addition of 300µL of 50% acetonitrile (in 0.1% TFA) and agitation at 700rpm for 5 mins at 37°C. Samples were then washed again by the addition of 300µL of 100% acetonitrile and agitation at 700rpm for 5 mins at 37°C. Samples were then lyophilised using a SpeedVac® for approximated 10 mins. Trypsin digest was then performed by the addition of 100µL of 200ng of Trypsin at a pH of 7-8 50nM TEAB buffer followed by overnight incubation at 37°C. The supernatant containing peptides were then transferred to a new tube. 1µL of formic acid was added to end the digest reaction and adjust the pH to 3. The volume was then increased to 1.5mL and subsequently lyophilised to 100µL using a SpeedVac®. The supernatant was then transferred to a 200µL c18 resin tip (Pierce™) to which 30µL of 100% acetonitrile was added. c18 tips were then centrifuged at 350-400 x g for 1 minute. The c18 tip was then washed by addition of 30µL of 0.1% TFA and centrifuged at 1830rpm for 3 mins. The peptide containing supernatant was transferred to a new c18 tip then centrifuged at 500 x g for 4.5 mins. The flow-through from this wash step was saved. A final

wash was then performed by the addition of 100µL of 0.1% TFA, followed by centrifugation at 500 x g for 4-5 mins. The flow-through from this wash step was also saved. Elution was achieved by the addition of 60µL of 50% acetonitrile/0.1%. Peptides were then identified using mass spectrometric analysis.

5.2.2 Cloning for the production of SIVmac-Vpx, SIVmac-Vpr, and HIV-1 Vpr expressing plasmids

SIVmac251-Vpx or SIVmac251-Vpr sequence was PCR amplified to introduce overhangs containing SpeI at the 5' end and BstXI at the 3' end. DNA sequences used for Vpx and Vpr can be found in Table 2.3. Amplified transgene sequences were cloned (refer to Section 2.3 Cloning Techniques) into the '2nd generation' pEF1-IRES-Puro (refer to Table 2.5) self-inactivating (SIN) lentiviral vector at the appropriate restriction sites (refer to Figure 5.1). Successful cloning was confirmed by sequencing the completed lentiviral vector for Vpr (Figure 5.2) and Vpx (data not shown) using the SIVmac251 Vpr forward Primer and the SIVmac251 Vpx forward primers, respectively (refer to Table 2.3, Sigma) complementary to the end of the EF1α promoter, and IRESstartReverse primer (refer to Table 2.3, Sigma). Plasmids for the expression of SIVmac251 Vpx, and SIVmac251 Vpr were labelled, pEF1-Vpx-IRES-PuroR and pEF1-SVpr-IRES-PuroR, respectively. The control construct was pEF1-IRES-PuroR (refer to Table 2.5). The plasmid used for expression of HIV-1 Vpr (pVPR) was a gift from Dr. Michael (Kenny) Moore (refer to Table 2.5). HIV-1 Vpr gene encoding was confirmed by sanger sequencing (Figure 5.3) by using the CMV forward primer (refer to Table 2.3).

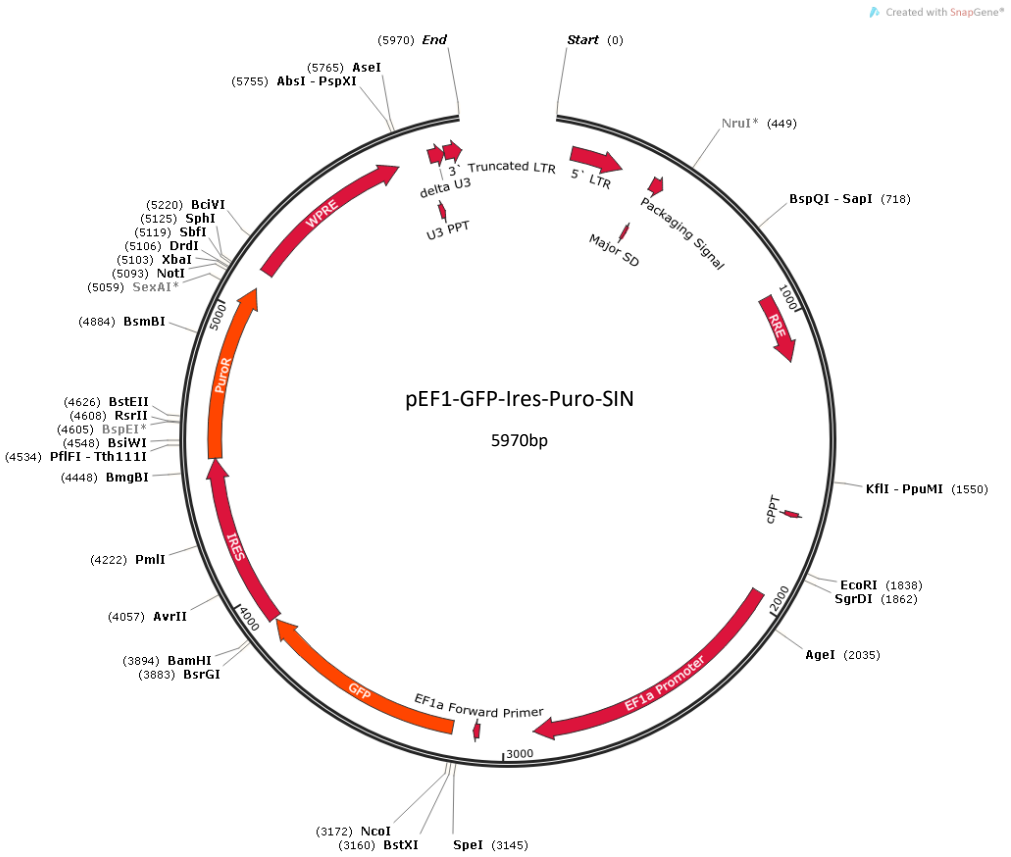


Figure 5.1 Plasmid pEF1-IRES-Puro-SIN.



Figure 5.2 SIVmac251 Vpr incorporation into pEF1-IRES-Puro.

Sequencing of pEF1-SVpr-IRES-PuroR to confirm the successful incorporation of the SIVmac251 Vpr gene sequence. The trace (433229801_VPR251_FWDVPR_F03.ab1) aligns with the Vpr sequence from the SIVmac251 genome fragment encoded by the pSIV3+ vector (accession number M19499). Generated using DNADynamo™ software.



Figure 5.3 HIV-1 Vpr incorporation into pVpr (HIV-1).

Sequencing of pVpr(HIV-1) plasmid to confirm coding of HIV-1 Vpr gene. The trace (433229801_VPRHIV_CMVF.ab1) aligns with the Vpr sequence encoded in the HIV-1 genome (accession number NC_001802.1). Generated using DNADynamo™ software.

5.3 Results

5.3.1 Modulation of dNTP concentrations and HIV-1 restriction by SAMHD1 RKP

Transgene expression systems offer a robust and simple method for the suppression of genes via shRNA expression in loss of function experiments. The efficiency of shRNA suppressed gene expression varies depending on the gene, the cell type, and the expression system used, but in most cases, gene knock-down is not 100%, and a small amount of residual knock-down protein (RKP) is translated. For most genes, RKP is insufficient to enact the cell-wide effects attributed to the gene, and therefore, the function is considered lost, however in a few cases, particularly with genes encoding enzymes, the functional effects of RKP can be quantifiable.

Several investigations probing the activity of SAMHD1 via knockdown with shRNA or siRNA have questioned the functionality that residual SAMHD1 protein remaining after knockdown can retain. Reinhard et al. [590] showed that reductions in HIV-1 restriction seen after knockdown of SAMHD1 with

siRNA can be further enhanced after exogenous application of Vpx VLPs. Similarly, Kyei et al. [118] concluded that the incomplete neutralisation of HIV-1 restriction induced by the tandem knockdown of cyclin-L2 (which results in an increase in HIV-1 restriction) and SAMHD1 (which results in reduced HIV-1 restriction), might be due to RKP. Finally, data presented in Chapter 3 of this thesis showed that knock-down of SAMHD1 in esYDMs resulted in higher protein levels, lower dNTP concentrations, and less potent rescue of HIV-1 infection compared to that observed with Vpx expressing esYDMs. It was concluded that this could be due to either functional RKP expressed in shSAM esYSDMs, or an additional SAMHD1 independent mechanism by which Vpx increased HIV-1 infection and dNTP concentrations in esYDMs. A myeloid cell line devoid of SAMHD1 was required to test these suggestions, and hence, the SAMHD1-KO esYDMs created and described in Chapter 4 were used in this regard.

First, the effects of SAMHD1 RKP on HIV-1 infection dynamics were investigated. WT and SAMHD1-KO esYDMs were incubated for 2 hrs with Virus-like particles (VLP's) encoding Vpx (Vpx-VLPs) or a non-functional cassette (empty-VLPs) and subsequently infected with VSV.G pseudotyped HIV-1.GIP virus (refer to 2.4.3.2 HIV-1 Infection assay (GFP) with VLPs). Application of Vpx-VLPs to WT esYDMs resulted in a 5.2-fold increase in HIV-1 infection versus WT cells treated with empty-VLPs. (Figure 5.4B). In the absence of Vpx, SAMHD1-KO esYDMs were 12-fold more permissive to HIV-1 infection compared to WT esYDMs (Figure 5.4A). Infection levels of SAMHD1-KO cells were 2.3-fold greater than infection in WT cells treated with Vpx-VLPs (Figure 5.4C). In SAMHD1-KO cells, HIV-1 infection levels, either in the presence or absence of Vpx, were not significantly different (Figure 5.4D).

Next, the effects of SAMHD1 RKP on dNTP concentrations were probed. WT and SAMHD1-KO esYDM cells were incubated for ~2 hrs with Vpx-VLPs or empty-VLPs. Post incubation dNTPs were extracted and quantified as previously described (refer to Section 3.2.2 Tritium based enzymatic assay for the determination of intracellular dNTP concentrations). The application of Vpx-VLPs to WT esYDMs resulted in a statistically significant increase in dATP (Figure 5.4F). In the absence of Vpx, dATP

concentrations in SAMHD1-KO esYDMs were 4-fold higher than observed in WT esYDMs (Figure 5.4E). dATP concentrations in SAMHD1-KO cells were 2.5-fold higher than in WT cells treated with Vpx-VLPs (Figure 5.4G). Interestingly, dATP concentrations in SAMHD1-KO esYDMs were 3-fold higher in the presence of Vpx-VLPs (Figure 5.4H) than SAMHD1-KO cells treated with empty VLPs.

These results show that in esYDMs, SAMHD1 RKP is active in dNTP hydrolysis and HIV-1 restriction. These results also show marked differences between HIV-1 rescue and dNTP concentrations in cells treated with Vpx exogenously versus cells expressing Vpx endogenous.

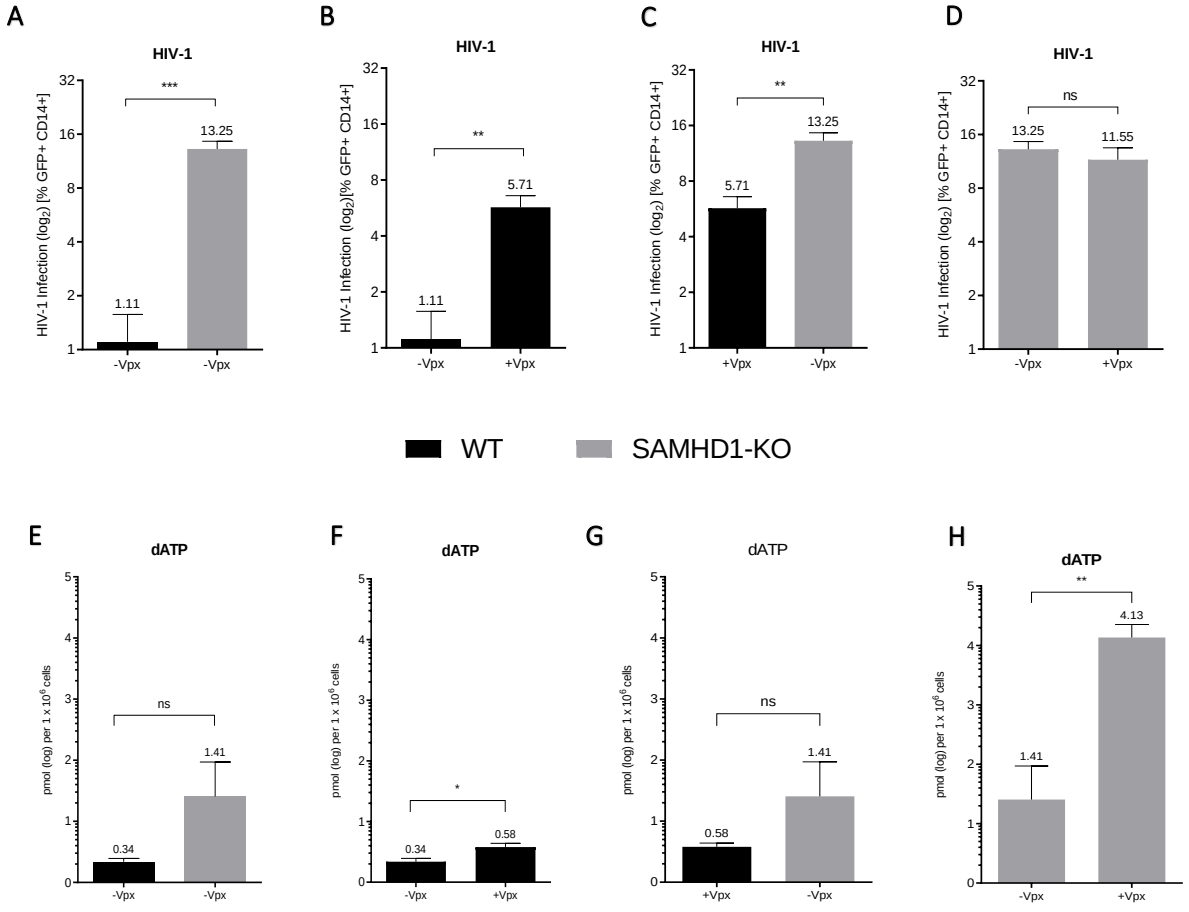


Figure 5.4 HIV-1 infection and dNTP concentrations in SAMHD1-KO cells.

Wild type (WT) esYDMs and SAMHD1 knockout (SAMHD1-KO) esYDMs were treated with VLPs encoding Vpx protein or an empty cassette (empty VLPs). After 2 hrs, cells were either infected with HIV-1 or harvested for dNTP quantification. For the HIV-1 infection assay VSV.G pseudotyped HIV-1.GIP was used. Post-infection cells were incubated for 3.5 days, then harvested, and CD14 stained. Frequency of HIV-1 infection were quantified by flow cytometry. In the absence of Vpx, HIV-1 infection in SAMHD1-KO esYDMs was 12-fold higher than in WT esYDMs, (**A**). Application of Vpx to WT cells significantly increases HIV-1 infection (**B**), but not to levels observed in SAMHD1-KO cells, (**C**). Application of Vpx to SAMHD1-KO cells did not alter the level of HIV-1 infection compared to SAMHD1-KO cells treated with empty VLPs, (**D**). For dNTP quantification, post-VLP incubation cells were harvested and counted. dNTPs were then isolated via methanoic extraction and subsequently quantified using the tritiated thymidine-based dNTP quantification assay established in Chapter 3 (refer to Section 3.2.2). In the absence of Vpx, dATP concentrations in SAMHD1-KO cells were at levels higher than in WT cells, (**E**). Application of Vpx to WT cells increased dATP concentrations, (**F**), but not to levels observed in SAMHD1-KO cells treated with empty VLPs, (**G**). Application of Vpx to SAMHD1-KO cells resulted in a significant increase in dATP versus SAMHD1-KO cells treated with empty VLPs, (**H**). Data presented as the mean +\- SEM and is representative of three independent experiments (n=3). One-tailed, unpaired, parametric t-test; ns=non-significant, *p<0.05, **p<0.01, ***p<0.001.

5.3.2 Probing the identity of SAMHD1 independent Vpx interacting partners

As previously described, RNAi mediated silencing or application of Vpx to cells expressing SAMHD1 with a functional dNTPase result in an increase in dNTP concentrations. However, there have been observations that fall outside of this well-established relationship. For example, in cycling CD4+ T-cells dNTP concentrations are high, despite strong expression of catalytically active SAMHD1, and in MDDCs matured with LPS, Vpx mediated degradation of SAMHD1 did not result in a concomitant rise in dNTP concentrations [590]. This could indicate the presence of additional mechanisms of regulation in the case of the former observation, or effects of SAMHD1 RKP or additional means of dNTP hydrolysis in the case of the latter, yet both observations imply that there may be aspects of the SAMHD1-Vpx relationship with dNTP concentrations in cells that remain to be described. SAMHD1 is the only dNTPase described in the human genome, however searching for an additional dNTPase to explain unchanged dNTP concentrations on addition of Vpx may not be necessary since the data presented in the previous section provided compelling evidence that the phenotype of unchanged dNTP concentrations post-application of Vpx may simply be due to SAMHD1 RKP (See Chapter 5, Section 5.3.1). Explanations regarding the phenotype of high dNTP concentrations in cells with robust expression of catalytically active SAMHD1 have yet to resolve conflicting reports regarding the contribution of posttranslational regulation by phosphorylation at T592 of the dNTPase (see Chapter 1, Section 1.1.5.4 SAMHD1) or alternatively, settle the requirement for regulation of any novel mechanism driving dNTP synthesis. Investigations that have probed novel dNTP synthesis in the context of HIV-1 infection have primarily focussed on the cell cycle regulator p21/Waf1/Cip1 (p21) [208, 211]. As previously described, p21 is a cyclin-dependent kinase inhibitor that functions in the regulation of differentiation and maturation in myeloid cells but is also implicated in functioning in HIV-1 restriction in these cells [208]. In MDDCs and MDMs, the mechanism underlying p21-mediated HIV-1 restriction is believed to involve the reduction of dNTP concentrations via suppression of enzymes involved in dNTP synthesis such as RNR2, TYMS, and TK-1, and indeed RNA interference of p21 results in an increase in dNTP concentrations [208, 211]. Curiously, a mechanism for p21 antagonisation by primate lentiviruses has yet to be described. Data

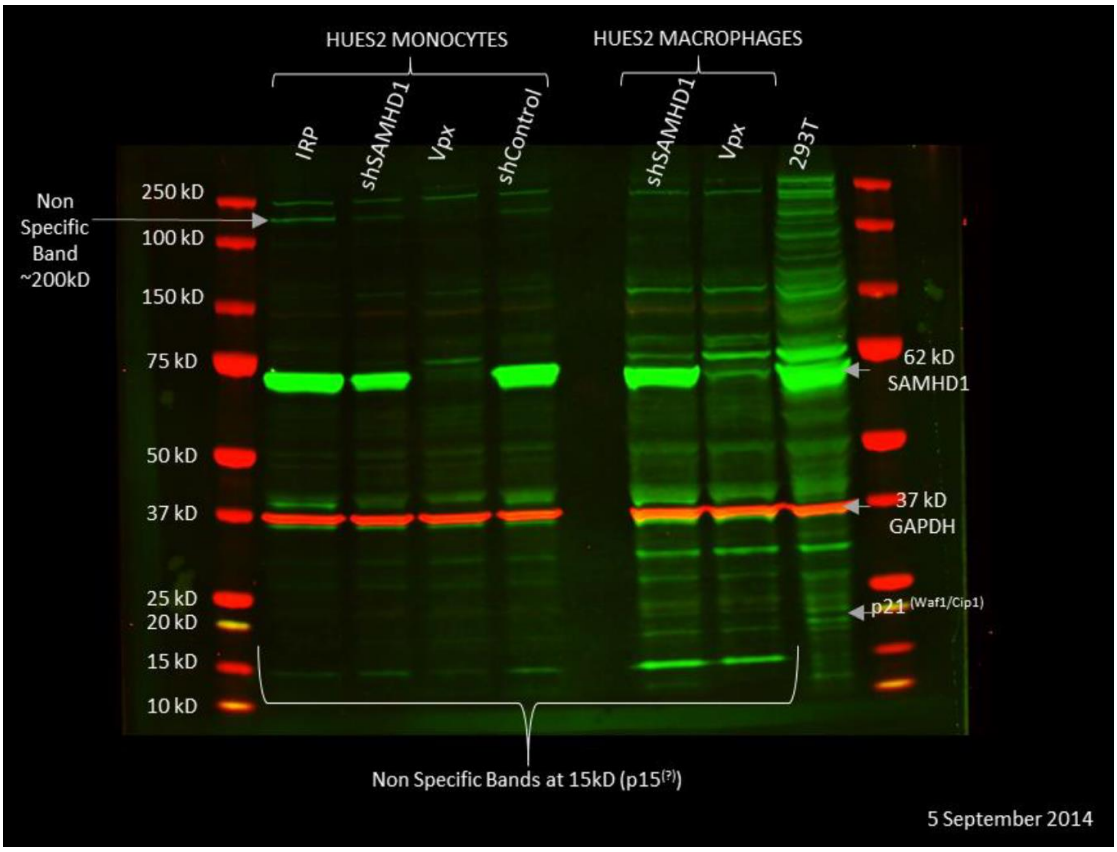
from section 5.3.1 showed that in SAMHD1-KO cells, the application of Vpx results in a small increase in dATP in esYDM, which implies that Vpx modulated dNTPs via a SAMHD1 independent mechanism. This, therefore, presents the possibility that Vpx interacts with a cellular factor, such as p21, to facilitate an increase in dNTP concentrations.

In order to test for interactions between p21, and Vpx in esYDMs and esYDMPs, cell lysates from esYDMs and esYDMPs treated with Vpx protein were extracted and probed for p21 via immunoblot (Figure 5.5A and Figure 5.5C). p21 protein was not identified in either esYDMs or esYDMPs. However, two unidentified proteins were present of sizes ~15kD and ~200kD. Interestingly, the expression profile of these proteins showed almost complete depletion in Vpx expressing cell lines, strongly implying that these two proteins interact with Vpx (Figure 5.5B and 5.2D).

In order to identify the two unknown proteins at ~15kD and ~200kD, an immunoprecipitation was performed using HA-tagged Vpx protein (HA-Vpx) in THP-1 monocytes (see Section 5.2.1). Unfortunately, only the ~200kD band was clearly present in the Vpx eluate (Figure 5.5E). Proteomic analysis of the ~200kD band revealed eight proteins present with a protein score of over 60 (Table 5.1). Of these eight proteins only one was relevant to primate lentiviral microbiology, VPRBP. VPRBP is also known as DCAF1 and is a subunit of the CLR4 E3 ubiquitin ligase complex usurped by both Vpx and Vpr in order to degrade host antagonistic proteins, such as SAMHD1 (refer to Section 1.1.4.2 Vpr, and Section 1.1.4.3 Vpx). Interestingly, a protein present in both the control and HA-Vpx samples but not in the HA-Vpx eluate, Regulation of nuclear pre-mRNA domain-containing protein 2 (RPRD2), also referred to as RNA-associated early-stage antiviral factor (REAF), has recently been identified as an interacting partner of Vpr that is active in HIV-1 restriction [613]. Since REAF was identified in the control sample, in this experiment at least, it cannot be considered a specific binding partner for Vpx.

These results show that in THP-1 cells, HA-Vpx interacts with DCAF1.

A



B

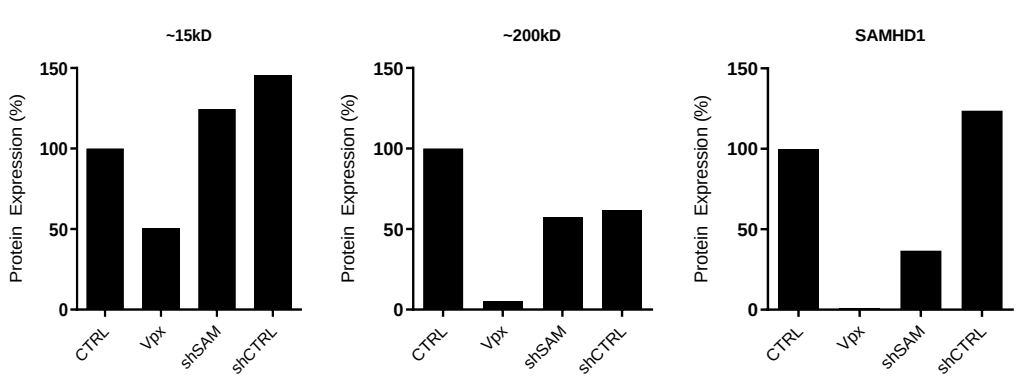
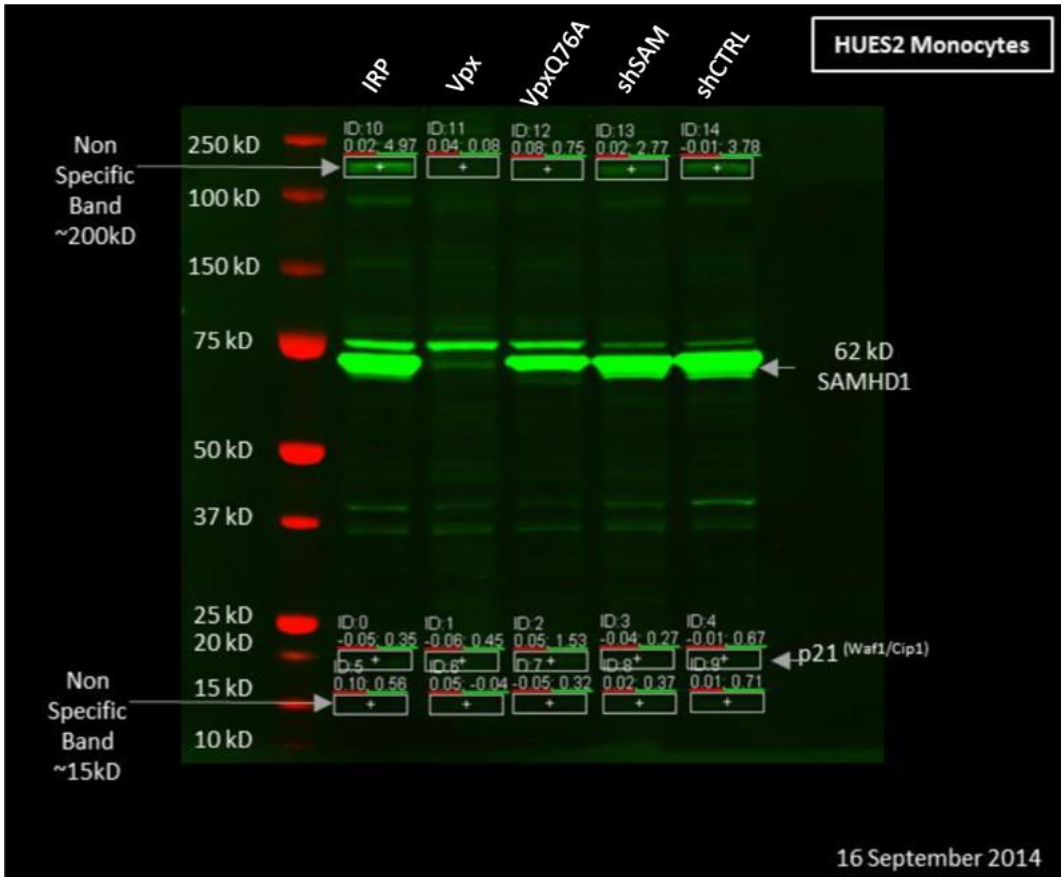


Figure 5.5 Potential novel Vpx interacting partners.

Unknown proteins binding non-specifically to SAMHD1 antibody in the ~200kD and ~15kD regions were detected when probing esYDM lysates for p21 and SAMHD1 by immunoblot. esYDM (referred to as HUES2 Macrophages) and esYDMP (referred to as HUES2 Monocytes) cell lines expressing Vpx, VpxQ76A (see below), shSAM (also referred to as shSAMHD1) or controls, and HEK293T cells were lysed and probed using α-SAMHD1, α-p21, and α-GAPDH monoclonal antibodies (**A**) and (**C**). Protein expression levels for SAMHD1 and the unknown proteins at ~200kD and ~15kD regions were then quantified (**B**) and (**D**) (n=1). Immunoprecipitation for the identification of novel Vpx interacting partners was performed using THP-1 monocytes expressing HA-tagged Vpx protein or a control construct (IRP). Following expansion, cells were lysed, and Vpx bound antigen precipitated using α-HA beads. Protein precipitates and control lysates were separated using a polyacrylamide gel and silver stained. The ~200kD protein and associated control bands were excised, de-silver stained, and processed for protein identification via mass spectrometry, (**E**).

C



D

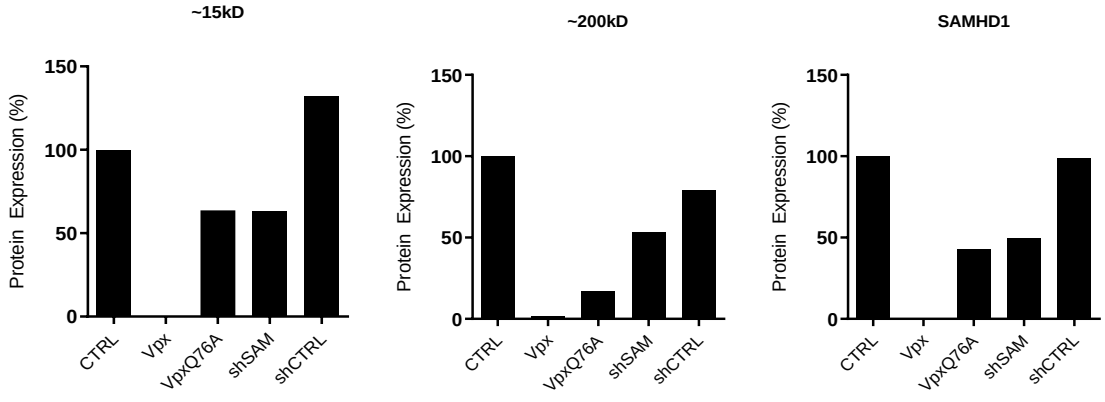


Figure 5.5 Potential novel Vpx interacting partners (continued).

Unknown proteins binding non-specifically to SAMHD1 antibody in the ~200kD and ~15kD regions were detected when probing esYDM lysates for p21 and SAMHD1 by immunoblot. esYDM (referred to as HUES2 Macrophages) and esYDMP (referred to as HUES2 Monocytes) cell lines expressing Vpx, VpxQ76A (see below), shSAM (also referred to as shSAMHD1) or controls, and HEK293T cells were lysed and probed using α-SAMHD1, α-p21, and α-GAPDH monoclonal antibodies (**A**) and (**C**). Protein expression levels for SAMHD1 and the unknown proteins at ~200kD and ~15kD regions were then quantified (**B**) and (**D**) (n=1). Immunoprecipitation for the identification of novel Vpx interacting partners was performed using THP-1 monocytes expressing HA-tagged Vpx protein or a control construct (IRP). Following expansion, cells were lysed, and Vpx bound antigen precipitated using α-HA beads. Protein precipitates and control lysates were separated using a polyacrylamide gel and silver stained. The ~200kD protein and associated control bands were excised, de-silver stained, and processed for protein identification via mass spectrometry, (**E**).

E

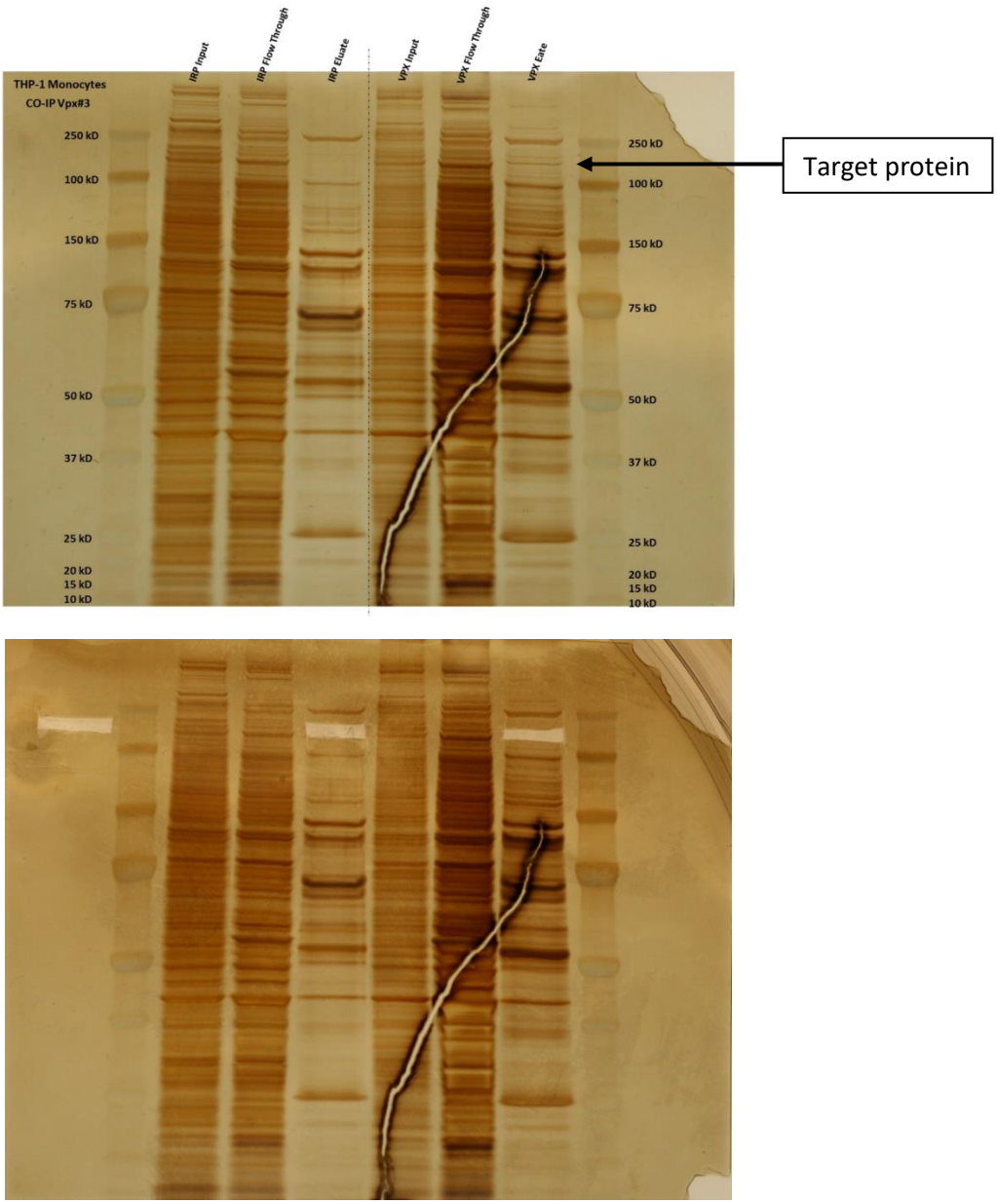


Figure 5.5 Potential novel Vpx interacting partners (continued).

Unknown proteins binding non-specifically to SAMHD1 antibody in the ~200kD and ~15kD regions were detected when probing esYDM lysates for p21 and SAMHD1 by immunoblot. esYDM (referred to as HUES2 Macrophages) and esYDMP (referred to as HUES2 Monocytes) cell lines expressing Vpx, VpxQ76A (see below), shSAM (also referred to as shSAMHD1) or controls, and HEK293T cells were lysed and probed using α-SAMHD1, α-p21, and α-GAPDH monoclonal antibodies (**A**) and (**C**). Protein expression levels for SAMHD1 and the unknown proteins at ~200kD and ~15kD regions were then quantified (**B**) and (**D**) (n=1). Immunoprecipitation for the identification of novel Vpx interacting partners was performed using THP-1 monocytes expressing HA-tagged Vpx protein or a control construct (IRP). Following expansion, cells were lysed, and Vpx bound antigen precipitated using α-HA beads. Protein precipitates and control lysates were separated using a polyacrylamide gel and silver stained. The ~200kD protein and associated control bands were excised, de-silver stained, and processed for protein identification via mass spectrometry, (**E**).

A

			20141103 IRP Control Sample		
Number	prot_fami	prot_acc	Protein Desctiption	prot_score	prot_mass
1	1	sp|P04264|K2C1_HUMAN	Keratin, type II cytoskeletal 1 OS=Homo sapiens GN=KRT1 PE=1 SV=6	571	66170
2	1	sp|P02533|K1C14_HUMAN	Keratin, type I cytoskeletal 14 OS=Homo sapiens GN=KRT14 PE=1 SV=4	480	51872
3	1	sp|P46940|IQGA1_HUMAN	Ras GTPase-activating-like protein IQGAP1 OS=Homo sapiens GN=IQGAP1 PE=1 SV=1	363	189761
4	1	sp|Q5VT52|RPRD2_HUMAN	Regulation of nuclear pre-mRNA domain-containing protein 2 OS=Homo sapiens GN=RPRD2 PE=1 SV=1	175	156380
5	1	sp|P07814|SYEP_HUMAN	Bifunctional glutamate/proline--tRNA ligase OS=Homo sapiens GN=EPRS PE=1 SV=5	157	172080
6	1	sp|Q00610-2|CLH1_HUMAN	Isoform 2 of Clathrin heavy chain 1 OS=Homo sapiens GN=CLTC	155	189538
7	1	sp|P15924-2|DESP_HUMAN	Isoform DPII of Desmoplakin OS=Homo sapiens GN=DSP	95	262237
8	1	sp|P81605-2|DCD_HUMAN	Isoform 2 of Dermcidin OS=Homo sapiens GN=DCD	76	12520
9	1	sp|Q92608|DOCK2_HUMAN	Dedicator of cytokinesis protein 2 OS=Homo sapiens GN=DOCK2 PE=1 SV=2	51	213123
10	1	sp|P35579|MYH9_HUMAN	Myosin-9 OS=Homo sapiens GN=MYH9 PE=1 SV=4	46	227646
11	1	sp|P47929|LEG7_HUMAN	Galectin-7 OS=Homo sapiens GN=LGALS7 PE=1 SV=2	40	15123
12	1	tr|J3KNX9|J3KNX9_HUMAN	Unconventional myosin-XVIIIa OS=Homo sapiens GN=MYO18A PE=2 SV=1	40	234193
13	1	sp|Q8TF72|SHRM3_HUMAN	Protein Shroom3 OS=Homo sapiens GN=SHROOM3 PE=1 SV=2	40	218321
14	1	tr|B1AN99|B1AN99_HUMAN	Trypsin-3 (Fragment) OS=Homo sapiens GN=PRSS3 PE=2 SV=1	39	19674
15	1	tr|M0R081|M0R081_HUMAN	C-type lectin domain family 11 member A OS=Homo sapiens GN=CLEC11A PE=2 SV=1	34	33570
16	1	tr|H0YEH2|H0YEH2_HUMAN	Pumilio homolog 1 (Fragment) OS=Homo sapiens GN=PUM1 PE=4 SV=1	30	120836
17	1	tr|M0R1V7|M0R1V7_HUMAN	Ubiquitin-60S ribosomal protein L40 (Fragment) OS=Homo sapiens GN=UBA52 PE=2 SV=1	26	7128
18	1	sp|Q96BF6|NACC2_HUMAN	Nucleus accumbens-associated protein 2 OS=Homo sapiens GN=NACC2 PE=2 SV=1	22	63538
19	1	sp|Q9NPQ8-2|RIC8A_HUMAN	Isoform 2 of Synembryn-A OS=Homo sapiens GN=RIC8A	17	59476
20	1	tr|E7EX82|E7EX82_HUMAN	Polyhomeotic-like protein 3 OS=Homo sapiens GN=PHC3 PE=2 SV=1	14	89826

B

			20141103 Vpx Sample		
Number	prot_fami	prot_acc	Protein Description	prot_score	prot_mass
1	1	sp|P04264|K2C1_HUMAN	Keratin, type II cytoskeletal 1 OS=Homo sapiens GN=KRT1 PE=1 SV=6	945	66170
2	1	sp|P13645|K1C10_HUMAN	Keratin, type I cytoskeletal 10 OS=Homo sapiens GN=KRT10 PE=1 SV=6	633	59020
3	1	sp|P46940|IQGA1_HUMAN	Ras GTPase-activating-like protein IQGAP1 OS=Homo sapiens GN=IQGAP1 PE=1 SV=1	568	189761
4	1	sp|Q00610-2|CLH1_HUMAN	Isoform 2 of Clathrin heavy chain 1 OS=Homo sapiens GN=CLTC	560	189538
5	1	sp|P07814|SYEP_HUMAN	Bifunctional glutamate/proline--tRNA ligase OS=Homo sapiens GN=EPRS PE=1 SV=5	442	172080
6	1	sp|Q9Y4B6-2|VPRBP_HUMAN	Isoform 2 of Protein VPRBP OS=Homo sapiens GN=VPRBP	194	170597
7	1	sp|Q9NYU2-2|UGGG1_HUMAN	Isoform 2 of UDP-glucose:glycoprotein glucosyltransferase 1 OS=Homo sapiens GN=UGGT1	122	175437
8	1	sp|Q5VT52-3|RPRD2_HUMAN	Isoform 3 of Regulation of nuclear pre-mRNA domain-containing protein 2 OS=Homo sapiens GN=RPRD2	111	153238
9	1	tr|F5H335|F5H335_HUMAN	Eukaryotic translation initiation factor 3 subunit A OS=Homo sapiens GN=EIF3A PE=2 SV=1	87	162936
10	1	sp|P81605-2|DCD_HUMAN	Isoform 2 of Dermcidin OS=Homo sapiens GN=DCD	69	12520
11	1	sp|Q8TEQ6|GEMI5_HUMAN	Gem-associated protein 5 OS=Homo sapiens GN=GEMIN5 PE=1 SV=3	68	170821
12	1	sp|P11388-2|TOP2A_HUMAN	Isoform 2 of DNA topoisomerase 2-alpha OS=Homo sapiens GN=TOP2A	64	178131
13	1	sp|Q5H9U9|DDX6L_HUMAN	Probable ATP-dependent RNA helicase DDX60-like OS=Homo sapiens GN=DDX60L PE=2 SV=2	64	199828
14	1	tr|S4R3H4|S4R3H4_HUMAN	Apoptotic chromatin condensation inducer in the nucleus OS=Homo sapiens GN=ACIN1 PE=4 SV=1	63	145755
15	1	sp|O60306|AQR_HUMAN	Intron-binding protein aquarius OS=Homo sapiens GN=AQR PE=1 SV=4	60	172270
16	1	sp|Q8TF72|SHRM3_HUMAN	Protein Shroom3 OS=Homo sapiens GN=SHROOM3 PE=1 SV=2	44	218321
17	1	sp|Q9Y6Q9-2|NCOA3_HUMAN	Isoform 2 of Nuclear receptor coactivator 3 OS=Homo sapiens GN=NCOA3	42	154611
18	1	sp|P15924|DESP_HUMAN	Desmoplakin OS=Homo sapiens GN=DSP PE=1 SV=3	41	334021
19	1	tr|B1AM27|B1AM27_HUMAN	Protein unc-13 homolog B OS=Homo sapiens GN=UNC13B PE=2 SV=1	40	186397
20	1	sp|Q8NDA8|MROH1_HUMAN	Maestro heat-like repeat-containing protein family member 1 OS=Homo sapiens GN=MROH1 PE=2 SV=3	40	183700
21	1	sp|Q8N3K9|CMYA5_HUMAN	Cardiomyopathy-associated protein 5 OS=Homo sapiens GN=CMYA5 PE=1 SV=3	31	450760
22	1	tr|I1E4Y6|I1E4Y6_HUMAN	PERQ amino acid-rich with GYF domain-containing protein 2 OS=Homo sapiens GN=GIGYF2 PE=2 SV=1	28	152891
23	1	sp|Q08499-12|PDE4D_HUMAN	Isoform 12 of cAMP-specific 3~,5~-cyclic phosphodiesterase 4D OS=Homo sapiens GN=PDE4D	28	24584
24	1	tr|I3L4V6|I3L4V6_HUMAN	Nucleoredoxin (Fragment) OS=Homo sapiens GN=NXN PE=4 SV=1	23	26188
25	1	tr|K7EKA6|K7EKA6_HUMAN	Integrin alpha-IIb light chain, form 2 (Fragment) OS=Homo sapiens GN=ITGA2B PE=4 SV=1	22	3618
26	1	tr|M0QY65|M0QY65_HUMAN	Sialic acid-binding Ig-like lectin 7 (Fragment) OS=Homo sapiens GN=SIGLEC7 PE=2 SV=1	20	21455
27	1	sp|Q5VU43-2|MYOME_HUMAN	Isoform 2 of Myomegalin OS=Homo sapiens GN=PDE4DIP	20	129810
28	1	tr|C9JFK9|C9JFK9_HUMAN	BAG family molecular chaperone regulator 3 (Fragment) OS=Homo sapiens GN=BAG3 PE=2 SV=1	20	34910
29	1	tr|E7EWQ4|E7EWQ4_HUMAN	Diacylglycerol kinase iota OS=Homo sapiens GN=DGKI PE=2 SV=2	19	120201
30	1	tr|J3QR65|J3QR65_HUMAN	Myotubularin-related protein 4 OS=Homo sapiens GN=MTMR4 PE=2 SV=1	18	129440
31	1	tr|F6QF33|F6QF33_HUMAN	Killer cell immunoglobulin-like receptor 3DL1 OS=Homo sapiens GN=KIR3DL1 PE=2 SV=1	16	51000

C

			Proteins in Vpx **sample and NOT in control with a protein score over 60**		
Number	prot_fami	prot_acc	Protein Description	prot_score	prot_mass
6	1	sp|Q9Y4B6-2|VPRBP_HUMAN	Isoform 2 of Protein VPRBP OS=Homo sapiens GN=VPRBP	194	170597
7	1	sp|Q9NYU2-2|UGGG1_HUMAN	Isoform 2 of UDP-glucose:glycoprotein glucosyltransferase 1 OS=Homo sapiens GN=UGGT1	122	175437
9	1	tr|F5H335|F5H335_HUMAN	Eukaryotic translation initiation factor 3 subunit A OS=Homo sapiens GN=EIF3A PE=2 SV=1	87	162936
11	1	sp|Q8TEQ6|GEMI5_HUMAN	Gem-associated protein 5 OS=Homo sapiens GN=GEMIN5 PE=1 SV=3	68	170821
12	1	sp|P11388-2|TOP2A_HUMAN	Isoform 2 of DNA topoisomerase 2-alpha OS=Homo sapiens GN=TOP2A	64	178131
13	1	sp|Q5H9U9|DDX6L_HUMAN	Probable ATP-dependent RNA helicase DDX60-like OS=Homo sapiens GN=DDX60L PE=2 SV=2	64	199828
14	1	tr|S4R3H4|S4R3H4_HUMAN	Apoptotic chromatin condensation inducer in the nucleus OS=Homo sapiens GN=ACIN1 PE=4 SV=1	63	145755
15	1	sp|O60306|AQR_HUMAN	Intron-binding protein aquarius OS=Homo sapiens GN=AQR PE=1 SV=4	60	172270

Table 5.1 Mass Spectrometry.

Proteins identified by mass spectrometry in the control sample, (**A**), the sample containing HA-Vpx bound antigen, (**B**), and those found in the Vpx sample but not in the control sample with a protein score over 60, (**C**).

5.3.3 SIVmac251 Vpr rescues HIV-1 infection in esYDMs in a SAMHD1 dependent manner

Although a DCAF-1 independent interacting partner for Vpx protein was not identified, the notion that Vpx influences dNTP concentrations in the absence of SAMHD1 highlight the importance of high dNTP concentrations in SIV microbiology (see Section 5.3.1). Moreover, in addition to confirming the multifunctionality of accessory proteins, it shows how one requirement (dNTP modulation in this case), might be manipulated by multiple means by a given effector (Vpx). This trend has been observed elsewhere in primate lentiviral microbiology in the antagonisation of SAMHD1 by Vpx and Vpr proteins [96]. As previously described, while SAMHD1 antagonisation is typically attributed to Vpx proteins, Vpr proteins of some primate lentiviruses are functional in this regard. These Vpr proteins are encoded by SIVs that do not encode a Vpx protein such as SIVdeb, SIVmus, and SIVagm [96]. To date, no virus encoding both Vpx and Vpr has been shown to encode a Vpr protein functional in SAMHD1 antagonisation. The interaction between SAMHD1 and Vpx/Vpr proteins is highly variable in terms of species specificity. Indeed, small sequence variations within given Vpx or Vpr genes can dramatically alter species-specificity with regards to SAMHD1 antagonisation. For example, both VpxROD2 and Vpx7312a are associated with HIV-2, distinguished by very small sequence variations. Yet when tested for antagonisation of SAMHD1s from 8 primate species, VpxROD2 was effective against SAMHD1 from two species, whereas Vpx7312a was effective against all eight. Similarly, both VprGri and VprVer are associated with SIVagm and distinguished by small sequence variations. When probed in the same manner for SAMHD1 degradation ability, VprGri was effective against SAMHD1 from one species, whereas VprVer was effective against SAMHD1 from seven different species [96] (refer to Table 1.2 Species-Specific SAMHD1 Degradation by Vpr and Vpx). It has been proposed that this diversity and adaptability in SAMHD1 degradation phenotypes may result from evolutionary pressure exerted by SAMHD1 during primate lentiviral evolution, the latter evidenced in part by the toggling between the C and N terminus of SAMHD1 for binding by Vpx and Vpr proteins, as previously described [96, 136]. It is therefore plausible that Vpr proteins encoded by primate lentiviruses that also possess a Vpx protein

may also be active in SAMHD1 antagonisation outside of their natural host environment. The original identification of Vpr proteins active in SAMHD1 antagonisation resulted from the phylogenetic analysis of divergent lentiviral Vpr and Vpx genes (refer to Figure 1.6) [96]. The Vpr genes that clustered closest to Vpx genes were tested for SAMHD1 antagonisation. SIVmac Vpr genes clustered closer to HIV-1 and SIVcpz Vpr genes than to Vpx genes and thus have not been extensively probed for SAMHD1 antagonistic ability in tissue-resident macrophages [96].

In order to determine SIVmac251 Vpr (herein referred to as Vpr) effects on HIV-1 infection in esYDMs, WT, SAMHD1-KO, or SAMHD1-MUT, esYDMs were treated with Vpr-VLPs or empty VLPs, incubated for 2hrs and subsequently infected with VSV.G pseudotyped HIV-1.GIP virus (refer to 2.4.3.2 HIV-1 Infection assay (GFP) with VLPs). Surprisingly, the application of Vpr rendered WT and SAMHD1-MUT esYDMs 12-fold and 3.7-fold more permissive to VSV.G-HIV-1.GIP, respectively (Figure 5.6A). Application of Vpr rendered WT cells 10-fold more permissive to JRFL pseudotyped HIV-1.GIP virus compared to controls; however, no significant difference was observed in SAMHD1-MUT esYDMs (Figure 5.6B). In SAMHD1-KO cells, regardless of the HIV-1 env used, there was no significant difference in HIV-1 infection in the presence or absence of Vpr protein (Figure 5.6A & B).

Given that SIVmac251 Vpx protein is active in SAMHD1 degradation, it seemed unlikely that SIVmac251 Vpr would encode an identical mechanism. However, potential Vpr-mediated SAMHD1 degradation was, nevertheless, investigated. esYDMs were treated with Vpr-VLPs, incubated for 2 hrs after which cells were lysed and probed for the presence of SAMHD1 via immunoblot. In esYDMs treated with Vpr-VLPs, SAMHD1 protein was depleted compared to WT controls (Figure 5.6C & D).

These results show that in esYDMs, SIVmac Vpr is active in the rescue of HIV-1 infection by a mechanism dependent on SAMHD1.

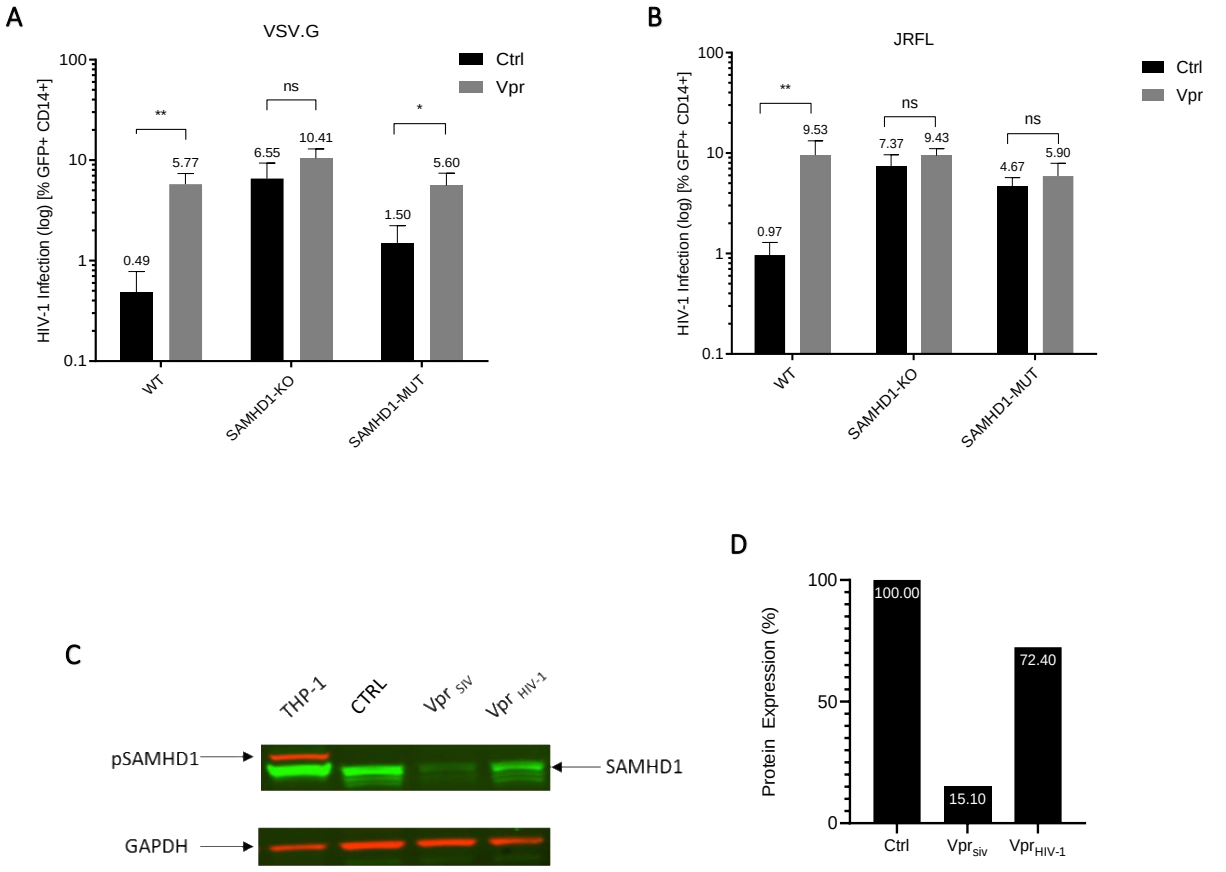


Figure 5.6 Vpr regulation of HIV-1 infection in esYDMs.

Wild type (WT), SAMHD1 knockout (SAMHD1-KO), and SAMHD1 dNTPase-defective (SAMHD1-MUT) esYDMs were treated with VLPs packaging SIVmac251 Vpr (Vpr) or an empty cassette (empty VLPs, Ctrl). After 2 hrs, cells were either infected with VSV.G pseudotyped HIV-1.GIP, or JRFL pseudotyped HIV-1.GIP virus. Cells were incubated for 3.5 days, then harvested, and CD14 stained. Frequency of HIV-1 infection was quantified by flow cytometry. In WT esYDMs, Vpr VLPs rescued HIV-1 infection significantly independent of the env used versus cells treated with empty VLPs. In SAMHD1-KO cells, there was no significant difference between cells treated with Vpr VLPs and cells treated with empty VLPs. In SAMHD1-MUT cells application of Vpr VLPs resulted in the rescue of VSV.G pseudotyped HIV-1.GIP infection but not JRFL pseudotyped HIV-1.GIP infection versus cells treated with empty VLPs. Data are presented as the mean +\- SEM and is representative of the three independent experiments (n=3). One-tailed, unpaired, parametric t-test; ns=non-significant, *p<0.05, **p<0.01, (**A**), & (**B**). The effect of Vpr on SAMHD1 expression levels in WT esYDMs was determined by immunoblot. Genetically unmodified (wild type – WT) esYDMs were treated with Vpr VLPs (Vpr_{SIV}) and incubated for 2 hrs or HIV-1 Vpr VLPs (Vpr_{HIV-1}) and incubated for 6 hrs. Cells were then lysed, and proteins separated using a polyacrylamide gel. α-SAMHD1, α-pSAMHD1 (SAMHD1 phosphorylated at T592) and α-GAPDH monoclonal antibodies were then used to probe the gel for protein expression levels (**C**), which were then quantified, (**D**) (n=1).

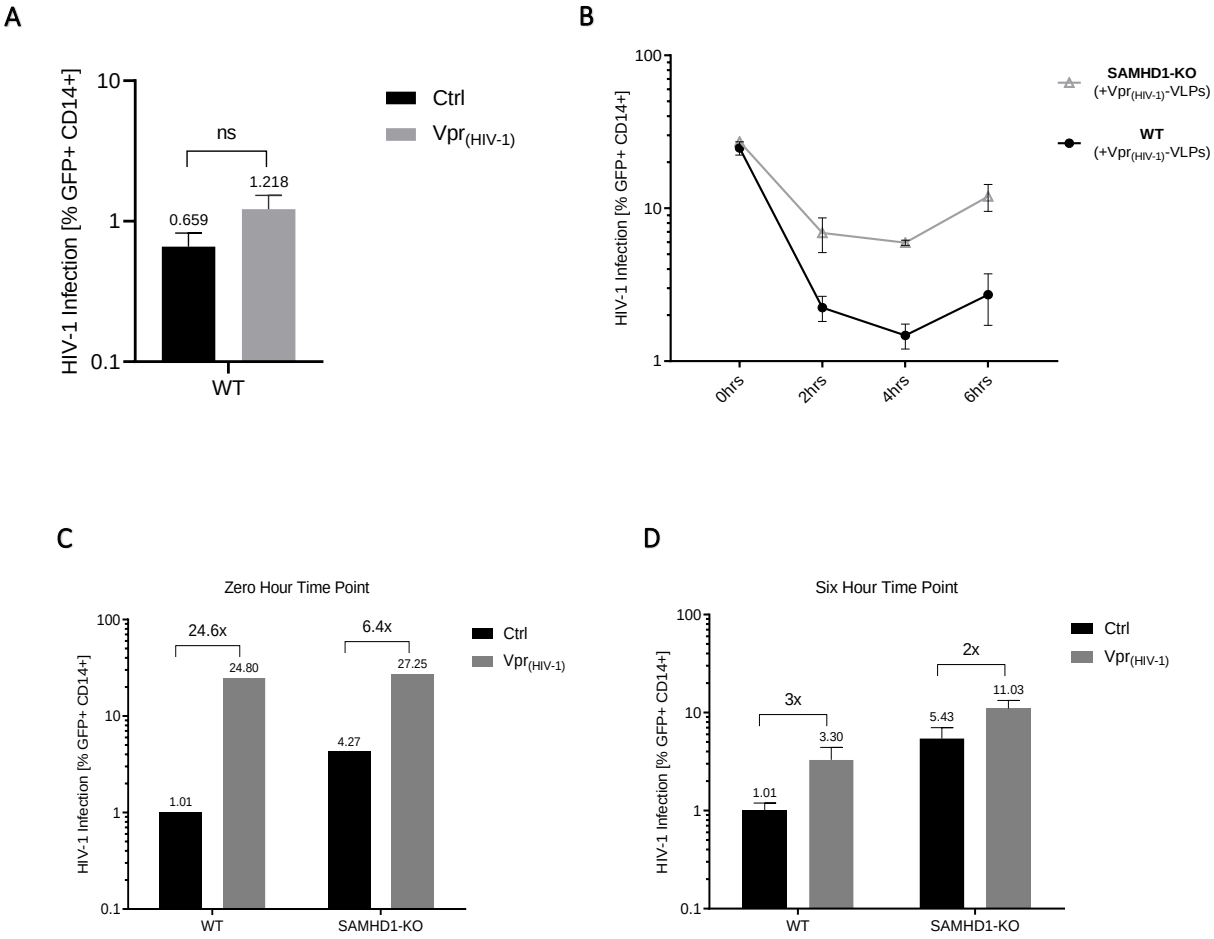


Figure 5.7 HIV-1 Vpr regulation of HIV-1 infection in esYDMs.

Wild type (WT) and SAMHD1 knockout (SAMHD1-KO) esYDMs were pre-treated with VLPs packaging HIV-1 Vpr ($Vpr_{(HIV-1)}$) or an empty cassette (empty VLPs, Ctrl). After the designated time frame, cells were infected with JRFL pseudotyped HIV-1.GIP virus and incubated for 3.5 days after which cells were lifted, CD14 stained, and infection quantified by flow cytometry. In WT cells pre-treatment with $Vpr_{(HIV-1)}$ 2-3 hrs before infection did not render cells significantly more permissive to HIV-1 infection than pre-treatment with empty VLPs (Ctrl); data are presented as the mean +/- SEM and is representative of multiple independent experiments (n=4); one-tailed, unpaired, parametric t-test; ns=non-significant, (**A**). In WT and SAMHD1-KO cells, frequency of HIV-1 infection in cells pre-treated with $Vpr_{(HIV-1)}$-VLPs 0, 2, 4, and 6 hrs prior to infection with JRFL pseudotyped HIV-1.GIP decreases sharply from the 0hr point to the 4hr point before recovering at the 6hr point, data represents the mean +/- SEM of a single experiment (n=1) in technical triplicate, **(B)**. When $Vpr_{(HIV-1)}$-VLPs were applied simultaneously with JRFL pseudotyped HIV-1.GIP (0hr time point), $Vpr_{(HIV-1)}$ rescued HIV-1 infection 24.6-fold and 6.4-fold compared to empty VLPs in wild type and SAMHD1-KO esYDMs, respectively; data represents the mean of a single experiment (n=1) in technical duplicate, (**C**). When Vpr-VLPs were applied 6hrs prior to infection with JRFL pseudotyped HIV-1.GIP (at the 6hour time point), $Vpr_{(HIV-1)}$ rescued HIV-1 infection 3.3-fold and 2-fold compared to empty VLPs in wild type and SAMHD1-KO esYDMs, respectively; data represents the mean +/- SEM of two experiments in technical triplicate, (**D**).

5.3.4 HIV-1 Vpr rescues HIV-1 infection in esYDMs

The importance of HIV-1 Vpr protein to successful infection of macrophages *in vitro* is well established [78, 93, 126], and while the mechanism underlying this effect remained elusive for some time, data from recent reports suggests, as previously described, that interaction between Vpr and the SLX4-MUS81-EME1 may be a key component of the pathway [90]. Vpr initiates both the premature activation and subsequent degradation of the SLX4-complex in a manner dependent on the binding of DCAF1. Both activities appear to support HIV-1 replication in macrophages; however, the underlying mechanism is still not entirely clear [89, 90, 107]. Despite HIV-1 Vpr binding DCAF1, HIV-1 Vpr has not been shown to directly bind and degrade SAMHD1 in macrophages. However, given the high variability in SAMHD1 motif recognition by divergent Vpr and Vpx proteins, the close phylogenetic proximity to SIVmac251 Vpr and the cell type dependence of much of SAMHD1 activty, the phenotype of potential HIV-1 Vpr rescue of HIV-1 infection in esYDM was investigated.

esYDMs were treated with HIV-1 Vpr (herein referred to as $Vpr_{(HIV-1)}$) VLPs and infected with JRFL pseudotyped HIV-1.GIP virus (refer to 2.4.3.2 HIV-1 Infection assay (GFP) with VLPs). Application of $Vpr_{(HIV-1)}$-VLPs to WT esYDMs resulted in an approximately 2-fold increase in HIV-1 infection (Figure 5.7A). $Vpr_{(HIV-1)}$-VLPs were applied according to the Vpx infection protocol, i.e., approximately 2-3 hrs prior to HIV-1 infection. Reports elsewhere suggested a temporal dynamic to HIV-1 infection in macrophages that may relate to Vpr [118]. Therefore, in order to determine whether the timing of $Vpr_{(HIV-1)}$-VLPs application influenced rescue of HIV-1 infection in esYDMs, cells were treated with $Vpr_{(HIV-1)}$-VLPs either, 0hr, 2hr, 4hr or 6hr prior to infection with JRFL pseudotyped HIV-1.GIP virus. In WT esYDMs pre-treatment with $Vpr_{(HIV-1)}$-VLPs at the 0hr, 2hr, 4hr, and 6hr resulted in HIV-1 infection frequency of 24.8%, 2.2%, 1.5% and 2.8%, respectively (Figure 5.7B). In SAMHD1-KO esYDMs, pre-treatment with $Vpr_{(HIV-1)}$-VLPs at the 0hr, 2hr, 4hr and 6hr resulted in HIV-1 infection frequency of 27.3%, 6.9%, 6.0% and 11.9% (Figure 5.7B). These data showed a clear dip in HIV-1 infection frequency with the lowest level (4hr) very close to pre-treatment timing for the previous comparison of $Vpr_{(HIV-1)}$

application in WT versus SAMHD1-KO cells (Figure 5.7A). The higher positioning of the time course curve for Vpr rescue of HIV-1 infection in SAMHD1-KO cells compared to WT cells may also be evidence of a SAMHD1 independent mechanism (Firgure 5.7b). In order to determine the $Vpr_{(HIV-1)}$-mediated HIV-1 infection fold increase at these additional time points, $Vpr_{(HIV-1)}$ or empty VLPs were applied 0hr and 6hr prior to infection with JRFL pseudotyped HIV.GIP both in wild type esYDMs and SAMHD1-KO esYDMs. At the 0hr time point, $Vpr_{(HIV-1)}$ rescued HIV-1 infection 24.6-fold and 6.4-fold compared to empty VLPs in wild type and SAMHD1-KO esYDMs, respectively (Figure 5.7C). At the 6hr time point, $Vpr_{(HIV-1)}$ rescued HIV-1 infection 3.3-fold and 2-fold compared to empty VLPs in wild type and SAMHD1-KO esYDMs, respectively (Figure 5.7D).

These results present evidence for a temporally dependent $Vpr_{(HIV-1)}$ mediated rescue of HIV-1 infection in esYDMs, which is most potent when $Vpr_{(HIV-1)}$ and HIV-1 virus are applied simultaneously.

5.3.5 The dNTPase function of SAMHD1 is dispensable for restriction of HIV-1 in esYDMs

In further complication of the controversy surrounding the existence of the SAMHD1-nuclease detailed earlier, evidence is mounting in support of an additional, dNTPase independent mechanism by which SAMHD1 restricts HIV-1 in myeloid cells (refer to Chapter 1, Section 1.1.5.4 SAMHD1). Furthermore, whilst there is also controversy surrounding the regulation of the dNTPase, there is a growing consensus that the dNTPase independent anti-HIV-1 function is regulated by phosphorylation at T592, the cell cycle, and type I IFNs (refer to Chapter 1, Section 1.1.5.4 SAMHD1). Some of the conflicts in published results regarding SAMHD1-mediated dNTPase independent HIV-1 restriction have been attributed to differences in experimental procedure, and particularly differences in cell lines used. The cell type and cell cycle specificity of SAMHD1 expression and activity are well established, and therefore, it was proposed that in order to assist in resolving conflicting data, investigations probing SAMHD1-mediated dNTPase independent HIV-1 restriction should preferably be executed in physiologically relevant cells [202].

In order to contribute data in this regard, the dynamics of SAMHD1-mediated dNTPase independent HIV-1 restriction were investigated in esYDMs. This was achieved by the use of an esYDM cell line encoding a dNTPase defective SAMHD1 mutant (SAMHD1-MUT) resulting from a deletion in the region coding for the dNTPase active site. As previously described, deletions in this region have been shown by several studies to completely abolish dNTPase activity (see Chapter 4, section 4.3.2). The deletion was confirmed by extrapolation from Sanger sequencing data (not shown), and dNTPase inactivity was confirmed by dNTP quantification and comparison to dNTP concentrations observed in SAMHD1-KO cells (Figure 4.14).

WT, SAMHD1-KO, or SAMHD1-MUT esYDMs were infected with VSV.G pseudotyped HIV-1.GIP virus (refer to 2.4.3.2 HIV-1 Infection assay (GFP)). As has been previously observed in this thesis, SAMHD1-KO macrophages were approximately 12-fold more permissive to HIV-1 infection than WT cells (Figure 5.8A). Interestingly, HIV-1 infection was also restricted in SAMHD1-MUT cells, showing a ~3-fold increase versus WT cells (Figure 5.8A).

These results show that in esYDMs, SAMHD1 exerts an antiviral effect that is mechanistically distinct from the dNTPase.

5.3.6 Env effects on HIV-1 infection in esYDMs

The use of VSV env in the construction of HIV-1 viral-like particles or vectors is a common practice in experimental microbiology [614, 615]. Pseudotyping with VSV.G presents several advantages. Firstly, VSV.G has a wide host range [614] and has been shown to be effective in infecting cells with low cell surface densities of native receptors such as macrophages. Ease of particle production (e.g., ability to use ultracentrifugation) and storage are additional motivations since VSV.G is considered highly mechanically stable, far more so than natural HIV-1 env [614]. However, the nature of the pseudotyped env dictates the mechanism of cell entry, which, depending on the aspect of HIV-1 dynamics being investigated, may influence results [616]. HIV-1 entry into macrophages is mediated by env fusion with

early endosome membranes., (refer to Section 1.1.6 HIV and SIV life cycle). In contrast, VSV.G drives cell entry via fusion with late endosomes and hence the intact viral particles traverse the intracellular environment within a vesicle for a distance before fusion occurs [616, 617]. From the perspective of Vpr and Vpx, the ability of these proteins to perform their functions appears delayed with VSV.G compared to HIV-1 env (e.g. JRFL). Similarly, the theoretical ability for SAMHD1 to access, and possibly restrict the contents of the viral particles are also delayed with VSV.G compared to HIV-1 env.

SAMHD1 localises to the nucleus [155], but a recent report has identified a small fraction that is localised to the cytoplasm in macrophages [186], the density of which varies greatly even between cells of the same cell type and polarisation state. Vpx requires SAMHD1 localised to the nucleus in order to facilitate degradation [618], which implies that the small fraction of SAMHD1 localised to the cytoplasm should be resistant to Vpx-mediated degradation. Indeed, it has been proposed that cells harbouring SAMHD1, which are resistant to Vpx mediated degradation (such as pDCs), accomplish this by translocating SAMHD1 to the cytoplasm, either as a steady-state phenomenon [580] or in relation to immunomodulatory stimulation such as IFNα [580]. Cytoplasmic SAMHD1 may explain the portion of SAMHD1 remaining after Vpx application (refer to Chapter 3, Figure 3.5E) and the differentiation temporal anomaly (refer to Chapter 3, Section 3.4 Discussion, and Chapter 4, Section 4.4 Discussion), both reported in this thesis. Moreover, the controversial dNTPase independent anti-HIV-1 mechanism of SAMHD1 may also require cytoplasmic localisation [202]. Thus, it follows that if env indirectly modulates interaction with (cytoplasmic) SAMHD1 and viral components, this may translate to systemic effects on the efficiency of HIV-1 infection.

In order to assess any impact that the use of VSV env may have on HIV-1 infection data in esYDMs, HIV-1 viral-like particles were constructed using HIV-1 env or JRFL, then used to infect esYDMs. VSV.G pseudotyped, or JRFL pseudotyped HIV-1.GIP virus was applied to esYDMs, either in the presence or absence of Vpx-VLPs or Vpr-VLPs (refer to 2.4.3.2 HIV-1 Infection assay (GFP) with VLPs). In WT esYDMs

either in the presence or absence of Vpx or Vpr, JRFL pseudotyped HIV-1.GIP virus was ~2-fold more infectious than VSV.G pseudotyped HIV-1.GIP virus (Figure 5.8B). In SAMHD1-KO esYDMs either in the presence or absence of Vpx or Vpr, there was no significant difference between the infectivity of JRFL or VSV.G pseudotyped HIV-1.GIP virus (Figure 5.8C). Curiously, in SAMHD1-MUT-G9 cells, in the absence of Vpx, JRFL pseudotyped HIV-1.GIP virus was 3-fold more infectious than VSV.G pseudotyped HIV-1.GIP virus, whereas in the presence of Vpx there was no significant difference between JRFL and VSV.G pseudotyped HIV-1.GIP viruses (Figure 5.8D).

These results show that JRFL pseudotyped HIV-1.GIP virus was more infectious than VSV.G pseudotyped HIV-1.GIP virus in SAMHD1-MUT esYDMs in a manner that may depend on SAMHD1.

5.3.7 Vpx and Vpr mediated rescue from the innate immune response in esYDMs

Observation of the effects of endogenous expression of the Vpx mutant Q76A on HIV-1 infection in esYDMs resulted in the hypothesis that VpxQ76A may restrict HIV-1 in ipsYDMs via a DCAF1 and SAMHD1 independent mechanism (refer to Chapter 3, Section 3.3.7 SAMHD1 independent functions of Vpx in esYDMs and ipsYDM). In order to test this hypothesis, WT and SAMHD1-KO esYDMs were infected with JRFL or VSV.G pseudotyped HIV-1.GIP virus particles in the presence or absence of exogenously applied VpxQ76A-VLPs. In WT cells, the application of VpxQ76A rendered cells 4.8-fold more permissive to JRFL pseudotyped HIV-1.GIP virus infection than WT cells treated with empty-VLPs (Figure 5.9A). Interestingly, VpxQ76A had no effect on HIV-1.GIP infection when pseudotyped with VSV.G (Figure 5.9B). In SAMHD1-KO cells, the application of VpxQ76A or Vpx did not significantly influence HIV-1.GIP infection versus SAMHD1-KO cells treated with empty-VLPs regardless of the env used (Figure 5.9A & B).

Data from Chapter 3 (refer to Chapter 3, Section 3.3.7 SAMHD1 independent functions of Vpx in esYDMs and ipsYDM) combined with observations elsewhere supported a SAMHD1 independent mechanism for

the rescue of HIV-1 infection attributable to VpxQ76A (and hence Vpx), which appears to have been refuted by the data presented above. Closer examination of other studies of this topic revealed that the HIV-1 restrictive phenotype of VpxQ76A most commonly manifested when infection of myeloid cells was preceded by stimulation with cytokines such as IFN-I and PMA [158, 204]. Therefore, in order to probe the effects of cytokines on potential VpxQ76A-mediated SAMHD1-independent mechanisms of HIV-1 restriction in esYDMs further, WT esYDMs and SAMDH1-KO esYDMs were pre-treated with IFNα, IFNβ, IFNγ or PMA, followed by treatment with empty-VLPs or VLPs containing Vpx, VpxQ76A, Vpr or $Vpr_{(HIV-1)}$ and subsequently infected with JRFL pseudotyped HIV-1.LUC virus (refer to Section 2.4.3.4 HIV-1 Infection assay (Luciferase) with VLPs). Interestingly, in SAMHD1-KO esYDMs, HIV-1 infection in the presence of IFNα, IFNβ, and IFNγ, but not PMA, showed a potential SAMHD1-independent HIV-1 restrictive function for Vpx (Figure 5.9C, D & E). VpxQ76A was active in the rescue of HIV-1 infection in SAMHD1-KO cells but only from the antiviral state established by IFNβ and PMA (Figure 5.9F). There was also evidence for $Vpr_{(HIV-1)}$ mediated rescue from all agents used in a SAMHD1-independent manner, as indeed there was also for SIVmac Vpr, which displayed the greatest magnitude rescue of HIV-1 infection of all accessory proteins tested (Figure 5.9C, D, E & F).

These results show that in unstimulated esYDMs, Vpx protein does not exert a SAMHD1 independent mechanism for HIV-1 restriction. However, in esYDMs stimulated with IFNα, IFNβ or IFNγ, Vpx may exert a SAMHD1 independent mechanism for HIV-1 restriction as may VpxQ76A in esYDMs stimulated with IFNβ & PMA. Furthermore, these results show that both Vpr and $Vpr_{(HIV-1)}$ may encode SAMHD1-independent mechanisms to rescue HIV-1 infection from the antiviral state or PMA stimulation in esYDMs.

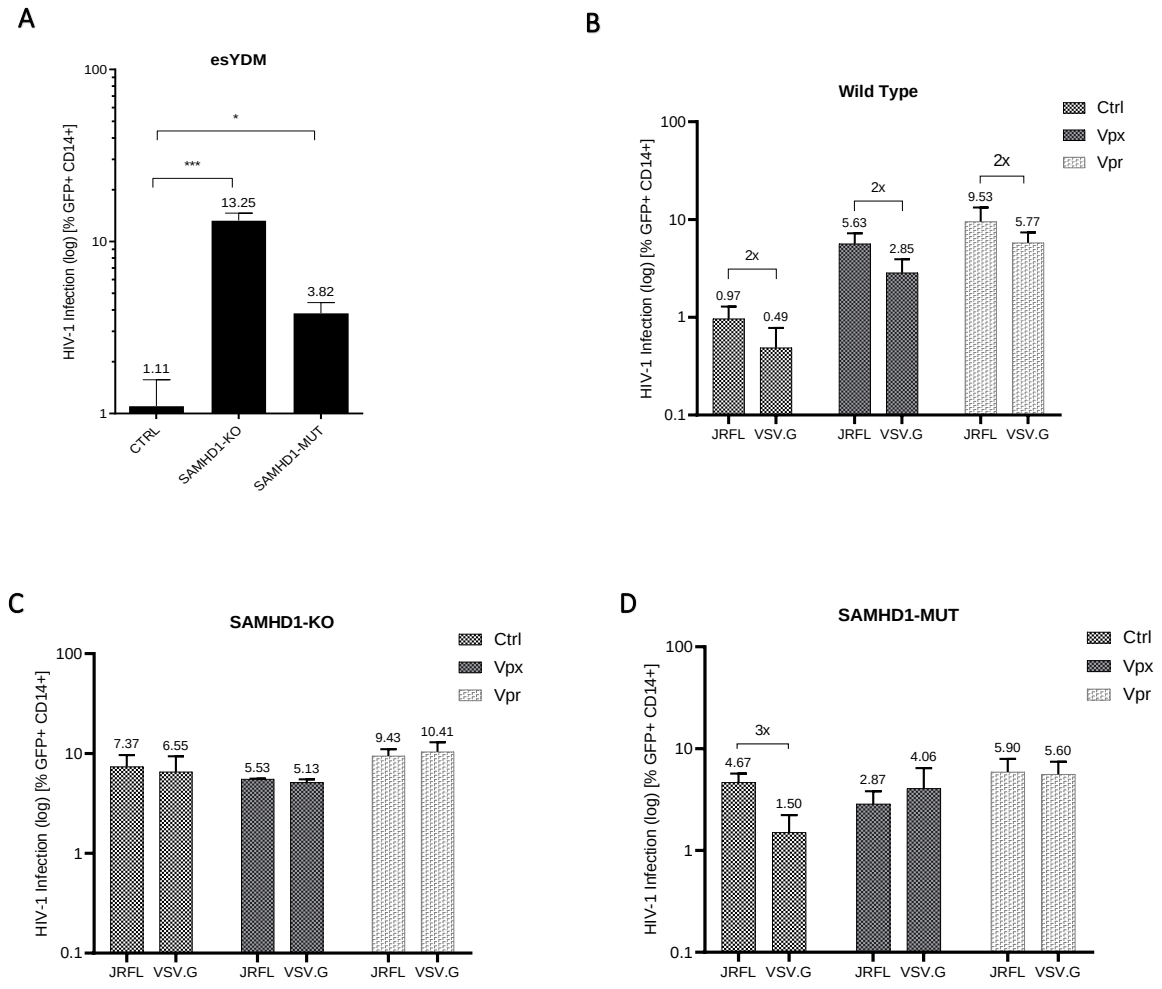


Figure 5.8 dNTPase independent mechanism for HIV-1 restriction encoded by SAMHD1 may be sensitive to env.

Wild type (WT), SAMHD1 knockout (SAMHD1-KO), and SAMHD1 dNTPase-defective (SAMHD1-MUT) esYDMs were infected with VSV.G pseudotyped HIV-1.GIP virus. Cells were incubated for 3.5 days, then harvested, and CD14 stained. Frequency of HIV-1 infection were then quantified by flow cytometry. In esYDMs dNTPase defective SAMHD1 rescued HIV-1 infection significantly (3.4x) versus esYDMs expressing fully functional SAMHD1, data are presented as the mean +\- SEM and is representative of the three independent experiments, (n=3). One-tailed, unpaired, parametric t-test; *p<0.05, ***p<0.001, (**A**). WT, SAMHD1-KO, and SAMHD1-MUT esYDMs were treated with Vpx-VLPs (Vpx), Vpr-VLPs (Vpr), or VLPs encoding an empty transgene cassette (CTRL). After 2 hrs, cells were infected with either VSV.G pseudotyped HIV-1.GIP virus, or JRFL pseudotyped HIV-1.GIP virus. Cells were incubated for 3.5 days then harvested and CD14 stained. Frequency of HIV-1 infection were then quantified by flow cytometry. In WT or SAMHD1-KO esYDMs, the magnitude of change in HIV-1 infection was consistent whether pre-treated with Vpx, Vpr, or empty VLPs regardless of the env used, (n=1); data are representative of a the mean +/- SEM of a single experiment executed in technical triplicate (**B**), & (**C**). In SAMHD1-MUT cells pre-treated with empty VLPs, HIV-1 infection was 3-fold higher when using JRFL pseudotyped virus versus VSV.G pseudotyped virus whereas in SAMHD1-MUT esYDMs pre-treated with Vpx or Vpr, no apparent difference in HIV-1 infection was observed regardless of the env used, (n=1); data are representative of a the mean +/- SEM of a single experiment executed in technical triplicate, (**D**).

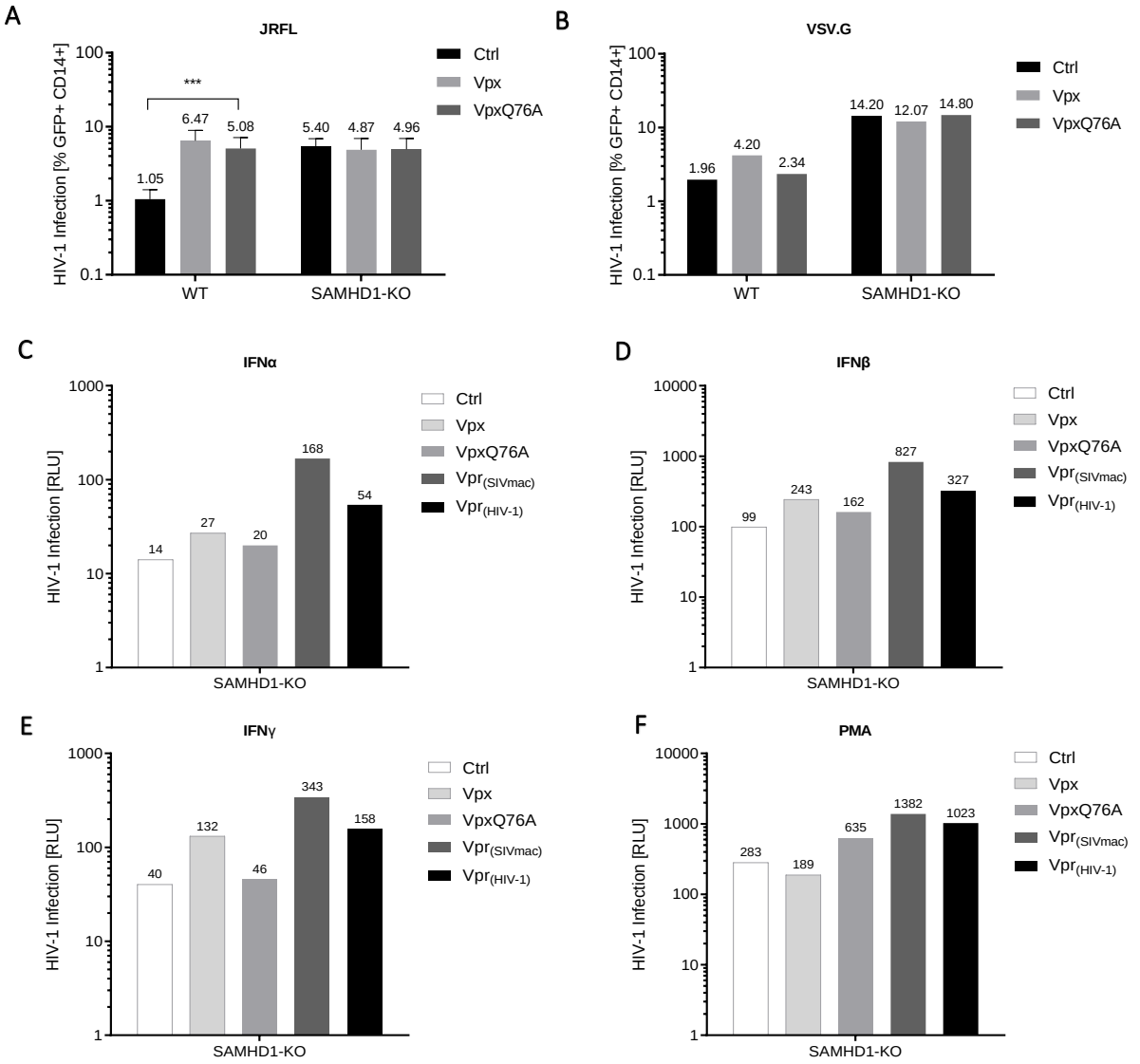


Figure 5.9 Vpx, Vpr, and Vpr$_{(HIV-1)}$ rescue HIV-1 infection from the antiviral state.

Wild type (WT) and SAMHD1 knockout (SAMHD1-KO) esYDMs were pre-treated with Vpx, VpxQ76A, or empty VLPs and subsequently infected with JRFL pseudotyped or VSV.G pseudotyped HIV-1.GIP virus. Cells were incubated for 3.5 days, then harvested, CD14 stained, and infection quantified via flow cytometry. In WT cells, VpxQ76A rescued JRFL pseudotyped HIV-1.GIP virus versus controls but showed no effect on SAMHD1-KO esYDMs, data are presented as the mean +\- SEM and are representative of three independent experiments (n=3); one-tailed, unpaired, parametric t-test; ***p<0.001, (**A**). VSV.G pseudotyped HIV-1.GIP was not rescued in either WT or SAMHD1-KO esYDMs by pre-treatment with VpxQ76A, (**B**). SAMHD1-KO cells were pre-treated with Vpx, VpxQ76A, SIVmacVpr (Vpr$_{(SIVmac)}$), HIV-1 Vpr (Vpr$_{(HIV-1)}$), or empty VLPs, then stimulated by IFNα, IFNβ, IFNγ or PMA and subsequently infected with JRFL pseudotyped HIV-1.LUC virus. VpxQ76A appeared unable to rescue SAMHD1-KO cells from the antiviral state, (**C**), & (**E**), but may function in the rescue of HIV-1 infection in SAMHD1-KO cells from the antiviral state established by IFNβ, (**D**), and stimulation by PMA, (**F**). Vpx showed evidence in support of rescue of HIV-1 infection in SAMHD1-KO cells from the antiviral state established by IFNα, IFNβ, IFNγ, (**C**), (**D**), & (**E**) but not stimulation by PMA, (**F**). Both Vpr and Vpr$_{(HIV-1)}$ showed evidence of rescue of HIV-1 infection in SAMHD1-KO cells from the antiviral state and PMA stimulation (**C**), (**D**), (**E**), & (**F**). For B, C, D, E, & F, data represent the mean of technical duplicates (n=1).

5.3.8 LPS assists HIV-1 infection in esYDMs

As previously described, while LPS is not a component of viruses, it (and therefore, by extension, bacteria) do appear to exert a positive effect on HIV-1 replication *in vivo* (refer to Section 5.1 Introduction). The effects of LPS on HIV-1 infection of es-derived tissue-resident macrophages *in vitro* have yet to be described as has the impact of Vpx, Vpr, or $Vpr_{(HIV-1)}$ in this regard. In order to investigate these questions, WT and SAMHD1-KO esYDMs were infected with JRFL or VSV.G pseudotyped HIV-1.GIP virus either in the presence or absence of Vpx, VpxQ76A, Vpr or $Vpr_{(HIV-1)}$. Interestingly, the application of LPS resulted in a modest rescue of HIV-1 infection in both WT and SAMHD1-KO cells regardless of the viral envelope glycoprotein used (Figure 5.10A). Moreover, esYDMs treated with LPS and infected with JRFL pseudotyped HIV-1 virus in the presence of Vpx, VpxQ76A Vpr, and $Vpr_{(HIV-1)}$ resulted in the modest rescue of HIV-1 infection over cells not treated with LPS, both in WT and SAMHD1-KO cells (Figure 5.10B). These data hint at a potential pro-HIV-1 replication role for LPS in esYDMs. The implication of a SAMHD1 independent function stimulated by LPS, as evidenced by HIV-1 infection profiles in SAMHD1-KO esYDMs, prompted quantification of dNTP concentrations in esYDMs stimulated with LPS. Interestingly, stimulation with LPS did not appear to affect dNTP concentrations in esYDMs (Figure 5.10C) implying that the application of LPS does not modulate SAMHD1 dNTPase activity.

These results show that bacterial components may exert a positive effect on HIV-1 replication in scYDMs.

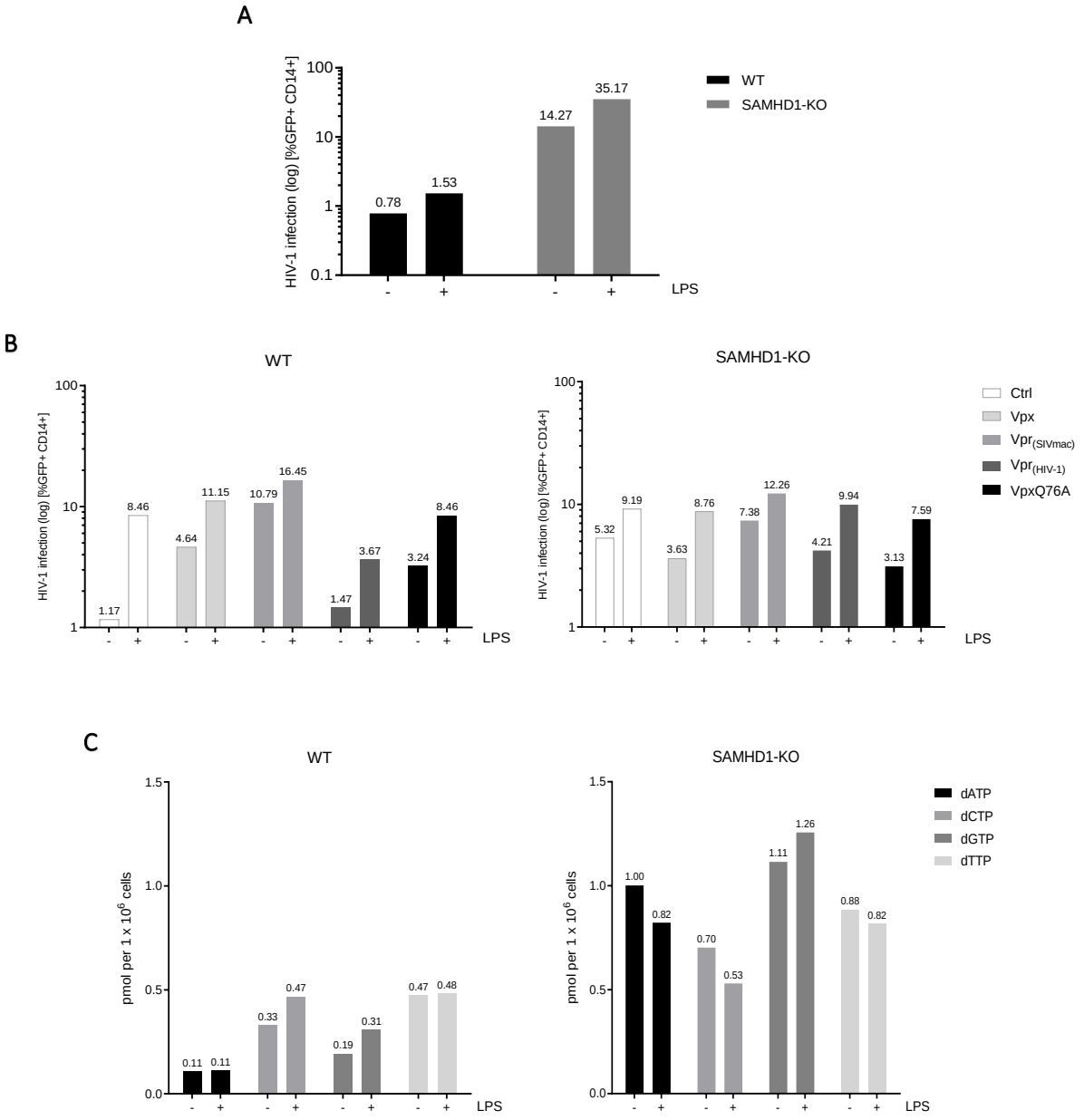


Figure 5.10 LPS regulation of HIV-1 infection in esYDMs.

Wild type (WT) and SAMHD1 knockout (SAMHD1-KO) esYDMs were pre-treated with LPS. After 2 hrs, cells were either infected with HIV-1 lentiviral vectors or harvested for dNTP quantification. For the HIV-1 infection assay VSV.G pseudotyped HIV-1.GIP virus was used. LPS pre-treatment of esYDMs showed evidence of LPS mediated HIV-1 rescue that may be SAMHD1-independent, (**A**). The mechanism underlying LPS mediated HIV-1 rescue may be independent of SAMHD1 and facilitation by Vpx and Vpr proteins, (**B**). For dNTP quantification, post LPS incubation cells were harvested and counted. dNTPs were then isolated via methanoic extraction and subsequently quantified using the dNTP assay. The application of LPS did not show evidence of altered dNTP concentrations in WT or SAMHD1-KO cells, (**C**). For all experiments, (n=1).

5.4 Discussion

Observations documented in Chapter 3 detailed the differential effects on SAMHD1 expression, HIV-1 infection, and dNTP concentrations in Vpx-expressing cells compared to SAMHD1-KD cells. This was hypothesised to be a result of the activity of residual SAMHD1 protein (RKP) or potential SAMHD1 independent effects attributable to Vpx. Investigating these differential effects was complicated by the constitutive expression of Vpx throughout the stem cell differentiation process, which may have influenced the phenotype of end-stage macrophages. Investigation of the effects of residual SAMHD1 protein was only possible by use of a SAMHD1-KO cell line, and thus the SAMHD1-KO esYDMs created and characterised in Chapter 4 were used to probe the activity of SAMHD1 RKP further.

Comparison of HIV-1 infection and dNTP concentrations in SAMHD1-KO esYDMs showed that complete depletion of SAMHD1 rescued both HIV-1 infection and dNTP concentrations to levels that surpassed those observed in WT esYDMs treated with Vpx (Figure 5.4). Whilst this increase was significant for HIV-1 infection (Figure 5.4A), it was not significant dNTP concentrations (Figure 5.4E). The lack of significance in the latter is believed to be due to experimental error incorporated from the use of aged equipment. From these data, it is possible to conclude that RKP is indeed functional in HIV-1 restriction and potentially dNTP hydrolysis in SAMHD1-KD esYDMs detailed in Chapter 3, but moreover that even the small amount of SAMHD1 protein remaining in Vpx-expressing esYDMs may be functional in this regard. The observation that knockout of SAMHD1 was more potent in the rescue of HIV-1 infection and potentially dNTP concentrations than the application of Vpx was intriguing. A possible explanation could involve SAMHD1 localisation. As previously discussed, SAMHD1 localised to the cytoplasm has been shown to be resistant to Vpx-mediated degradation [580, 618], and thus, it is possible that this fraction (that would be absent in SAMHD1-KO cells) is functional in HIV-1 restriction and dNTP hydrolysis in the presence of Vpx. This result shows the potency of SAMHD1 activity and highlights the importance of high-efficiency RNAi-mediated interference required for investigations into SAMHD1 activity. In addition, this result implied the hypothesis attributing the additional increases in HIV-1 infections and

dNTP hydrolysis in Vpx expressing esYDMs to additional functions of Vpx is likely false, and indeed the application of exogenous Vpx protein to SAMHD1-KO cells did not show any significant increases in HIV-1 infection versus SAMHD1-KO esYDMs treated with empty VLPs (Figure 5.4D). Curiously, however, the application of Vpx to SAMHD1-KO cells did result in a significant increase in dATP versus controls (Figure 5.4H). While the observation for dATP was consistently documented, reproducible increases in the other dNTPs were not observed. This may be due to the use of cell count for normalisation rather than ATP concentrations, which may have allowed error to accumulate. It is also possible that optimisation of enzyme concentrations specific to a given dNTP was required as per published protocols elsewhere [570]. The dNTPassay established in this thesis used the same enzyme and concentration for all four dNTPs. Nevertheless, the result can still be considered as evidence supporting a Vpx-mediated increase in dATP in esYDMs in a manner independent of SAMHD1.

The potential mechanism by which Vpx increases dATP in esYDMs should involve either stimulation of dNTP synthesis or degradation of an additional dNTPase. An additional dNTPase has not been identified as a Vpx interacting partner; indeed, SAMHD1 is the only dNTPase identified in the human genome. Moreover, a Vpx interacting partner functional in the synthesis of dNTPs has also not been described, but, interestingly, a mechanism involving dNTP synthesis in HIV-1 rescue, has [211]. The model involves the degradation of p21, which resulted in increased dNTP concentration and HIV-1 rescue. p21 is a regulator of the cell cycle that suppresses the expression of proteins involved in dNTP synthesis such as RNR. Thus, the hypothesis was formulated that Vpx targets p21 for degradation resulting in increased dNTP concentrations. Probing for p21 in esYDMs and esYDMPs via immunoblot did not show any significant difference in expression between WT and Vpx expressing cells, arguing against Vpx degradation of p21 in esYDMs. However, two unknown proteins, ~p15 and ~p200 did show a depletion profile that implied degradation by Vpx. Immunoprecipitation in THP-1 monocytes identified the ~p200 protein as VprBP. This protein, also known as DCAF1, is a subunit of the CLR4 E3 ubiquitin ligase complex and a well-established Vpx interacting partner. Whilst this protein may be involved in the degradation

of the target protein it was not the co-factor being searched for. It is possible that the unknown interacting partner was in the p15 region; however, this band was not of sufficient definition to enable analysis by mass spectrometry. Alternatively, the inability to identify a novel interacting partner may have been due to the use of THP-1 monocytes. THP-1 cells were used due to the high number of cells required for immunoprecipitations. The phenotype of Vpx-mediated increases in dATP in SAMHD1-KO cells was identified in esYDMs and not in THP-1 monocytes, and thus, it's possible that this interacting partner is unique to esYDMs.

Results from Chapter 3 showed that SAMHD1 expression and phosphorylation at T592, hydrolysis of dNTPs, and restriction of HIV-1 in esYDMs are like that seen in blood MDMs. However, the potency of the dNTPase and any unidentified dNTPase-independent antiviral activity of SAMHD1 in HIV-1 restriction in esYDMs remained uninvestigated. The CRISPR- Cas9-mediated creation of a cell line encoding a mutant SAMHD1 devoid of dNTPase activity (SAMHD1-MUT) allowed this phenotype to be probed. Western blot of SAMHD1 in SAMHD1-MUT esYDMs revealed that SAMHD1 expression level was very low, nevertheless SAMHD1-MUT esYDMs restricted HIV-1, and only 3.4-fold less efficiently than WT SAMHD1. HIV-1 infection of SAMHD1-KO esYDMs was 12-fold more effective compared to WT esYDMs, which when compared to the fold change in SAMHD1-MUT esYDMs (3.4-fold), and considered in relation to SAMHD1-MUT expression level implies that the antiviral activity manifest in esYDMs is extremely potent. Abolition of the dNTPase activity was confirmed by Sanger sequencing and quantification of all four dNTPs, which were similar to those observed in two other SAMHD1-KO esYDM cell lines. Therefore, it is possible to conclude that the SAMHD1 HIV-1 restrictive function observed in SAMHD1-MUT esYDMs is dNTPase independent. The difference in expression levels of SAMHD1 in WT versus SAMHD1-MUT esYDMs is noteworthy, but since the cell line with the highest expression of SAMHD1 (WT) is at the bottom of the HIV-1 restriction gradient (as observed in WT vs. SAMHD1-KO vs. SAMHD1-MUT cells), the result (3.4-fold HIV-1 restriction in SAMHD1-MUT vs. WT esYDMs) would not be artificially magnified by the lower expression levels of SAMHD1 in SAMHD1-MUT cells. In other

words, because active SAMHD1 expression is positively correlated with HIV-1 restriction, the low expression levels of SAMHD1 in SAMHD1-MUT cells cannot result in artificial inflation if HIV-1 restriction. Finally, with regards to the effects of residual SAMHD1 protein (RKP) discussed previously, the potency of the SAMHD1-MUT antiviral activity in relation to the protein expression levels further confirms the conclusions drawn above.

Although there is controversy surrounding the fundamental mechanism underlying the SAMHD1 dNTPase-independent HIV-1 restrictive activity, there is some consensus supporting the cytoplasm as the location where it might occur [202]. The pseudotyped glycoprotein used for much of this, and other studies, VSV.G, mediates cell entry via endocytosis and fusion in late endosomes rather than fusion in early endosomes as mediated by HIV-1 env, and it is unknown whether the different consequent subcellular cytoplasmic pathways would affect SAMHD1 antiviral activity in esYDMs [247, 248] (refer to Section 1.1.6 HIV and SIV lifecycle). WT, SAMHD1-KO, and SAMHD1-MUT cells were infected with JRFL or VSV.G pseudotyped HIV-1 GFP encoding virus in the presence or absence of Vpx or Vpr. In WT cells, the fold change between JRFL and VSV.G enveloped virus was consistent at ~2-fold, whether in the presence of Vpx, Vpr or empty VLPs. In SAMHD1-KO cells, the fold change between JRFL and VSV.G enveloped HIV-1 viruses was also consistent, with no substantial difference observed. In SAMHD1-MUT cells, however, a 3-fold change was observed in empty VLP treated cells, whereas there was no substantial change in Vpx or Vpr VLP treated cells. The observation of fold changes between JRFL and VSV.G in SAMHD1 expressing cells (WT and SAMHD1-MUT) but not in SAMHD1 depleted cells (SAMHD1-KO, SAMHD1-MUT+Vpr, SAMHD1-MUT+Vpx) implies that there may be determining factors of env that mediate HIV-1 restriction that is dependent on SAMHD1. However, the fact that pseudotyping HIV-1 with JRFL env renders the virus more permissive than pseudotyping with VSV.G is counterintuitive to the model suggesting VSV.G may subvert SAMHD1 restriction, perhaps due to intravesicular cytoplasmic transit. These data suggest that fusion at the plasma membrane or in early endosomes is advantageous to HIV-1 infection in a SAMHD1 dependent manner. Perhaps the early distribution of Vpx and Vpr are

the determining factors as with VSV.G nether would be active until intracellular transit and vesicle fusion is complete. Alternatively, these results may indicate antagonisation by IFITMs which has been shown to collect in late endosomes restricting certain strains of HIV-1 (as well as IAV). However, it is not clear how SAMHD1 might facilitate HIV-1 infection in this scenario [246].

In addition to Vpx, the interacting protein identified in the pulldown, DCAF1, has also been shown, as previously discussed, to interact with Vpr proteins (refer to Chapter 1, Section 1.1.4.2 Vpr). Whilst with Vpx, SAMHD1-independent functions attributed to DCAF1 interaction have yet to be defined, for Vpr proteins interaction with DCAF1 has been linked to cell cycle arrest in addition to SAMHD1 antagonisation, in a species-specific manner [91, 98, 104, 151, 152]. Curiously, while many different Vpr proteins have been probed in this regard, the phenotype of SIVmac251 Vpr remained to be described, as indeed had the HIV-1 restrictive phenotype of SIVmac251 Vpr in esYDMs or macrophages in general. Exogenous application of Vpr via VLPs to WT esYDMs resulted in a 12-fold rescue of HIV-1 infection and showed that SIVmac251 Vpr is active in enhancing viral replication in a manner independent of Vpr-mediated G2 arrest (due to the non-dividing phenotype of macrophages). In SAMHD1-KO cells, however, there was no significant difference in HIV-1 infection either in the presence or absence of Vpr [Figure 5.6 A&B]. This strongly implied that the Vpr mediated rescue of HIV-1 infection in esYDMs was dependent on SAMHD1. The SIVmac251 Vpr mediated mechanism for SAMHD1 antagonisation was hypothesised to be independent of SAMHD1-degradation due to SIVmac251 encoding Vpx protein, which functions in this manner. However, surprisingly, immunoblot for SAMHD1 in esYDMs pretreated with Vpr revealed significantly depleted SAMHD1 levels versus controls. This showed that in esYDMs, at least, SIVmac251 Vpr mediates the degradation of SAMHD1.

Interestingly, this result is in conflict with data produced elsewhere, which indicated that SIVmac239 Vpr protein is not active in the degradation and antagonisation of human SAMHD1 [96]. The conflict may be due to experimental differences since these experiments (immunoblot) were performed by co-

transfection of epitope-tagged SAMHD1 protein with SIVmac239 Vpr in HEK293T cells, whereas in this thesis experiments were performed by exogenous application of SIVmac251 Vpr-VLPs to macrophages. As previously described, SIVmac Vpx degradation of human SAMHD1 is intimately tied to cell type, and therefore, SIVmac Vpr may be similarly sensitive. Thus, a combination of differences in SIVmac Vpr strain (239 versus 251), cell type (HEK293T versus macrophages), SAMHD1 expression mechanism (transfection versus endogenous expression), and Vpr expression mechanism (transfection versus exogenous application via VLPs) may have resulted in the conflicting data observed.

Diverse Vpr proteins interaction with DCAF1 is well documented as previously described; however, whether SIVmac Vpr mediates SAMHD1 degradation via recruitment to DCAF1, remains unknown. As previously mentioned, SAMHD1 expression and phosphorylation status can be regulated by proteins intrinsic to cell cycle control. G2 cell cycle arrest is a Vpr function highly conserved across primate lentiviruses [106], and while not pertinent in macrophages, may contribute, in part, to a cell-cycle-governed pathway that results in SAMHD1 degradation. Immunoblot of SAMHD1 in WT esYDMs treated with Vpr-VLPs showed that Vpr did not regulate phosphorylation at T592, which remained unchanged in these cells. This potentially argues against cell-cycle-governed regulation by Vpr since phosphorylation at T592 is regulated by cyclin-dependent kinases. An alternative and perhaps more simple explanation is that whilst SIVmac251 Vpr does not recognize or antagonise SAMHD1 in its natural host, the sequence divergence inherent in human SAMHD1 allows recognition by SIVmac251 Vpr and hence, antagonisation. As previously discussed, two main models exist detailing the origin of Vpx protein, one suggests Vpx protein was lost by an ancestral primate lentivirus, and the second suggests that Vpx protein arose from the duplication (or the acquisition) of a Vpr protein that had evolved to antagonise SAMHD1 in a select few SIVs [96]. These data clearly show antagonisation of human SAMHD1 by SIVmac251 Vpr, a function SIVmac251 Vpr does not possess in its natural host and hence may be a novel instance of a primate lentivirus encoding SAMHD1 antagonisation by both Vpr and Vpx. Since the transfer of defective SAMHD1 antagonisation from an active Vpx to Vpr, or acquisition of a

new Vpx/Vpr protein active in SAMHD1 antagonisation while encoding a Vpr already active in SAMHD1 antagonisation, is unlikely, the ability of SIVmac251 Vpr to degrade human SAMHD1 is possibly the remnant of a previously (ancestral) encoded function. Hence, these data support the model where in SIVmac (or rather the naturally occurring ancestor, SIVsm), Vpx arose via transfer (duplication) of SAMHD1 antagonisation from an ancestral resident Vpr protein.

Current thinking supports the neofunctionalization of SAMHD1 antagonisation by Vpr after the divergence of HIV-1 Vpr from an ancestral SIV, a notion based partly on the observation that neither HIV-1 Vpr nor SIVmac239 Vpr was active in SAMHD1 antagonisation [96]. However, the data presented here showing that SIVmac251 Vpr is active in depletion of human SAMHD1 raised the possibility that SAMHD1 antagonisation may have arisen in an earlier ancestral primate lentivirus than originally suggested and, moreover, that HIV-1 Vpr may be active in SAMHD1 antagonisation in esYDMs. As previously described, the importance of HIV-1 Vpr to successful infection in macrophages *in vitro* is well established, however, while the inability of HIV-1 Vpr to antagonise SAMHD1 has also been widely described, data has emerged supporting a role for HIV-1 in SAMHD1 antagonisation indirectly via manipulation of cyclin L2 [118]. In WT esYDMs, pretreatment with HIV-1 Vpr VLPs 2-3 hrs before viral challenge resulted in a modest (~2-fold) but not significant increase in HIV-1 infection, and therefore it is not possible to conclude that HIV-1 Vpr rescues HIV-1 infection in esYDMs. The magnitude and therefore significance of Vpr-mediated rescue of HIV-1 infection, however, may depend on how long before HIV-1 infection that Vpr is applied. In both WT and SAMHD1-KO cells, the greatest increase was observed on the simultaneous application of Vpr and infection with HIV-1. Interestingly, this is also the most physiologically relevant process since in natural infection, Vpr would inhabit the same endosome as the viral core by virtue of being packaged in the same particle or be deposited into the cytoplasm immediately upon completion of particle fusion with the host cell. The substantial reduction in activity at the 2hr and 4hr time points could imply that Vpr protein is no longer localised such that it can perform the function that rescues infectivity at the 0hr time point. The identity of this process or activity remains

unknown, however a potential clue may be found in the modest rebound in Vpr-mediated rescue of HIV-1 infection at the 6hr time point following an initial inhibition at the 2hr time point which has been observed elsewhere in relation to HIV indirect antagonisation of SAMHD1 via cyclin L2 [118]. Since this temporal phenotype was also observed in SAMHD1-KO cells, the phenomenon can be considered, at least in part, independent of SAMHD1. The reduction in fold change from 6.4-fold at 0hrs to 2-fold at 6hrs of SAMHD1-KO cells treated with Vpr versus SAMHD1-KO cells treated with empty VLPs is further evidence of a SAMHD1-independent factor and shows a reduction in the activity of this factor, over time. The data appears to support HIV-1 Vpr rescue of HIV-1 infection in esYDMs independent of SAMHD1, which would be in line with reports elsewhere for Vpr functionality in blood MDMs. However, further HIV-1 infection experimental repeats are required before the significance of this observation can be confirmed.

Several lines of evidence were presented in Chapter 3 for HIV-1 restrictive functions encoded by Vpx protein in addition to the DCAF1 mediated degradation of SAMHD1. In esYDMPs and PMA-treated THP-1 cells, this was evidenced by the rescue of HIV-1 infection by VpxQ76A and in esYDMs by the rescue of HIV-1 infection by co-expression of shSAM (SAMHD1-KD cells) and VpxQ76A. Mutating the alanine to glutamine at amino acid position 76 renders VpxQ76A unable to bind DCAF1 and hence initiate DCAF1 mediated SAMHD1 degradation (refer to Chapter 1, Section 1.1.4.3 Vpx). In this chapter, the exogenous application of VpxQ76A did not rescue HIV-1 infection of VSV.G pseudotyped HIV-1.GIP virus, in agreement with results from the endogenous expression of VpxQ76A detailed in Chapter 3 [refer to Chapter 3, Section 3.3.7 SAMHD1 independent functions of Vpx in esYDMs and ipsYDM). Interestingly, exogenous application of VpxQ76A did rescue HIV-1 infection with JRFL pseudotyped virus, however [Figure 5.9A]. Unfortunately, due to the lack of experimental repeats for exogenous application of VpxQ76A in addition to infection with VSV.G pseudotyped HIV-1 virus, it is not possible to draw conclusions relating to env nor expression mechanism (exogenous vs. endogenous) of VpxQ76A. However, from the significant increases in JRFL HIV-1 infection observed in WT esYDMs combined with

the lack of significant increases in JRFL HIV-1 infection observed in SAMHD1-KO esYDMs it is possible to conclude that in esYDMs VpxQ76A can rescue HIV-1 infection in a manner dependent on SAMHD1 but independent of direct binding of VpxQ76A to DCAF1. Interestingly, this phenotype has also been proposed for VpxQ76A rescue of HIV-1 infection from an LPS induced antiviral state in MDDCs [590]. Such a mechanism may involve indirect activation of SAMHD1 degradation such as is suggested to be mediated by cyclin L2 [118] and p21 proteins [208, 210, 211]. Alternatively, VpxQ76A may inhibit SAMHD1 function via direct binding and destabilisation of the oligomerised catalytically active state, as has been proposed elsewhere [195]. The potential SAMHD1 independent mechanism proposed in Chapter 3 as a result of HIV-1 infection studies in esYDMs expressing both VpxQ76A and shSAM can, therefore, be considered false, and while effects of env and expression mode of VpxQ76A should be considered, the effect observed was likely a result of VpxQ76A antagonisation of SAMHD1 RKP remaining in SAMHD1-KD cells.

Application of VpxQ76A rescued HIV-1 infection of PMA treated esYDMs and adds data for this phenomenon to that existing for esYDMPs, and PMA treated THP-1 cells reported in Chapter 3 (refer to Chapter 3, Section 3.3.7 and Section 3.4). Curiously, the application of VpxQ76A to PMA treated SAMHD1-KO esYDMs resulted in an increase in JRFL HIV-1 infection versus controls [Figure 5.9F]. This may be an indication that in PMA treated esYDMs, Vpx rescues HIV-1 infection by a mechanism that is independent of both DCAF1 and SAMHD1. VpxQ76A rescue was not observed for SAMHD1-KO cells treated with IFNα, IFNβ, or IFNγ arguing against a DCAF1 *and* SAMHD1 independent mechanism for HIV-1 restriction in esYDMs stimulated by these cytokines (Figure 5.9C, D & E). Of note, Vpx protein was active in rescue of HIV-1 restriction in SAMHD1-KO cells treated with of IFNα, IFNβ or IFNγ versus controls and shows that Vpx may indeed be active in the rescue of HIV-1 from the antiviral state, as has been reported elsewhere [576, 590], but moreover that this rescue is dependent on binding to DCAF1 (Figure 5.9C, D & E). The mechanism underlying Vpx rescue from the antiviral state is unknown but may involve additional IFN-stimulated restriction factors antagonizable by Vpx. Finally, both SIVmac Vpr and

HIV-1 Vpr protein displayed rescue of HIV-1 infection in esYDMs from IFNα, IFNβ, or IFNγ induced antiviral state or stimulation with PMA via mechanisms that may be both dependent and independent of SAMHD1 (Figure 5.9A, B, C & D). Several reports have implicated Vpr in the regulation of the IFN response, an activity that may well be manifest in the data presented in this thesis. It is not possible, however, to draw further conclusions from HIV-1 infection experiments in the presence of Vpr proteins, IFNα, IFNβ, IFNγ, or PMA due to the lack of experimental repeats.

In contrast to reports regarding the effects of LPS in MDMs and MDDCs (refer to Section 5.1 Introduction), stimulation of esYDMs with LPS appeared to render these cells more permissive to HIV-1 infection than controls (Figure 5.10A & B). This was observed in both WT and SAMHD1-KO cells. These data may support a model in which bacterial components enhance HIV-1 replication in tissue-resident macrophages. Additionally, in esYDMs, the LPS mediated mechanism may be independent of SAMHD1 since no change in dNTPs was observed (Figure 5.10C); as well as independent of regulation by Vpx, SIVmac Vpr or HIV-1 Vpr (Figure 5.10B). As previously described, *in vivo*, even during AIDS, whilst virus production is primarily associated with macrophages, viral production appears to be at a relatively low level. When high titre virus-producing tissue-resident macrophages are isolated, they have been shown to be associated with opportunistic pathogens such as *Mycobacterium avium* complex and *Pneumocystis carinii* [399]. This could imply that bacterial components (such as LPS) may enhance viral replication in macrophages, which, if confirmed, may have important implications for HIV-1 pathogenesis and disease progression *in vivo*.

In summary, the small amount of SAMHD1 protein remaining after shRNA knockdown (RKP) or indeed Vpx degradation is not only active in HIV-1 restriction and dNTP hydrolysis but potent enough such that effects were quantifiable. Hence the hypothesis attributing the different efficiencies of HIV-1 restriction and dNTP hydrolysis in SAMHD1-KD esYDMs compared to Vpx expressing esYDMs to RKP was accepted as true. Consequently, the hypothesis attributing different efficiencies of HIV-1 restriction and dNTP

hydrolysis in SAMHD1-KD esYDMs compared to Vpx expressing esYDMs to additional functions encoded by Vpx was rejected as false. An increase in dNTPs in SAMHD1-KO esYDMs on the application of Vpx VLPs, however, provided evidence for an additional (SAMHD1 independent) mechanism by which Vpx increased dATP concentrations in esYDMs. However, an immunoprecipitation probe using HA-Vpx in THP-1 monocytes did not identify an effector.

Evidence was presented showing SIVmac251 Vpr functions in SAMHD1 degradation and hence, antagonisation in esYDMs. Similar experiments probing SAMHD1 dependent HIV-1 Vpr functions in esYDMs, however, did not identify any $Vpr_{(HIV-1)}$ attributable activities but did supply evidence for a potentially SAMHD1-independent pro-HIV-1 infection role for $Vpr_{(HIV-1)}$ in esYDMs.

The use of a dNTPase defective SAMHD1 mutant esYDM cell line identified dNTPase-independent HIV-1 restriction in esYDMs, adding data in support of this controversial function. And evidence of potential indirect modulatory effects on HIV-1 infection dependent on type of pseudotyped env was discussed.

Finally, evidence was presented implicating Vpx activity in the rescue of HIV-1 infection from the antiviral state established by type I and type II IFNs, and to a lesser extent, by LPS. Furthermore, SIVmac251 Vpr and HIV-1 Vpr accessory proteins were implicated in the rescue of HIV-1 infection from the antiviral state in esYDMs.

Chapter 6

Chapter 6: Discussion

6.1 Summary of Results

In this thesis, I set out to investigate the biology of the HIV-1 restriction factor SAMHD1 in human stem cell-derived macrophages. These macrophages had recently been shown to differentiate along a pathway that *in vivo* is indicative of a yolk sac lineage and hence, tissue-resident macrophages (refer to Chapter 1, Section 1.3.4 Ontogenesis). SAMHD1 expression and behaviour in macrophages have been shown to vary, dependent on several factors including lineage and stimulation from the microenvironment (polarisation) (refer to Chapter 1, Section 1.3.5 Differentiation). Thus, it followed that the biology of SAMHD1 in stem cell (yolk sac derived) macrophages might be unique to that already established using primary blood (bone marrow-derived) macrophages.

A loss-of-function experimental strategy in stem cell-derived macrophages was established in order to investigate SAMHD1 behaviour. This involved using shRNA interference and the SIVmac accessory protein Vpx to knockdown SAMHD1 and degrade SAMHD1 in target cells, respectively. The stem cell differentiation protocol allowed the use of lentivectors for stable transduction and hence, the expression of shRNA or transgenes, which could be executed with little immunological resistance at the stem cell stage. Hence, the iPS cell line NHDF-1 and the es cell line, HUES-2, were transduced with lentivectors encoding transgenes Vpx, VpxQ76A (Vpx control - a mutant unable to bind DCAF1 and hence initiate DCAF1-mediated degradation of SAMHD1), IRP (a transgene control), shSAM (shRNA targeting SAMHD1), and shCTRL (an shRNA control). An iPS cell line was used in addition to the es cell line in order to investigate what effects, if any, the reprogramming procedure to induce pluripotency may have on end-stage macrophage biology with regards to SAMHD1, and HIV-1 infection in general.

All stem cell lines were successfully differentiated to macrophages showing that lentiviral transduction and continual selection (via puromycin) did not inhibit differentiation. The differentiation protocol was

well established in the laboratory, and consequently, the macrophages produced had been extensively characterised in both published reports and a doctoral thesis [377, 569]. Hence, at this stage, macrophages and precursors were identified by morphology. IRP and VpxQ76A expressing factories produced the monocyte-like macrophage precursor cells (esYDMPs) after approximately 2 weeks. Vpx expressing factories produced esYDMPs after approximately 3 weeks, whereas SAMHD1-KD and shCTRL expressing factories produced esYDMPs after approximately 5 weeks. This esYDMPs production temporal anomaly was observed with both iPS and es cell lines, and it raised the question of whether the delay in production observed in SAMHD1-KD cells was a consequence of SAMHD1 depletion or whether it was a defect inherent in the RNA interference system being used. Moreover, if SAMHD1 depletion was responsible, then it implied that knockdown of SAMHD1 was detrimental to the differentiation process, but that depletion of SAMHD1 by Vpx was less detrimental to the differentiation process. This appeared contradictory as Vpx was more potent in SAMHD1 depletion than RNA interference and therefore presented the possibility of alternative functions encoded by Vpx that may accelerate differentiation.

SAMHD1 is a deoxynucleotide triphosphate hydrolase, an activity which is believed to be central to both retroviral restriction and homeostasis (refer to Chapter 1, Section 1.1.5.4 SAMHD1). Hence the ability to quantify dNTPs in cells used in SAMHD1 investigations was considered of high importance. Since an assay to determine intracellular dNTP concentrations was lacking in the department, I established and optimised an assay to do the same. The “dNTPassay” established used enzymatic incorporation of tritiated thymidine or tritiated adenosine into oligo pairs of known sequence. Incorporation of the tritiated dNTP and the dNTP being measured was proportional, and so quantification of the radioisotope emitted by the tritiated dNTP could be used to quantify the dNTP in question. The assay was considered functional after quantification for dNTPs in several cell types was shown to be like those detailed in published reports.

In esYDMs SAMHD1 expression levels, phosphorylation at T592 and hydrolysis of dNTPs were all like those observed in the monocytic cell line THP-1 and also similar to published data for blood MDMs. These data also showed that neither the yolk sac lineage nor the *in vitro* differentiation significantly altered these parameters from those observed in THP-1 cells and published reports for blood MDMs.

In the steady-state, both esYDMs and ipsYDMs were restrictive to HIV-1 infection with a potency that was similar to that detailed in published reports for blood MDMs and peripheral tissue-resident macrophages. Expression of Vpx or shSAM resulted in depleted SAMHD1 protein levels, increased dNTP concentrations, and rescue of HIV-1 infection in esYDMs and ipsYDMs. This showed that SAMHD1 was active in HIV-1 restriction in stem cell-derived macrophages but also that the phenotype upon expression of Vpx or shRNA targeting SAMHD1 is like that reported in blood MDMs. SAMHD1 depletion, rebound in dNTP concentrations, and rescue of HIV-1 infection were all more potent when facilitated by Vpx compared to shRNA knockdown of SAMHD1 in both esYDM and ipsYDMs. Two hypotheses were formed to explain this observation: i) shRNA is less efficient at SAMHD1 depletion than Vpx, and the larger portion of SAMHD1 protein present in SAMHD1-KD cells versus Vpx expressing cells allows for greater hydrolysis of dNTPs and HIV-1 restriction. This portion of SAMHD1 protein remaining after shRNA-mediated knockdown was referred to as residual knockdown protein (RKP); ii) Vpx encodes an additional mechanism to increase dNTPs and rescue HIV-1 infection that is independent of SAMHD1 protein levels. These hypotheses were tested using the SAMHD1 knockout cells detailed below.

Comparison of HIV-1 infection frequency in all esYDM and ipsYDM cell lines showed no significant differences between iPS and es-derived cell lines. This appeared to be evidence for the absence of donor-derived differences often observed with HIV-1 infection kinetics in blood MDMs.

The control construct for Vpx, VpxQ76A, was chosen because the mutation at reside 76 had been widely reported to abolish binding to DCAF1, and hence degradation of SAMHD1. However, in esYDMs expressing VpxQ76A, SAMHD1 protein levels were depleted, although no concomitant rebound of dNTP

concentrations or rescue of HIV-1 infection was observed. Interestingly, VpxQ76A rescue of HIV-1 infection was observed in ipsYDMs when co-expressed with shSAM; moreover, HIV-1 rescue was to levels greater than that observed in SAMHD1-KD cells alone. This result could imply a weak HIV-1 rescue phenotype for VpxQ76A in this cell type. Reports elsewhere had documented HIV-1 rescue by VpxQ76A in a manner that appeared to depend on cell type and activation, hence the phenotype of VpxQ76A was investigated in PMA treated THP-1 cells and esYDMPs (macrophage precursors). Surprisingly, VpxQ76A rescued HIV-1 infection in both PMA treated THP-1 cells and esYDMPs, but moreover, the rescue of HIV-1 infection in PMA treated THP-1 cells was more potent than that observed with Vpx. This provided more evidence for the cell type dependence of this phenomenon as previously discussed; however, SAMHD1 protein levels were not determined in either cell type nor dNTP concentrations in esYDMPs, thus limiting the scope of further conclusions drawn from these observations. The combination of observations of VpxQ76A phenotype in esYDMs, ipsYDMs, esYDMPs, and PMA treated THP-1 cells, however, did appear to imply a DCAF1 independent mechanism and therefore potentially a SAMHD1 independent mechanism by which VpxQ76A rescues HIV-1 infection.

The temporal anomaly associated with Vpx expressing factories, the difference in potency of SAMHD1 depletion, dNTP hydrolysis and HIV-1 restriction in Vpx expressing cells versus SAMHD1-KO cells, and finally the restrictive cell type-dependent phenotype of VpxQ76A, taken together appeared to implicate additional, potentially SAMHD1-independent, functions encoded by Vpx. Hence a SAMHD1 knockout cell line was created. Differentiating macrophages from SAMHD1 knockout stem cells negated any influence that unknown effects of Vpx or shRNA would have had on end-stage macrophages differentiated from Vpx or shRNA expressing stem cells. SAMHD1-KO cells would also enable definitive testing of the two hypotheses detailed above relating to the differences in potency of SAMHD1 depletion, dNTP hydrolysis, and HIV-1 restriction in Vpx expressing cells versus SAMHD1-KO cells. Finally, SAMHD1-KO cells would also enable identification of any Vpx (and hence VpxQ76A) functions that were truly independent of SAMHD1.

The CRISPR- Cas9 gene-editing system was used to create SAMHD1 knockout stem cells. In addition, a SAMHD1-KO stem cell line encoding a dNTPase defective SAMHD1 gene was also created (SAMHD1-MUT). These cells were then differentiated into macrophages. Interestingly, SAMHD1-KO and SAMHD1-MUT factories produced esYDMPs with a similar temporal delay observed in SAMHD1-KD cells. esYDMs were positive for common myeloid markers as well as HIV-1 entry receptors. SAMHD1 abolition in SAMHD1-KO cells was confirmed by western blot and also by quantification of dNTPs, which were substantially elevated in these cells. Similar probes of SAMHD1-MUT cells identified a very small fraction of SAMHD1 protein present as well as dNTP concentrations elevated to levels observed in SAMHD1-KO cells, thus confirming non-function of the dNTPase.

The two hypotheses relating to SAMHD1 RKP detailed above were tested by observing HIV-1 infection dynamics in SAMHD1-KO cells in the presence and absence of Vpx. In steady-state SAMHD1-KO cells, the application of Vpx via Vpx-VLPs did not rescue HIV-1 infection significantly more than HIV-1 infection in the absence of Vpx. This showed that in esYDMs Vpx does not function in the rescue of HIV-1 infection via a SAMHD1 independent mechanism and that the observations relating to the difference in potency of SAMHD1 depletion, dNTP hydrolysis and HIV-1 restriction in Vpx expressing cells versus SAMHD1-KD cells was due to the activity of residual knockdown protein (RKP). Interestingly, whilst the application of Vpx did not affect HIV-1 infection in SAMHD1-KO cells, it did significantly elevate dATP concentrations in SAMHD1-KO cells treated with empty VLPs. This *did* imply a SAMHD1 independent mechanism for dATP modulation. Such an additional mechanism may involve either upregulation of dNTP synthesis or antagonisation of an alternative dNTPase to SAMHD1. An attempt was made to identify any potential novel Vpx interacting partner by immunoprecipitation in THP-1 monocytes with HA-tagged Vpx; however, no novel proteins were identified.

The creation of an esYDM cell line, which encoded a dNTPase defective SAMHD1 mutant, allowed the testing of dNTPase independent mechanisms of HIV-1 restriction of SAMHD1. The activity of the

dNTPase was confirmed as abolished by Sanger sequencing and quantification of dNTP concentrations. Although SAMHD1 expression was very low, HIV-1 was still restricted significantly versus SAMHD1-KO cells. This showed that in esYDMs, the dNTPase is dispensable for HIV-1 restriction but also that only small concentrations of SAMHD1 protein are required for HIV-1 restriction to occur.

An investigation probing the effects of env on HIV-1 infection in esYDMs showed that pseudotyping with HIV-1 envelope (JRFL) rendered HIV-1 more infectious than pseudotyping with VSV.G envelope in esYDMs. This was hypothesised to be a result of the reduced exposure of the HIV-1 core to the cytoplasm, and hence SAMHD1, a consequence of VSV.G mediated cell entry via fusion with late endosomes. Furthermore, this appears to map to the dNTPase independent HIV-1 restrictive mechanism of SAMHD1 alluded to earlier.

Due to the significant overlap in Vpx and Vpr functions (refer to Chapter 1, Section 1.1.4 HIV and SIV accessory proteins), particularly in interaction with both DCAF1 and SAMHD1, I decided to investigate any functions of both SIVmac Vpr and HIV-1 Vpr that may be SAMHD1 specific using the SAMHD1-KO cells. Surprisingly, SIVmac Vpr appeared active in the rescue of HIV-1 infection but, moreover, in a manner dependent on the antagonisation and degradation of SAMHD1. This was surprising since SIVmac already encoded an accessory protein that antagonised human SAMHD1, i.e., Vpx. This observation is hypothesised to be due to the resurrection of an ancestral ability to antagonise SAMHD1 encoded by SIVmac Vpr. It has been suggested that acquisition of the ability to antagonise SAMHD1 resulted in the duplication (or acquisition) of the ancestral Vpr and the birth of Vpx [96]. Vpx then specialised in antagonisation of the host (Macquaqe) SAMHD1 allowing the resident Vpr to specialise in SAMHD1-independent functions. Hence, the sequence divergence of human SAMHD1 may have been recognised by ancestral anti-SAMHD1 SIVmac Vpr residues. This observation was also taken as additional evidence for the model of the acquisition of SAMHD1 antagonisation by an ancestral SIV Vpr protein as the event that resulted in the birth of Vpx [96].

Similar probing of HIV-1 Vpr ($Vpr_{(HIV-1)}$) revealed that, as widely described for $Vpr_{(HIV-1)}$ in human macrophages, $Vpr_{(HIV-1)}$ was active in rescue of HIV-1 infection in esYDMs and that this rescue appears to be independent of interactions with SAMHD1 when Vpr and HIV-1 virus is applied simultaneously. However, further experimental repeats are required before these observations can be confirmed.

The SAMHD1-KO esYDMs were utilised again in order to probe the observation of VpxQ76A rescue of HIV-1 infection in SAMHD1-KD ipsYDMs further. Exogenous application of VpxQ76A did not rescue HIV-1 infection in SAMHD1-KO esYDMs, which implied that in ipsYDMs VpxQ76A-mediated rescue of HIV-1 infection was probably SAMHD1 dependent but independent of DCAF1-CLR4-mediated depletion. Moreover, in wild type esYDMs, VpxQ76A rescued HIV-1 virus pseudotyped with JRFL but not HIV-1 virus pseudotyped with VSV.G.

Vpx and VpxQ76A had been shown to rescue HIV-1 infection from the antiviral state in myeloid cells and so I decided to investigate whether this was a phenotype manifest in esYDMs, whether SIVmac Vpr or $Vpr_{(HIV-1)}$ were functional in this regard, and finally by using the SAMHD1-KO cells, whether any effects could be attributable to SAMHD1. Interestingly, preliminary experiments showed that Vpx, VpxQ76A, Vpr, and $Vpr_{(HIV-1)}$ all rescued HIV-1 infection from the antiviral state established by IFNs or LPS, and by a mechanism that appeared to be independent of SAMHD1.

Unfortunately, effects on dNTP concentrations and SAMHD1 expression levels resulting from of the antiviral state or PMA stimulation in esYDMs was not probed; however, the effects of LPS on dNTP concentrations in esYDMs were. Application of LPS to esYDMs did not result in an increase in dNTP concentrations, which may constitute additional evidence for the dispensability of SAMHD1's dNTPase in HIV-1 restriction in esYDMs. Further experimental repeats are required in order to corroborate data from these observations, but if confirmed, it would constitute additional evidence for unidentified interacting partners of Vpx and Vpr proteins and also for the potential importance of bacterial components in facilitating HIV-1 replication in tissue-resident macrophages.

6.2 Implications and perspectives

6.2.1 Implications

A widely used in vitro model for studying HIV-1 dynamics in macrophages are blood MDMs. Studies in the mouse show that these macrophages derive from the bone marrow in a manner dependent on the transcription factor MYB. They are believed to closely resemble monocyte-derived infiltrating macrophages that are short-lived and do not self-renew. Recent advances in our understanding of macrophage ontology have revealed that tissue-resident macrophages derive from the embryonic yolk sac in a manner that is independent of MYB. These macrophages can be very long-lived and capable of self-renewal. Blood MDMs have been shown to be a good model for primary tissue-resident macrophages such as AMs and PMs, but not microglia [567]. Thus, blood MDMs may not always represent an ideal model for certain tissue-resident macrophage subsets. Macrophages derived from stem cells using the protocol found in this thesis have been shown to arise in a manner independent of MYB which, in addition to dependence on the transcription factors RUNX1- and SPI1-, indicates an origin in the primitive wave of haematopoiesis and hence the yolk sac [4]. Thus, esYDMs may represent a more relevant model of longer-lived tissue-resident macrophage subsets in which to investigate SAMHD1 and HIV-1 microbiology.

esYDMs have a well-established HIV-1 restrictive phenotype [265], which is corroborated by findings in this thesis. Whilst blood MDMs were not directly probed in this work, the data obtained from esYDMs was similar to that documented for blood MDMs in several published reports. PMA treated THP-1 cells; however, *were* probed and were shown to be more permissive to HIV-1 and contain higher dNTP concentrations at a steady-state then esYDMs. In addition to adding data to the HIV-1 restrictive phenotype in esYDMs, the phenotype of SAMHD1 expression levels, hydrolysis of dNTPs, and depletion by Vpx were also shown to be similar to that detailed in published reports in blood MDMs. Overall, my results imply that the microbiology of SAMHD1-mediated HIV-1 restriction in scYDMs is similar to the

phenotype documented for blood MDMs, when both are at the steady-state. Thus, the working hypothesis of this thesis has been rejected.

Peripheral tissue-resident macrophages such as AMs and PMs have also been shown to mimic blood MDMs in terms of SAMHD1-mediated HIV-1 restriction and rescue by Vpx [567]. Therefore, given the myb-independent nature of scYDMs, my data suggests that esYDMs may more accurately model peripheral tissue-resident macrophages of AM and PM subsets rather than subsets such as microglia. In support of this, a recent publication has detailed the production of microglia from stem cells using the protocol documented in this thesis as a base but which, importantly, requires alternative growth factors (and hence a different differentiation pathway) to those detailed here [619]. Repeats of these experiments, perhaps including blood MDMs from multiple donors and primary tissue-resident macrophages, would be required for confirmation of any similarity to SAMHD1-mediated HIV-1 restrictive phenotype found in scYDMs.

Whilst data in this thesis shows that Vpx potently degrades human SAMHD1, amplifies dNTP concentrations, and rescues HIV-1 restriction in esYDMs, the interdependence of these phenotypes could not be confirmed. This was due to separate cell cultures being used for SAMHD1 expression quantification, dNTP quantification, and HIV-1 infection experiments; primarily due to the large number of cells required for dNTP quantification with a sufficient number of repeats. Particularly in light of the dispensability of dNTPase in HIV-1 restriction detailed in this report, a future experiment should use protein and dNTPs extracted from the same cells previously exposed to Vpx or Vpr (or indeed HIV-1). This would enable the definitive documentation of any interdependence of SAMHD1 protein expression levels (or phosphorylation status) and dNTP concentrations in relation to Vpx, Vpr, or HIV-1 in scYDMs.

HIV-1 infection kinetics in human stem cell-derived macrophages also gave some insight into the source of donor-derived differences often observed in HIV-1 infection frequency in blood MDMs. Whilst the source of donor-derived differences is not entirely clear, they are believed to be caused, at least in part,

by transcriptional differences unique to the individuals (donors) genome. Observation of HIV-1 infection kinetics of es and iPS cells cultured, differentiated into macrophages, and then infected with HIV-1 in parallel, did not show any significant differences in frequency of HIV-1 infection. The es and iPS cells were derived from different donors and therefore suggested that donor-derived differences are not a result of transcriptional (and hence genetic) activity. Instead, this suggests that donor-derived differences are more likely a function of stimulation from the microenvironment and are thus representative of macrophage polarisation or activation state. Extensions to this investigation, perhaps utilising multiple human stem cell lines, blood MDMs, and primary tissue-resident macrophages, would assist greatly in not only corroborating the observations detailed above but also in discerning what external stimulatory elements might be involved.

esYDMPs were produced by SAMHD1-KO factories approximately 4 weeks after EB plating, and 2 weeks after wild type factories started to produce. This was similar to the production kinetics observed in SAMHD1-KD cells and thus supported the hypothesis that the absence of SAMHD1 was responsible for the production kinetics observed rather than being a consequence of an anomaly associated with the RNA interference system. It also confirmed the apparent acceleratory effect of Vpx on esYDMP production. The mechanism underlying this effect was not determined in this thesis, but it could involve a cytoplasmic fraction of SAMHD1, which has been shown to be resistant to Vpx-mediated degradation [156]. Data presented in this work has shown that small quantities of SAMHD1 are potent in both dNTP hydrolysis and HIV-1 restriction and therefore it is possible that the cytoplasmic SAMHD1 fraction, which represents a very low percentage of SAMHD1 protein in myeloid cells [186], is sufficient to “rescue” differentiation. In support of this, VpxQ76A factories produced esYDMPs at the same time point as wild type factories indicating that a binding partner of DCAF1 (such as SAMHD1) functions by directly regulating the timing of esYDMP production. It should also be noted, however, that the binding partner of DCAF1 may also be a novel factor that is accelerating differentiation. This uncertainty could potentially be solved by creating a SAMHD1-KO cell line that was also transduced with a lentiviral vector

expressing Vpx (as previously discussed). If the factor regulating esYDMP production was only SAMHD1, then factories would produce at approximately the same time as SAMHD1-KO factories. If additional functions of Vpx were involved, then factories would produce esYDMPs prior to SAMHD1-KO factories.

As previously discussed, several published reports hypothesise a ribonuclease activity of SAMHD1 that functions in HIV-1 restriction independent of the dNTPase. One objection to this hypothesis was that SAMHD1 is believed to restrict HIV-1 in the nucleus (where the majority of SAMHD1 is localised), whereas the ribonuclease is believed to function in the cytoplasm once the HIV-1 core has uncoated sufficiently. The frequency of HIV-1 infection in the dNTPase mutant esYDMs presented compelling evidence for a dNTPase independent function for HIV-1 restriction encoded by SAMHD1. Interestingly, the data presented in this thesis showing the differential effects of env on HIV-1 restriction in SAMHD1-MUT cells could be interpreted as confirmatory of the cytoplasm as an area important for SAMHD1-mediated restriction of HIV-1 by the dNTPase independent mechanism. Taken together, these data appear to corroborate the hypothesis put forward in the literature for a dNTPase independent mechanism of HIV-1 restriction by SAMHD1 localised to the cytoplasm [114, 115, 235]. More robust conclusions would require additional experiments, perhaps including the use of a dNTPase mutant cell line with SAMHD1 at expression levels comparable to wild type non-genetically modified cells. However, if confirmed, the dispensability of SAMHD1's dNTPase in HIV-1 restriction does raise some interesting questions. For example, exogenous application of dNs has been shown to rescue HIV-1 infection in macrophages. If low dNTPs are not restricting HIV-1, as data presented in this thesis suggests, then what is the mechanism rescuing HIV-1 infection upon the addition of dNs?

In esYDMs at the steady-state, VpxQ76A rescues JRFL pseudotyped HIV-1 by a mechanism dependent on SAMHD1 but independent of DCAF1, however does not rescue VSV.G pseudotyped HIV-1. The nature of this mechanism is unclear, as is the dependency on env. It is possible that VpxQ76A directly inhibits the unknown HIV-1 restrictive mechanism encoded by SAMHD1 in a similar manner to which

Vpr antagonises UNG2 (refer to Chapter 1, Section 1.1.4.2 Vpr). Interestingly, the JRFL dependence of this phenotype may position the activity of VpxQ76A in the cytoplasm for reasons detailed in the preceding paragraph and thus may also indicate the cytoplasm as an important region for SAMHD1 mediated HIV-1 restriction.

The rescue of HIV-1 infection by VpxQ76A in esYDMPs and PMA treated THP-1 cells, and by Vpx in esYDMs with an established antiviral state shown in this thesis implies a novel mechanism to rescue HIV-1 infection encoded by Vpx. Interestingly, the rescue of HIV-1 infection by Vpx and VpxQ76A has also been documented in published reports in blood MDDCs with an established antiviral state [590], as has rescue of HIV-1 infection independent of Vpx interaction with DCAF1 in PMA treated THP-1 cells [153]. Taken together, these data imply that a novel HIV-1 restriction factor may exist in myeloid cells, including esYDMs and esYDMPs that is antagonised by Vpx in a manner independent of DCAF1 and probably, therefore, SAMHD1. However, experimental repeats are required to establish greater confidence in this conclusion. Whether it is the same novel factor restricting HIV-1 infection in stem cell-derived macrophages, PMA treated THP-1 cells, and primary MDDCs remains to be determined. Identification of this novel factor by, for example immunoprecipitations, will likely be frustrated by the requirement for cells to be in an antiviral state. A solution to this problem may be found in esYDMPs, the monocyte like macrophage precursor cells. Preliminary evidence was documented in this thesis indicating that VpxQ76A may rescue HIV-1 infection in these cells, and thus may antagonise the same novel restriction factor detailed above (which may thus be expressed in these cells at a steady state). If this result is reproducible in SAMHD1-KO esYDMPs then these cells could be used in immunoprecipitation for identification of this unknown factor.

Intriguingly, both SIVmac Vpr and HIV-1 Vpr ($Vpr_{(HIV-1)}$) appeared to rescue HIV-1 infection from the antiviral state in esYDMs in a manner independent of SAMHD1. The factor antagonised in esYDMs by Vpr and $Vpr_{(HIV-1)}$ is unknown, but the phenotype of rescue is analogous to that observed for Vpx.

Experimental repeats are required to corroborate these findings, but if confirmed, there are two notable implications. Firstly, if the novel factor antagonised by Vpx, Vpr, and $Vpr_{(HIV-1)}$ is the same protein, then it suggests this factor is very important in retroviral restriction given that diverse accessory proteins have evolved to neutralise it. Secondly, if the novel factor antagonised by Vpx and Vprs are different proteins, then this could imply a class of functions in HIV-1 rescue encoded by accessory proteins that may primarily be active during an antiviral state, which are currently poorly described.

In addition to SIVmac Vpr rescue of HIV-1 from the antiviral state, it was also shown that SIVmac Vpr functions in the rescue of HIV-1 in esYDMs at the steady-state. This was surprising since SIVmac also antagonises human SAMHD1 using Vpx. The fact that SIV Vpr was active in antagonisation of human SAMHD1 may be evidence of the high flexibility inherent in antagonisation by these proteins. This could imply that these proteins are not good targets for novel pharmacological design due to the high likelihood of escape mutations arising not only by the accessory protein in question but perhaps by redundancy inherent in ancillary accessory proteins encoded within the same viral genome (e.g., SIVmac Vpx & Vpr antagonisation of human SAMHD1).

The successful creation of SAMHD1-KO macrophages shows that CRISPR- Cas9 gene editing is compatible with the human stem cell differentiation protocol used in this thesis. The CRISPR- Cas9 system was not onerous in terms of technical or financial requirements and proved very efficient in targeting SAMHD1 with few off-target events. Moreover, the high degree of potential targeting accuracy enabled the creation of an enzymatic mutant SAMHD1 cell line all without additional experimental procedure (compared to the creation of knockout (homozygous indels)). As such, I feel genetic manipulation using CRISPR- Cas9 in human stem cell-derived macrophages is an extremely powerful tool for gene function studies in macrophages, which typically offer significant immunological resistance to genetic modification.

Gene editing has already been used successfully in T-Cells for therapeutic clinical application. Zinc finger nucleases were used to perturb the CCR5 gene in hematopoietic stem cells extracted from HIV-1 positive patients [620]. These cells were then reintroduced with the notion that all cell lineages differentiated from these cells (such as lymphocytes and myeloid cells) would not express the CCR5 co-receptor and hence halt HIV-1 entry and replication ($CCR5^{--}$). Whilst clinical interventions of this kind have had limited success they are a promising indication of how gene editing can be used in therapy or control of HIV-1 infection [620]. Although CRISPR- Cas9 gene editing and stem cell-induced pluripotency are still techniques in relative infancy, combined they may present an extremely powerful progression in genetic engineering for HIV-1 therapeutics. For example, the acquisition of stem cells via induced pluripotency is far less invasive and expensive than the current procedures, such as a lumbar puncture. IPS cells could then be genetically modified using CRISPR- Cas9 in a manner that is retardive to HIV replication, quickly expanded, and then reintroduced into the individual, differentiated *in vitro* for further investigations, or frozen in liquid nitrogen for long term storage. All cell lineages derived from the reintroduced modified iPS cells would be genetically engineered to resist HIV-1 replication, target existing infected cells for termination, or perhaps both. The most promising cellular factor identified to date that could be manipulated in such a procedure is the host restriction factor TRIM5α. The advantages inherent in TRIM5α compared to all other restriction factors are two-fold. Firstly, TRIM5 proteins appear to be highly specific to retrovirus capsids. Thus, altering the function of TRIM5α is highly unlikely to affect cellular homeostasis or even the activity of endogenous retroviral elements (e.g., LINE-1 retrotransposon) due to their lack of encoded capsid proteins. Secondly, data has been published showing that only a single amino acid change is necessary in order to render human TRIM5α restrictive to HIV-1 [621]. The requirement to change so few amino acids would reduce the technical (and hence temporal) burden on *in vitro* gene editing. In the spirit of the lessons learned from HAART, additional HIV-1 restrictive mechanisms should also be introduced in addition to mutated TRIM5α, such as destruction of the CCR5 gene, so that the combined TRIM5α-$CCR5^{--}$ restrictive capacity reduces the emergence of HIV-1 compensatory mutations. And indeed, the previously mentioned technical and

financial ease inherent in the CRISPR- Cas9 system makes it ideal for such multitargeted editing. Of course, advancement in the iPSC production protocol such as refining fibroblast reprogramming so that iPSCs are transcriptionally indistinguishable from hematopoietic stem cells extracted from patients, and elimination of all off-target cutting by CRISPR- Cas9 [622], are fundamental requirements for any meaningful progress in this field.

The stem cell derived macrophage model used in this thesis represents a powerful tool for the investigation of macrophage biology primarily due to the range of genetic manipulation techniques that can be applied at the stem cell stage, but also due to the large number of genetically homogenous cells that can be produced over a long period of time. This is particularly advantageous when investigating a pathogen for which macrophages are the natural host cell type, such as HIV-1. Macrophages are highly specialised immune effectors and are equipped with a range of function specific attributes (such as enhanced antiviral defences via upregulation of ISGs), components which, if absent in non-natural host cells utilised in an HIV-1-related investigation, could facilitate the generation of anomalous results. Preliminary novel observations reported in this work, such as the SAMHD1 independent Vpx-mediated increases in dATP (refer to Section 5.3.1 Modulation of dNTP concentrations and HIV-1 restriction by SAMHD1 RKP, Figure 5.4H) and the env receptor influence on HIV-1 infection (refer to Section 5.3.6 Env effects on HIV-1 infection in esYDMs), may represent incidences of this phenomenon and hence may manifest only in macrophages. Intriguingly, the unidentified mechanism underlying the pro-HIV-1 replication role for Vpr hypothesised in the wider literature (refer to Section 1.1.4.2 Vpr) and hinted at in this thesis (refer to Section 5.3.4 HIV-1 Vpr rescues HIV-1 infection in esYDMs), has since been defined. HIV-1 Vpr has recently been shown to antagonise the host restriction factor REAF (also known as RPRD2, (refer to Section 5.3.2 Probing the identity of SAMHD1 independent Vpx interacting partners) in a CLR4-DCAF1 dependant manner, in macrophages [613]. The authors showed that REAF was minimally restrictive to HIV-1 in cycling CD4+ T-cells but potent in HIV-1 restriction in primary MDMs. The identification of REAF as a Vpr sensitive HIV-1 restricting factor in primary MDMs highlights the value of

investigating the nature of a pathogen using natural host cells and, moreover, suggests that a robust and versatile macrophage model, such as that derived from stem cells defined in this thesis, would be of great value for future investigations into pathogen-macrophage interactions.

6.2.2 Perspectives

Possibly the most intriguing results detailed in this thesis is the rescue of HIV-1 infection in esYDMs by SIVmac251 Vpr and HIV-1 Vpr. The HIV-1 restriction factor in human macrophages neutralised by HIV-1 Vpr appears to have since been identified as REAF [613], however it has not been established whether this is the same factor interacting with SIVmac251 Vpr. Thus, a potential future experiment would be to perform SIVmac251 Vpr immunoprecipitations in macrophages, such as esYDMs, in an attempt to determine whether SIVmac251 Vpr interacts with REAF and if not, identify the unknown entity neutralised by SIVmac251 Vpr.

Data that may also be of interest is that regarding potential SIVmac251 Vpr rescue of SIV infection in human macrophages, or indeed macaque macrophages, as data detailed in this thesis is concerned only with SIVmac251 Vpr rescue of HIV-1 in human macrophages (esYDMs). Thus, a further potential future experiment could involve the application SIVmac251 Vpr followed by a challenge with SIVmac251 virus to human or macaque macrophages in order to gain more insight into the restrictive scope of this potentially unknown entity antagonised by SIVmac251 Vpr.

Chapter 7

Chapter 7: References

7.1 Licences

7.1.1 Licence for Figure 1.2 “Phylogeny of lentiviruses”.

Sharp, P.M. and B.H. Hahn, [623] *Origins of HIV and the AIDS pandemic.* Cold Spring Harb Perspect Med, 2011. **1**(1): p. a006841. Page 3, Figure 2. Copyright Cold Spring Harbour Laboratory Press.

7.1.2 Licence for Figure 1.6 “Some Vpr Proteins Degrade SAMHD1” and Table 1.2 “Species-Specific SAMHD1 Degradation by Vpr and Vpx”.

Lim, Fregoso [96] *The ability of primate lentiviruses to degrade the monocyte restriction factor SAMHD1 preceded the birth of the viral accessory protein Vpx.* Cell Host Microbe, 2012. **11**(2): p. 194-204. Original Figure numbers: Figure 2. Some Vpr Proteins Degrade SAMHD1" Part A only - the unrooted phylogeny of 115 vpr and vpx sequences. Table 1. Species-Specific SAMHD1 degradation by Vpr and Vpx". License number: 4646390301204. License date: Aug 12, 2019.

7.2 Bibliography

1. Puigdomenech, I., et al., *SAMHD1 restricts HIV-1 cell-to-cell transmission and limits immune detection in monocyte-derived dendritic cells.* J Virol, 2013. **87**(5): p. 2846-56.
2. Hrecka, K., et al., *Vpx relieves inhibition of HIV-1 infection of macrophages mediated by the SAMHD1 protein.* Nature, 2011. **474**(7353): p. 658-61.
3. Laguette, N., et al., *SAMHD1 is the dendritic- and myeloid-cell-specific HIV-1 restriction factor counteracted by Vpx.* Nature, 2011. **474**(7353): p. 654-7.
4. Buchrieser, J., W. James, and M.D. Moore, *Human Induced Pluripotent Stem Cell-Derived Macrophages Share Ontogeny with MYB-Independent Tissue-Resident Macrophages.* Stem Cell Reports, 2017. **8**(2): p. 334-345.
5. van Wilgenburg, B., et al., *Efficient, long term production of monocyte-derived macrophages from human pluripotent stem cells under partly-defined and fully-defined conditions.* PLoS One, 2013. **8**(8): p. e71098.
6. Weagel, E., et al., *Macrophage polarization and its role in cancer.* 2015. **6**: p. 338.
7. Martinez, F.O. and S. Gordon, *The M1 and M2 paradigm of macrophage activation: time for reassessment.* F1000Prime Rep, 2014. **6**: p. 13.
8. Blayney, D.W., W.A. Blattner, and R.C. Gallo, *Isolation procedures for patients with leukemia or lymphoma associated with human T-cell leukemia virus.* N Engl J Med, 1983. **308**(14): p. 844.
9. Barre-Sinoussi, F., et al., *Isolation of a T-lymphotropic retrovirus from a patient at risk for acquired immune deficiency syndrome (AIDS).* Science, 1983. **220**(4599): p. 868-71.
10. Popovic, M., et al., *Detection, isolation, and continuous production of cytopathic retroviruses (HTLV-III) from patients with AIDS and pre-AIDS.* Science, 1984. **224**(4648): p. 497-500.
11. Gartner, S., et al., *Virus isolation from and identification of HTLV-III/LAV-producing cells in brain tissue from a patient with AIDS.* JAMA, 1986. **256**(17): p. 2365-71.
12. Koenig, S., et al., *Detection of AIDS virus in macrophages in brain tissue from AIDS patients with encephalopathy.* Science, 1986. **233**(4768): p. 1089-93.
13. Deeks, S.G., et al., *HIV infection.* Nature Reviews Disease Primers, 2015. **1**: p. 15035.
14. HIV, *HIV Global Statistics.* 2019.

15. Kouri, V., et al., *High frequency of antiviral drug resistance and non-b subtypes in HIV-1 patients failing antiviral therapy in Cuba.* J Int AIDS Soc, 2014. **17**(4 Suppl 3): p. 19754.
16. Ruane, P.J., et al., *Antiviral activity, safety, and pharmacokinetics/pharmacodynamics of tenofovir alafenamide as 10-day monotherapy in HIV-1-positive adults.* J Acquir Immune Defic Syndr, 2013. **63**(4): p. 449-55.
17. (W.H.O), W.H.O., *HIV Pre Exposure Prophylaxsis.* 2019.
18. BBC, *The truth about.. HIV.* 2017.
19. Vallari, A., et al., *Confirmation of putative HIV-1 group P in Cameroon.* J Virol, 2011. **85**(3): p. 1403-7.
20. W.H.O. *The World Health Organisation www.who.int/gho/hiv/en/*. 2018.
21. Clavel, F., et al., *Isolation of a new human retrovirus from West African patients with AIDS.* Science, 1986. **233**(4761): p. 343-6.
22. Damond, F., et al., *Identification of a highly divergent HIV type 2 and proposal for a change in HIV type 2 classification.* AIDS Res Hum Retroviruses, 2004. **20**(6): p. 666-72.
23. Ayouba, A., et al., *Evidence for continuing cross-species transmission of SIVsmm to humans: characterization of a new HIV-2 lineage in rural Cote d'Ivoire.* AIDS, 2013. **27**(15): p. 2488-91.
24. Reeves, J.D. and R.W. Doms, *Human immunodeficiency virus type 2.* J Gen Virol, 2002. **83**(Pt 6): p. 1253-65.
25. Tienen, C., et al., *Two distinct epidemics: the rise of HIV-1 and decline of HIV-2 infection between 1990 and 2007 in rural Guinea-Bissau.* J Acquir Immune Defic Syndr, 2010. **53**(5): p. 640-7.
26. Visseaux, B., et al., *Hiv-2 molecular epidemiology.* Infect Genet Evol, 2016. **46**: p. 233-240.
27. Bottiger, D., et al., *Simian immunodeficiency virus (SIVsm) isolation from blood and brain of experimentally infected macaques.* AIDS, 1991. **5**(4): p. 445-9.
28. Tsujimoto, H., et al., *Isolation and characterization of simian immunodeficiency virus from mandrills in Africa and its relationship to other human and simian immunodeficiency viruses.* J Virol, 1988. **62**(11): p. 4044-50.
29. Fultz, P.N., et al., *Isolation of a T-lymphotropic retrovirus from naturally infected sooty mangabey monkeys (Cercocebus atys).* Proc Natl Acad Sci U S A, 1986. **83**(14): p. 5286-90.
30. Kanki, P.J., J. Alroy, and M. Essex, *Isolation of T-lymphotropic retrovirus related to HTLV-III/LAV from wild-caught African green monkeys.* Science, 1985. **230**(4728): p. 951-4.
31. Peeters, M., et al., *Isolation and characterization of a new chimpanzee lentivirus (simian immunodeficiency virus isolate cpz-ant) from a wild-captured chimpanzee.* AIDS, 1992. **6**(5): p. 447-51.
32. Huet, T., et al., *Genetic organization of a chimpanzee lentivirus related to HIV-1.* Nature, 1990. **345**(6273): p. 356-9.
33. Plantier, J.C., et al., *A new human immunodeficiency virus derived from gorillas.* Nat Med, 2009. **15**(8): p. 871-2.
34. Van Heuverswyn, F., et al., *Human immunodeficiency viruses: SIV infection in wild gorillas.* Nature, 2006. **444**(7116): p. 164.
35. Bibollet-Ruche, F., et al., *New simian immunodeficiency virus infecting De Brazza's monkeys (Cercopithecus neglectus): evidence for a cercopithecus monkey virus clade.* J Virol, 2004. **78**(14): p. 7748-62.
36. Carr, M., et al., *Isolation of a simian immunodeficiency virus from a malbrouck (Chlorocebus cynosuros).* Arch Virol, 2017. **162**(2): p. 543-548.
37. Hirsch, V.M., et al., *Phylogeny and natural history of the primate lentiviruses, SIV and HIV.* Curr Opin Genet Dev, 1995. **5**(6): p. 798-806.
38. Gao, F., et al., *Origin of HIV-1 in the chimpanzee Pan troglodytes troglodytes.* Nature, 1999. **397**(6718): p. 436-41.
39. Keele, B.F., et al., *Chimpanzee reservoirs of pandemic and nonpandemic HIV-1.* Science, 2006. **313**(5786): p. 523-6.

40. Worobey, M., et al., *Direct evidence of extensive diversity of HIV-1 in Kinshasa by 1960.* Nature, 2008. **455**(7213): p. 661-4.
41. Rodgers, M.A., et al., *Identification of rare HIV-1 Group N, HBV AE, and HTLV-3 strains in rural South Cameroon.* Virology, 2017. **504**: p. 141-151.
42. Vallari, A., et al., *Four new HIV-1 group N isolates from Cameroon: Prevalence continues to be low.* AIDS Res Hum Retroviruses, 2010. **26**(1): p. 109-15.
43. Villabona-Arenas, C.J., et al., *HIV-1 group O infection in Cameroon from 2006 to 2013: Prevalence, genetic diversity, evolution and public health challenges.* Infect Genet Evol, 2015. **36**: p. 210-216.
44. Hirsch, V.M., et al., *An African primate lentivirus (SIVsm) closely related to HIV-2.* Nature, 1989. **339**(6223): p. 389-92.
45. Lemey, P., et al., *Tracing the origin and history of the HIV-2 epidemic.* Proc Natl Acad Sci U S A, 2003. **100**(11): p. 6588-92.
46. Smith, S.M., et al., *Isolation of a new HIV-2 group in the US.* Retrovirology, 2008. **5**: p. 103.
47. Yamaguchi, J., S.G. Devare, and C.A. Brennan, *Identification of a new HIV-2 subtype based on phylogenetic analysis of full-length genomic sequence.* AIDS Res Hum Retroviruses, 2000. **16**(9): p. 925-30.
48. Chen, Z., et al., *Genetic characterization of new West African simian immunodeficiency virus SIVsm: geographic clustering of household-derived SIV strains with human immunodeficiency virus type 2 subtypes and genetically diverse viruses from a single feral sooty mangabey troop.* J Virol, 1996. **70**(6): p. 3617-27.
49. Apetrei, C., et al., *Detection and partial characterization of simian immunodeficiency virus SIVsm strains from bush meat samples from rural Sierra Leone.* J Virol, 2005. **79**(4): p. 2631-6.
50. Fryer, H.R., et al., *Predicting the extinction of HIV-2 in rural Guinea-Bissau.* AIDS, 2015. **29**(18): p. 2479-86.
51. Chen, Z., et al., *Human immunodeficiency virus type 2 (HIV-2) seroprevalence and characterization of a distinct HIV-2 genetic subtype from the natural range of simian immunodeficiency virus-infected sooty mangabeys.* J Virol, 1997. **71**(5): p. 3953-60.
52. Pepin, J. and A.C. Labbe, *Noble goals, unforeseen consequences: control of tropical diseases in colonial Central Africa and the iatrogenic transmission of blood-borne viruses.* Trop Med Int Health, 2008. **13**(6): p. 744-53.
53. Schneider, W.H. and E. Drucker, *Blood transfusions in the early years of AIDS in sub-Saharan Africa.* Am J Public Health, 2006. **96**(6): p. 984-94.
54. Marx, P.A., P.G. Alcabes, and E. Drucker, *Serial human passage of simian immunodeficiency virus by unsterile injections and the emergence of epidemic human immunodeficiency virus in Africa.* Philos Trans R Soc Lond B Biol Sci, 2001. **356**(1410): p. 911-20.
55. Sousa, J., V. Müller, and A.-M. Vandamme, *The epidemic emergence of HIV: What novel enabling factors were involved?* Vol. 12. 2017. 685-707.
56. Knipe, D.M. and P.M. Howley, *Fields Virology*. 4th ed. 2001, Philadelphia: Lippincott, Williams & Wilkins.
57. Arrigo, S.J. and I.S. Chen, *Rev is necessary for translation but not cytoplasmic accumulation of HIV-1 vif, vpr, and env/vpu 2 RNAs.* Genes Dev, 1991. **5**(5): p. 808-19.
58. Pollard, V.W. and M.H. Malim, *The HIV-1 Rev protein.* Annu Rev Microbiol, 1998. **52**: p. 491-532.
59. Marcello, A., M. Zoppe, and M. Giacca, *Multiple modes of transcriptional regulation by the HIV-1 Tat transactivator.* IUBMB Life, 2001. **51**(3): p. 175-81.
60. Rossenkhan, R., et al., *Viral diversity and diversification of major non-structural genes vif, vpr, vpu, tat exon 1 and rev exon 1 during primary HIV-1 subtype C infection.* PLoS One, 2012. **7**(5): p. e35491.
61. Hearps, A.C. and D.A. Jans, *Regulating the functions of the HIV-1 matrix protein.* AIDS Res Hum Retroviruses, 2007. **23**(3): p. 341-6.

62. Bell, N.M. and A.M. Lever, *HIV Gag polyprotein: processing and early viral particle assembly.* Trends Microbiol, 2013. **21**(3): p. 136-44.
63. Jaeger, J., T. Restle, and T.A. Steitz, *The structure of HIV-1 reverse transcriptase complexed with an RNA pseudoknot inhibitor.* EMBO J, 1998. **17**(15): p. 4535-42.
64. Kent, S., G.R. Marshall, and A. Wlodawer, *Determining the 3D structure of HIV-1 protease.* Science, 2000. **288**(5471): p. 1590.
65. Rosa, A., et al., *HIV-1 Nef promotes infection by excluding SERINC5 from virion incorporation.* Nature, 2015. **526**(7572): p. 212-7.
66. Greenway, A.L., G. Holloway, and D.A. McPhee, *HIV-1 Nef: a critical factor in viral-induced pathogenesis.* Adv Pharmacol, 2000. **48**: p. 299-343.
67. Collette, Y., et al., *HIV-2 and SIV nef proteins target different Src family SH3 domains than does HIV-1 Nef because of a triple amino acid substitution.* J Biol Chem, 2000. **275**(6): p. 4171-6.
68. Barker, E. and D.T. Evans, *HLA-C Downmodulation by HIV-1 Vpu.* Cell Host Microbe, 2016. **19**(5): p. 570-1.
69. Rosenberg, M.R., L.M. Weaver, and M.G. Casarotto, *Probing interactions of Vpu from HIV-1 with amiloride-based compounds.* Biochim Biophys Acta, 2016. **1858**(4): p. 733-9.
70. Bour, S., C. Perrin, and K. Strebel, *Cell surface CD4 inhibits HIV-1 particle release by interfering with Vpu activity.* J Biol Chem, 1999. **274**(47): p. 33800-6.
71. Reddy, K., et al., *Functional characterization of Vif proteins from HIV-1 infected patients with different APOBEC3G haplotypes.* AIDS, 2016. **30**(11): p. 1723-9.
72. Inubushi, R. and A. Adachi, *Cell-dependent function of HIV-1 Vif for virus replication (Review).* Int J Mol Med, 1999. **3**(5): p. 473-6.
73. Cohen, E.A., et al., *Identification of HIV-1 vpr product and function.* J Acquir Immune Defic Syndr, 1990. **3**(1): p. 11-8.
74. Tristem, M., et al., *Evolution of the primate lentiviruses: evidence from vpx and vpr.* EMBO J, 1992. **11**(9): p. 3405-12.
75. Balliet, J.W., et al., *Distinct effects in primary macrophages and lymphocytes of the human immunodeficiency virus type 1 accessory genes vpr, vpu, and nef: mutational analysis of a primary HIV-1 isolate.* Virology, 1994. **200**(2): p. 623-31.
76. Campbell, B.J. and V.M. Hirsch, *Vpr of simian immunodeficiency virus of African green monkeys is required for replication in macaque macrophages and lymphocytes.* J Virol, 1997. **71**(7): p. 5593-602.
77. Connor, R.I., et al., *Vpr is required for efficient replication of human immunodeficiency virus type-1 in mononuclear phagocytes.* Virology, 1995. **206**(2): p. 935-44.
78. Hattori, N., et al., *The human immunodeficiency virus type 2 vpr gene is essential for productive infection of human macrophages.* Proc Natl Acad Sci U S A, 1990. **87**(20): p. 8080-4.
79. Balotta, C., et al., *Antisense phosphorothioate oligodeoxynucleotides targeted to the vpr gene inhibit human immunodeficiency virus type 1 replication in primary human macrophages.* J Virol, 1993. **67**(7): p. 4409-14.
80. Lang, S.M., et al., *Importance of vpr for infection of rhesus monkeys with simian immunodeficiency virus.* J Virol, 1993. **67**(2): p. 902-12.
81. Gibbs, J.S., et al., *Progression to AIDS in the absence of a gene for vpr or vpx.* J Virol, 1995. **69**(4): p. 2378-83.
82. Hoch, J., et al., *vpr deletion mutant of simian immunodeficiency virus induces AIDS in rhesus monkeys.* J Virol, 1995. **69**(8): p. 4807-13.
83. Paxton, W., R.I. Connor, and N.R. Landau, *Incorporation of Vpr into human immunodeficiency virus type 1 virions: requirement for the p6 region of gag and mutational analysis.* J Virol, 1993. **67**(12): p. 7229-37.

84. Lavallee, C., et al., *Requirement of the Pr55gag precursor for incorporation of the Vpr product into human immunodeficiency virus type 1 viral particles.* J Virol, 1994. **68**(3): p. 1926-34.
85. Checroune, F., et al., *Incorporation of Vpr into human immunodeficiency virus type 1: role of conserved regions within the P6 domain of Pr55gag.* J Acquir Immune Defic Syndr Hum Retrovirol, 1995. **10**(1): p. 1-7.
86. Kondo, E., et al., *The p6gag domain of human immunodeficiency virus type 1 is sufficient for the incorporation of Vpr into heterologous viral particles.* J Virol, 1995. **69**(5): p. 2759-64.
87. Jowett, J.B., et al., *The human immunodeficiency virus type 1 vpr gene arrests infected T cells in the G2 + M phase of the cell cycle.* J Virol, 1995. **69**(10): p. 6304-13.
88. Romani, B., et al., *HIV-1 Vpr Protein Enhances Proteasomal Degradation of MCM10 DNA Replication Factor through the Cul4-DDB1[VprBP] E3 Ubiquitin Ligase to Induce G2/M Cell Cycle Arrest.* J Biol Chem, 2015. **290**(28): p. 17380-9.
89. Berger, G., et al., *G2/M cell cycle arrest correlates with primate lentiviral Vpr interaction with the SLX4 complex.* J Virol, 2015. **89**(1): p. 230-40.
90. Laguette, N., et al., *Premature activation of the SLX4 complex by Vpr promotes G2/M arrest and escape from innate immune sensing.* Cell, 2014. **156**(1-2): p. 134-45.
91. Hakata, Y., M. Miyazawa, and N.R. Landau, *Interactions with DCAF1 and DDB1 in the CRL4 E3 ubiquitin ligase are required for Vpr-mediated G2 arrest.* Virol J, 2014. **11**: p. 108.
92. Chen, R., et al., *Vpr-mediated incorporation of UNG2 into HIV-1 particles is required to modulate the virus mutation rate and for replication in macrophages.* J Biol Chem, 2004. **279**(27): p. 28419-25.
93. Subbramanian, R.A., et al., *Human immunodeficiency virus type 1 Vpr is a positive regulator of viral transcription and infectivity in primary human macrophages.* J Exp Med, 1998. **187**(7): p. 1103-11.
94. Eckstein, D.A., et al., *HIV-1 Vpr enhances viral burden by facilitating infection of tissue macrophages but not nondividing CD4+ T cells.* J Exp Med, 2001. **194**(10): p. 1407-19.
95. Agostini, I., et al., *Phosphorylation of Vpr regulates HIV type 1 nuclear import and macrophage infection.* AIDS Res Hum Retroviruses, 2002. **18**(4): p. 283-8.
96. Lim, E.S., et al., *The ability of primate lentiviruses to degrade the monocyte restriction factor SAMHD1 preceded the birth of the viral accessory protein Vpx.* Cell Host Microbe, 2012. **11**(2): p. 194-204.
97. Morellet, N., et al., *NMR structure of the HIV-1 regulatory protein VPR.* J Mol Biol, 2003. **327**(1): p. 215-27.
98. Wu, Y., et al., *The DDB1-DCAF1-Vpr-UNG2 crystal structure reveals how HIV-1 Vpr steers human UNG2 toward destruction.* Nat Struct Mol Biol, 2016. **23**(10): p. 933-940.
99. Bourbigot, S., et al., *The C-terminal domain of the HIV-1 regulatory protein Vpr adopts an antiparallel dimeric structure in solution via its leucine-zipper-like domain.* Biochem J, 2005. **387**(Pt 2): p. 333-41.
100. Guenzel, C.A., C. Herate, and S. Benichou, *HIV-1 Vpr-a still "enigmatic multitasker".* Front Microbiol, 2014. **5**: p. 127.
101. Higa, L.A. and H. Zhang, *Stealing the spotlight: CUL4-DDB1 ubiquitin ligase docks WD40-repeat proteins to destroy.* Cell Division, 2007. **2**(1): p. 5.
102. Zhao, L.J., S. Mukherjee, and O. Narayan, *Biochemical mechanism of HIV-I Vpr function. Specific interaction with a cellular protein.* J Biol Chem, 1994. **269**(22): p. 15577-82.
103. Zhang, S., et al., *Cytoplasmic retention of HIV-1 regulatory protein Vpr by protein-protein interaction with a novel human cytoplasmic protein VprBP.* Gene, 2001. **263**(1-2): p. 131-40.
104. Cassiday, P.A., et al., *Understanding the molecular manipulation of DCAF1 by the lentiviral accessory proteins Vpr and Vpx.* Virology, 2015. **476**: p. 19-25.
105. He, J., et al., *Human immunodeficiency virus type 1 viral protein R (Vpr) arrests cells in the G2 phase of the cell cycle by inhibiting p34cdc2 activity.* J Virol, 1995. **69**(11): p. 6705-11.

106. Planelles, V., et al., *Vpr-induced cell cycle arrest is conserved among primate lentiviruses.* J Virol, 1996. **70**(4): p. 2516-24.
107. Zhou, X., M. DeLucia, and J. Ahn, *SLX4-SLX1 Protein-independent Down-regulation of MUS81-EME1 Protein by HIV-1 Viral Protein R (Vpr).* J Biol Chem, 2016. **291**(33): p. 16936-16947.
108. DePaula-Silva, A.B., et al., *Determinants for degradation of SAMHD1, Mus81 and induction of G2 arrest in HIV-1 Vpr and SIVagm Vpr.* Virology, 2015. **477**: p. 10-17.
109. Fassati, A. and S.P. Goff, *Characterization of intracellular reverse transcription complexes of human immunodeficiency virus type 1.* J Virol, 2001. **75**(8): p. 3626-35.
110. Poon, B. and I.S. Chen, *Human immunodeficiency virus type 1 (HIV-1) Vpr enhances expression from unintegrated HIV-1 DNA.* J Virol, 2003. **77**(7): p. 3962-72.
111. Schwefel, D., et al., *Molecular determinants for recognition of divergent SAMHD1 proteins by the lentiviral accessory protein Vpx.* Cell Host Microbe, 2015. **17**(4): p. 489-99.
112. Schwefel, D., et al., *Structural basis of lentiviral subversion of a cellular protein degradation pathway.* Nature, 2013. **505**: p. 234.
113. Oh, C., et al., *A central role for PI3K-AKT signaling pathway in linking SAMHD1-deficiency to the type I interferon signature.* Sci Rep, 2018. **8**(1): p. 84.
114. Ryoo, J., et al., *The ribonuclease activity of SAMHD1 is required for HIV-1 restriction.* Nat Med, 2014. **20**(8): p. 936-41.
115. Choi, J., et al., *SAMHD1 specifically restricts retroviruses through its RNase activity.* Retrovirology, 2015. **12**: p. 46.
116. Beloglazova, N., et al., *Nuclease activity of the human SAMHD1 protein implicated in the Aicardi-Goutieres syndrome and HIV-1 restriction.* J Biol Chem, 2013. **288**(12): p. 8101-10.
117. Gao D, W.J., Wu YT, Du F, Aroh C, Yan N, *Cyclic GMP-AMP synthase is an innate immune sensor of HIV and other retroviruses.* Science (New York, N.Y.), 2013: p. 341:903–6.
118. Kyei, G.B., et al., *Cyclin L2 is a critical HIV dependency factor in macrophages that controls SAMHD1 abundance.* Cell Host Microbe, 2015. **17**(1): p. 98-106.
119. Bouhamdan, M., et al., *Human immunodeficiency virus type 1 Vpr protein binds to the uracil DNA glycosylase DNA repair enzyme.* J Virol, 1996. **70**(2): p. 697-704.
120. Sleigh, R., et al., *Differential association of uracil DNA glycosylase with SIVSM Vpr and Vpx proteins.* Virology, 1998. **245**(2): p. 338-43.
121. Fassati, A., et al., *Nuclear import of HIV-1 intracellular reverse transcription complexes is mediated by importin 7.* EMBO J, 2003. **22**(14): p. 3675-85.
122. Heinzinger, N.K., et al., *The Vpr protein of human immunodeficiency virus type 1 influences nuclear localization of viral nucleic acids in nondividing host cells.* Proc Natl Acad Sci U S A, 1994. **91**(15): p. 7311-5.
123. Popov, S., et al., *Viral protein R regulates docking of the HIV-1 preintegration complex to the nuclear pore complex.* J Biol Chem, 1998. **273**(21): p. 13347-52.
124. Fouchier, R.A., et al., *Interaction of the human immunodeficiency virus type 1 Vpr protein with the nuclear pore complex.* J Virol, 1998. **72**(7): p. 6004-13.
125. Takeda, E., et al., *Nuclear exportin receptor CAS regulates the NPI-1-mediated nuclear import of HIV-1 Vpr.* PLoS One, 2011. **6**(11): p. e27815.
126. Nitahara-Kasahara, Y., et al., *Novel nuclear import of Vpr promoted by importin alpha is crucial for human immunodeficiency virus type 1 replication in macrophages.* J Virol, 2007. **81**(10): p. 5284-93.
127. Trinite, B., et al., *HIV-1 Vpr- and Reverse Transcription-Induced Apoptosis in Resting Peripheral Blood CD4 T Cells and Protection by Common Gamma-Chain Cytokines.* J Virol, 2016. **90**(2): p. 904-16.
128. Murakami, T. and Y. Aida, *Visualizing Vpr-induced G2 arrest and apoptosis.* PLoS One, 2014. **9**(1): p. e86840.
129. Ma, B., et al., *HIV-1 viral protein R (Vpr) induction of apoptosis and cell cycle arrest in multidrug-resistant colorectal cancer cells.* Oncol Rep, 2012. **28**(1): p. 358-64.

130. Guha, D., et al., *Neuronal apoptosis by HIV-1 Vpr: contribution of proinflammatory molecular networks from infected target cells.* J Neuroinflammation, 2012. **9**: p. 138.
131. Andersen, J.L., E. Le Rouzic, and V. Planelles, *HIV-1 Vpr: mechanisms of G2 arrest and apoptosis.* Exp Mol Pathol, 2008. **85**(1): p. 2-10.
132. Levy, D.N., Y. Refaeli, and D.B. Weiner, *Extracellular Vpr protein increases cellular permissiveness to human immunodeficiency virus replication and reactivates virus from latency.* J Virol, 1995. **69**(2): p. 1243-52.
133. Levy, D.N., et al., *Serum Vpr regulates productive infection and latency of human immunodeficiency virus type 1.* Proc Natl Acad Sci U S A, 1994. **91**(23): p. 10873-7.
134. Yurkovetskiy, L., et al., *Primate immunodeficiency virus proteins Vpx and Vpr counteract transcriptional repression of proviruses by the HUSH complex.* Nat Microbiol, 2018. **3**(12): p. 1354-1361.
135. Marcon, L., et al., *Dispensable role of the human immunodeficiency virus type 2 Vpx protein in viral replication.* J Virol, 1991. **65**(7): p. 3938-42.
136. Fregoso, O.I., et al., *Evolutionary toggling of Vpx/Vpr specificity results in divergent recognition of the restriction factor SAMHD1.* PLoS Pathog, 2013. **9**(7): p. e1003496.
137. Pancio, H.A. and L. Ratner, *Human immunodeficiency virus type 2 Vpx-Gag interaction.* J Virol, 1998. **72**(6): p. 5271-5.
138. Selig, L., et al., *Interaction with the p6 domain of the gag precursor mediates incorporation into virions of Vpr and Vpx proteins from primate lentiviruses.* J Virol, 1999. **73**(1): p. 592-600.
139. Belshan, M. and L. Ratner, *Identification of the nuclear localization signal of human immunodeficiency virus type 2 Vpx.* Virology, 2003. **311**(1): p. 7-15.
140. Singhal, P.K., et al., *Nuclear export of simian immunodeficiency virus Vpx protein.* J Virol, 2006. **80**(24): p. 12271-82.
141. Singhal, P.K., et al., *Simian immunodeficiency virus Vpx is imported into the nucleus via importin alpha-dependent and -independent pathways.* J Virol, 2006. **80**(1): p. 526-36.
142. Yu, X.F., et al., *The vpx gene of simian immunodeficiency virus facilitates efficient viral replication in fresh lymphocytes and macrophage.* J Virol, 1991. **65**(9): p. 5088-91.
143. Berger, G., et al., *SIVMAC Vpx improves the transduction of dendritic cells with nonintegrative HIV-1-derived vectors.* Gene Ther, 2009. **16**(1): p. 159-63.
144. Guyader, M., et al., *VPX mutants of HIV-2 are infectious in established cell lines but display a severe defect in peripheral blood lymphocytes.* EMBO J, 1989. **8**(4): p. 1169-75.
145. Negre, D., et al., *Characterization of novel safe lentiviral vectors derived from simian immunodeficiency virus (SIVmac251) that efficiently transduce mature human dendritic cells.* Gene Ther, 2000. **7**(19): p. 1613-23.
146. Mangeot, P.E., et al., *High levels of transduction of human dendritic cells with optimized SIV vectors.* Mol Ther, 2002. **5**(3): p. 283-90.
147. Bergamaschi, A., et al., *The human immunodeficiency virus type 2 Vpx protein usurps the CUL4A-DDB1 DCAF1 ubiquitin ligase to overcome a postentry block in macrophage infection.* J Virol, 2009. **83**(10): p. 4854-60.
148. Srivastava, S., et al., *Lentiviral Vpx accessory factor targets VprBP/DCAF1 substrate adaptor for cullin 4 E3 ubiquitin ligase to enable macrophage infection.* PLoS Pathog, 2008. **4**(5): p. e1000059.
149. Sharova, N., et al., *Primate lentiviral Vpx commandeers DDB1 to counteract a macrophage restriction.* PLoS Pathog, 2008. **4**(5): p. e1000057.
150. Ahn, J., et al., *HIV/simian immunodeficiency virus (SIV) accessory virulence factor Vpx loads the host cell restriction factor SAMHD1 onto the E3 ubiquitin ligase complex CRL4DCAF1.* J Biol Chem, 2012. **287**(15): p. 12550-8.
151. Romani, B. and E.A. Cohen, *Lentivirus Vpr and Vpx accessory proteins usurp the cullin4-DDB1 (DCAF1) E3 ubiquitin ligase.* Curr Opin Virol, 2012. **2**(6): p. 755-63.

152. Wei, W., et al., *A novel DCAF1-binding motif required for Vpx-mediated degradation of nuclear SAMHD1 and Vpr-induced G2 arrest.* Cell Microbiol, 2012. **14**(11): p. 1745-56.
153. Goujon, C., et al., *Characterization of simian immunodeficiency virus SIVSM/human immunodeficiency virus type 2 Vpx function in human myeloid cells.* J Virol, 2008. **82**(24): p. 12335-45.
154. Gramberg, T., N. Sunseri, and N.R. Landau, *Evidence for an activation domain at the amino terminus of simian immunodeficiency virus Vpx.* J Virol, 2010. **84**(3): p. 1387-96.
155. Brandariz-Nunez, A., et al., *Role of SAMHD1 nuclear localization in restriction of HIV-1 and SIVmac.* Retrovirology, 2012. **9**: p. 49.
156. Hofmann, H., et al., *The Vpx lentiviral accessory protein targets SAMHD1 for degradation in the nucleus.* J Virol, 2012. **86**(23): p. 12552-60.
157. Berger, A., et al., *Interaction of Vpx and apolipoprotein B mRNA-editing catalytic polypeptide 3 family member A (APOBEC3A) correlates with efficient lentivirus infection of monocytes.* J Biol Chem, 2010. **285**(16): p. 12248-54.
158. Schaller, T., et al., *New insights into an X-traordinary viral protein.* Front Microbiol, 2014. **5**: p. 126.
159. DeLucia, M., et al., *HIV-2 and SIVmac accessory virulence factor Vpx down-regulates SAMHD1 enzyme catalysis prior to proteasome-dependent degradation.* J Biol Chem, 2013. **288**(26): p. 19116-26.
160. Hu, J., et al., *Characterization and comparison of recombinant simian immunodeficiency virus from drill (Mandrillus leucophaeus) and mandrill (Mandrillus sphinx) isolates.* J Virol, 2003. **77**(8): p. 4867-80.
161. Bailes, E., et al., *Hybrid origin of SIV in chimpanzees.* Science, 2003. **300**(5626): p. 1713.
162. Manel, N., et al., *A cryptic sensor for HIV-1 activates antiviral innate immunity in dendritic cells.* Nature, 2010. **467**(7312): p. 214-7.
163. Cribier, A., et al., *Phosphorylation of SAMHD1 by cyclin A2/CDK1 regulates its restriction activity toward HIV-1.* Cell Rep, 2013. **3**(4): p. 1036-43.
164. Sheehy, A.M., N.C. Gaddis, and M.H. Malim, *The antiretroviral enzyme APOBEC3G is degraded by the proteasome in response to HIV-1 Vif.* Nat Med, 2003. **9**(11): p. 1404-7.
165. Mangeat, B., et al., *Broad antiretroviral defence by human APOBEC3G through lethal editing of nascent reverse transcripts.* Nature, 2003. **424**(6944): p. 99-103.
166. Yu, X., et al., *Induction of APOBEC3G ubiquitination and degradation by an HIV-1 Vif-Cul5-SCF complex.* Science, 2003. **302**(5647): p. 1056-60.
167. Malim, M.H., *APOBEC proteins and intrinsic resistance to HIV-1 infection.* Philos Trans R Soc Lond B Biol Sci, 2009. **364**(1517): p. 675-87.
168. Fletcher, A.J., et al., *Trivalent RING Assembly on Retroviral Capsids Activates TRIM5 Ubiquitination and Innate Immune Signaling.* Cell Host & Microbe, 2018. **24**(6): p. 761-775.e6.
169. Li, X., et al., *Unique features of TRIM5α among closely related human TRIM family members.* Virology, 2007. **360**(2): p. 419-433.
170. Kim, K., et al., *Cyclophilin A protects HIV-1 from restriction by human TRIM5α.* Nature Microbiology, 2019. **4**(12): p. 2044-2051.
171. Perez-Caballero, D., et al., *Tetherin inhibits HIV-1 release by directly tethering virions to cells.* Cell, 2009. **139**(3): p. 499-511.
172. Neil, S.J., T. Zang, and P.D. Bieniasz, *Tetherin inhibits retrovirus release and is antagonized by HIV-1 Vpu.* Nature, 2008. **451**(7177): p. 425-30.
173. Lim, E.S., H.S. Malik, and M. Emerman, *Ancient adaptive evolution of tetherin shaped the functions of Vpu and Nef in human immunodeficiency virus and primate lentiviruses.* J Virol, 2010. **84**(14): p. 7124-34.
174. Malim, M.H. and P.D. Bieniasz, *HIV Restriction Factors and Mechanisms of Evasion.* Cold Spring Harbor perspectives in medicine, 2012. **2**(5): p. a006940-a006940.

175. Bruce, E.A., et al., *Release of filamentous and spherical influenza A virus is not restricted by tetherin.* J Gen Virol, 2012. **93**(Pt 5): p. 963-9.
176. Neil, S.J., et al., *An interferon-alpha-induced tethering mechanism inhibits HIV-1 and Ebola virus particle release but is counteracted by the HIV-1 Vpu protein.* Cell Host Microbe, 2007. **2**(3): p. 193-203.
177. Goldstone, D.C., et al., *HIV-1 restriction factor SAMHD1 is a deoxynucleoside triphosphate triphosphohydrolase.* Nature, 2011. **480**(7377): p. 379-82.
178. Franzolin, E., et al., *The deoxynucleotide triphosphohydrolase SAMHD1 is a major regulator of DNA precursor pools in mammalian cells.* Proc Natl Acad Sci U S A, 2013. **110**(35): p. 14272-7.
179. Chen, Z., et al., *Inhibition of Hepatitis B virus replication by SAMHD1.* Biochem Biophys Res Commun, 2014. **450**(4): p. 1462-8.
180. Resources, N., *SAMHD1 SAM and HD domain containing deoxynucleoside triphosphate triphosphohydrolase 1 [Homo sapiens (human)].* 2019.
181. White, T.E., et al., *Contribution of SAM and HD domains to retroviral restriction mediated by human SAMHD1.* Virology, 2013. **436**(1): p. 81-90.
182. Ji, X., et al., *Mechanism of allosteric activation of SAMHD1 by dGTP.* Nat Struct Mol Biol, 2013.
183. Brandariz-Nunez, A., et al., *Contribution of oligomerization to the anti-HIV-1 properties of SAMHD1.* Retrovirology, 2013. **10**: p. 131.
184. Arnold, L.H., et al., *Phospho-dependent Regulation of SAMHD1 Oligomerisation Couples Catalysis and Restriction.* PLoS Pathog, 2015. **11**(10): p. e1005194.
185. Welbourn, S., et al., *Identification and characterization of naturally occurring splice variants of SAMHD1.* Retrovirology, 2012. **9**: p. 86.
186. St Gelais, C., et al., *A Putative Cyclin-binding Motif in Human SAMHD1 Contributes to Protein Phosphorylation, Localization, and Stability.* J Biol Chem, 2016. **291**(51): p. 26332-26342.
187. Zhu, C., et al., *Structural insight into dGTP-dependent activation of tetrameric SAMHD1 deoxynucleoside triphosphate triphosphohydrolase.* Nat Commun, 2013. **4**: p. 2722.
188. Yan, J., et al., *Tetramerization of SAMHD1 is required for biological activity and inhibition of HIV infection.* J Biol Chem, 2013. **288**(15): p. 10406-17.
189. Ji, X., et al., *Structural basis of cellular dNTP regulation by SAMHD1.* Proc Natl Acad Sci U S A, 2014. **111**(41): p. E4305-14.
190. Amie, S.M., R.A. Bambara, and B. Kim, *GTP is the primary activator of the anti-HIV restriction factor SAMHD1.* J Biol Chem, 2013. **288**(35): p. 25001-6.
191. Hansen, E.C., et al., *GTP activator and dNTP substrates of HIV-1 restriction factor SAMHD1 generate a long-lived activated state.* Proc Natl Acad Sci U S A, 2014. **111**(18): p. E1843-51.
192. Ji, X., et al., *Mechanism of allosteric activation of SAMHD1 by dGTP.* Nat Struct Mol Biol, 2013. **20**(11): p. 1304-9.
193. Rocha-Perugini, V., et al., *CD81 association with SAMHD1 enhances HIV-1 reverse transcription by increasing dNTP levels.* Nat Microbiol, 2017. **2**(11): p. 1513-1522.
194. Morrissey, C., et al., *The eukaryotic elongation factor eEF1A1 interacts with SAMHD1.* Biochem J, 2015. **466**(1): p. 69-76.
195. Ji, X. and Y. Xiong, *Two tales (tails) of SAMHD1 destruction by Vpx.* Cell Host Microbe, 2015. **17**(4): p. 425-7.
196. Wang, Z., et al., *Allosteric Activation of SAMHD1 Protein by Deoxynucleotide Triphosphate (dNTP)-dependent Tetramerization Requires dNTP Concentrations That Are Similar to dNTP Concentrations Observed in Cycling T Cells.* J Biol Chem, 2016. **291**(41): p. 21407-21413.
197. Seamon, K.J., et al., *SAMHD1 is a single-stranded nucleic acid binding protein with no active site-associated nuclease activity.* Nucleic Acids Res, 2015. **43**(13): p. 6486-99.
198. Goncalves, A., et al., *SAMHD1 is a nucleic-acid binding protein that is mislocalized due to aicardi-goutieres syndrome-associated mutations.* Hum Mutat, 2012. **33**(7): p. 1116-22.

199. Seamon, K.J., N.N. Bumpus, and J.T. Stivers, *Single-Stranded Nucleic Acids Bind to the Tetramer Interface of SAMHD1 and Prevent Formation of the Catalytic Homotetramer.* Biochemistry, 2016. **55**(44): p. 6087-6099.
200. Tungler, V., et al., *Single-stranded nucleic acids promote SAMHD1 complex formation.* J Mol Med (Berl), 2013. **91**(6): p. 759-70.
201. Daddacha, W., et al., *SAMHD1 Promotes DNA End Resection to Facilitate DNA Repair by Homologous Recombination.* Cell Rep, 2017. **20**(8): p. 1921-1935.
202. Mauney, C.H. and T. Hollis, *SAMHD1: Recurring roles in cell cycle, viral restriction, cancer, and innate immunity.* Autoimmunity, 2018. **51**(3): p. 96-110.
203. Pauls, E., et al., *Restriction of HIV-1 replication in primary macrophages by IL-12 and IL-18 through the upregulation of SAMHD1.* J Immunol, 2013. **190**(9): p. 4736-41.
204. Goujon, C., et al., *Evidence for IFNalpha-induced, SAMHD1-independent inhibitors of early HIV-1 infection.* Retrovirology, 2013. **10**: p. 23.
205. Liao W, B.Z., Cheng C, et al, *Dendritic cell-derived interferon gamma induced protein mediates tumor necrosis factor alpha stimulation of human lung fibroblasts.* Proteomics, 2008(8): p. 2640–2650.
206. Yan, J., et al., *CyclinA2-Cyclin-dependent Kinase Regulates SAMHD1 Protein Phosphohydrolase Domain.* J Biol Chem, 2015. **290**(21): p. 13279-92.
207. Pauls, E., et al., *Cell Cycle Control and HIV-1 Susceptibility Are Linked by CDK6-Dependent CDK2 Phosphorylation of SAMHD1 in Myeloid and Lymphoid Cells.* J Immunol, 2014. **193**(4): p. 1988-97.
208. Valle-Casuso, J.C., et al., *p21 Restricts HIV-1 in Monocyte-Derived Dendritic Cells through the Reduction of Deoxynucleoside Triphosphate Biosynthesis and Regulation of SAMHD1 Antiviral Activity.* J Virol, 2017. **91**(23).
209. White, T.E., et al., *The retroviral restriction ability of SAMHD1, but not its deoxynucleotide triphosphohydrolase activity, is regulated by phosphorylation.* Cell Host Microbe, 2013. **13**(4): p. 441-51.
210. Pauls, E., et al., *p21 regulates the HIV-1 restriction factor SAMHD1.* Proc Natl Acad Sci U S A, 2014. **111**(14): p. E1322-4.
211. Allouch, A., et al., *p21-mediated RNR2 repression restricts HIV-1 replication in macrophages by inhibiting dNTP biosynthesis pathway.* Proc Natl Acad Sci U S A, 2013. **110**(42): p. E3997-4006.
212. Tang, C., et al., *Impaired dNTPase Activity of SAMHD1 by Phosphomimetic Mutation of Thr-592.* J Biol Chem, 2015. **290**(44): p. 26352-9.
213. Welbourn, S., et al., *Restriction of virus infection but not catalytic dNTPase activity is regulated by phosphorylation of SAMHD1.* J Virol, 2013. **87**(21): p. 11516-24.
214. Bhattacharya, A., et al., *Effects of T592 phosphomimetic mutations on tetramer stability and dNTPase activity of SAMHD1 can not explain the retroviral restriction defect.* Sci Rep, 2016. **6**: p. 31353.
215. Wang, J.L., et al., *SAMHD1 is down regulated in lung cancer by methylation and inhibits tumor cell proliferation.* Biochem Biophys Res Commun, 2014. **455**(3-4): p. 229-33.
216. Rentoft, M., et al., *Heterozygous colon cancer-associated mutations of SAMHD1 have functional significance.* Proc Natl Acad Sci U S A, 2016. **113**(17): p. 4723-8.
217. Herold, N., et al., *SAMHD1 protects cancer cells from various nucleoside-based antimetabolites.* Cell Cycle, 2017. **16**(11): p. 1029-1038.
218. Lee, E.J., et al., *SAMHD1 acetylation enhances its deoxynucleotide triphosphohydrolase activity and promotes cancer cell proliferation.* Oncotarget, 2017. **8**(40): p. 68517-68529.
219. Li, M., et al., *Roles of SAMHD1 in antiviral defense, autoimmunity and cancer.* Rev Med Virol, 2017. **27**(4).
220. Rice, G.I., et al., *Mutations involved in Aicardi-Goutieres syndrome implicate SAMHD1 as regulator of the innate immune response.* Nat Genet, 2009. **41**(7): p. 829-32.

221. du Moulin, M., et al., *Cerebral vasculopathy is a common feature in Aicardi-Goutieres syndrome associated with SAMHD1 mutations.* Proceedings of the National Academy of Sciences of the United States of America, 2011. **108**(26): p. E232-E232.
222. Ramesh, V., et al., *Intracerebral large artery disease in Aicardi-Goutieres syndrome implicates SAMHD1 in vascular homeostasis.* Dev Med Child Neurol, 2010. **52**(8): p. 725-32.
223. Dale, R.C., et al., *Familial Aicardi-Goutieres syndrome due to SAMHD1 mutations is associated with chronic arthropathy and contractures.* Am J Med Genet A, 2010. **152A**(4): p. 938-42.
224. Ramantani, G., et al., *Expanding the phenotypic spectrum of lupus erythematosus in Aicardi-Goutieres syndrome.* Arthritis Rheum, 2010. **62**(5): p. 1469-77.
225. du Moulin, M., et al., *Cerebral vasculopathy is a common feature in Aicardi-Goutieres syndrome associated with SAMHD1 mutations.* Proc Natl Acad Sci U S A, 2011. **108**(26): p. E232; author reply E233.
226. Leshinsky-Silver, E., et al., *A large homozygous deletion in the SAMHD1 gene causes atypical Aicardi-Goutieres syndrome associated with mtDNA deletions.* European Journal of Human Genetics, 2011. **19**(3): p. 287-292.
227. Zhao, K., et al., *Modulation of LINE-1 and Alu/SVA retrotransposition by Aicardi-Goutieres syndrome-related SAMHD1.* Cell Rep, 2013. **4**(6): p. 1108-15.
228. Li, N., W. Zhang, and X. Cao, *Identification of human homologue of mouse IFN-gamma induced protein from human dendritic cells.* Immunol Lett, 2000. **74**(3): p. 221-4.
229. Baldauf, H.M., et al., *SAMHD1 restricts HIV-1 infection in resting CD4(+) T cells.* Nat Med, 2012. **18**(11): p. 1682-7.
230. Ayinde, D., N. Casartelli, and O. Schwartz, *Restricting HIV the SAMHD1 way: through nucleotide starvation.* Nat Rev Microbiol, 2012. **10**(10): p. 675-80.
231. Antonucci, J.M., et al., *SAMHD1-mediated HIV-1 restriction in cells does not involve ribonuclease activity.* Nat Med, 2016. **22**(10): p. 1072-1074.
232. Fassati, A., *Multiple roles of the capsid protein in the early steps of HIV-1 infection.* Virus Research, 2012. **170**(1): p. 15-24.
233. Fassati, A., *HIV infection of non-dividing cells: a divisive problem.* Retrovirology, 2006. **3**: p. 74.
234. Greber, U.F. and A. Fassati, *Nuclear import of viral DNA genomes.* Traffic, 2003. **4**(3): p. 136-43.
235. Ryoo, J., et al., *Reply to SAMHD1-mediated HIV-1 restriction in cells does not involve ribonuclease activity.* Nat Med, 2016. **22**(10): p. 1074-1075.
236. Ryoo, J., et al., *SAMHD1, the Aicardi-Goutieres syndrome gene and retroviral restriction factor, is a phosphorolytic ribonuclease rather than a hydrolytic ribonuclease.* Biochem Biophys Res Commun, 2016. **477**(4): p. 977-981.
237. Herrmann, A., et al., *Correction to: The SAMHD1-mediated block of LINE-1 retroelements is regulated by phosphorylation.* Mob DNA, 2018. **9**: p. 16.
238. Herrmann, A., et al., *The SAMHD1-mediated block of LINE-1 retroelements is regulated by phosphorylation.* Mob DNA, 2018. **9**: p. 11.
239. Hu, S., et al., *SAMHD1 Inhibits LINE-1 Retrotransposition by Promoting Stress Granule Formation.* PLoS Genet, 2015. **11**(7): p. e1005367.
240. White, T.E., et al., *Modulation of LINE-1 Retrotransposition by a Human SAMHD1 Polymorphism.* Virol Rep, 2016. **6**: p. 53-60.
241. Sze, A., et al., *Host restriction factor SAMHD1 limits human T cell leukemia virus type 1 infection of monocytes via STING-mediated apoptosis.* Cell Host Microbe, 2013. **14**(4): p. 422-34.
242. Kodigepalli, K.M., et al., *Exogenous expression of SAMHD1 inhibits proliferation and induces apoptosis in cutaneous T-cell lymphoma-derived HuT78 cells.* Cell Cycle, 2017. **16**(2): p. 179-188.

243. Bonifati, S., et al., *SAMHD1 controls cell cycle status, apoptosis and HIV-1 infection in monocytic THP-1 cells.* Virology, 2016. **495**: p. 92-100.
244. Feng, Y., et al., *HIV-1 entry cofactor: functional cDNA cloning of a seven-transmembrane, G protein-coupled receptor.* Science, 1996. **272**(5263): p. 872-7.
245. Wu, L., et al., *CD4-induced interaction of primary HIV-1 gp120 glycoproteins with the chemokine receptor CCR-5.* Nature, 1996. **384**(6605): p. 179-83.
246. Foster, T.L., et al., *Resistance of Transmitted Founder HIV-1 to IFITM-Mediated Restriction.* Cell Host Microbe, 2016. **20**(4): p. 429-442.
247. van Wilgenburg, B., et al., *The productive entry pathway of HIV-1 in macrophages is dependent on endocytosis through lipid rafts containing CD4.* PLoS One, 2014. **9**(1): p. e86071.
248. Carter, G.C., et al., *HIV-1 infects macrophages by exploiting an endocytic route dependent on dynamin, Rac1 and Pak1.* Virology, 2011. **409**(2): p. 234-50.
249. Briggs, J.A., et al., *Structural organization of authentic, mature HIV-1 virions and cores.* EMBO J, 2003. **22**(7): p. 1707-15.
250. Campbell, E.M. and T.J. Hope, *HIV-1 capsid: the multifaceted key player in HIV-1 infection.* Nature reviews. Microbiology, 2015. **13**(8): p. 471-483.
251. Goff, S.P., *Retroviridae: the retroviruses and their replication*, in *Fields Virology*. 2001, LIPPINCOTT WILLIAMS & WILKINS.
252. McDonald, D., et al., *Visualization of the intracellular behavior of HIV in living cells.* J Cell Biol, 2002. **159**(3): p. 441-52.
253. Lukic, Z., et al., *HIV-1 uncoating is facilitated by dynein and kinesin 1.* J Virol, 2014. **88**(23): p. 13613-25.
254. Varadarajan, P., et al., *The functionally conserved nucleoporins Nup124p from fission yeast and the human Nup153 mediate nuclear import and activity of the Tf1 retrotransposon and HIV-1 Vpr.* Mol Biol Cell, 2005. **16**(4): p. 1823-38.
255. Sertznig, H., et al., *Behind the scenes of HIV-1 replication: Alternative splicing as the dependency factor on the quiet.* Virology, 2018. **516**: p. 176-188.
256. Freed, E.O., *HIV-1 assembly, release and maturation.* Nature Reviews Microbiology, 2015. **13**: p. 484.
257. Accola, M.A., et al., *A conserved dileucine-containing motif in p6(gag) governs the particle association of Vpx and Vpr of simian immunodeficiency viruses SIV(mac) and SIV(agm).* J Virol, 1999. **73**(12): p. 9992-9.
258. Baskaran, D., *Investigating the role of a dynamic actin cytoskeleton and its regulators for HIV-1 entry in macrophages.* 2013.
259. Milone, M.C. and U. O'Doherty, *Clinical use of lentiviral vectors.* Leukemia, 2018. **32**(7): p. 1529-1541.
260. Oldham, R.A.A., E.M. Berinstein, and J.A. Medin, *Lentiviral vectors in cancer immunotherapy.* Immunotherapy, 2015. **7**(3): p. 271-284.
261. Durand, S. and A. Cimarelli, *The inside out of lentiviral vectors.* Viruses, 2011. **3**(2): p. 132-159.
262. Naldini, L., et al., *In Vivo Gene Delivery and Stable Transduction of Nondividing Cells by a Lentiviral Vector.* Science, 1996. **272**(5259): p. 263.
263. Miyoshi, H., et al., *Development of a self-inactivating lentivirus vector.* Journal of virology, 1998. **72**(10): p. 8150-8157.
264. Dull, T., et al., *A Third-Generation Lentivirus Vector with a Conditional Packaging System.* Journal of Virology, 1998. **72**(11): p. 8463.
265. Baskaran, D., *Investigating the role of dynamic actin cytoskeleton and it's regulators for HIV-1 entry into macrophages.* 2013.
266. Lucas, T., et al., *Differential roles of macrophages in diverse phases of skin repair.* J Immunol, 2010. **184**(7): p. 3964-77.

267. Henson, P.M. and D.A. Hume, *Apoptotic cell removal in development and tissue homeostasis.* Trends Immunol, 2006. **27**(5): p. 244-50.
268. Erwig, L.P. and P.M. Henson, *Clearance of apoptotic cells by phagocytes.* Cell Death Differ, 2008. **15**(2): p. 243-50.
269. Duffield, J.S., et al., *Host responses in tissue repair and fibrosis.* Annu Rev Pathol, 2013. **8**: p. 241-76.
270. Heredia, J.E., et al., *Type 2 innate signals stimulate fibro/adipogenic progenitors to facilitate muscle regeneration.* Cell, 2013. **153**(2): p. 376-88.
271. Davies, L.C., et al., *Tissue-resident macrophages.* Nat Immunol, 2013. **14**(10): p. 986-95.
272. Boyle, W.J., W.S. Simonet, and D.L. Lacey, *Osteoclast differentiation and activation.* Nature, 2003. **423**: p. 337.
273. Yoshida, H., et al., *The murine mutation osteopetrosis is in the coding region of the macrophage colony stimulating factor gene.* Nature, 1990. **345**: p. 442.
274. Chow, A., et al., *CD169(+) macrophages provide a niche promoting erythropoiesis under homeostasis and stress.* Nat Med, 2013. **19**(4): p. 429-36.
275. Jaiswal, S., et al., *CD47 is upregulated on circulating hematopoietic stem cells and leukemia cells to avoid phagocytosis.* Cell, 2009. **138**(2): p. 271-85.
276. Rao, S., et al., *Obligatory participation of macrophages in an angiopoietin 2-mediated cell death switch.* Development, 2007. **134**(24): p. 4449-58.
277. Stefater, J.A., 3rd, et al., *Regulation of angiogenesis by a non-canonical Wnt-Flt1 pathway in myeloid cells.* Nature, 2011. **474**(7352): p. 511-5.
278. Li, Q. and B.A. Barres, *Microglia and macrophages in brain homeostasis and disease.* Nat Rev Immunol, 2018. **18**(4): p. 225-242.
279. Squarzoni, P., et al., *Microglia modulate wiring of the embryonic forebrain.* Cell Rep, 2014. **8**(5): p. 1271-9.
280. Money, K.M. and G.D. Stanwood, *Developmental origins of brain disorders: roles for dopamine.* Front Cell Neurosci, 2013. **7**: p. 260.
281. Wang, Y., et al., *IL-34 is a tissue-restricted ligand of CSF1R required for the development of Langerhans cells and microglia.* Nature immunology, 2012. **13**(8): p. 753-760.
282. Buchrieser, J., *Unserstanding human mononuclear phagocyte ontogeny using human induced pluripotent stem cells (iPSCs).* 2016.
283. Wynn, T.A., A. Chawla, and J.W. Pollard, *Macrophage biology in development, homeostasis and disease.* Nature, 2013. **496**(7446): p. 445-55.
284. Haupt, R., et al., *Langerhans cell histiocytosis (LCH): guidelines for diagnosis, clinical work-up, and treatment for patients till the age of 18 years.* Pediatric blood & cancer, 2013. **60**(2): p. 175-184.
285. Barnes, P.J., *Alveolar macrophages in chronic obstructive pulmonary disease (COPD).* Cell Mol Biol (Noisy-le-grand), 2004. **50 Online Pub**: p. Ol627-37.
286. Hotamisligil, G.S., *Inflammation and metabolic disorders.* Nature, 2006. **444**(7121): p. 860-7.
287. Wu, D., et al., *Eosinophils sustain adipose alternatively activated macrophages associated with glucose homeostasis.* Science, 2011. **332**(6026): p. 243-7.
288. Olefsky, J.M. and C.K. Glass, *Macrophages, inflammation, and insulin resistance.* Annu Rev Physiol, 2010. **72**: p. 219-46.
289. Odegaard, J.I., et al., *Macrophage-specific PPARgamma controls alternative activation and improves insulin resistance.* Nature, 2007. **447**(7148): p. 1116-20.
290. Kang, K., et al., *Adipocyte-derived Th2 cytokines and myeloid PPARdelta regulate macrophage polarization and insulin sensitivity.* Cell Metab, 2008. **7**(6): p. 485-95.
291. Sun, K., C.M. Kusminski, and P.E. Scherer, *Adipose tissue remodeling and obesity.* J Clin Invest, 2011. **121**(6): p. 2094-101.
292. Nguyen, K.D., et al., *Alternatively activated macrophages produce catecholamines to sustain adaptive thermogenesis.* Nature, 2011. **480**(7375): p. 104-8.

293. Zaidi, M.R., et al., *Interferon-gamma links ultraviolet radiation to melanomagenesis in mice.* Nature, 2011. **469**(7331): p. 548-53.
294. Deng, L., et al., *A novel mouse model of inflammatory bowel disease links mammalian target of rapamycin-dependent hyperproliferation of colonic epithelium to inflammation-associated tumorigenesis.* Am J Pathol, 2010. **176**(2): p. 952-67.
295. Arthur, J.C., et al., *Intestinal inflammation targets cancer-inducing activity of the microbiota.* Science, 2012. **338**(6103): p. 120-3.
296. Lin, E.Y., et al., *Macrophages regulate the angiogenic switch in a mouse model of breast cancer.* Cancer Res, 2006. **66**(23): p. 11238-46.
297. Condeelis, J. and J.W. Pollard, *Macrophages: obligate partners for tumor cell migration, invasion, and metastasis.* Cell, 2006. **124**(2): p. 263-6.
298. DeNardo, D.G., P. Andreu, and L.M. Coussens, *Interactions between lymphocytes and myeloid cells regulate pro- versus anti-tumor immunity.* Cancer Metastasis Rev, 2010. **29**(2): p. 309-16.
299. Hanahan, D. and L.M. Coussens, *Accessories to the crime: functions of cells recruited to the tumor microenvironment.* Cancer Cell, 2012. **21**(3): p. 309-22.
300. Psaila, B. and D. Lyden, *The metastatic niche: adapting the foreign soil.* Nat Rev Cancer, 2009. **9**(4): p. 285-93.
301. Kinne, R.W., et al., *Macrophages in rheumatoid arthritis.* Arthritis Res, 2000. **2**(3): p. 189-202.
302. Mahida, Y.R., *The key role of macrophages in the immunopathogenesis of inflammatory bowel disease.* Inflamm Bowel Dis, 2000. **6**(1): p. 21-33.
303. Vogel, D.Y.S., et al., *Macrophages in inflammatory multiple sclerosis lesions have an intermediate activation status.* Journal of neuroinflammation, 2013. **10**: p. 35-35.
304. Wynn, T.A. and K.M. Vannella, *Macrophages in Tissue Repair, Regeneration, and Fibrosis.* Immunity, 2016. **44**(3): p. 450-462.
305. Moore, K.J., F.J. Sheedy, and E.A. Fisher, *Macrophages in atherosclerosis: a dynamic balance.* Nature reviews. Immunology, 2013. **13**(10): p. 709-721.
306. Orme, J. and C. Mohan, *Macrophage subpopulations in systemic lupus erythematosus.* Discov Med, 2012. **13**(69): p. 151-8.
307. Peters-Golden, M., *The alveolar macrophage: the forgotten cell in asthma.* Am J Respir Cell Mol Biol, 2004. **31**(1): p. 3-7.
308. Ghafouri, M., et al., *HIV-1 associated dementia: symptoms and causes.* Retrovirology, 2006. **3**: p. 28-28.
309. Cerrato, E., et al., *Cardiovascular disease in HIV patients: from bench to bedside and backwards.* Open Heart, 2015. **2**(1): p. e000174.
310. Saccomanno, M.F. and A. Ammassari, *Bone disease in HIV infection.* Clinical cases in mineral and bone metabolism : the official journal of the Italian Society of Osteoporosis, Mineral Metabolism, and Skeletal Diseases, 2011. **8**(1): p. 33-36.
311. Cassetta, L. and J.W. Pollard, *Targeting macrophages: therapeutic approaches in cancer.* Nature Reviews Drug Discovery, 2018.
312. Ostuni, R., et al., *Macrophages and cancer: from mechanisms to therapeutic implications.* Trends in Immunology, 2015. **36**(4): p. 229-239.
313. Fricker, M. and P.G. Gibson, *Macrophage dysfunction in the pathogenesis and treatment of asthma.* Eur Respir J, 2017. **50**(3).
314. Chalmers, S.A., et al., *Therapeutic targeting of macrophages in lupus nephritis.* Discov Med, 2015. **20**(108): p. 43-9.
315. Kaufmann, S.H.E. and A. Dorhoi, *Molecular Determinants in Phagocyte-Bacteria Interactions.* Immunity, 2016. **44**(3): p. 476-491.
316. Nicola, A.M., A. Casadevall, and D.L. Goldman, *Fungal killing by mammalian phagocytic cells.* Current opinion in microbiology, 2008. **11**(4): p. 313-317.

317. Mercer, J. and U.F. Greber, *Virus interactions with endocytic pathways in macrophages and dendritic cells.* Trends in Microbiology, 2013. **21**(8): p. 380-388.
318. Mogensen, S.C., *Role of macrophages in natural resistance to virus infections.* Microbiological reviews, 1979. **43**(1): p. 1-26.
319. Janeway CA Jr, T.P., Walport M, et al. , *Immunobiology: The Immune System in Health and Disease.* . 2001, New York: Garland Science
320. Gordon, S., *Pattern Recognition Receptors: Doubling Up for the Innate Immune Response.* Cell, 2002. **111**(7): p. 927-930.
321. Linehan, S.A., L. Martinez-Pomares, and S. Gordon, *Mannose receptor and scavenger receptor: two macrophage pattern recognition receptors with diverse functions in tissue homeostasis and host defense.* Adv Exp Med Biol, 2000. **479**: p. 1-14.
322. Janssens, S. and R. Beyaert, *Role of Toll-Like Receptors in Pathogen Recognition.* Clinical Microbiology Reviews, 2003. **16**(4): p. 637.
323. Thompson, M.R., et al., *Pattern recognition receptors and the innate immune response to viral infection.* Viruses, 2011. **3**(6): p. 920-940.
324. Aderem, A. and D.M. Underhill, *Mechanisms of phagocytosis in macrophages.* Annu Rev Immunol, 1999. **17**: p. 593-623.
325. Slauch, J.M., *How does the oxidative burst of macrophages kill bacteria? Still an open question.* Molecular microbiology, 2011. **80**(3): p. 580-583.
326. Junt, T., et al., *Subcapsular sinus macrophages in lymph nodes clear lymph-borne viruses and present them to antiviral B cells.* Nature, 2007. **450**: p. 110.
327. Underhill, D.M., et al., *Dynamic interactions of macrophages with T cells during antigen presentation.* The Journal of experimental medicine, 1999. **190**(12): p. 1909-1914.
328. Alberts B, J.A., Lewis J, et al., *Helper T Cells and Lymphocyte Activation.*, in *Molecular Biology of the Cell.* 2002, New York: Garland Science;.
329. Samuel, C.E., *Antiviral actions of interferons.* Clinical microbiology reviews, 2001. **14**(4): p. 778-809.
330. Levy, D.E., I.J. Marié, and J.E. Durbin, *Induction and function of type I and III interferon in response to viral infection.* Current opinion in virology, 2011. **1**(6): p. 476-486.
331. Ivashkiv, L.B. and L.T. Donlin, *Regulation of type I interferon responses.* Nature reviews. Immunology, 2014. **14**(1): p. 36-49.
332. Nasr, N., et al., *Mechanism of Interferon-Stimulated Gene Induction in HIV-1-Infected Macrophages.* Journal of Virology, 2017. **91**(20): p. e00744-17.
333. Towers, G.J., *The control of viral infection by tripartite motif proteins and cyclophilin A.* Retrovirology, 2007. **4**(1): p. 40.
334. Kirmaier, A., A. Krupp, and W.E. Johnson, *Understanding restriction factors and intrinsic immunity: insights and lessons from the primate lentiviruses.* Future virology, 2014. **9**(5): p. 483-497.
335. Palis, J., et al., *Development of erythroid and myeloid progenitors in the yolk sac and embryo proper of the mouse.* Development, 1999. **126**(22): p. 5073-84.
336. Bertrand, J.Y., et al., *Three pathways to mature macrophages in the early mouse yolk sac.* Blood, 2005. **106**(9): p. 3004-11.
337. Ginhoux, F., et al., *Origin and differentiation of microglia.* Front Cell Neurosci, 2013. **7**: p. 45.
338. Ginhoux, F., et al., *Fate mapping analysis reveals that adult microglia derive from primitive macrophages.* Science, 2010. **330**(6005): p. 841-5.
339. Schulz, C., et al., *A lineage of myeloid cells independent of Myb and hematopoietic stem cells.* Science, 2012. **336**(6077): p. 86-90.
340. Yona, S., et al., *Fate mapping reveals origins and dynamics of monocytes and tissue macrophages under homeostasis.* Immunity, 2013. **38**(1): p. 79-91.

341. Epelman, S., et al., *Embryonic and adult-derived resident cardiac macrophages are maintained through distinct mechanisms at steady state and during inflammation.* Immunity, 2014. **40**(1): p. 91-104.
342. Hashimoto, D., et al., *Tissue-resident macrophages self-maintain locally throughout adult life with minimal contribution from circulating monocytes.* Immunity, 2013. **38**(4): p. 792-804.
343. Cumano, A. and I. Godin, *Ontogeny of the hematopoietic system.* Annu Rev Immunol, 2007. **25**: p. 745-85.
344. Ginhoux, F. and M. Guilliams, *Tissue-Resident Macrophage Ontogeny and Homeostasis.* Immunity, 2016. **44**(3): p. 439-449.
345. Gordon, S. and A. Pluddemann, *Tissue macrophages: heterogeneity and functions.* BMC Biol, 2017. **15**(1): p. 53.
346. Kanitakis, J., et al., *Self-renewal capacity of human epidermal Langerhans cells: observations made on a composite tissue allograft.* Exp Dermatol, 2011. **20**(2): p. 145-6.
347. Stanley, E.R., et al., *Biology and action of colony-stimulating factor-1.* Molecular Reproduction and Development, 1997. **46**(1): p. 4-10.
348. Hamilton, J.A., *Colony-stimulating factors in inflammation and autoimmunity.* Nature Reviews Immunology, 2008. **8**: p. 533.
349. Pollard, J.W., *Trophic macrophages in development and disease.* Nat Rev Immunol, 2009. **9**(4): p. 259-70.
350. Hume, D.A. and K.P. MacDonald, *Therapeutic applications of macrophage colony-stimulating factor-1 (CSF-1) and antagonists of CSF-1 receptor (CSF-1R) signaling.* Blood, 2012. **119**(8): p. 1810-20.
351. Ryan, G.R., et al., *Rescue of the colony-stimulating factor 1 (CSF-1)–nullizygous mouse (Csf1 ^{op} /Csf1 ^{op}) phenotype with a CSF-1 transgene and identification of sites of local CSF-1 synthesis.* Blood, 2001. **98**(1): p. 74.
352. Cecchini, M.G., et al., *Role of colony stimulating factor-1 in the establishment and regulation of tissue macrophages during postnatal development of the mouse.* Development, 1994. **120**(6): p. 1357.
353. Hume, D.A., et al., *The effect of human recombinant macrophage colony-stimulating factor (CSF-1) on the murine mononuclear phagocyte system in vivo.* J Immunol, 1988. **141**(10): p. 3405-9.
354. Davies, L.C., et al., *Tissue-resident macrophages.* Nature Immunology, 2013. **14**: p. 986.
355. Davies, L.C., et al., *A quantifiable proliferative burst of tissue macrophages restores homeostatic macrophage populations after acute inflammation.* European Journal of Immunology, 2011. **41**(8): p. 2155-2164.
356. Jenkins, S.J., et al., *Local Macrophage Proliferation, Rather than Recruitment from the Blood, Is a Signature of T_H2 Inflammation.* Science, 2011. **332**(6035): p. 1284.
357. Greter, M., et al., *Stroma-derived interleukin-34 controls the development and maintenance of langerhans cells and the maintenance of microglia.* Immunity, 2012. **37**(6): p. 1050-1060.
358. Shibata, Y., et al., *GM-CSF Regulates Alveolar Macrophage Differentiation and Innate Immunity in the Lung through PU.1.* Immunity, 2001. **15**(4): p. 557-567.
359. Robb, L., et al., *Hematopoietic and lung abnormalities in mice with a null mutation of the common beta subunit of the receptors for granulocyte-macrophage colony-stimulating factor and interleukins 3 and 5.* Proc Natl Acad Sci U S A, 1995. **92**(21): p. 9565-9.
360. Hamilton, J.A. and G.P. Anderson, *Mini ReviewGM-CSF Biology.* Growth Factors, 2004. **22**(4): p. 225-231.
361. Zucali, J.R., et al., *Interleukin 1 stimulates fibroblasts to produce granulocyte-macrophage colony-stimulating activity and prostaglandin E2.* J Clin Invest, 1986. **77**(6): p. 1857-63.

362. Ozawa, H., et al., *Interferon-gamma and interleukin-10 inhibit antigen presentation by Langerhans cells for T helper type 1 cells by suppressing their CD80 (B7-1) expression.* Eur J Immunol, 1996. **26**(3): p. 648-52.
363. Lukens, J.R., et al., *Inflammasome-derived IL-1beta regulates the production of GM-CSF by CD4(+) T cells and gammadelta T cells.* J Immunol, 2012. **188**(7): p. 3107-15.
364. Jansen, J.H., et al., *Inhibition of human macrophage colony formation by interleukin 4.* J Exp Med, 1989. **170**(2): p. 577-82.
365. Gasson, J.C., *Molecular physiology of granulocyte-macrophage colony-stimulating factor.* Blood, 1991. **77**(6): p. 1131-45.
366. El-Behi, M., et al., *The encephalitogenicity of T(H)17 cells is dependent on IL-1- and IL-23-induced production of the cytokine GM-CSF.* Nat Immunol, 2011. **12**(6): p. 568-75.
367. Bagby, G.C., Jr., et al., *Interleukin 1 stimulates granulocyte macrophage colony-stimulating activity release by vascular endothelial cells.* J Clin Invest, 1986. **78**(5): p. 1316-23.
368. Ushach, I. and A. Zlotnik, *Biological role of granulocyte macrophage colony-stimulating factor (GM-CSF) and macrophage colony-stimulating factor (M-CSF) on cells of the myeloid lineage.* Journal of Leukocyte Biology, 2016. **100**(3): p. 481-489.
369. Young, D.A., L.D. Lowe, and S.C. Clark, *Comparison of the effects of IL-3, granulocyte-macrophage colony-stimulating factor, and macrophage colony-stimulating factor in supporting monocyte differentiation in culture. Analysis of macrophage antibody-dependent cellular cytotoxicity.* The Journal of Immunology, 1990. **145**(2): p. 607.
370. Xu, W., et al., *IL-10–producing macrophages preferentially clear early apoptotic cells.* Blood, 2006. **107**(12): p. 4930-4937.
371. Xu, W., et al., *Human peritoneal macrophages show functional characteristics of M-CSF-driven anti-inflammatory type 2 macrophages.* European Journal of Immunology, 2007. **37**(6): p. 1594-1599.
372. Komuro, I., et al., *Human alveolar macrophages and granulocyte-macrophage colony-stimulating factor-induced monocyte-derived macrophages are resistant to H2O2 via their high basal and inducible levels of catalase activity.* J Biol Chem, 2001. **276**(26): p. 24360-4.
373. Thomson, J.A., et al., *Embryonic Stem Cell Lines Derived from Human Blastocysts.* Science, 1998. **282**(5391): p. 1145.
374. Yu, J.T., James A. . *NIH Stem Cell Information Home Page.* 2016; Available from: https://stemcells.nih.gov/info/Regenerative_Medicine/2006Chapter1.htm.
375. Takahashi, K. and S. Yamanaka, *Induced pluripotent stem cells in medicine and biology.* Development, 2013. **140**(12): p. 2457.
376. Takahashi, K. and S. Yamanaka, *Induction of Pluripotent Stem Cells from Mouse Embryonic and Adult Fibroblast Cultures by Defined Factors.* Cell, 2006. **126**(4): p. 663-676.
377. Wilgenburg, B.v., et al., *Efficient, Long Term Production of Monocyte-Derived Macrophages from Human Pluripotent Stem Cells under Partly-Defined and Fully-Defined Conditions.* PLOS ONE, 2013. **8**(8): p. e71098.
378. Gomez Perdiguero, E., et al., *Tissue-resident macrophages originate from yolk-sac-derived erythro-myeloid progenitors.* Nature, 2014. **518**: p. 547.
379. Smith, P.D., et al., *Intestinal macrophages and response to microbial encroachment.* Mucosal Immunol, 2011. **4**(1): p. 31-42.
380. Bain, C.C., et al., *Constant replenishment from circulating monocytes maintains the macrophage pool in the intestine of adult mice.* Nature immunology, 2014. **15**(10): p. 929-937.
381. Hong, H.S., W. Ahn, and Y. Son, *CD45+/CD11b+ monocytes are required for mesenchymal stem cell proliferation In Vitro.* Tissue Engineering and Regenerative Medicine, 2014. **11**(3): p. 224-229.

382. Walker, D.G. and L.-F. Lue, *Immune phenotypes of microglia in human neurodegenerative disease: challenges to detecting microglial polarization in human brains.* Alzheimer's research & therapy, 2015. **7**(1): p. 56-56.
383. Hopperton, K.E., et al., *Markers of microglia in post-mortem brain samples from patients with Alzheimer's disease: a systematic review.* Molecular Psychiatry, 2017. **23**: p. 177.
384. Pilling, D., et al., *Identification of markers that distinguish monocyte-derived fibrocytes from monocytes, macrophages, and fibroblasts.* PloS one, 2009. **4**(10): p. e7475-e7475.
385. Vega, M.A.C., A.L., *Human macrophage activation: Too many functions and phenotypes for a single cell type.* Inmunología, 2006. **25**: p. 248-272.
386. Albright, A.V., et al., *Microglia express CCR5, CXCR4, and CCR3, but of these, CCR5 is the principal coreceptor for human immunodeficiency virus type 1 dementia isolates.* J Virol, 1999. **73**(1): p. 205-13.
387. Clayton, K.L., et al., *HIV Infection of Macrophages: Implications for Pathogenesis and Cure.* Pathogens & immunity, 2017. **2**(2): p. 179-192.
388. Mills, C.D., et al., *M-1/M-2 macrophages and the Th1/Th2 paradigm.* J Immunol, 2000. **164**(12): p. 6166-73.
389. Goerdt, S., et al., *Alternative versus classical activation of macrophages.* Pathobiology, 1999. **67**(5-6): p. 222-6.
390. Mosser, D.M., *The many faces of macrophage activation.* J Leukoc Biol, 2003. **73**(2): p. 209-12.
391. Gordon, S. and P.R. Taylor, *Monocyte and macrophage heterogeneity.* Nat Rev Immunol, 2005. **5**(12): p. 953-64.
392. Gordon, S. and F.O. Martinez, *Alternative activation of macrophages: mechanism and functions.* Immunity, 2010. **32**(5): p. 593-604.
393. Mosser, D.M. and J.P. Edwards, *Exploring the full spectrum of macrophage activation.* Nat Rev Immunol, 2008. **8**(12): p. 958-69.
394. Mantovani, A., et al., *The chemokine system in diverse forms of macrophage activation and polarization.* Trends Immunol, 2004. **25**(12): p. 677-86.
395. Chung, E.Y., S.J. Kim, and X.J. Ma, *Regulation of cytokine production during phagocytosis of apoptotic cells.* Cell Res, 2006. **16**(2): p. 154-61.
396. Bogdan, C., Y. Vodovotz, and C. Nathan, *Macrophage deactivation by interleukin 10.* J Exp Med, 1991. **174**(6): p. 1549-55.
397. McElrath, M.J., et al., *Comprehensive assessment of HIV target cells in the distal human gut suggests increasing HIV susceptibility toward the anus.* Journal of acquired immune deficiency syndromes (1999), 2013. **63**(3): p. 263-271.
398. Cassol, E., et al., *M1 and M2a Polarization of Human Monocyte-Derived Macrophages Inhibits HIV-1 Replication by Distinct Mechanisms.* The Journal of Immunology, 2009. **182**(10): p. 6237.
399. Orenstein, J.M., C. Fox, and S.M. Wahl, *Macrophages as a Source of HIV During Opportunistic Infections.* Science, 1997. **276**(5320): p. 1857.
400. Koenig, S., et al., *Detection of AIDS virus in macrophages in brain tissue from AIDS patients with encephalopathy.* Science, 1986. **233**(4768): p. 1089.
401. Jambo, K.C., et al., *Small alveolar macrophages are infected preferentially by HIV and exhibit impaired phagocytic function.* Mucosal immunology, 2014. **7**(5): p. 1116-1126.
402. Olafsson, K., et al., *Variation of HIV Infectibility of Macrophages as a Function of Donor, Stage of Differentiation, and Site of Origin.* 1991. **4**(2): p. 154-164.
403. Tschachler, E., et al., *Epidermal Langerhans cells--a target for HTLV-III/LAV infection.* J Invest Dermatol, 1987. **88**(2): p. 233-7.
404. Matsuzawa, T., et al., *Immunological function of Langerhans cells in HIV infection.* Journal of Dermatological Science, 2017. **87**(2): p. 159-167.

405. Kawamura, T., et al., *The role of Langerhans cells in the sexual transmission of HIV.* Journal of Dermatological Science, 2005. **40**(3): p. 147-155.
406. de Witte, L., et al., *Langerin is a natural barrier to HIV-1 transmission by Langerhans cells.* Nature Medicine, 2007. **13**: p. 367.
407. Hufert, F.T., et al., *Human Kupffer cells infected with HIV-1 in vivo.* J Acquir Immune Defic Syndr, 1993. **6**(7): p. 772-7.
408. Zalar, A., et al., *Macrophage HIV-1 infection in duodenal tissue of patients on long term HAART.* Antiviral Research, 2010. **87**(2): p. 269-271.
409. Castellano, P., L. Prevedel, and E.A. Eugenin, *HIV-infected macrophages and microglia that survive acute infection become viral reservoirs by a mechanism involving Bim.* Scientific Reports, 2017. **7**(1): p. 12866.
410. Clayton, K.L., et al., *Resistance of HIV-infected macrophages to CD8(+) T lymphocyte-mediated killing drives activation of the immune system.* Nature immunology, 2018. **19**(5): p. 475-486.
411. Honeycutt, J.B., et al., *Macrophages sustain HIV replication in vivo independently of T cells.* The Journal of clinical investigation, 2016. **126**(4): p. 1353-1366.
412. Gorry, P.R., et al., *Macrophage tropism of human immunodeficiency virus type 1 isolates from brain and lymphoid tissues predicts neurotropism independent of coreceptor specificity.* J Virol, 2001. **75**(21): p. 10073-89.
413. Rose, R., et al., *HIV Maintains an Evolving and Dispersed Population in Multiple Tissues during Suppressive Combined Antiretroviral Therapy in Individuals with Cancer.* Journal of Virology, 2016. **90**(20): p. 8984.
414. Gavegnano, C. and R.F. Schinazi, *Antiretroviral therapy in macrophages: implication for HIV eradication.* Antiviral chemistry & chemotherapy, 2009. **20**(2): p. 63-78.
415. Salimi, H., et al., *Macrophage-tropic HIV-1 variants from brain demonstrate alterations in the way gp120 engages both CD4 and CCR5.* Journal of leukocyte biology, 2013. **93**(1): p. 113-126.
416. Mefford, M.E., et al., *Bioinformatic analysis of neurotropic HIV envelope sequences identifies polymorphisms in the gp120 bridging sheet that increase macrophage-tropism through enhanced interactions with CCR5.* Virology, 2015. **481**: p. 210-22.
417. Chesebro, B., et al., *Macrophage-tropic human immunodeficiency virus isolates from different patients exhibit unusual V3 envelope sequence homogeneity in comparison with T-cell-tropic isolates: definition of critical amino acids involved in cell tropism.* Journal of virology, 1992. **66**(11): p. 6547-6554.
418. Arrildt, K.T., et al., *Phenotypic Correlates of HIV-1 Macrophage Tropism.* Journal of Virology, 2015. **89**(22): p. 11294.
419. Peters, P.J., et al., *Biological analysis of human immunodeficiency virus type 1 R5 envelopes amplified from brain and lymph node tissues of AIDS patients with neuropathology reveals two distinct tropism phenotypes and identifies envelopes in the brain that confer an enhanced tropism and fusigenicity for macrophages.* J Virol, 2004. **78**(13): p. 6915-26.
420. Peters, P.J., et al., *Non-macrophage-tropic human immunodeficiency virus type 1 R5 envelopes predominate in blood, lymph nodes, and semen: implications for transmission and pathogenesis.* J Virol, 2006. **80**(13): p. 6324-32.
421. Thomas, E.R., et al., *Macrophage entry mediated by HIV Envs from brain and lymphoid tissues is determined by the capacity to use low CD4 levels and overall efficiency of fusion.* Virology, 2007. **360**(1): p. 105-19.
422. Korber, B.T., et al., *Genetic differences between blood- and brain-derived viral sequences from human immunodeficiency virus type 1-infected patients: evidence of conserved elements in the V3 region of the envelope protein of brain-derived sequences.* J Virol, 1994. **68**(11): p. 7467-81.

423. Ohagen, A., et al., *Genetic and functional analysis of full-length human immunodeficiency virus type 1 env genes derived from brain and blood of patients with AIDS.* J Virol, 2003. **77**(22): p. 12336-45.
424. Cormier, E.G. and T. Dragic, *The crown and stem of the V3 loop play distinct roles in human immunodeficiency virus type 1 envelope glycoprotein interactions with the CCR5 coreceptor.* J Virol, 2002. **76**(17): p. 8953-7.
425. Ritola, K., et al., *Increased human immunodeficiency virus type 1 (HIV-1) env compartmentalization in the presence of HIV-1-associated dementia.* J Virol, 2005. **79**(16): p. 10830-4.
426. Yi, Y., et al., *An unusual syncytia-inducing human immunodeficiency virus type 1 primary isolate from the central nervous system that is restricted to CXCR4, replicates efficiently in macrophages, and induces neuronal apoptosis.* J Neurovirol, 2003. **9**(4): p. 432-41.
427. Korber, B.T., et al., *Mutational trends in V3 loop protein sequences observed in different genetic lineages of human immunodeficiency virus type 1.* J Virol, 1994. **68**(10): p. 6730-44.
428. Duncan, C.J.A. and Q.J. Sattentau, *Viral determinants of HIV-1 macrophage tropism.* Viruses, 2011. **3**(11): p. 2255-2279.
429. Alkhatib, G., et al., *CC CKR5: a RANTES, MIP-1alpha, MIP-1beta receptor as a fusion cofactor for macrophage-tropic HIV-1.* Science, 1996. **272**(5270): p. 1955-8.
430. Dragic, T., et al., *HIV-1 entry into CD4+ cells is mediated by the chemokine receptor CC-CKR-5.* Nature, 1996. **381**(6584): p. 667-73.
431. Salazar-Gonzalez, J.F., et al., *Genetic identity, biological phenotype, and evolutionary pathways of transmitted/founder viruses in acute and early HIV-1 infection.* The Journal of experimental medicine, 2009. **206**(6): p. 1273-1289.
432. Li, S., et al., *Persistent CCR5 utilization and enhanced macrophage tropism by primary blood human immunodeficiency virus type 1 isolates from advanced stages of disease and comparison to tissue-derived isolates.* J Virol, 1999. **73**(12): p. 9741-55.
433. Gray, L., et al., *Uncoupling coreceptor usage of human immunodeficiency virus type 1 (HIV-1) from macrophage tropism reveals biological properties of CCR5-restricted HIV-1 isolates from patients with acquired immunodeficiency syndrome.* Virology, 2005. **337**(2): p. 384-98.
434. Kugelberg, E., *Capturing HIV-infected T cells.* Nature Reviews Immunology, 2014. **15**: p. 2.
435. Lambotte, O., et al., *Detection of Infectious HIV in Circulating Monocytes From Patients on Prolonged Highly Active Antiretroviral Therapy.* 2000. **23**(2): p. 114-119.
436. Bracq, L., et al., *T Cell-Macrophage Fusion Triggers Multinucleated Giant Cell Formation for HIV-1 Spreading.* Journal of Virology, 2017. **91**(24).
437. Baxter, A.E., et al., *Macrophage infection via selective capture of HIV-1-infected CD4+ T cells.* Cell host & microbe, 2014. **16**(6): p. 711-721.
438. Gartner, S., et al., *The role of mononuclear phagocytes in HTLV-III/LAV infection.* Science, 1986. **233**(4760): p. 215-9.
439. Baxter, A.E., et al., *Single-Cell Characterization of Viral Translation-Competent Reservoirs in HIV-Infected Individuals.* Cell host & microbe, 2016. **20**(3): p. 368-380.
440. Welsch, S., et al., *HIV-1 buds predominantly at the plasma membrane of primary human macrophages.* PLoS pathogens, 2007. **3**(3): p. e36-e36.
441. Giese, S. and M. Marsh, *Tetherin Can Restrict Cell-Free and Cell-Cell Transmission of HIV from Primary Macrophages to T Cells.* PLOS Pathogens, 2014. **10**(7): p. e1004189.
442. Wang, L., et al., *Visualization of HIV T Cell Virological Synapses and Virus-Containing Compartments by Three-Dimensional Correlative Light and Electron Microscopy.* Journal of virology, 2017. **91**(2): p. e01605-16.
443. Jouve, M., et al., *HIV-1 Buds and Accumulates in “Nonacidic” Endosomes of Macrophages.* Cell Host & Microbe, 2007. **2**(2): p. 85-95.

444. Deneka, M., et al., *In macrophages, HIV-1 assembles into an intracellular plasma membrane domain containing the tetraspanins CD81, CD9, and CD53.* The Journal of cell biology, 2007. **177**(2): p. 329-341.
445. Sattentau, Q.J. and M. Stevenson, *Macrophages and HIV-1: An Unhealthy Constellation.* Cell host & microbe, 2016. **19**(3): p. 304-310.
446. Gousset, K., et al., *Real-Time Visualization of HIV-1 GAG Trafficking in Infected Macrophages.* PLOS Pathogens, 2008. **4**(3): p. e1000015.
447. Jolly, C. and Q.J. Sattentau, *Human immunodeficiency virus type 1 virological synapse formation in T cells requires lipid raft integrity.* Journal of virology, 2005. **79**(18): p. 12088-12094.
448. Martin, N., et al., *Virological Synapse-Mediated Spread of Human Immunodeficiency Virus Type 1 between T Cells Is Sensitive to Entry Inhibition.* Journal of Virology, 2010. **84**(7): p. 3516.
449. Chen, B.K., *T cell virological synapses and HIV-1 pathogenesis.* Immunol Res, 2012. **54**(1-3): p. 133-9.
450. Sharova, N., et al., *Macrophages archive HIV-1 virions for dissemination in trans.* The EMBO journal, 2005. **24**(13): p. 2481-2489.
451. Hashimoto, M., et al., *Potential Role of the Formation of Tunneling Nanotubes in HIV-1 Spread in Macrophages.* J Immunol, 2016. **196**(4): p. 1832-41.
452. Groot, F., S. Welsch, and Q.J. Sattentau, *Efficient HIV-1 transmission from macrophages to T cells across transient virological synapses.* Blood, 2008. **111**(9): p. 4660.
453. Alvarez, R.A., M.I. Barría, and B.K. Chen, *Unique Features of HIV-1 Spread through T Cell Virological Synapses.* PLOS Pathogens, 2014. **10**(12): p. e1004513.
454. Eugenin, E.A., P.J. Gaskill, and J.W. Berman, *Tunneling nanotubes (TNT) are induced by HIV-infection of macrophages: a potential mechanism for intercellular HIV trafficking.* Cellular immunology, 2009. **254**(2): p. 142-148.
455. Duncan, C.J.A., R.A. Russell, and Q.J. Sattentau, *High multiplicity HIV-1 cell-to-cell transmission from macrophages to CD4+ T cells limits antiretroviral efficacy.* AIDS (London, England), 2013. **27**(14): p. 2201-2206.
456. Chun, T.W., S. Moir, and A.S. Fauci, *HIV reservoirs as obstacles and opportunities for an HIV cure.* Nat Immunol, 2015. **16**(6): p. 584-9.
457. Rawlings, S.A., et al., *Elimination of HIV-1-Infected Primary T Cell Reservoirs in an In Vitro Model of Latency.* PLoS One, 2015. **10**(5): p. e0126917.
458. Chun, T.W., et al., *Effect of antiretroviral therapy on HIV reservoirs in elite controllers.* J Infect Dis, 2013. **208**(9): p. 1443-7.
459. Réu, P., et al., *The Lifespan and Turnover of Microglia in the Human Brain.* Cell reports, 2017. **20**(4): p. 779-784.
460. Clayton, K.L., et al., *Resistance of HIV-infected macrophages to CD8+ T lymphocyte–mediated killing drives activation of the immune system.* Nature Immunology, 2018. **19**(5): p. 475-486.
461. Letendre, S., et al., *Validation of the CNS Penetration-Effectiveness rank for quantifying antiretroviral penetration into the central nervous system.* Arch Neurol, 2008. **65**(1): p. 65-70.
462. Sharkey, M.E., et al., *Persistence of episomal HIV-1 infection intermediates in patients on highly active anti-retroviral therapy.* Nature Medicine, 2000. **6**: p. 76.
463. Dahl, V., et al., *An example of genetically distinct HIV type 1 variants in cerebrospinal fluid and plasma during suppressive therapy.* J Infect Dis, 2014. **209**(10): p. 1618-22.
464. Costiniuk, C.T. and M.A. Jenabian, *The lungs as anatomical reservoirs of HIV infection.* Rev Med Virol, 2014. **24**(1): p. 35-54.
465. Herskovitz, J. and H.E. Gendelman, *HIV and the Macrophage: From Cell Reservoirs to Drug Delivery to Viral Eradication.* Journal of Neuroimmune Pharmacology, 2018.
466. Yukl, S.A., et al., *Challenges in Detecting HIV Persistence during Potentially Curative Interventions: A Study of the Berlin Patient.* PLOS Pathogens, 2013. **9**(5): p. e1003347.

467. Hütter, G., et al., *Long-Term Control of HIV by CCR5 Delta32/Delta32 Stem-Cell Transplantation.* New England Journal of Medicine, 2009. **360**(7): p. 692-698.
468. Filippo, J.S., P. Sung, and H. Klein, *Mechanism of eukaryotic homologous recombination.* Annual Review of Biochemistry, 2008. **77**: p. 229-257.
469. Moynahan, M.E. and M. Jasin, *Mitotic homologous recombination maintains genomic stability and suppresses tumorigenesis.* Nat Rev Mol Cell Biol, 2010. **11**(3): p. 196-207.
470. Lieber, M.R., *The mechanism of double-strand DNA break repair by the nonhomologous DNA end-joining pathway.* Annu Rev Biochem, 2010. **79**: p. 181-211.
471. Jackson, S.P. and J. Bartek, *The DNA-damage response in human biology and disease.* Nature, 2009. **461**(7267): p. 1071-8.
472. Handel, E.M. and T. Cathomen, *Zinc-finger nuclease based genome surgery: it's all about specificity.* Curr Gene Ther, 2011. **11**(1): p. 28-37.
473. Yang, H., et al., *One-step generation of mice carrying reporter and conditional alleles by CRISPR/Cas-mediated genome engineering.* Cell, 2013. **154**(6): p. 1370-9.
474. Flynn, R., et al., *CRISPR-mediated genotypic and phenotypic correction of a chronic granulomatous disease mutation in human iPS cells.* Exp Hematol, 2015. **43**(10): p. 838-848 e3.
475. Flynn, R., et al., *CRISPR-mediated genotypic and phenotypic correction of a chronic granulomatous disease mutation in human iPS cells.* Exp Hematol, 2015.
476. Ran, F.A., et al., *Double nicking by RNA-guided CRISPR Cas9 for enhanced genome editing specificity.* Cell, 2013. **154**(6): p. 1380-9.
477. Richter, S., et al., *Zinc finger nuclease mediated knockout of ADP-dependent glucokinase in cancer cell lines: effects on cell survival and mitochondrial oxidative metabolism.* PLoS One, 2013. **8**(6): p. e65267.
478. Ren, Y., et al., *TALENs-directed knockout of the full-length transcription factor Nrf1α that represses malignant behaviour of human hepatocellular carcinoma (HepG2) cells.* Scientific Reports, 2016. **6**: p. 23775.
479. Shen, Z., et al., *Conditional knockouts generated by engineered CRISPR-Cas9 endonuclease reveal the roles of coronin in C. elegans neural development.* Developmental cell, 2014. **30**(5): p. 625-636.
480. Epinat, J.C., et al., *A novel engineered meganuclease induces homologous recombination in yeast and mammalian cells.* Nucleic Acids Res, 2003. **31**(11): p. 2952-62.
481. Thermes, V., et al., *I-SceI meganuclease mediates highly efficient transgenesis in fish.* Mech Dev, 2002. **118**(1-2): p. 91-8.
482. Choulika, A., et al., *The yeast I-Sce I meganuclease induces site-directed chromosomal recombination in mammalian cells.* C R Acad Sci III, 1994. **317**(11): p. 1013-9.
483. Silva, G., et al., *Meganucleases and other tools for targeted genome engineering: perspectives and challenges for gene therapy.* Curr Gene Ther, 2011. **11**(1): p. 11-27.
484. Smith, J., et al., *A combinatorial approach to create artificial homing endonucleases cleaving chosen sequences.* Nucleic Acids Res, 2006. **34**(22): p. e149.
485. Grabher, C., J.S. Joly, and J. Wittbrodt, *Highly efficient zebrafish transgenesis mediated by the meganuclease I-SceI.* Methods Cell Biol, 2004. **77**: p. 381-401.
486. Grabher, C. and J. Wittbrodt, *Meganuclease and transposon mediated transgenesis in medaka.* Genome Biol, 2007. **8 Suppl 1**: p. S10.
487. Grabher, C. and J. Wittbrodt, *Recent advances in meganuclease-and transposon-mediated transgenesis of medaka and zebrafish.* Methods Mol Biol, 2008. **461**: p. 521-39.
488. Babaryka, A., E. Kuhn, and R.W. Koster, *In vivo synthesis of meganuclease for generating transgenic zebrafish Danio rerio.* J Fish Biol, 2009. **74**(2): p. 452-7.
489. Ogino, H., W.B. McConnell, and R.M. Grainger, *High-throughput transgenesis in Xenopus using I-SceI meganuclease.* Nat Protoc, 2006. **1**(4): p. 1703-10.

490. Ishibashi, S., N.R. Love, and E. Amaya, *A simple method of transgenesis using I-SceI meganuclease in Xenopus.* Methods Mol Biol, 2012. **917**: p. 205-18.
491. Ochiai, H., et al., *The Ars insulator facilitates I-SceI meganuclease-mediated transgenesis in the sea urchin embryo.* Dev Dyn, 2008. **237**(9): p. 2475-82.
492. Bibikova, M., et al., *Enhancing gene targeting with designed zinc finger nucleases.* Science, 2003. **300**(5620): p. 764.
493. Miller, J.C., et al., *A TALE nuclease architecture for efficient genome editing.* Nat Biotechnol, 2011. **29**(2): p. 143-8.
494. Urnov, F.D., et al., *Highly efficient endogenous human gene correction using designed zinc-finger nucleases.* Nature, 2005. **435**(7042): p. 646-51.
495. Moscou, M.J. and A.J. Bogdanove, *A simple cipher governs DNA recognition by TAL effectors.* Science, 2009. **326**(5959): p. 1501.
496. Lombardo, A., et al., *Gene editing in human stem cells using zinc finger nucleases and integrase-defective lentiviral vector delivery.* Nat Biotechnol, 2007. **25**(11): p. 1298-306.
497. Berg, J.M., *Proposed structure for the zinc-binding domains from transcription factor IIIA and related proteins.* Proc Natl Acad Sci U S A, 1988. **85**(1): p. 99-102.
498. Kim, Y.G., J. Cha, and S. Chandrasegaran, *Hybrid restriction enzymes: zinc finger fusions to Fok I cleavage domain.* Proc Natl Acad Sci U S A, 1996. **93**(3): p. 1156-60.
499. Urnov, F.D., et al., *Genome editing with engineered zinc finger nucleases.* Nat Rev Genet, 2010. **11**(9): p. 636-46.
500. Christian, M., et al., *Targeting DNA double-strand breaks with TAL effector nucleases.* Genetics, 2010. **186**(2): p. 757-61.
501. Li, T., et al., *TAL nucleases (TALNs): hybrid proteins composed of TAL effectors and FokI DNA-cleavage domain.* Nucleic Acids Res, 2011. **39**(1): p. 359-72.
502. Kay, S., et al., *A bacterial effector acts as a plant transcription factor and induces a cell size regulator.* Science, 2007. **318**(5850): p. 648-51.
503. Boch, J., et al., *Breaking the code of DNA binding specificity of TAL-type III effectors.* Science, 2009. **326**(5959): p. 1509-12.
504. Bitinaite, J., et al., *FokI dimerization is required for DNA cleavage.* Proc Natl Acad Sci U S A, 1998. **95**(18): p. 10570-5.
505. Szczepek, M., et al., *Structure-based redesign of the dimerization interface reduces the toxicity of zinc-finger nucleases.* Nat Biotechnol, 2007. **25**(7): p. 786-93.
506. Miller, J.C., et al., *An improved zinc-finger nuclease architecture for highly specific genome editing.* Nat Biotechnol, 2007. **25**(7): p. 778-85.
507. Niu, Q., et al., *Knockout of the adp gene related with colonization in Bacillus nematocida B16 using customized transcription activator-like effectors nucleases.* Microbial Biotechnology, 2015. **8**(4): p. 681-692.
508. Carroll, D., *Genome Engineering With Zinc-Finger Nucleases.* Genetics, 2011. **188**(4): p. 773-782.
509. Li, T., et al., *Modularly assembled designer TAL effector nucleases for targeted gene knockout and gene replacement in eukaryotes.* Nucleic Acids Research, 2011.
510. Herrmann, F., et al., *p53 Gene Repair with Zinc Finger Nucleases Optimised by Yeast 1-Hybrid and Validated by Solexa Sequencing.* PLoS ONE, 2011. **6**(6): p. e20913.
511. Watanabe, T., S. Noji, and T. Mito, *GeneKnockout by Targeted Mutagenesis in a Hemimetabolous Insect, the Two-Spotted Cricket Gryllus bimaculatus, using TALENs.* Methods Mol Biol, 2016. **1338**: p. 143-55.
512. Miyamoto, K., et al., *The Expression of TALEN before Fertilization Provides a Rapid Knock-Out Phenotype in <italic>Xenopus laevis</italic> Founder Embryos.* PLoS ONE, 2015. **10**(11): p. e0142946.

513. Lei, Y., et al., *Efficient targeted gene disruption in Xenopus embryos using engineered transcription activator-like effector nucleases (TALENs).* Proceedings of the National Academy of Sciences, 2012. **109**(43): p. 17484-17489.
514. Qiu, C., et al., *Efficient knockout of transplanted green fluorescent protein gene in medaka using TALENs.* Mar Biotechnol (NY), 2014. **16**(6): p. 674-83.
515. Amacher, S.L., *Emerging gene knockout technology in zebrafish: zinc-finger nucleases.* Brief Funct Genomic Proteomic, 2008. **7**(6): p. 460-4.
516. Sung, Y.H., et al., *Knockout mice created by TALEN-mediated gene targeting.* Nat Biotech, 2013. **31**(1): p. 23-24.
517. Geurts, A.M., et al., *Knockout Rats via Embryo Microinjection of Zinc-Finger Nucleases.* Science, 2009. **325**(5939): p. 433-433.
518. Frank, S., B.V. Skryabin, and B. Greber, *A modified TALEN-based system for robust generation of knock-out human pluripotent stem cell lines and disease models.* BMC Genomics, 2013. **14**(1): p. 1-9.
519. Hofer, U., et al., *Pre-clinical modeling of CCR5 knockout in human hematopoietic stem cells by zinc finger nucleases using humanized mice.* J Infect Dis, 2013. **208 Suppl 2**: p. S160-4.
520. O'Connell, M.R., et al., *Programmable RNA recognition and cleavage by CRISPR/Cas9.* Nature, 2014. **516**(7530): p. 263-6.
521. Jansen, R., et al., *Identification of genes that are associated with DNA repeats in prokaryotes.* Mol Microbiol, 2002. **43**(6): p. 1565-75.
522. Jansen, R., et al., *Identification of a novel family of sequence repeats among prokaryotes.* OMICS, 2002. **6**(1): p. 23-33.
523. Sorek, R., V. Kunin, and P. Hugenholtz, *CRISPR--a widespread system that provides acquired resistance against phages in bacteria and archaea.* Nat Rev Microbiol, 2008. **6**(3): p. 181-6.
524. Sander, J.D. and J.K. Joung, *CRISPR-Cas systems for editing, regulating and targeting genomes.* Nat Biotechnol, 2014. **32**(4): p. 347-55.
525. Haft, D.H., et al., *A guild of 45 CRISPR-associated (Cas) protein families and multiple CRISPR/Cas subtypes exist in prokaryotic genomes.* PLoS Comput Biol, 2005. **1**(6): p. e60.
526. Wright, A.V., J.K. Nunez, and J.A. Doudna, *Biology and Applications of CRISPR Systems: Harnessing Nature's Toolbox for Genome Engineering.* Cell, 2016. **164**(1-2): p. 29-44.
527. Sapranauskas, R., et al., *The Streptococcus thermophilus CRISPR/Cas system provides immunity in Escherichia coli.* Nucleic Acids Res, 2011. **39**(21): p. 9275-82.
528. Gottesman, S., *Microbiology: Dicing defence in bacteria.* Nature, 2011. **471**(7340): p. 588-9.
529. Haurwitz, R.E., et al., *Sequence- and structure-specific RNA processing by a CRISPR endonuclease.* Science, 2010. **329**(5997): p. 1355-8.
530. Deltcheva, E., et al., *CRISPR RNA maturation by trans-encoded small RNA and host factor RNase III.* Nature, 2011. **471**(7340): p. 602-7.
531. Jinek, M., et al., *A programmable dual-RNA-guided DNA endonuclease in adaptive bacterial immunity.* Science, 2012. **337**(6096): p. 816-21.
532. Gasiunas, G., et al., *Cas9-crRNA ribonucleoprotein complex mediates specific DNA cleavage for adaptive immunity in bacteria.* Proc Natl Acad Sci U S A, 2012. **109**(39): p. E2579-86.
533. Bikard, D., et al., *Programmable repression and activation of bacterial gene expression using an engineered CRISPR-Cas system.* Nucleic Acids Res, 2013. **41**(15): p. 7429-37.
534. Mali, P., et al., *CAS9 transcriptional activators for target specificity screening and paired nickases for cooperative genome engineering.* Nat Biotechnol, 2013. **31**(9): p. 833-8.
535. Mali, P., et al., *RNA-guided human genome engineering via Cas9.* Science, 2013. **339**(6121): p. 823-6.
536. Kime, C., et al., *Efficient CRISPR/Cas9-Based Genome Engineering in Human Pluripotent Stem Cells.* Curr Protoc Hum Genet, 2016. **88**: p. Unit 21 4.
537. Wyvekens, N., S.Q. Tsai, and J.K. Joung, *Genome Editing in Human Cells Using CRISPR/Cas Nucleases.* Curr Protoc Mol Biol, 2015. **112**: p. 31 3 1-18.

538. Xue, H., et al., *Genetic Modification in Human Pluripotent Stem Cells by Homologous Recombination and CRISPR/Cas9 System.* Methods Mol Biol, 2014.
539. Wang, T., et al., *Genetic screens in human cells using the CRISPR-Cas9 system.* Science, 2014. **343**(6166): p. 80-4.
540. Shalem, O., et al., *Genome-scale CRISPR-Cas9 knockout screening in human cells.* Science, 2014. **343**(6166): p. 84-7.
541. Rong, Z., et al., *Homologous recombination in human embryonic stem cells using CRISPR/Cas9 nickase and a long DNA donor template.* Protein Cell, 2014.
542. Perez-Pinera, P., et al., *Synergistic and tunable human gene activation by combinations of synthetic transcription factors.* Nat Methods, 2013. **10**(3): p. 239-42.
543. Maeder, M.L., et al., *CRISPR RNA-guided activation of endogenous human genes.* Nat Methods, 2013. **10**(10): p. 977-9.
544. Hou, Z., et al., *Efficient genome engineering in human pluripotent stem cells using Cas9 from Neisseria meningitidis.* Proc Natl Acad Sci U S A, 2013. **110**(39): p. 15644-9.
545. Jiang, W., et al., *Demonstration of CRISPR/Cas9/sgRNA-mediated targeted gene modification in Arabidopsis, tobacco, sorghum and rice.* Nucleic Acids Res, 2013. **41**(20): p. e188.
546. Yang, Y.Y., et al., *Identification of rice varieties with high tolerance or sensitivity to lead and characterization of the mechanism of tolerance.* Plant Physiol, 2000. **124**(3): p. 1019-26.
547. Kasher, P.R., et al., *Characterization of samhd1 morphant zebrafish recapitulates features of the human type I interferonopathy Aicardi-Goutieres syndrome.* J Immunol, 2015. **194**(6): p. 2819-25.
548. Liu, D., et al., *Efficient gene targeting in zebrafish mediated by a zebrafish-codon-optimized cas9 and evaluation of off-targeting effect.* J Genet Genomics, 2014. **41**(1): p. 43-6.
549. Auer, T.O., et al., *Highly efficient CRISPR/Cas9-mediated knock-in in zebrafish by homology-independent DNA repair.* Genome Res, 2014. **24**(1): p. 142-53.
550. Jao, L.E., S.R. Wente, and W. Chen, *Efficient multiplex biallelic zebrafish genome editing using a CRISPR nuclease system.* Proc Natl Acad Sci U S A, 2013. **110**(34): p. 13904-9.
551. Hwang, W.Y., et al., *Efficient genome editing in zebrafish using a CRISPR-Cas system.* Nat Biotechnol, 2013. **31**.
552. Hwang, W.Y., et al., *Heritable and precise zebrafish genome editing using a CRISPR-Cas system.* PLoS One, 2013. **8**(7): p. e68708.
553. Hruscha, A., et al., *Efficient CRISPR/Cas9 genome editing with low off-target effects in zebrafish.* Development, 2013. **140**(24): p. 4982-7.
554. Chang, N., et al., *Genome editing with RNA-guided Cas9 nuclease in zebrafish embryos.* Cell Res, 2013. **23**(4): p. 465-72.
555. Gratz, S.J., et al., *CRISPR/Cas9-mediated genome engineering and the promise of designer flies on demand.* Fly (Austin), 2013. **7**(4).
556. Zhou, J., et al., *Dual sgRNAs facilitate CRISPR/Cas9-mediated mouse genome targeting.* FEBS J, 2014.
557. Wu, Y., et al., *Correction of a genetic disease in mouse via use of CRISPR-Cas9.* Cell Stem Cell, 2013. **13**(6): p. 659-62.
558. Li, D., et al., *Heritable gene targeting in the mouse and rat using a CRISPR-Cas system.* Nat Biotechnol, 2013. **31**(8): p. 681-3.
559. Ma, Y., et al., *Generating rats with conditional alleles using CRISPR/Cas9.* Cell Res, 2014. **24**(1): p. 122-5.
560. Cong, L., et al., *Multiplex genome engineering using CRISPR/Cas systems.* Science, 2013. **339**(6121): p. 819-23.
561. Pattanayak, V., et al., *High-throughput profiling of off-target DNA cleavage reveals RNA-programmed Cas9 nuclease specificity.* Nat Biotechnol, 2013. **31**(9): p. 839-43.
562. Fu, Y., et al., *High-frequency off-target mutagenesis induced by CRISPR-Cas nucleases in human cells.* Nat Biotechnol, 2013. **31**(9): p. 822-6.

563. Tsai, S.Q., et al., *GUIDE-seq enables genome-wide profiling of off-target cleavage by CRISPR-Cas nucleases.* Nat Biotechnol, 2015. **33**(2): p. 187-97.
564. Fu, Y., et al., *Improving CRISPR-Cas nuclease specificity using truncated guide RNAs.* Nat Biotechnol, 2014. **32**(3): p. 279-84.
565. Kim, E., et al., *Precision genome engineering with programmable DNA-nicking enzymes.* Genome Res, 2012. **22**(7): p. 1327-33.
566. Wyvekens, N., et al., *Dimeric CRISPR RNA-Guided FokI-dCas9 Nucleases Directed by Truncated gRNAs for Highly Specific Genome Editing.* Hum Gene Ther, 2015. **26**(7): p. 425-31.
567. Cenker, J.J., R.D. Stultz, and D. McDonald, *Brain Microglial Cells Are Highly Susceptible to HIV-1 Infection and Spread.* AIDS research and human retroviruses, 2017. **33**(11): p. 1155-1165.
568. Cowan, C.A., et al., *Derivation of embryonic stem-cell lines from human blastocysts.* N Engl J Med, 2004. **350**(13): p. 1353-6.
569. Wilgenburg, B.J., *Investigation into sub-cellular CD4 distribution in human Embryonic Stem Cell derived macrophages and its role in HIV-1 infection.* Doctoral Thesis, 2012.
570. Ferraro, P., et al., *Quantitation of cellular deoxynucleoside triphosphates.* Nucleic Acids Res, 2010. **38**(6): p. e85.
571. Solter, A.W. and R.E. Handschumacher, *A rapid quantitative determination of deoxyribonucleoside triphosphates based on the enzymatic synthesis of DNA.* Biochim Biophys Acta, 1969. **174**(2): p. 585-90.
572. Roesch, F. and O. Schwartz, *The SAMHD1 knockout mouse model: in vivo veritas?* EMBO J, 2013. **32**(18): p. 2427-9.
573. Li, D., et al., *Vpx mediated degradation of SAMHD1 has only a very limited effect on lentiviral transduction rate in ex vivo cultured HSPCs.* Stem Cell Res, 2015. **15**(2): p. 271-80.
574. Descours, B., et al., *SAMHD1 restricts HIV-1 reverse transcription in quiescent CD4(+) T-cells.* Retrovirology, 2012. **9**: p. 87.
575. St Gelais, C., et al., *SAMHD1 restricts HIV-1 infection in dendritic cells (DCs) by dNTP depletion, but its expression in DCs and primary CD4+ T-lymphocytes cannot be upregulated by interferons.* Retrovirology, 2012. **9**: p. 105.
576. Pertel, T., C. Reinhard, and J. Luban, *Vpx rescues HIV-1 transduction of dendritic cells from the antiviral state established by type 1 interferon.* Retrovirology, 2011. **8**: p. 49.
577. Chen, S., et al., *SAMHD1 suppresses innate immune responses to viral infections and inflammatory stimuli by inhibiting the NF-kappaB and interferon pathways.* Proc Natl Acad Sci U S A, 2018. **115**(16): p. E3798-E3807.
578. Kodigepalli, K.M., et al., *SAMHD1 modulates in vitro proliferation of acute myeloid leukemia-derived THP-1 cells through the PI3K-Akt-p27 axis.* Cell Cycle, 2018. **17**(9): p. 1124-1137.
579. Szaniawski, M.A., et al., *SAMHD1 Phosphorylation Coordinates the Anti-HIV-1 Response by Diverse Interferons and Tyrosine Kinase Inhibition.* MBio, 2018. **9**(3).
580. Bloch, N., et al., *HIV type 1 infection of plasmacytoid and myeloid dendritic cells is restricted by high levels of SAMHD1 and cannot be counteracted by Vpx.* AIDS Res Hum Retroviruses, 2014. **30**(2): p. 195-203.
581. Kim, B., et al., *Tight interplay among SAMHD1 protein level, cellular dNTP levels, and HIV-1 proviral DNA synthesis kinetics in human primary monocyte-derived macrophages.* J Biol Chem, 2012. **287**(26): p. 21570-4.
582. Lahouassa, H., et al., *SAMHD1 restricts the replication of human immunodeficiency virus type 1 by depleting the intracellular pool of deoxynucleoside triphosphates.* Nat Immunol, 2012. **13**(3): p. 223-8.
583. Hollenbaugh, J.A., et al., *dNTP pool modulation dynamics by SAMHD1 protein in monocyte-derived macrophages.* Retrovirology, 2014. **11**: p. 63.
584. Diamond, T.L., et al., *Macrophage tropism of HIV-1 depends on efficient cellular dNTP utilization by reverse transcriptase.* J Biol Chem, 2004. **279**(49): p. 51545-53.

585. Dragin, L., et al., *Interferon block to HIV-1 transduction in macrophages despite SAMHD1 degradation and high deoxynucleoside triphosphates supply.* Retrovirology, 2013. **10**: p. 30.
586. Welbourn, S. and K. Strebel, *Low dNTP levels are necessary but may not be sufficient for lentiviral restriction by SAMHD1.* Virology, 2016. **488**: p. 271-7.
587. Gramberg, T., et al., *Restriction of diverse retroviruses by SAMHD1.* Retrovirology, 2013. **10**: p. 26.
588. Franzolin, E., et al., *The Deoxynucleoside Triphosphate Triphosphohydrolase Activity of SAMHD1 Protein Contributes to the Mitochondrial DNA Depletion Associated with Genetic Deficiency of Deoxyguanosine Kinase.* J Biol Chem, 2015. **290**(43): p. 25986-96.
589. Fujita, M., et al., *SAMHD1-Dependent and -Independent Functions of HIV-2/SIV Vpx Protein.* Front Microbiol, 2012. **3**: p. 297.
590. Reinhard, C., et al., *Vpx rescue of HIV-1 from the antiviral state in mature dendritic cells is independent of the intracellular deoxynucleotide concentration.* Retrovirology, 2014. **11**: p. 12.
591. Schaller, T., et al., *Nuclear import of SAMHD1 is mediated by a classical karyopherin alpha/beta1 dependent pathway and confers sensitivity to VpxMAC induced ubiquitination and proteasomal degradation.* Retrovirology, 2014. **11**: p. 29.
592. Cheng, X. and L. Ratner, *HIV-2 Vpx protein interacts with interferon regulatory factor 5 (IRF5) and inhibits its function.* J Biol Chem, 2014. **289**(13): p. 9146-57.
593. Zhang, N., et al., *The poly-proline tail of SIVmac Vpx provides gain of function for resistance to a cryptic proteasome-dependent degradation pathway.* Virology, 2017. **511**: p. 23-29.
594. Jordan, C.A., et al., *Infection of brain microglial cells by human immunodeficiency virus type 1 is CD4 dependent.* Journal of virology, 1991. **65**(2): p. 736-742.
595. Baldauf, H.M., et al., *Vpx overcomes a SAMHD1-independent block to HIV reverse transcription that is specific to resting CD4 T cells.* Proc Natl Acad Sci U S A, 2017. **114**(10): p. 2729-2734.
596. Zang Lab, M., *CRISPR Design.* 2015.
597. Wittwer, C.T., et al., *High-Resolution Genotyping by Amplicon Melting Analysis Using LCGreen.* Clinical Chemistry, 2003. **49**(6): p. 853.
598. Hadden, J.M., et al., *Crystal structure of the Holliday junction resolving enzyme T7 endonuclease I.* Nat Struct Biol, 2001. **8**(1): p. 62-7.
599. White, M.F., et al., *Recognition and manipulation of branched DNA structure by junction-resolving enzymes.* J Mol Biol, 1997. **269**(5): p. 647-64.
600. Xin, B., et al., *Homozygous mutation in SAMHD1 gene causes cerebral vasculopathy and early onset stroke.* Proc Natl Acad Sci U S A, 2011. **108**(13): p. 5372-7.
601. Ryoo, J., et al., *The ribonuclease activity of SAMHD1 is required for HIV-1 restriction.* Nat Med, 2014.
602. Quintana-Murci, L. and M. Fellous, *The Human Y Chromosome: The Biological Role of a "Functional Wasteland".* Journal of biomedicine & biotechnology, 2001. **1**(1): p. 18-24.
603. Behrendt, R., et al., *Mouse SAMHD1 has antiretroviral activity and suppresses a spontaneous cell-intrinsic antiviral response.* Cell Rep, 2013. **4**(4): p. 689-96.
604. Jakobsen MR, B.R., Andersen A, Berg RK, Jensen SB, Tengchuan J,, *IFI16 senses DNA forms of the lentiviral replication cycle and controls HIV-1 replication.* Proc Natl Acad Sci U S A, 2013(110): p. E4571–80.
605. Hong, H.S., et al., *Exogenous HIV-1 Vpr disrupts IFN-alpha response by plasmacytoid dendritic cells (pDCs) and subsequent pDC/NK interplay.* Immunol Lett, 2009. **125**(2): p. 100-4.
606. Zahoor, M.A., et al., *HIV-1 Vpr induces interferon-stimulated genes in human monocyte-derived macrophages.* PLoS One, 2014. **9**(8): p. e106418.
607. Vodicka, M.A., et al., *HIV-1 Vpr interacts with the nuclear transport pathway to promote macrophage infection.* Genes Dev, 1998. **12**(2): p. 175-85.

608. Kornbluth, R.S., et al., *Interferons and bacterial lipopolysaccharide protect macrophages from productive infection by human immunodeficiency virus in vitro.* The Journal of experimental medicine, 1989. **169**(3): p. 1137-1151.
609. Zybarth, G., et al., *Activation-induced resistance of human macrophages to HIV-1 infection in vitro.* J Immunol, 1999. **162**(1): p. 400-6.
610. Pushkarsky, T., L. Dubrovsky, and M. Bukrinsky, *Lipopolysaccharide stimulates HIV-1 entry and degradation in human macrophages.* J Endotoxin Res, 2001. **7**(4): p. 271-6.
611. Pomerantz, R.J., et al., *Lipopolysaccharide is a potent monocyte/macrophage-specific stimulator of human immunodeficiency virus type 1 expression.* The Journal of experimental medicine, 1990. **172**(1): p. 253-261.
612. Equils, O., et al., *Repeated lipopolysaccharide (LPS) exposure inhibits HIV replication in primary human macrophages.* Microbes and Infection, 2006. **8**(9): p. 2469-2476.
613. Gibbons, J.M., et al., *HIV-1 Accessory Protein Vpr Interacts with REAF/RPRD2 To Mitigate Its Antiviral Activity.* Journal of Virology, 2020. **94**(4): p. e01591-19.
614. Bartz, S.R. and M.A. Vodicka, *Production of high-titer human immunodeficiency virus type 1 pseudotyped with vesicular stomatitis virus glycoprotein.* Methods, 1997. **12**(4): p. 337-42.
615. Sanders, D.A., *No false start for novel pseudotyped vectors.* Current Opinion in Biotechnology, 2002. **13**: p. 437–442.
616. Yu, D., et al., *The HIV envelope but not VSV glycoprotein is capable of mediating HIV latent infection of resting CD4 T cells.* PLoS pathogens, 2009. **5**(10): p. e1000633-e1000633.
617. Sun, X., et al., *Internalization and fusion mechanism of vesicular stomatitis virus and related rhabdoviruses.* Future virology, 2010. **5**(1): p. 85-96.
618. Guo, H., et al., *Identification of critical regions in human SAMHD1 required for nuclear localization and Vpx-mediated degradation.* PLoS One, 2013. **8**(7): p. e66201.
619. Haenseler, W., et al., *A Highly Efficient Human Pluripotent Stem Cell Microglia Model Displays a Neuronal-Co-culture-Specific Expression Profile and Inflammatory Response.* Stem cell reports, 2017. **8**(6): p. 1727-1742.
620. Haworth, K.G., C.W. Peterson, and H.-P. Kiem, *CCR5-edited gene therapies for HIV cure: Closing the door to viral entry.* Cytotherapy, 2017. **19**(11): p. 1325-1338.
621. Yap, M.W., S. Nisole, and J.P. Stoye, *A single amino acid change in the SPRY domain of human Trim5alpha leads to HIV-1 restriction.* Curr Biol, 2005. **15**(1): p. 73-8.
622. Cradick, T.J., et al., *CRISPR/Cas9 systems targeting beta-globin and CCR5 genes have substantial off-target activity.* Nucleic Acids Res, 2013. **41**(20): p. 9584-92.
623. Sharp, P.M. and B.H. Hahn, *Origins of HIV and the AIDS pandemic.* Cold Spring Harb Perspect Med, 2011. **1**(1): p. a006841.